Theoretical Studies on Transition Metal Complexes of Silicon Species: Their Novel Bonding Natures, Electronic Structures, and Fluxional Behavior

Mausumi Ray

2009

Preface

In recent years, interactions and reactions of transition metal complexes with species of heavy p-block elements have drawn a lot of interests because the interaction of d-block elements with heavy p-block elements can create a new series of compounds with interesting geometries, properties, and reactivities. The chemical bonds between the transition metal and heavy p-block element are expected to be distinctly different from the usual covalent and coordinate bonds of carbon, nitrogen, and oxygen compounds. Silicon is the most common and useful element among such heavy p-block elements. Moreover, the M-Si bond plays a key role in many conversion reactions of silicon compounds catalyzed by transition metal complexes. Thus, transition metal complexes of silicon species have been attractive research targets in inorganic chemistry, organometallic chemistry, catalytic chemistry, and physical chemistry. However, we do not have sufficient knowledge of geometries, bonding natures, and reaction behavior of transition metal silicon complexes compared to well established chemistry of their carbon analogues. One reason is that the synthesis of transition metal silicon complexes is difficult in contrast to their carbon analogue. Therefore, future studies are obligatory in this field to elucidate the characteristic features of the interactions and reactions between transition metal and silicon species. It is crucial to find out the general rules and fundamental properties that determine the geometries, interactions, and reactions of such complexes.

Considering these issues, theoretical study with modern electronic structure theory must be applied to such complexes because the electronic structure theory can present good knowledge and correct understanding of the geometry, bonding nature, and electronic structure of a chemical system. However, such theoretical study on transition metal complex with silicon species has been very limited, so far. It is also

noted that the computational approach is not easy for the large systems containing transition metal and heavy p-block elements.

In this thesis, the author presents theoretical studies on new transition metal complexes containing silicon species. The density functional theory (DFT) was mainly used in these theoretical studies. Møller-Plesset (MP) perturbation theory (MP2, MP3, and MP4) and coupled-cluster method with single and double substitutions and perturbation correction of triple excitations (CCSD(T)) were also employed to check the reliability of the DFT-calculated energies. To inspect the bonding interactions of these complexes, the LCMO (Linear Combination of Molecular Orbital) analysis was carried out, in which molecular orbital ψ_i of the total system is represented by a linear combination of molecular orbitals of the fragments. This thesis provides valuable and important results on interesting geometrical characteristics, bonding interactions, and electronic structures of transition metal complexes containing silicon species. The geometry changes, energetics, and electronic processes of their reactions as well as their fluxional behavior are clearly discussed based on the fundamental understanding of electronic structure. Correct understanding is provided on the reasons why the transition metal complexes of silicon species are similar to and/or different from their carbon analogues. Clear idea is proposed on how to synthesize new transition metal complexes of silicon species.

These studies were carried out at the Department of Molecular Engineering, Graduate School of Engineering, Kyoto University under the supervision of Professor Shigeyoshi Sakaki. At first, the author expresses her sincere thanks to Prof. Sakaki for his wonderful guidance, inspiration, valuable suggestions, and enthusiastic discussion throughout this research. All studies were performed with his full cooperation.

Contents

4. Theoretical Study of New Ethynediyl-Bridged Bis(Silylene) Dinuclear Tungsten Complex: Novel Bonding Nature and Electronic Structure   155

5. Tungsten Dihydride Silyl Complex: New Insight into Their Bonding Nature and Dynamic Behavior   187

General Conclusion   235

List of Publications   241

General Introduction

1　Background

In modern chemistry, the interactions and reactions of transition metal complexes have been investigated extensively. One of the reasons is that the application of transition metal complexes has become increasingly important due to their high technological demands for the production of new advanced materials which are valuable from various aspects of our modern life [1]. Among those studies, investigation of the interaction and reaction of transition metal complexes with species containing heavy p-block elements has been considerably focused because the interaction of d-block elements with p-block elements can create a new series of compounds with interesting properties and reactivities [1, 2-5]. In particular, the compounds containing the bond between d-block and heavy p-block elements can play a key role as intermediates in the transformations of such p-block compounds [3]. Because of large differences between s and p orbitals and very small electronegativities of heavy group 14 p-block elements compared to carbon, the chemical bonds between the transition metal and heavy group 14 elements are expected to be distinctly different from usual covalent and coordinate bonds of carbon compounds. Furthermore, heavy group 14 elements are able to expand their valence shells and to produce penta- or even hexa-valent species, which are well known as hypervalency [1e]. Hence, species containing the heavy group 14 element exhibit very diverse coordination chemistry and are becoming increasingly novel ligands to a wide range of transition metals [1, 2-5]. To synthesize a new series of compounds containing transition metal (M) and heavy group 14 elements (E), we need deep understanding of the nature of the M-E

interaction. In this regard, a lot of efforts have recently been devoted to the syntheses and characterizations of transition metal complexes containing heavy group 14 elements. However, in contrast to the well-advanced field of the transition metal complexes containing organic species, the chemistry of its heavier analogues is still in infancy. Various issues remain to be solved in this field. In addition to experimental breakthrough, detailed theoretical considerations of structures, bonding natures, and reactivities of such systems are highly and impatiently awaited.

2   Transition Metal Complexes of Silicon Species

Silicon is the most common and useful element among the heavy p-block elements of group 14. Silicon compounds are much different from their carbon analogues even if their compositions are similar to each other. For instance, acetylene is linear, whereas its

$$R-C\equiv C-R \qquad \overset{R}{\diagdown}Si\equiv Si\overset{}{\diagdown}_R$$
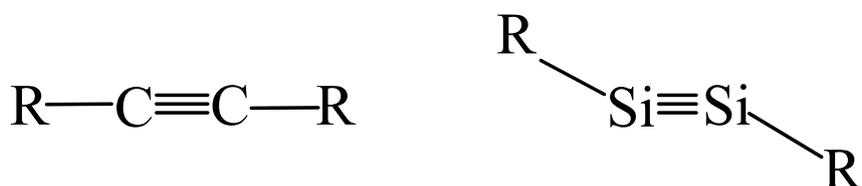
Scheme 1

silicon analogue is very reactive and takes trans-bent structure, as shown in Scheme 1 [1a-d, 5, 6-15]. Recently, transition metal complexes containing various silicon species have attracted considerable academic and industrial interests owing to their synthetic applications as well as physico-chemical properties [2, 3, 16-26]. Similar to the M-C bonds, the formation and cleavage of which play fundamental roles in the catalytic reactions of organic compounds, the reactivity of the M-Si bond play key roles in many conversion reactions of silicon compounds catalyzed by transition metal complexes [3]. In order to develop new synthetic routes of various transition metal complexes containing

silicon species, well understanding of the interaction between silicon species and transition metal center is indispensible. Thus, spectacular development of the transition metal chemistry of silicon species has been made [3, 18, 22-32]. However, the chemistry of transition metal silicon complexes is still insufficient compared to the well established chemistry of their carbon analogues. Deep understanding about the nature of the M-Si bond and its reactivity is considerably insufficient. It is unclear how and why silicon analogues of transition metal complexes are similar to or different from their carbon analogues. One of the reasons is that the syntheses of transition metal complexes containing silicon species are still difficult and challenging in contrast to their carbon analogues. For instance, the ferrocene derivatives with the cyclopentadienyl (Cp) ligands consisting entirely of group 14 heavy elements are most intriguing, representing an inorganic version of classical metallocenes [1e]. In contrast to a popular ferrocene (η^5-
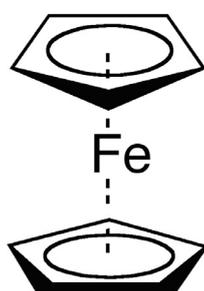
Scheme 2

$C_5H_5)_2Fe$ (Scheme 2), which was synthesized about 55 years ago, the synthesis of persilaferrocene, $(\eta^5\text{-}Si_5H_5)_2Fe$, has not been succeeded, yet [1e]. Also, in contrast to a number of known transition metal complexes of cyclobutadiene $\eta^4\text{-}R_4C_4$, those with the $\eta^4\text{-}R_4Si_4$ ligands have been limited; for instance, a few examples of Fe [1e, 33a] and Co [1e, 33b] complexes were recently reported, as shown in Scheme 3. Therefore, enormous future studies are necessary in this field; especially the detailed theoretical studies are obligatory to elucidate the characteristic features of the interaction and reaction between transition metal center and silicon species. It is crucial to find out the general rules and

E = Si or Ge

(A)   (B)
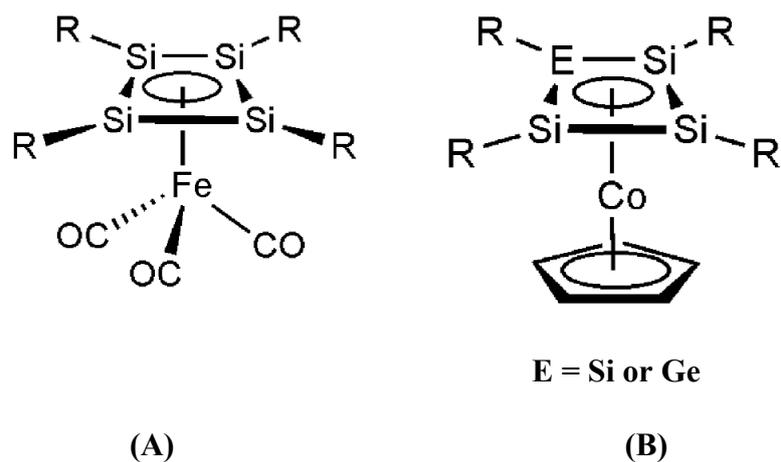
Scheme 3

fundamental properties that determine the geometries, interactions, and reactions of such complexes. Thus, theoretical study with modern electronic structure theory must be applied to such complexes, because electronic structure theory can present the fundamental chemical properties including the geometry, bonding nature, and electronic structure of a chemical system. This is specifically important when experimental results are difficult to obtain. However, such theoretical study on the transition metal complexes containing silicon species has been very limited, so far. Various electronic structure methods have been developed during the last two decades. At first, the common methods that are applied on the systems containing transition metals are briefly reviewed here.

3   Application of Electronic Structure Theory to Transition Metal Complexes

Application of electronic structure theory to the transition metal complex was comparatively limited in contrast to the organic compound until the end of 1980s. This is because the electronic structure of the transition metal complex is more complicated than that of the organic compound in general. Situation has dramatically changed in the last two decades due to the enormous developments of post-Hartree-Fock (post-HF) and

Density Functional Theory (DFT) methods and the small-core relativistic effective core potentials (ECPs). These set a new stage for the calculations of various important properties of the transition metal compounds [34-44].

To obtain reliable and accurate results for the transition metal system, inclusion of electron correlation effects is essential. This cannot be achieved within an independent-particle, single determinant Hartree-Fock (HF) approach. Hence, various post-HF methods have been developed to include the electron correlation effects.

The total energy (E) of the system is represented by eq 1,

$$E = E_N + E_T + E_V + E_J + E_X + E_C \qquad (1)$$

where E_N is the nuclei-nuclei repulsion energy, E_T is the kinetic energy of the electrons, E_V is the electron-nuclear attraction energy, E_J is the electron-electron repulsion energy, E_X is the electron-electron exchange energy, and E_C is the electron-electron correlation energy. It is noted that E_N is independent of the electron coordinates within the Born-Oppenheimer approximation. In the post-HF methods, the full HF exchange is employed for Ex and E_C is evaluated by the Configuration Interaction (CI), Møller-Plesset (MP) perturbation, or Coupled-Cluster (CC) methods. The CI method uses a variational wave function, which is a linear combination of configuration state functions (CSFs) consisting of spin orbitals. Advantage of the CI method is that it is variational, indicating that the calculated energy is always greater than the exact energy. A full CI calculation in which all possible electron configurations are taken into account provides exact correlation energy. However, it is very high cost calculation. Thus, truncation of the CI-space is necessary to save computational time. A popular way to truncate the CI expansion is to consider only singly and doubly excited configurations (CI-SD). In the MP method, the difference between the Fock operator ($\hat{H}_{HF}$) and the exact Hamiltonian ($\hat{H}$) is considered as a perturbation term and the wave function and the energy of the

5

system are represented by the perturbation expansion. Corrections can be made to any order of the energy and the wave function. The MP2 method takes into account correction up to the second order, and hence, it is a relatively cheap method for inclusion of the electron correlation effect. Third (MP3) and fourth (MP4) order MP calculations are computationally more expensive. The MP method works well when the zeroth-order wave function is good but displays poor convergence when the zeroyh-order wave function contains substantial multi-reference character. The CC wave function is generated by an excitation operator acting on a Slater determinant to produce a linear combination of excited Slater determinants. The CC method is non-variational, but very accurate. The CCSD(T) method, which is the CC method with single and double substitutions and perturbation correction of triple excitations, is often called "*the gold standard of quantum chemistry*" for its excellent accuracy for the molecule near equilibrium geometry. However, this calculation requires large computer resources and currently is not suitable for systems with more than ~400 basis functions. Unfortunately, the CI, MP, and CC methods require basis sets larger than DZP to exploit fully the inherent accuracy in these methods, which further reduces the size of the systems than can be handled. The Multi-Configuration SCF (MCSCF) method has been developed to study the system having non-degenerate character, i.e., large non-dynamical correlation. In the MCSCF calculation, the set of both coefficients of CSFs or determinants and the LCMO coefficients in molecular orbitals are optimized to present the electronic wave function incorporating full non-dynamical correlation with the best molecular orbitals. The major problem with the MCSCF method is to correctly select the configurations that are necessary for the property of interest. One approach is the Complete Active Space Self-Consistent Field (CASSCF) method, in which the selection of the configurations is done by partitioning MOs into active and inactive spaces. This method is used for describing

6

non-degenerate systems such as metal-metal multiple bonds, excited electronic states, and high-accuracy studies of dissociative processes. However, the numbers of active orbitals are limited to be about 14 at present due to its high demand of computational cost. This means that this method is limited to relatively smaller systems. Another weak point of the CASSCF method arises from the neglect of electron correlation in which the inactive space participates. CI calculation in which the configuration list is generated by allowing single or double excitations from the MCSCF or CASSCF reference space was proposed. Such methods are called Multireference CI (MRCI) and Second-order CI (SOCI) method, respectively. These methods include dynamical correlation beyond the MCSCF or CASSCF level. In MRMP2 or CASPT2 methods, the second order perturbation theory is also used to include the dynamic correlation to the MCSCF or CASSCF wave function. These methods can deal with extremely complex chemical situations and, if computing power permits, may be used to calculate both ground and excited states reliably.

The Density Functional Theory (DFT), another approach for the evaluation of the electron correlation, is very different from the HF and post-HF methods. In this method, the electronic structure is characterized by the electron density rather than by the wave function, where a functional is used for representing the exchange and correlation energies (E_X and E_C terms of eq 1). Interestingly, the DFT method is considerably less demanding on computational resources than the post-HF methods because the correlation energy is approximately evaluated with the density which is given by single determinant wave function. As a result, the DFT method can be applied to such large system as the transition metal complex. Nowadays the DFT method with the hybrid functionals such as B3LYP, B3P86, and B3PW91 seems to give reliable results for the ground state properties,
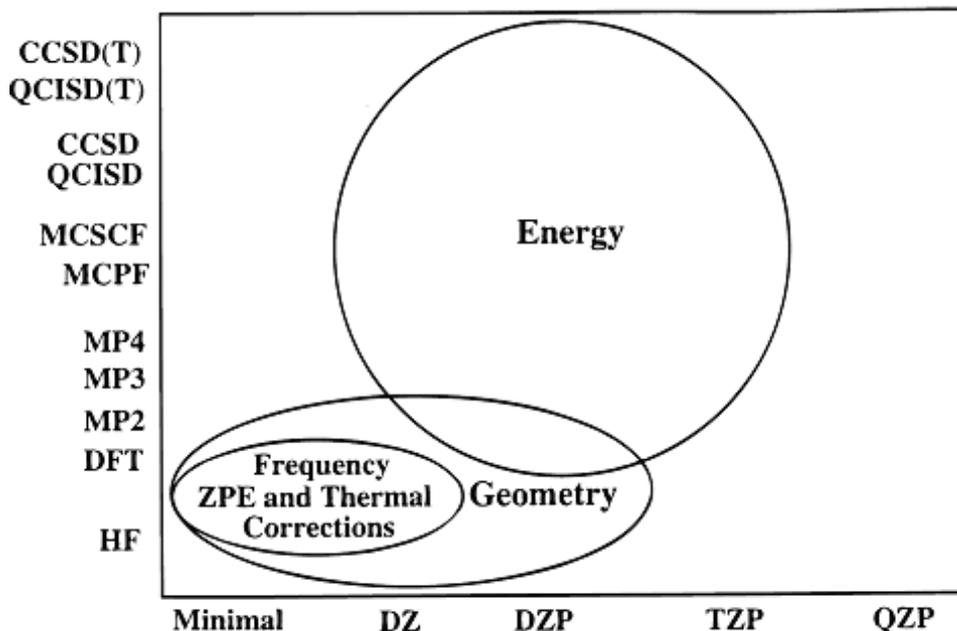
Figure 1. Strategic use of computational method and basis set in studies of transition metal complexes. Ref. [50(c)].

and therefore, has become an efficient and reliable computational tool for the large systems [34-53]. In the popular B3LYP functional, E_X is represented by the Becke three parameter hybrid exchange potential (B3) [54] and E_C is represented by the non-local correlation functional of Lee, Yang, and Parr (LYP) [55]. The E_C is also represented by the correlation functionals of Perdew (P86) in B3P86 [56] and of Perdew and Wang (PW91) [57] in B3PW91. The success of these hybrid functionals has often been attributed to the inclusion of the exact HF exchange and gradient corrections for the exchange and correlation. However, we need to remember that we do not know the correct exchange and correlation functions, indicating that the quality of the DFT method depends on the system: if the exchange-correlation functionals fit well the system, the DFT-calculated results are reliable. But, if not, the DFT-calculated results are not reliable.

Now, optimization of geometry and calculation of energetic of the species of interests are essential in quantum mechanical study. The accuracy of such calculations

8

depends on the theoretical methods as well as on the basis sets [34]. The strategic use of the computational methods and basis sets to study the transition metal systems is illustrated schematically in Figure 1 [50(c)]. Computational level becomes higher from the HF to the CCSD(T) and basis set quality increases from the minimal basis set through the double- and triple-ζ basis sets (DZ and TZ) with additional polarization functions (DZP and TZP) to the quadruple-ζ basis sets (QZ) with polarization functions (QZP). In other words, the quality of computational results increases upon going to the right-up direction in Figure 1.

3.1 Methods Useful for Geometry Optimization

Successful application of the electronic structure theory and reliable evaluation of the reaction and activation energies require correct geometries of reactant, transition state, intermediate, and product. Hence, geometry optimization is the first important step in the quantum chemical study of the transition metal complex. The most common geometry optimization of the system containing transition metal is performed at the MP2 or DFT levels of theory. However, recent theoretical studies show that the MP2 method cannot describe the electronic state of the transition metal system in many cases, because often the HF wave function becomes unstable due to multi-reference character in the transition metal complex. It has been proved from many studies that the DFT method with the hybrid functionals as B3P86, B3LYP, and B3PW91 provides better and more reliable description of geometries of transition metal complexes than the MP2 method [36, 41a,d,e, 48-53] except for some metal-metal multiple bonds bearing significant multireference character [52]. Actually, Table 1 shows that the B3LYP- and CISD-optimized geometries of a cobalt nitroso complex Cp(CO)(PH$_3$)(NOMe) **4** (see Scheme 4) are in much better agreement with the X-ray structure than the HF- and MP2-optimized geometries [50c].
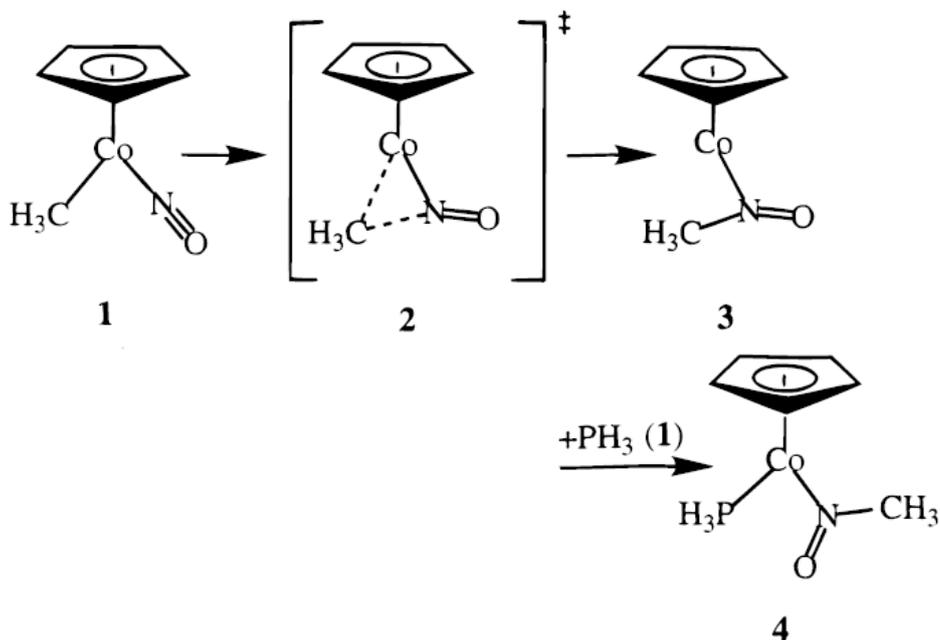
Scheme 4. Insertion of NO into a Co-CH₃ σ-bond followed by PH₃ addition. Ref [50(c)].

For instance, the metal-ligand distances are too long at the HF level and are too short at the MP2 level. The short Co-N distance and the long N-O distance of the MP2-optimized geometries indicate that the strength of the "back-donation" is overestimated by the MP2 method. As an additional example, Table 2 shows how much the geometry of [Cl₂Rh(CO)]⁻ depends on the level of theory [51]. The QCISD- and B3LYP-optimized geometries are close to that of the highest level CCSD(T)-optimized

Table 1. Selected optimized parameters of CpCo(PH₃)(NOMe) **4**.

	RHF/DZ	DFT/DZ	MP2/DZ	CISD/DZ	exp
Co−P	2.511	2.287	2.164	2.360	2.174
Co−N	1.991	1.772	1.711	1.787	1.780
N−O	1.226	1.324	1.378	1.295	1.282
N−C	1.487	1.514	1.527	1.504	1.484
P−Co−N	96.8	95.8	94.4	96.0	92.4
Co−N−O	124.2	126.4	128.3	125.4	125.6
Co−N−C	121.2	123.5	124.5	123.5	124.4

Bond lengths are in angstrom and bond angles are in degree.
Ref [50(c)].

Table 2. DFT, MP2, QCISD, and CCSD(T) Fully Optimized Geometries of [Cl$_2$Rh(CO)]$^-$.

	B3LYP	MP2	QCISD	CCSD(T)
R(Rh−C)	1.773	1.697	1.777	1.765
R(C−O)	1.157	1.178	1.161	1.166
R(Rh−Cl)	2.388	2.356	2.400	2.402
∠C−Rh−Cl	98.1	99.1	98.7	99.0
∠Cl−Rh−Cl	163.8	161.8	162.6	162.0

Ref [51].

geometry. On the other hand, the MP2-calculated Rh–C, C–O, and Rh–Cl distances considerably deviate from the CCSD(T)-calculated values. Also, the shorter Rh-CO distance accompanied with a longer C–O distance at the MP2 level indicates that Rh–CO π back-donation is overestimated by the MP2 method, too. In this regard, nowadays the DFT method with the hybrid functionals is commonly used for the geometry optimization of transition metal complexes.

3.2 Methods Useful for Energy calculation

Correct evaluation of energy at the optimized geometry is in particular important in the quantum chemical study of the transition metal complex. The energy is one index of the accuracy of the wave function. It has been proved in many recent studies that the DFT method with hybrid functionals such as B3LYP, B3PW91 etc. usually provides much better and more reliable description of relative energies than does the MP2 method except for some weak bonding interactions [44, 50, 52]. For example, as shown in Figure 2, the energetics by different levels of theory at the B3LYP/DZ-optimized geometries were investigated in the insertion of NO into a Co-CH$_3$ σ-bond (**1** to **3** in Scheme 4) clearly

11
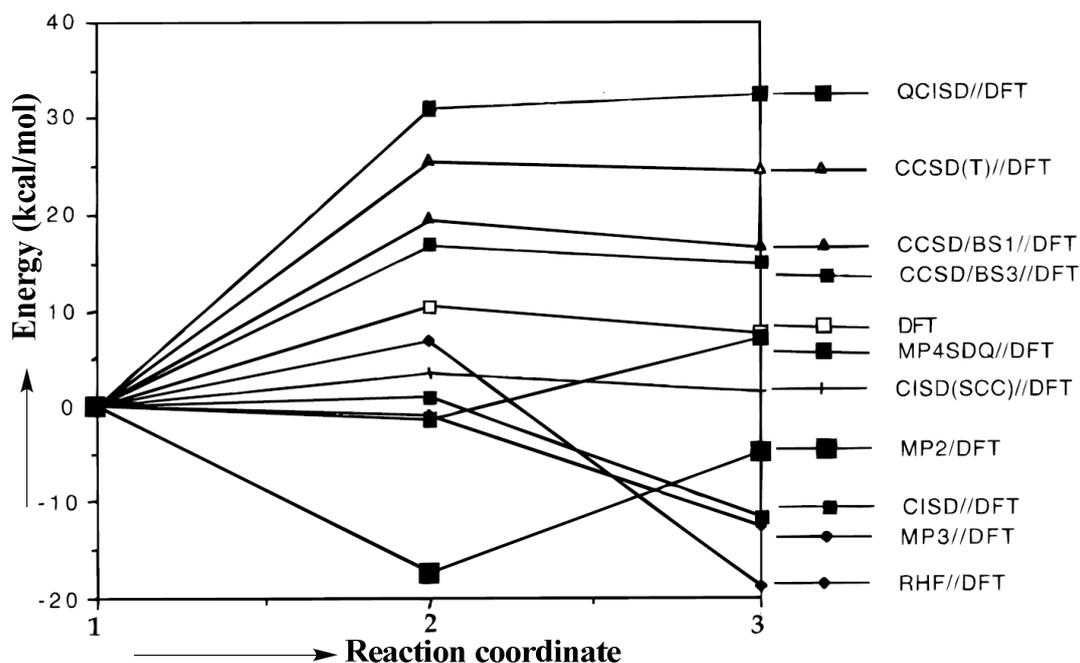
Figure 3. Energy profiles for the insertion of NO into a Co-CH$_3$ σ-bond; see Scheme 4. Ref [50(c)].

indicate that the MP perturbation method (MP2, MP3, MP4) fails to converge, while the B3LYP energy change is in good agreement with the higher post-HF methods such as CISD, QCISD, CCSD, and CCSD(T) [50a]. Also, the first dissociation energy of transition metal hexacarbonyls shows that the BP86- and B3LYP-calculated values are in good agreement with the CCSD(T)-calculated values; see Table 3 [44a]. In these

Table 3. First bond dissociation energies (kcal/mol) of isoelectronic transition metal hexacarbonyls.

method	$[Hf(CO)_6]^{2-}$	$[Ta(CO)_6]^-$	$W(CO)_6$	$[Re(CO)_6]^+$	$[Os(CO)_6]^{2+}$	$[Ir(CO)_6]^{3+}$
B3LYP	51.40 (49.61)	47.81 (45.95)	45.93 (43.84)	48.22 (45.99)	58.20 (55.87)	74.94 (72.59)
BP86	54.86 (53.18)	50.94 (49.08)	49.43 (47.34)	52.25 (50.02)	62.57 (60.24)	79.05 (76.70)
MP2		53.08 (51.21)	54.76 (52.67)	58.21 (55.98)	69.90 (67.27)	85.71 (83.36)
CCSD(T)		47.94 (46.07)	48.02 (45.93)	50.57 (48.34)	60.95 (58.62)	77.45 (75.10)
exptl			46.0 ± 2			

ZPE corrected values are given in parenthesis. Ref [44a].
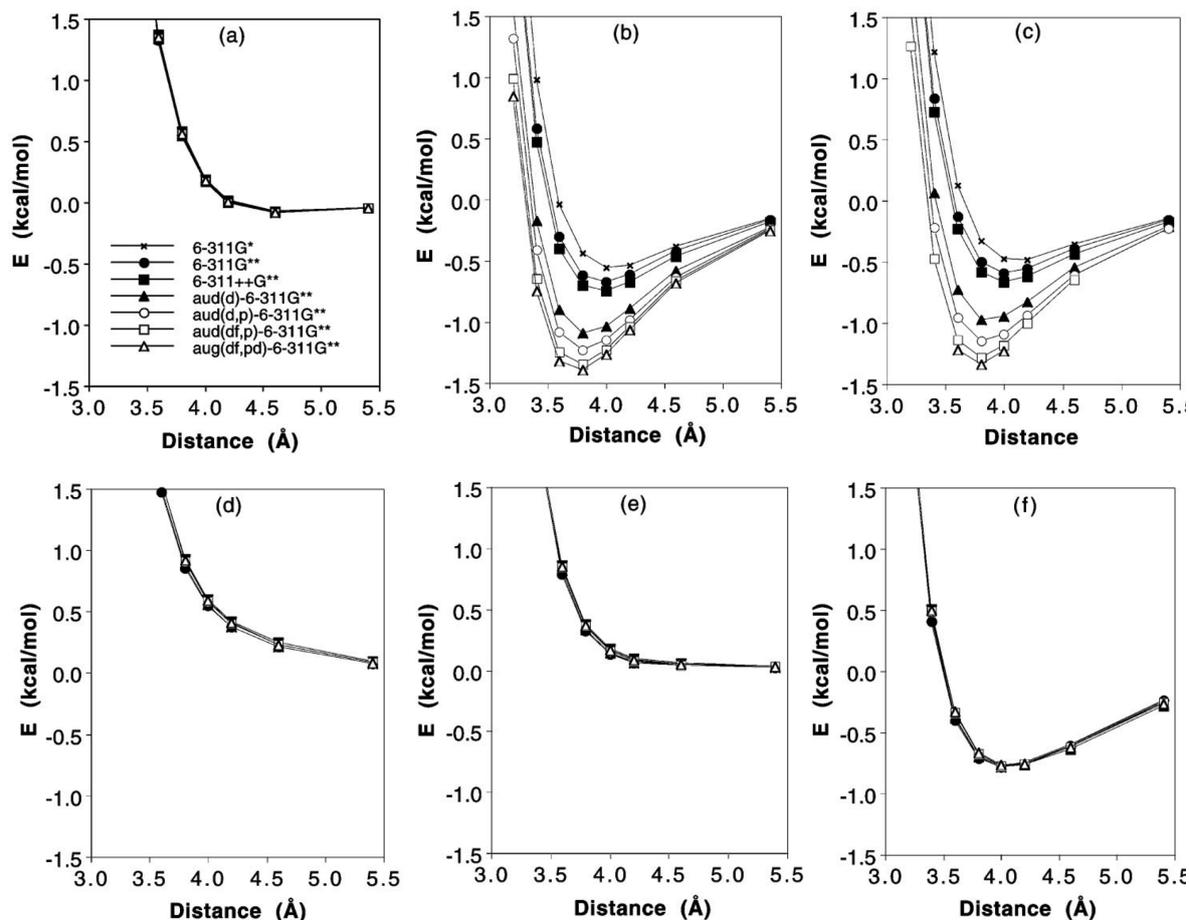
Figure 4. The (a) HF, (b) MP2, (c) CCSD(T), (d) BLYP, (e) B3LYP, and (f) PW91 potentials of the D_{2d} ethylene dimer. Ref. [62].

regards, the DFT method with the hybrid functionals becomes the standard computational tool nowadays for treating the large systems containing transition metal element [34-53]. However, it is reported in many works that the current DFT functionals do not correctly describe the weak interaction due to dispersion forces [50(c), 58-64]. For instance, the intermolecular interaction potential for the D_{2d} ethylene dimer is shown in Fig. 4 [62]. The calculated HF potentials have a very shallow potential minima (Figure 4a) and the MP2 and CCSD(T) potentials (Figure 4b and 4c) show that the dispersion interaction is mainly responsible for the attraction. On the other hand, the BLYP and B3LYP potentials do not have minima, indicating these functionals fail to evaluate the dispersion interaction and the PW91 potential has its minimum at an intermolecular distance of 4.0 Å,
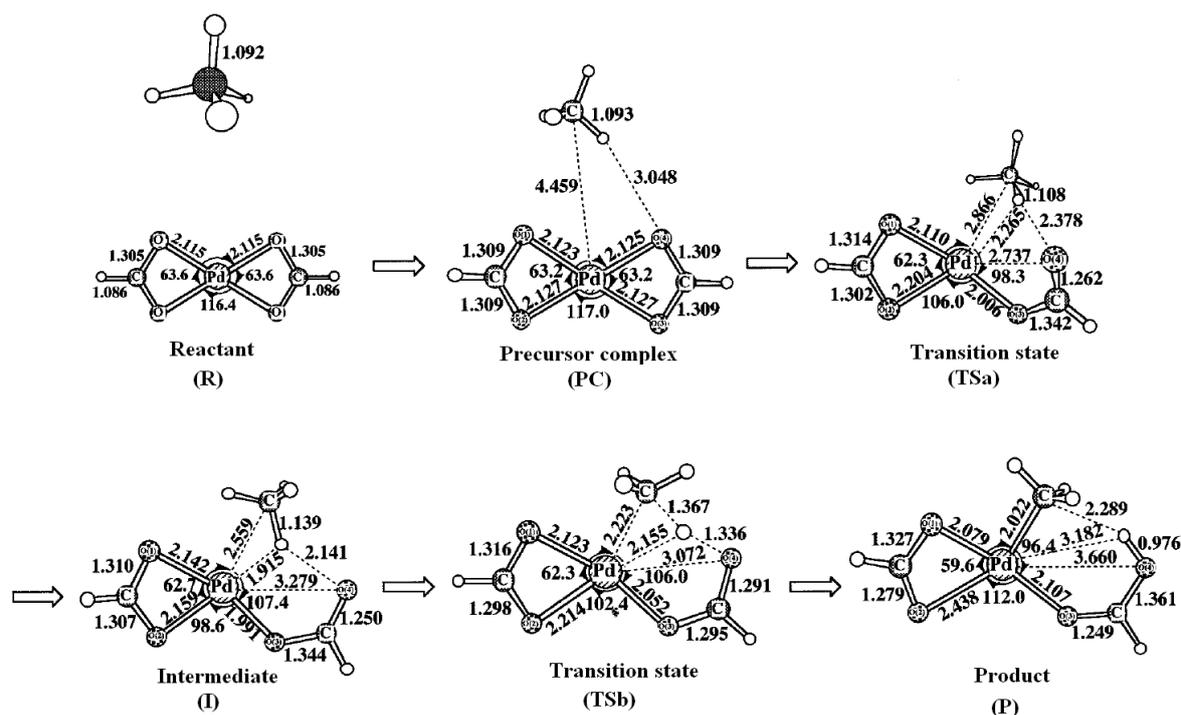
Figure 5. Geometry changes in the C-H bond activation of methane by Pd-(η^2-O$_2$CH)$_2$. Bond lengths are in angstrom and bond angles are in degree. Ref [67].

which is longer than those obtained by the MP2 and CCSD(T) calculations ~3.8 Å. Also, it was reported for several transition metal systems that the DFT-calculated energetic is much different from that calculated by the post-HF methods [50, 65-67]. For example, the DFT(B3LYP) method presented much smaller binding energy (BE), activation barrier (E_a), and reaction energy (ΔE) than the CCSD(T) method in the C-H σ-bond activation of methane by Pd(η^2-O$_2$CH)$_2$, while the MP4(SDQ) method presents better results than does the DFT; see Figure 5 for the reaction and Table 4 for the energies [67]. Hence, though the post-HF methods such as the CCSD(T) are computationally expensive, the application of post-HF methods at least to the small model system is recommended as a check of the reliability of the DFT computational results of the transition metal complexes.

Table 4. Binding energy (BE), activation barrier (E_a), and reaction energy (ΔE) in the C-H σ-bond activation of methane by $Pd(\eta^2\text{-}O_2CH)_2$ (kcal/mol unit).

Method	BE[a]	E_a[b]	ΔE[c]
DFT	-0.6	13.9	-4.9
MP2	-1.3	17.5	-12.8
MP3	-1.2	19.8	-12.8
MP4(DQ)	-1.2	21.1	-12.0
MP4(SDQ)	-1.3	21.5	-8.3
CCSD(T)	-1.5	20.5	-6.1

[a] BE=E_t(Precursor complex)-E_t(Sum of reactants).   [b] E_a=E_t(**TSb**)-E_t(**PC**)
[c] ΔE=E_t(Product)-E_t(Sum of reactants).   Ref [67].

4   The Aims of This Thesis

Recently, research on the transition metal silylene, silaallyl, silapropargyl, and dihydride silyl complexes gets momentum because of their importance as intermediates in the conversion processes of metal-catalyzed transformation reactions of various organosilicon compounds.   They are also attractive research subjects in theoretical/computational chemistry, because transition metal complexes of such silicon species would have novel bonding nature and electronic structure, as described below.

The silylene species involves a singlet spin state in general, and as a result, the sp^2 lone-pair orbital and the empty p-orbital (Scheme 5) of silylene play important roles in the interaction with the transition metal center. This means that the coordinate bond of silylene with the transition metal center is expected to be similar to that of CO. Unexpectedly, however, transition metal silylene complexes are not stable unlike the transition metal CO complexes. In this regard, careful theoretical investigation is required to elucidate the bonding nature and electronic structure of the transition metal silylene complexes.

Empty p orbital

R

R

Doubly-occupied sp^2 orbital
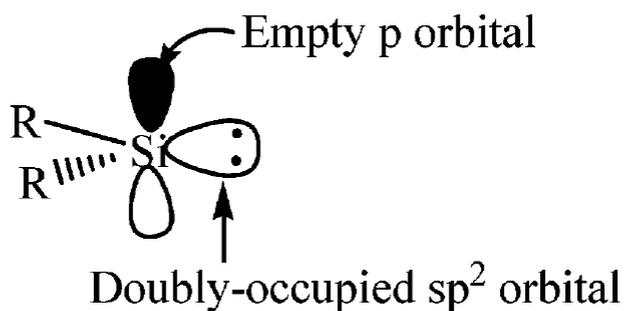
Scheme 5

Also, multiple bond including Si element is interesting because it is considerably different from its carbon analogue. Syntheses of such chemical species are interesting and challenging in recent chemistry.   The silaallyl and silapropargyl species are silicon analogues of the allyl and propargyl, respectively (Scheme 6).   These species are very reactive and free silaallyl and silapropargyl species have not been isolated yet, to our best knowledge.   However, it is expected that the interaction with transition metal complex is able to stabilize them.   In spite of this expectation, isolations of the transition metal η^3-silaallyl and η^3-silapropargyl complexes are very difficult in contrast to many isolated

Allyl

Propargyl

Silaallyl

Silapropargyl

Scheme 6

16
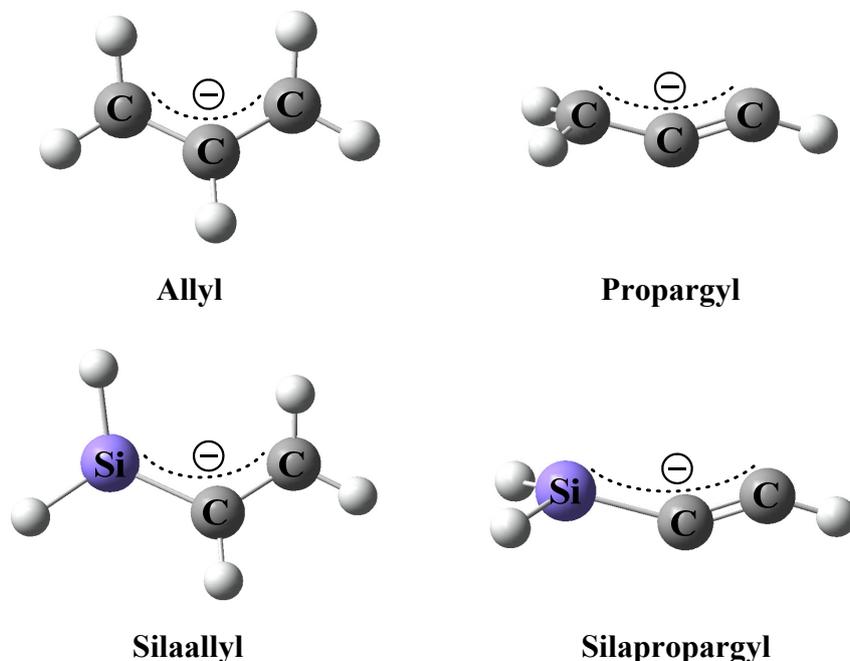
transition metal η^3-allyl and η^3-propargyl complexes. Thus, their syntheses are one of the challenging research targets in the transition metal organosilicon chemistry. Recently, the η^3-silaallyl complex was isolated only for tungsten which is Cp*(CO)$_2$W(η^3-Me$_2$SiCHCMe$_2$) [68a] but the similar tungsten η^3-silapropargyl complex has not been isolated yet [68b]. These results indicate that the interaction of these silicon species with the transition metal center must be different from their carbon analogues. In this regard, detailed theoretical study of the transition metal η^3-silaallyl and η^3-silapropargyl complexes is necessary to clarify their geometries, electronic structures, and bonding natures and to find out how to stabilize these complexes. However, no theoretical study of these complexes has been reported yet, to our best knowledge.

In chapter 1, we wish to present theoretical study of tungsten acetylide silylene and tungsten η^3-silapropargyl complexes. Detailed discussions of their geometrical characteristics and novel bonding natures as well as geometry changes, energetics, and electronic process of their interconversion reaction will be presented here.

In chapter 2, we wish to present theoretical study of tungsten η^3-silaallyl and tungsten vinyl silylene complexes. Our purposes here are to make clear comparison of these complexes with the tungsten η^3-silapropargyl and tungsten acetylide silylene complexes and to clarify the reasons why the tungsten η^3-silaallyl complex can be isolated but the tungsten η^3-silapropargyl complex cannot.

In chapter 3, we wish to present theoretical prediction how to stabilize transition metal η^3-silapropargyl complex. Our purposes here are to clarify how and why the stabilities, bonding natures, and electronic structures of the transition metal η^3-silapropargyl complex depend on the substituents of Si, C, ligands, and metal center.

In chapter 4, we wish to present theoretical study of a new μ-CC-bridged dinuclear tungsten silylene complex to elucidate its novel bonding nature and electronic structure.

In addition to the transition metal silylene complexes, transition metal dihydride silyl complexes of the $L_nM(H)_2(SiR_3)$ type have drawn recent interests due to their unusual bonding natures and high fluxionality of their geometries. Also, these complexes are possible intermediates in hydrosilation. Bonding natures of such complexes vary between

Silyl dihydride · **η^2-Silane** · **η^3-Silicate**

Classical · **Non-classical** · **Non-classical**
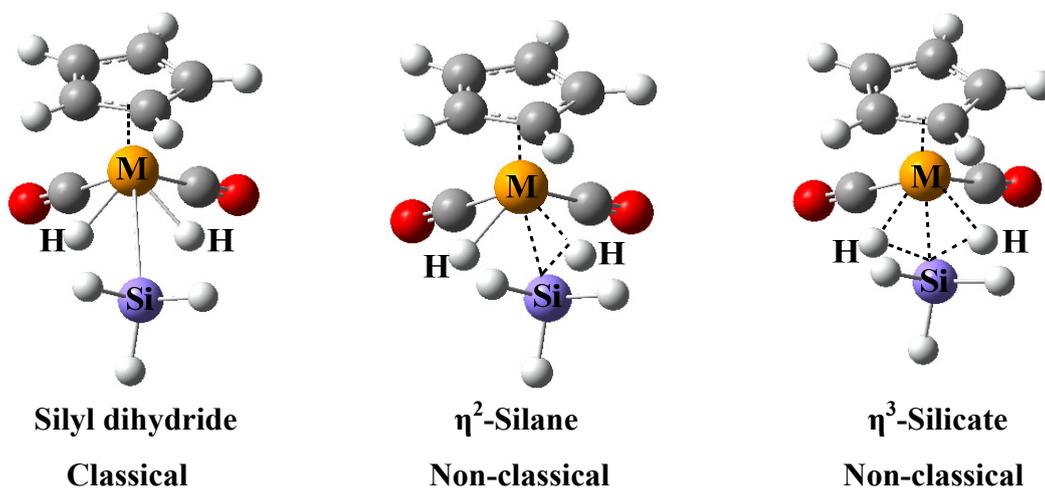
Scheme 7

the classical dihydride silyl form [69a], non-classical η^2-silane form [69a, 70], and non-classical η^3-silicate form [69] depending on the strength of the Si-H inter-ligand interaction; see Scheme 7. It is noted that the non-classical η^3-silicate form is the rarest mode among these three bonding modes. The $L_nM(H)_2(SiR_3)$ type complexes are quite rare for group 6 transition metals [68c-e]. Only $Cp^*(CO)_2W(H)_2(SiR_3)$ type complexes have been synthesized and characterized, recently [68c-e, 71]. Experimental analyses of these tungsten complexes suggest the presence of the non-classical Si-H interaction [68c, d] and unusually high fluxionality [68d], indicating that the group 6 metals add new features in the chemistry of the transition metal dihydride silyl complexes. In these regards, detailed theoretical study of the transition metal dihydride silyl complex is essential to elucidate the interesting structural feature, bonding nature, electronic structure, and mechanism of the unusually high fluxionality. Theoretical study of the transition metal dihydride silyl complexes are very limited [69] and no theoretical study to elucidate

18

the mechanism of fluxionality of such complexes has yet been reported, to our best knowledge.

In chapter 5, we wish to present theoretical study of the tungsten dihydride silyl complex to elucidate its interesting electronic structure including the oxidation state of the tungsten center, non-classical bonding nature, and novel fluxional behavior.

In the present study, the DFT method with such hybrid functionals as B3LYP and B3PW91 is mainly used and the MP perturbation (MP2, MP3, and MP4) theory and CCSD(T) method were also employed to check the reliability of the DFT-calculated energies. Moreover, the LCMO (Linear Combination of Molecular Orbital) analysis was employed to inspect the bonding interaction of these complexes, in which a molecular orbital ψ_i of the total system is represented by a linear combination of molecular orbitals of the fragments.

Bibliography

[1]   (a) Sekiguchi, A.; Zigler, S.; Robert, W.; Josef, M. *J. Am. Chem. Soc.* **1986**, *108*, 4241. (b) Sekiguchi, A.; Rei, K.; Masaaki, I. *Science* **2004**, *305*, 1755. (c) Frenking, G.; Krapp, A.; Nagase, S.; Takagi, N.; Sekiguchi, A. *Chemphyschem* **2006**, *7*, 799. (d) Sekiguchi, A.; Ichinohe, M.; Kinjo, R. *Bull. Chem. Soc. Jpn.* **2006**, *6*, 825. (e) Sekiguchi, A.; Lee, V. Y. *Chem. Soc. Rev.* **2008**, *37*, 1652.

[2]   *The Chemistry of Organic Silicon Compounds*; Patai, S., Rappoprt, Z., Eds.; Wiley: Chichester, UK, **1989**.

[3]   (a) Marciniec, B. In *Comprehensive Handbook on Hydrosilylation*; Pergamon Press, Oxford, **1992**. (b) Marciniec, B. *New J. Chem.* **1997**, *21*, 815. (c) Marciniec, B. *Appl. Organomet. Chem.* **2000**, *14*, 527. (d) Marciniec, B. *Silicon Chem.* **2002**, *1*, 155. (e) Marciniec, B. In *Applied Homogeneous Catalysis with Organometallic Compounds (2 ed.)*; Cornils, B., Herrman, W., Eds.; **2002**, pp. 491. (f) Marciniec, B.; Pietraszuk, C. In *Handbook of Metathesis*; Grubbs, R., Eds.; Wiley: VCH, **2003**, pp. 445. (g) Marciniec, B. *Coord. Chem. Rev.* **2005**, *249*, 2374.

[4]   Paver, M. A.; Russell, C. A.; Wright, D. S. *Angew. Chem. Int. Ed. Engl.* **1995**, *34*, 1545 and references therein.

[5]   (a) Power, P. P. *Chem. Rev.* **1999**, *99*, 3463. (b) Power, P. P. *Chem. Comm.* **2003**, *17*, 2091 and references therein. (c) Power, P. P. *Organometallics* **2007**, *26*, 4362.

[6]   Lischka, H.; Kohler, H.-J. *J. Am. Chem. Soc.* **1983**, *105*, 6646.

[7]   Binkley, J. S. *J. Am. Chem. Soc.* **1984**, *106*, 603.

[8]   Kalcher, J.; Sax, A.; Olbrich, G. *Int. J. Quantum Chem.* **1984**, *25*, 543.

[9]   Kohler, H.-J.; Lischka, H. *Chem. Phys. Lett.* **1984**, *112*, 33.

[10]   Thies, B. S.; Grev, R. S.; Schaefer, H. F. *Chem. Phys. Lett.* **1987**, *140*, 355.

[11] (a) Koseki, S.; Gordon, M. S. *J. Phys. Chem.* **1988**, *92*, 364. (b) Koseki, S.; Gordon, M. S. *J. Phys. Chem.* **1989**, *93*, 118.

[12] (a) Bogey, M.; Bolvin, H.; Demuynck, C.; Destombes, J. L. *Phys. Rev. Lett.* **1991**, *66*, 413. (b) Cordonnier, M.; Bogey, M.; Demuynck, C.; Destombes, J.-L. *J. Chem. Phys.* **1992**, *97*, 7984.

[13] Jutzi, P. *Angew. Chem. Int. Ed.* **2000**, *39*, 3797.

[14] (a) Weidenbruch, M. *J. Organomet. Chem.* **2002**, *646*, 39. (b) Weidenbruch, M. *Angew. Chem., Int. Ed.* **2005**, *44*, 514.

[15] (a) Kobayashi, K.; Nagase, S. *Organometallics* **1997**, *16*, 2489. (b) Nagase, S.; Kobayashi, K.; Takagi, N. *J. Organomet. Chem.* **2000**, *611*, 264. (c) Takagi, N.; Nagase, S. *Chem. Lett.* **2001**, *10*, 966. (d) Kobayashi, K.; Takagi, N.; Nagase, S. *Organometallics* **2001**, *20*, 234. (e) Takagi, N.; Nagase, S. *Organometallics* **2001**, *20*, 5498. (f) Takagi, N.; Nagase, S. *Eur. J. Inorg. Chem.* **2002**, *11*, 2775.

[16] Piper, T. S.; Lemal, D.; Wilkinson, G. *Naturwiss.* **1956**, *43*, 129.

[17] Höfler, F. *Top. Curr. Chem.* **1974**, *50*, 129.

[18] Curtis, M. D.; Epstein, P. S.; *Adv. Organomet. Chem.* **1981**, *19*, 213.

[19] Colomer, E.; Corriu, R. J. P. *Top. Curr. Chem.* **1981**, *96*, 79.

[20] Aylett, B. J. *Adv. Inorg. Chem. Radiochem.* **1982**, *25*, 1.

[21] In *Silicon-Based Polymer Science, Advances in Chemistry Series*, Ziegler, J. M.; Fearon, F.W.G. Eds., American Chemical Society: Washington, DC, **1990**; pp 224.

[22] Tilley, T. D. In *Transition Metal-Silyl Derivatives*; Patai, S., Rappoprt, Z., Eds.; Wiley: New York, **1991**; pp 245.

[23] Seyferth, D. *In Organosilicon Chemistry, from Molecules to Materials*; Auner, N.; Weis, J. Eds.; VCH: Weinheim, Germany, **1994**; pp 269.

[24]   (a) In *Organosilicon Chemistry I, from Molecules to Materials*, Auner, N.; Weis, J. Eds.; VCH: Weinheim, Germany, **1994**. (b) In *Organosilicon Chemistry I, from Molecules to Materials*, Auner, N.; Weis, J. Eds.; VCH: Weinheim, Germany, **1996**.

[25]   Shimada, S.; Tanaka, M. *Coor. Chem. Rev.* **2006**, *250*, 991 and references therein.

[26]   Ottoson, H.; Steel, P. G.; *Chem. Eur. J.* **2006**, *12*, 1576 and references therein.

[27]   Ojima, I.; Li, Z.; Zhu, J. *The Chemistry of Organic Silicon Compounds*, John Wiley and Sons: Chichester, **1998**.

[28]   Reichl, J. A.; Berry, D. H.; *Recent Progress in Trans. Metal-Catalyzed Reaction on Silicon, Germanium and Tin*, Academic Presss: **1999**.

[29]   Horn, K. A. *Chem. Rev.* **1995**, *95*, 1317.

[30]   Sharma, H. K.; Pannell, K. H. *Chem. Rev.* **1995**, *95*, 1351.

[31]   Corey, J. Y.; Braddock-Wilking, J. *Chem. Rev.* **1999**, *99*, 175.

[32]   Ikedo, S.; Chatani, N.; Kajikawa, Y.; Ohne, K.; Murai, S. *J. Org. Chem.* **1992**, *57*, 2.

[33]   (a) Takanashi, K.; Lee, V. Ya.; Ichinohe, M.; Sekiguchi, A. *Angew. Chem., Int. Ed.*, **2006**, *45*, 3269. (b) Takanashi, K.; Lee, V. Ya.; Ichinohe, M.; Sekiguchi, A. *Eur. J. Inorg. Chem.*, **2007**, 5471.

[34]   Hehre, W. J.; Radom, L.; Schleyer, P. V. R.; Pople, J. A. *Ab initio Molecular Orbital Theory*; John Wiley & Sons: New York, **1986**.

[35]   *Reviews in Computational Chemistry*; Lipkowitz, K. B., Boyd, D. B., Eds.; VCH: New York, **1990-1999**; Vols. 1-13.

[36]   Ziegler, T. *Chem. Rev.* **1991**, *91*, 651.

[37]   Davidson, E. R. *Chem. Rev.* **1991**, *91*, 649.

[38]   (a) Koga, K.; Morokuma, K. *Chem. Rev.* **1991**, *91*, 823. (b) Musaev, D. G.; Morokuma, K. In *Advances in Chemical Physics*; Rice, S. A., Prigogine, I., Eds.; John Wiley & Sons: New York, **1996**; Vol. XCV, p 61.

[39]   Yoshida, S.; Sakaki, S.; Kobayashi, H. *Electronic Processes in Catalyst*; VCH: New York, **1992**.

[40]   *Transition Metal Hydrides*, Dedieu, A., Ed.; VCH: New York, **1992**.

[41]   (a) Siegbahn, P. E. M.; Svensson, M. *Chem. Phys. Lett.* **1993**, *216*, 147. (b) Siegbahn, P. E. M.; Blomberg, M. R. A. In *Theoretical Aspects of Homogeneous Catalysts, Applications of Ab Initio Molecular Orbital Theory*; van Leeuwen, P. W. N. M., van Lenthe, J. H., Morokuma, K., Eds.; Kluwer Academic: Hingham, MA, **1995**. (c) Siegbahn, P. E. M. *In Advances in Chemical Physics*; Rice, S. A., Prigogine, I., Eds.; John Wiley & Sons: New York, **1996**; Vol. XCIII, p 333. (d) Siegbahn, P. E. M.; Blomberg, M. R. A. *Annu. Rev. Phys. Chem.* **1999**, *50*, 221. (e) Siegbahn, P. E. M. *J. Biol. Inorg. Chem.* **2006**, *11*, 695.

[42]   *Theoretical Aspects of Homogeneous Catalysis, Applications of Ab Initio Molecular Orbital Theory*; van Leeuwen, P. W. N. M., van Lenthe, J. H., Morokuma, K., Eds.; The Netherlands, **1994**.

[43]   Salahub, D. R.; Castro, M.; Fournier, R.; Calaminici, P.; Godbout, N.; Goursot, A.; Jamorski, C.; Kobayashi, H.; Martinez, A.; Papai, I.; Proynov, E.; Russo, N.; Sirois, S.; Ushio, J.; Vela, A. In *Theoretical and Computational Approaches to Interface Phenomena*; Sellers H., Olab, J., Eds.; Plenum Press: New York, **1995**; p 187.

[44]   (a) Szilagyi, R. K.; Frenking, G. *Organometallics* **1997**, *16*, 4807. (b) Frenking, G.; Fröhlich, N. *Chem. Rev.* **2000**, *100*, 717.

[45]   Müller, K. *Angew. Chem., Int. Ed. Engl.* **1980**, *19*, 1.

[46]   Schlegel, H. B. In *Ab Initio Methods in Quantum Chemistry,* Lawley, Ed.; John Wiley & Sons Ltd.: New York, **1987**.

[47]   Foresman, J. B.; Frish, A. E. *Exploring Chemistry with Electronic Structure Mothods*; Gaussian, Inc.: The Woodlands, TX, **1993**.

[48]   Jonas, V.; Thiel, W. *J. Chem. Phys*. **1995**, *102*, 8474.

[49]   Bögel, H.; Tobisch, S.; Nowak, T. *Int. J. Quant. Chem*. **1998**, *69*, 387.

[50]   (a) Niu, S.; Hall, M. B. *J. Am. Chem. Soc*. **1997**, *119*, 3077. (b) Niu, S.; Hall, M. B. *J. Phys. Chem. A*. **1997**, *101*, 1360. (c) Niu, S.; Hall, M. B. *Chem. Rev*. **2000**, *100*, 353.

[51]   Hu, Z.; Boyd, R. J. *J. Chem. Phys*. **2000**, *113*, 9393.

[52]   Schultz, N. E.; Zhao, Y.; Truhlar, D. G. *J. Phys. Chem. A* **2005**, *109*, 11127.

[53]   Waller, M. P.; Braun, H.; Hojdis, N.; Bühl, M. *J. Chem. Theory Comput*. **2007**, *3*, 2234.

[54]   (a) Becke, A. D. *Phys Rev. A*. **1988**, *38*, 3098. (b) Becke, A. D. *J. Chem. Phys*. **1993**, *98*, 5648.

[55]   Lee, C.; Yang, W.; Parr, R. G. *Phys. Rev. B*. **1988**, *37*, 785.

[56]   Perdew, J. P. *Phys. Rev. B*. **1986**, *33*, 8822.

[57]   (a) Perdew, J. P. *In Electronic Structure of Solids`91*, Ziesche, P., Eschrig, H., Ed.; Akademic Verlag: Berlin, **1991**; p 11. (b) Perdew, J. P.; Chevary, J. A.; Vosko, S. H.; Jackson, K. A.; Pederson, M. R.; Singh, D. J.; Fiolhais, C. *Phys. Rev. B*. **1992**, *46*, 6671. (c) Perdew, J. P.; Chevary, J. A.; Vosko, S. H.; Jackson, K. A.; Pederson, M. R.; Singh, D. J.; Fiolhais, C. *Phys. Rev. B*. **1993**, *48*, 4978. (d) Perdew, J. P.; Burke, K.; Wang, Y. *Phys Rev. B*. **1996**, *54*, 16533.

[58]   Kristyan, S.; Pulay, P. *Chem. Phys. Lett*. **1994**, *229*, 175.

[59]   Perez-Jorda, J. M.; Becke, A. D. *Chem. Phys. Lett*. **1995**, *233*, 134.

[60] Zhang, Y.; Pan, W.; Yang, W. *J. Chem. Phys*. **1997**, *107*, 7921.

[61] Sponer, J.; Hobza, P. *Chem. Phys. Lett*. **1997**, *267*, 263.

[62] Tsuzuki, S.; Lüthi, H. P. *J. Chem. Phys*. **2001**, *114*, 3949.

[63] Wu, Q.; Yang, W. *J. Chem. Phys*. **2002**, *116*, 515.

[64] Cybulski, S. M.; Seversen, C. P.; *J. Chem. Phys*. **2005**, *122*, 014117.

[65] Siegbahn, P. E. M. *J. Am. Chem. Soc*. **1996,** *118,* 1487.

[66] Zaric, S.; Hall, M. B.; *J. Phys. Chem. A* **1997**, *101*, 4646.

[67] Biswas, B.; sugimoto, M.; Sakaki, S. *Organometallics* **2000**, *19*, 3895.

[68] (a) Sakaba, H.; Watanabe, S.; Kabuto, K. *J. Am. Chem. Soc*. **2003**, *125*, 2842. (b) Sakaba, H.; Yoshida, M.; Kabuto, C.; Kabuto, K. *J. Am. Chem. Soc*. **2005**, *127*, 7276. (c) Sakaba, H.; Hirata, T.; Kabuto, C.; Horino, H. *Chem. Lett*. **2001**, 1078. (d) Sakaba, H.; Hirata, T.; Kabuto, C.; Kabuto, K. *Organometallics* **2006**, *25*, 5145. (e) Sakaba, H.; Hirata, T.; Kabuto, C.; Kabuto, K. *J. Organomet. Chem*. **2007**, *692*, 402.

[69] (a) Vyboishchikov, S. F.; Nikonov, G. I. *Organometallics* **2007**, *26,* 4160. (b) Gutsilyak, D. V.; Kuzmina, L. G.; Howard, JA. K.; Vyboishchikov, S. F.; Nikonov, G. I. *J. Am. Chem. Soc*. **2008**, *130,* 3732.

[70] Taw, F. L.; Bergman, R. G.; Brookhart, M. *Organometallics* **2004**, *23*, 886.

[71] (a) Hashimoto, H.; Ochiai M.; Tobita, H. *J. Organomet. Chem*. **2007**, *692*, 36. (b) Watanabe, T.; Hashimoto, H.; Tobita, H. *Unpublished*.

Chapter 1

Silapropargyl/Silaallenyl and Silylene Acetylide Complexes of [Cp(CO)₂W]⁺. Theoretical Study of Their Interesting Bonding Nature and Formation Reaction

1.1　Introduction

Transition-metal silylene complexes are important and interesting research targets in coordination chemistry, organometallic chemistry, and synthetic chemistry [1-5]. The geometry, bonding nature, and electronic structure are of considerable interest because of its similarities to and differences from the carbon analogue. The important role as intermediates was also proposed in various metal-catalyzed transformation reactions of organosilicon compounds. To understand well its properties and reaction behavior, a considerable effort has been made to isolate transition-metal silylene complex [1-5]. The first example of isolated transition-metal silylene complex was previously reported by Schmidt and Welz in 1977 [6]. However, $(CO)_4Fe(=SiMe_2NHEt_2)$, which they synthesized, was very unstable and its X-ray characterization was not successful. In 1987, Zybill and Müller synthesized a transition-metal silylene complex and presented the first structural evidence for the TM=Si unit (TM = transition-metal) [7]. Since then, many successful results have been reported on the syntheses and characterization of transition-metal silylene complexes [1-5]. For instance, the Ogino group [8] and the Pannell group [9] successfully synthesized many transition-metal silylene complexes from disilanyl complexes through a 1,2-silyl shift. The Tilley group successfully

synthesized base-stabilized ruthenium silylene complexes [10] and then base-free osmium and platinum silylene complexes [11]. The Corriu [12] and Braunstein groups [13] successfully synthesized HMPA- and amine-stabilized silylene complexes, respectively. The 1,2-H shift from a silyl ligand to a metal center was also employed to synthesize transition-metal silylene complexes [14-16]. It is noted that σ-bond activation was involved as an important process in these syntheses of transition-metal silylene complexes. Besides these studies, transition-metal silylene complexes have also been synthesized by ligation of free silylene with metal center [17-21].

The transition-metal silylene complex has attracted considerable interests, as well [22-26]. The silylene species involves a singlet spin state, and as a result, the sp^2 lone pair orbital and the empty p orbital (Scheme 1.1) play important roles in the interaction with the metal center.
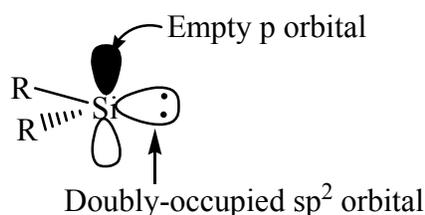
Scheme 1.1

This means that the coordinate bond with transition-metal center is expected to be similar to that of CO. Unexpectedly, however, the transition-metal silylene complexes are not stable unlike the transition-metal CO complexes. In this regard, the geometry and the bonding nature of the transition-metal silylene complexes were theoretically discussed in many works [22-25]. The reaction of a transition-metal silylene complex is another attractive research subject to theoreticians. For instance, Hall and his collaborators theoretically investigated the hydrosilation reaction catalyzed by ruthenium-silylene complex [26].

28
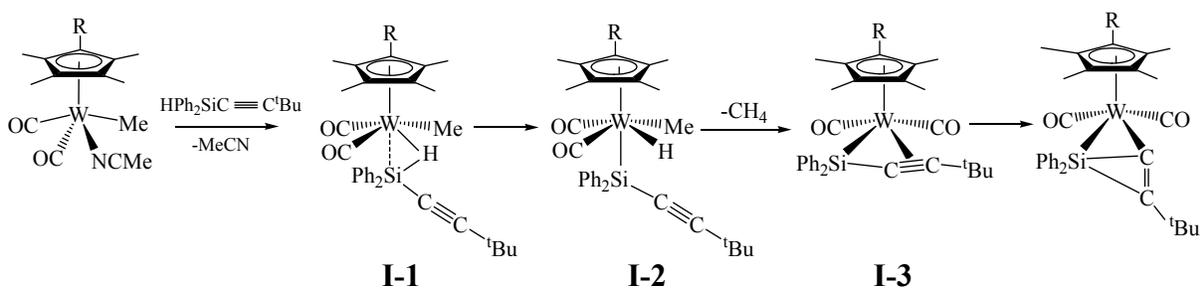
Scheme 1.2. Formation reaction of Cp*(CO)$_2$W(C≡C^{t}Bu)(SiPh$_2$) from Cp*(CO)$_2$W(Me)(MeCN).

Recently, an interesting tungsten complex with composition of Cp*(CO)$_2$W(C≡C^{t}Bu)(SiPh$_2$) was synthesized from Cp*(CO)$_2$(MeCN)W(Me) and the alkynylsilane (HPh$_2$SiC≡C^{t}Bu) [27], as shown in Scheme 1.2. Cp*(CO)$_2$W(C≡C^{t}Bu)(SiPh$_2$) is understood in terms of a tungsten silylene complex stabilized by an intramolecular charge-transfer (CT) interaction with the acetylide group, as schematically shown by **Form-A** in Scheme 1.3, which is a new canonical structure of transition-metal silylene complex. The other two renderings of this complex were also experimentally proposed; one is a tungsten complex involving a silacyclopropenyl group (**Form-B)** and the other is a tungsten complex with a four-membered ring including silyl and alkenyl groups (**Form-C)**; Scheme 1.3. It is
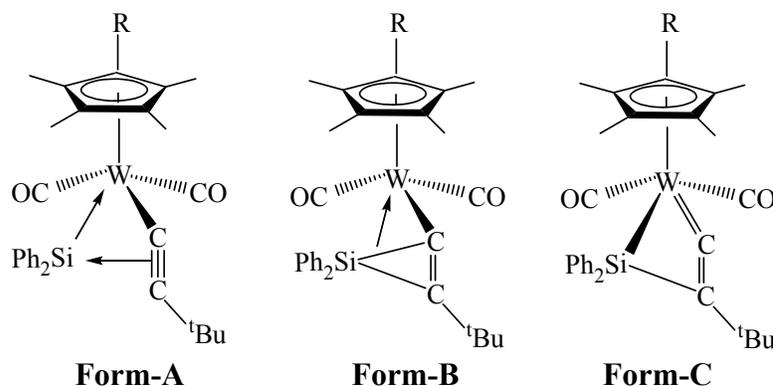
Scheme 1.3. Three possible limiting forms of Cp*(CO)$_2$W(C≡C^{t}Bu)(SiPh$_2$)

worthwhile to investigate theoretically the bonding nature of $Cp^*(CO)_2W(C\equiv C^tBu)(SiPh_2)$ and to clarify which structure is correct. The formation of this compound is also very interesting, because this reaction takes place through a variety of σ-bond activation processes, as follows: In the experimentally proposed reaction scheme [27], the first step is displacement of coordinated MeCN by the silylacetylene to give an intermediate $Cp^*(CO)_2W(Me)(HSi(Ph)_2C\equiv C^tBu)$ **I-1**, followed by the Si-H oxidative addition to the W center to form the second intermediate $Cp^*(CO)_2W(Me)(H)(Si(Ph)_2C\equiv C^tBu)$ **I-2**. The next step is the C-H reductive elimination of methane to form the third intermediate $Cp^*(CO)_2\overline{W(Si(Ph)_2C\equiv C}^tBu)$ **I-3**, and the final step is either Si-C σ-bond activation to afford **Form-A** and **Form-C** or Si-C bond formation to afford **Form-B** (Scheme 1.3). If either **Form-A** or **Form-C** is correct, $Cp^*(CO)_2W(C\equiv C^tBu)(SiPh_2)$ is produced via a 1,2-alkynyl shift from a tungsten 1-alkynylsilyl complex **I-3**, which, to our knowledge, is interesting α-Si-C σ-bond activation [28]. Thus, it is worthwhile to investigate theoretically this formation reaction. Also, the bonding nature and geometry of **I-3** are interesting, because **I-3** is considered to be a silapropargyl complex, i.e., a silicon analogue of a propargyl complex; such species has not been reported yet, while the silicon analogue of a π-allyl complex has been experimentally reported [29].

In the present study, the bonding nature of $Cp^*(CO)_2W(C\equiv C^tBu)(SiPh_2)$ and $Cp^*(CO)_2\overline{W(Si(Ph)_2C\equiv C}^tBu)$ **I-3** and the formation reaction of $Cp^*(CO)_2W(C\equiv C^tBu)(SiPh_2)$ from $Cp^*(CO)_2W(Me)(HSi(Ph)_2C\equiv C^tBu)$ were theoretically investigated with DFT, MP2 to MP4(SDTQ), and CCSD(T) methods. The main purpose of this work is to present a proper understanding of the geometries and bonding nature of these complexes and to clarify

electronic processes and characteristic features of the transformation reaction of **I-1** to Cp*(CO)$_2$W(C≡C^{t}Bu)(SiPh$_2$).

1.2   Computational Details

We employed here Cp(CO)$_2$W(C≡CH)(SiH$_2$) **1** as the simplest model of Cp*(CO)$_2$W(C≡C^{t}Bu)(SiPh$_2$). Geometries were optimized with the density functional theory (DFT) method, where B3PW91 functional was adopted for the exchange-correlation terms[30, 31]. The B3PW91 functional presented much better agreements of the optimized geometry of **1** with experimental one of Cp*(CO)$_2$W(C≡C^{t}Bu)(SiPh$_2$) [27] than the B3LYP [30,32] and MPWPW91 [31, 33] functionals, as shown in Appendix A.1.1. We ascertained that none of the equilibrium geometry exhibited an imaginary frequency and each transition state exhibited only one imaginary frequency. Energy was evaluated with the DFT, MP2 to MP4(SDTQ), and CCSD(T) methods, where the DFT-optimized geometries were adopted.

Two kinds of basis set systems, BS-I and BS-II, were used in this work. In BS-I, usual LANL2DZ [34] basis set was employed for W. cc-pVDZ basis sets [35] were employed for Si, C, and O, and 6-31G basis set was used for H [36]. This BS-I system was used for geometry optimization. The basis set effects on the optimized geometry were examined with 6-31G(d) [37] basis set for Si, C, and O and Huzinaga-Dunning [38] basis set for Si. However, no significant difference was observed between BS-I and these basis set systems (see Appendix A.1.1).   In BS-II, valence electrons of W were represented with a (541/541/111/1) basis set [34, 39, 40] with the same effective core potentials as those of BS-I. For the other atoms, the same basis sets as those of BS-I were employed. This BS-II was used to evaluate energy and population changes.

Gaussian 03 program package (revision C.02) [41] was used for all these computations. Population analysis was carried out with the method proposed by Weinhold et al [42]. Molecular orbitals were drawn with MOLEKEL program package (version 4.3) [43].

1.3   Results and Discussion

We wish to discuss first the bonding nature and geometry of $Cp^*(CO)_2W(C{\equiv}C^tBu)(SiPh_2)$ and then the reaction leading to its formation from $Cp^*(CO)_2W(Me)(Si(Ph)_2HC{\equiv}C^tBu)$.   Also, we will discuss the bonding nature and characterization of $Cp^*(CO)_2\overline{W(Si(Ph)_2C{\equiv}}C^tBu)$ in comparison with those of similar propargyl/allenyl complex.

1.3.1 Geometry of $Cp(CO)_2W(C{\equiv}CR^1)(SiR^2{}_2)$ (R^1 = H, Me, or ^tBu; R^2 = H or Me)

The optimized geometry of $Cp(CO)_2W(C{\equiv}CH)(SiH_2)$ **1** agrees well with the experimental one [27], except for several geometrical parameters; the W-Si and Si-C1 distances are moderately longer but the W-C1 and Si-C2 distances are moderately shorter than the corresponding experimental values (see Figure 1.1 and Table 1.1 for important geometrical parameters). Introduction of Me and ^tBu groups on the acetylide C atom leads to excellent agreement of the optimized geometry with the experimental one, as will be discussed below in more detail.

For a better understanding of the geometry and bonding nature of **1**, we optimized an ideal complex, $Cp(CO)_2W(C{\equiv}CH)(SiH_2)$ **2**, in which the acetylide group is at a position

32
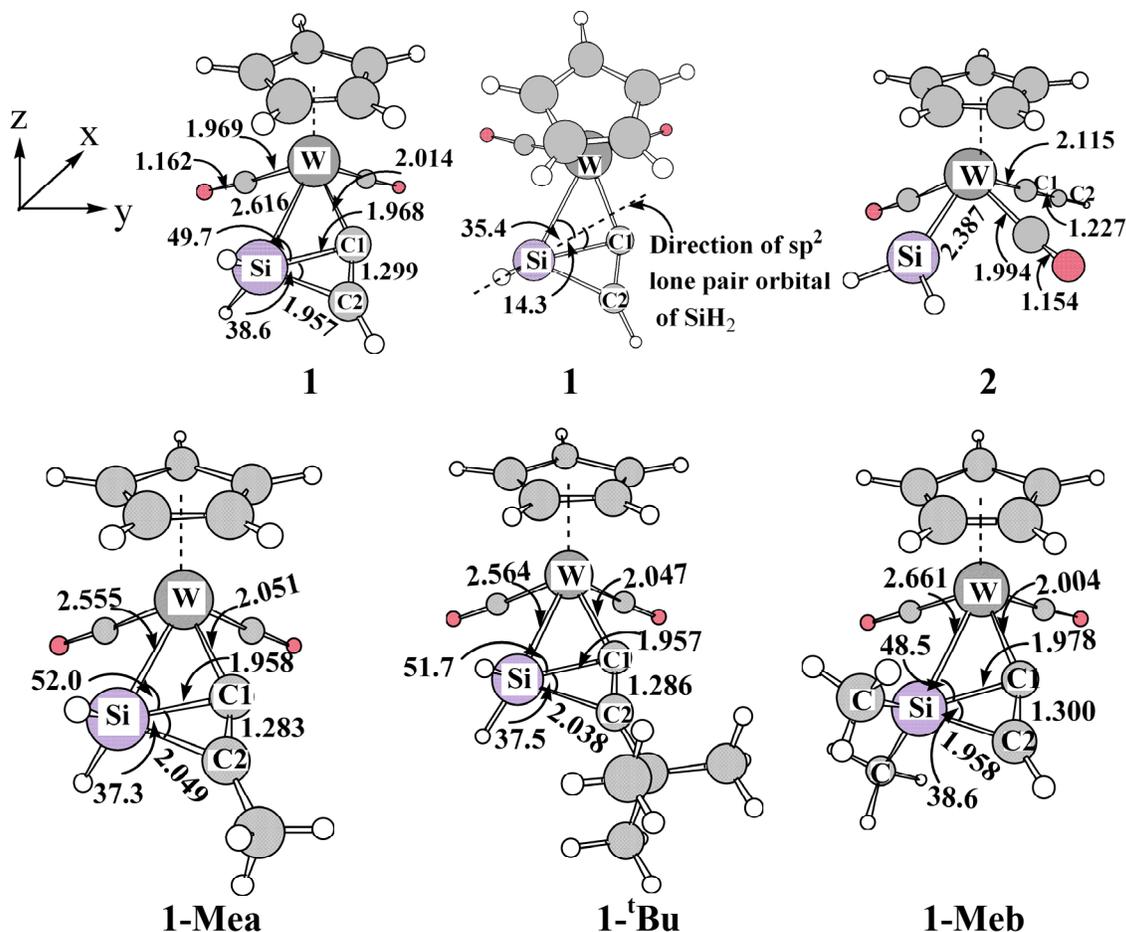
Figure 1.1. DFT/BS-I optimized geometries of $Cp(CO)_2W(C\equiv CR^1)(SiR^2_2)$ (R^1=H, Me, or ^tBu and R^2=H or Me). Bond lengths are in angstrom and bond angles are in degree.

Table 1.1. Selected optimized parameters of $Cp(CO)_2W(C\equiv CR^1)(SiR^2_2)$.

	1 R^1=H, R^2=H	**1-Mea** R^1=Me, R^2=H	**1-^tBu** R^1=^tBu, R^2= H	**1-Meb** R^1=H, R^2=Me	**Expt.**[a] R^1=^tBu, R^2=Ph
W-Si	2.616	2.555	2.564	2.661	2.567
W-C1	2.014	2.051	2.047	2.004	2.050
Si-C1	1.968	1.958	1.957	1.978	1.937
Si-C2	1.957	2.049	2.038	1.958	2.009
C1-C2	1.299	1.283	1.286	1.300	1.270
∠W-Si-C1	49.7	52.0	51.7	48.5	51.9
∠C1-Si-C2	39.0	37.3	37.5	38.6	37.5

Bond lengths are in angstrom and bond angles are in degree.
[a] Reference 27.
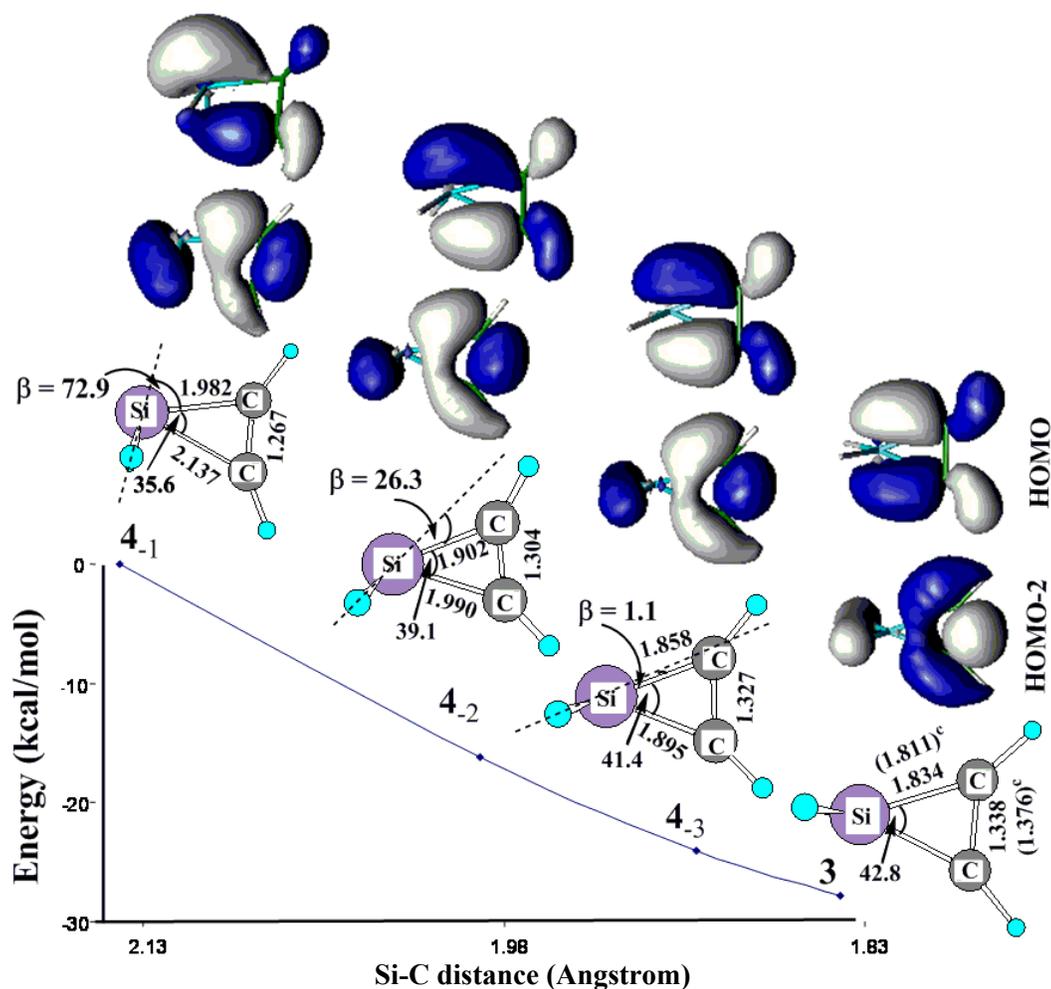
Figure 1.2. Changes of geometry,[a] total energy,[b] and important Kohn-Sham orbital[b] in the formation reaction of silacyclopropene from silylene and acetylene.
[a] DFT/ BS-I optimization was carried out. Bond lengths are in angstrom and bond angles are in degree. [b] DFT/BS-II calculation. [c] In parentheses are experimental values [45].

opposite to the SiH_2 group, as shown in Figure 1.1; in other words, no interaction exists between these two moieties. The W-C1 and C1-C2 distances of **2** agree well with those of a typical tungsten acetylide complex [44]. Silacyclopropene **3** was also optimized, as shown in Figure 1.2. The Si-C and C-C distances of **3** agree well with the experimental values [45].

The Si-C1 and Si-C2 distances in **1** are considerably longer than the Si-C bond of **3**. Consistent with these long Si-C1 and Si-C2 distances, the C1-C2 distance of **1** is somewhat

shorter than that of **3**. Also, the C1-C2 distance is longer in **1** than in **2**. It is noted that the acetylide moiety somewhat distorts in **1** (C1-C2-H angle=145.7º) unlike the linear alignment in **2**. The W-C1 distance of **1** is almost the same as that of **2**, while the W-Si distance of **1** is longer than those of **2** and a typical donor-stabilized tungsten-silylene complex [8m, 46]. Consistent with the longer W-Si distance in **1** than in **2** and the longer Si-C1 and Si-C2 distances in **1** than in **3**, the sp^2 lone pair orbital of SiH$_2$ expands neither toward the W center nor toward the midpoint of the C1-C2 bond, i.e., the sp^2 lone pair orbital expands at an angle of 35° with the W-Si bond and at an angle of 14° with the Si-C1 bond, as shown in Figure 1.1.

All these geometrical features of **1** suggest that the CCH(SiH$_2$) moiety in **1** is neither a pure silacyclopropenyl group nor the sum of pure silylene and acetylide groups. It is likely that the CCH(SiH$_2$) moiety is intermediate between them, which will be discussed below in more detail.

To shed clear light on the CCH(SiH$_2$) moiety, we investigated the formation reaction of silacyclopropene from silylene and acetylene, as shown in Figure 1.2. This reaction takes place without barrier, as previously reported by Gordon et al [47] and Koch et al [48]. Because no precursor complex could be optimized in this reaction, the starting geometry **4$_{-1}$** was optimized under assumption that the SiH$_2$ plane was placed to be parallel to the C-C bond. In **4$_{-1}$**, the Si-C distances are long and the sp^2 lone pair orbital of SiH$_2$ makes a large angle (72.9º) with the Si-C bond. Upon going to **4$_{-3}$** from **4$_{-1}$**, the sp^2 lone pair orbital of SiH$_2$ is changing its direction toward the center of the C-C bond with concomitant formation of two Si-C bonds. The angle (14.3º) between the sp^2 lone pair orbital and the Si-C1 bond in **1** is smaller than that (26.3º) of **4$_{-2}$** but larger than that (1.1º) of **4$_{-3}$**. The Si-C1 and Si-C2 distances of **1** are not different very much from those of **4$_{-2}$**. From these geometrical features, it is

concluded that the CCH(SiH$_2$) moiety of **1** is similar to the HCCH(SiH$_2$) species halfway to the formation of silacyclopropene from silylene and acetylene; in other words, the CCH(SiH$_2$) moiety of **1** is understood to be an interesting intermediate species trapped by the W center in the reaction leading to the formation of silacyclopropene.

Substituent effects on the geometry of **1** were investigated by introducing Me and ^{t}Bu on C2 and Me on Si (see **1-Mea**, **1-^{t}Bu**, and **1-Meb** in Figure 1.1). Introduction of Me and ^{t}Bu groups on C2 considerably shortens the W-Si distance by 0.061 Å and 0.052 Å, respectively, and considerably lengthens the Si-C2 distance by 0.092 Å and 0.081 Å, respectively (see **1-Mea** and **1-^{t}Bu** in Figure 1.1). The C1-C2 bond also becomes moderately shorter by introduction of Me and ^{t}Bu groups on C2. Consistent with the shortening of the W-Si distance, the angle between the sp^2 lone pair orbital of SiH$_2$ and the W-Si bond decreases to 25.4º in **1-Mea** and 27.4º in **1-^{t}Bu**, compared to that (35.4º) of **1**. These optimized geometries of **1-Mea** and **1-^{t}Bu** extremely agree with the experimental one. On the other hand, Me groups on Si little change the geometry except for moderate lengthening of the W-Si distance in **1-Meb**. These substituent effects will be discussed below on the basis of bonding nature.

1.3.2   Bonding Nature of Cp(CO)$_2$W(C≡CH)(SiH$_2$) 1

To clearly understand the bonding nature of **1**, we investigated molecular orbitals of **1**. The HOMO and HOMO-1 mainly consist of a W d-orbital, as shown in Figure 1.3A. The presence of two doubly-occupied d orbitals is consistent with the +2 oxidation state of W (d^4 system). The HOMO-2 of **1** closely resembles the HOMO of silacyclopropene, and the HOMO-6 of **1** is similar to the HOMO-2 of **4$_{-1}$** ~ **4$_{-3}$** (see also Figure 1.2). These features suggest that the HOMO-2 and HOMO-6 of **1** mainly consist of the sp^2 lone pair and empty p

HOMO   **HOMO-1**   **HOMO-2**   **HOMO-5**   **HOMO-6**   **HOMO-8**

(-5.4)   (-6.0)   (-7.3)   (-8.4)   (-10.1)   (-10.9)

(A) Cp(CO)$_2$W(C≡CH)(SiH$_2$) 1

HOMO   **HOMO-1**   **HOMO-2**   **HOMO-3**   **HOMO-6**   **HOMO-8**

(-5.7)   (-6.0)   (-7.0)   (-7.3)   (-8.7)   (-9.8)
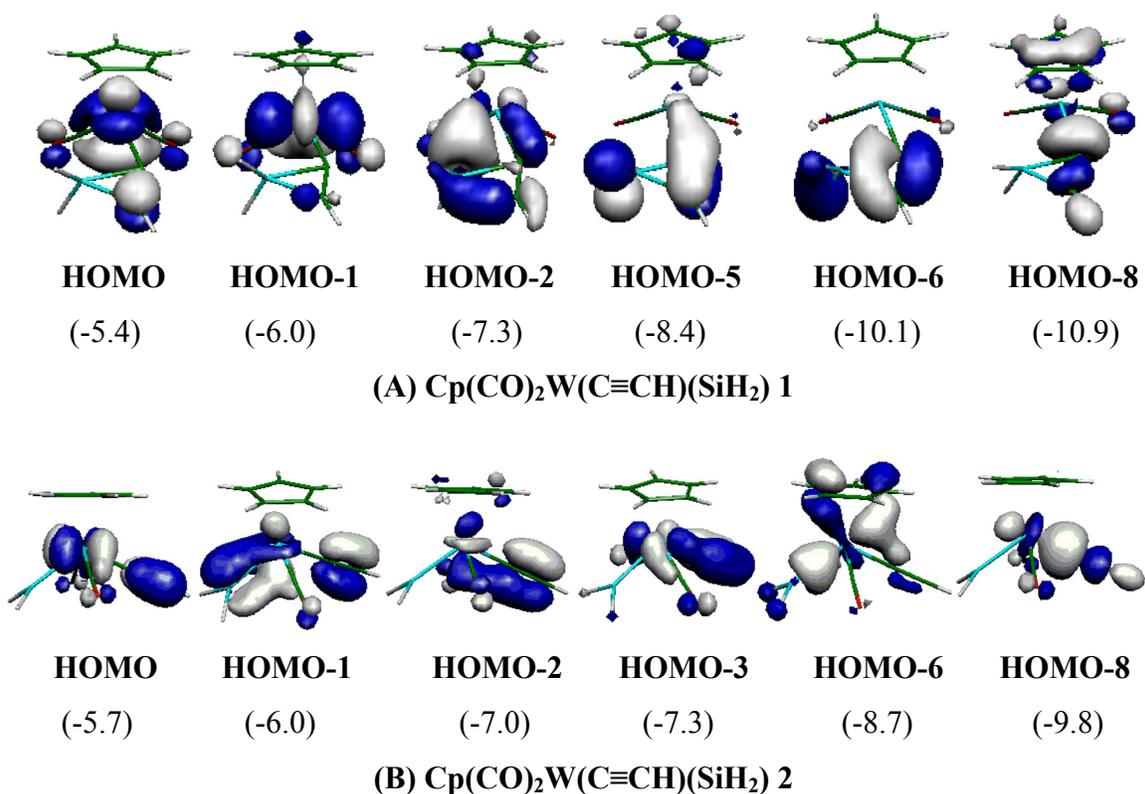
(B) Cp(CO)$_2$W(C≡CH)(SiH$_2$) 2

Figure 1.3. Several important Kohn-Sham orbitals observed in Cp(CO)$_2$W(C≡CH)(SiH$_2$) **1** and ideal complex Cp(CO)$_2$W(C≡CH)(SiH$_2$) **2**. In parentheses are orbital energies (eV unit).

orbitals of silylene and the π and π* orbitals of acetylide. The sp^2 lone pair orbital of silylene overlaps with the π* orbital of acetylide in a bonding way, because the π* orbital is at higher energy than the sp^2 lone pair orbital, and with the π orbital of acetylide in an anti-bonding way, because the π orbital is at lower energy than the sp^2 lone pair orbital, as shown in Scheme 1.4(A). As a result, the contribution of C1 p orbital considerably decreases and that of C2 p orbital considerably increases, which leads to the HOMO-2. In other words, the HOMO-2 involves CT from the sp^2 lone pair of silylene to the π* orbital of acetylide and a four-electron repulsion between the sp^2 lone pair of silylene and the π orbital of acetylide. The HOMO-6 is formed through slightly different orbital mixing; the π orbital of acetylide overlaps with the

(A) HOMO-2

Main   Small   Small   Very small

(B) HOMO-6

Main   Small   Small   Very small
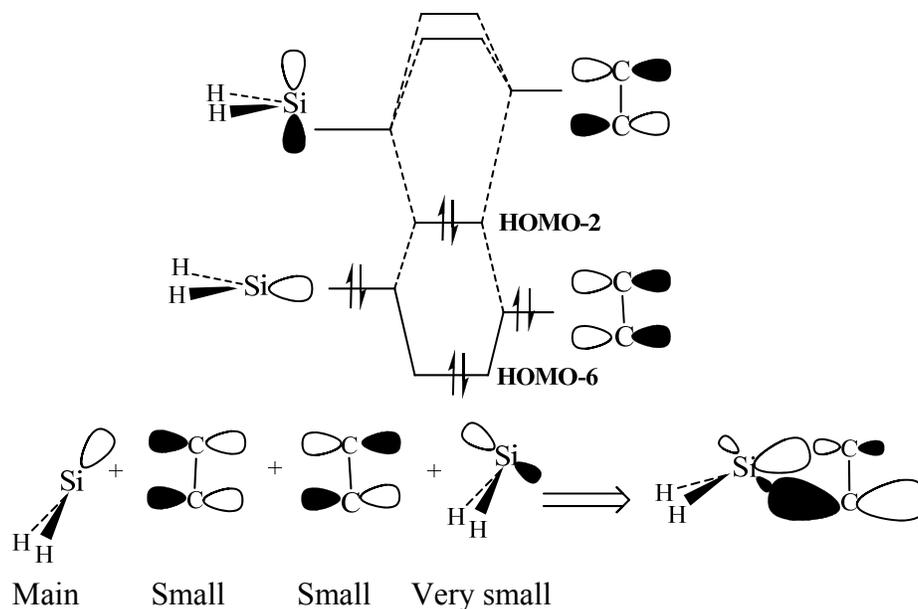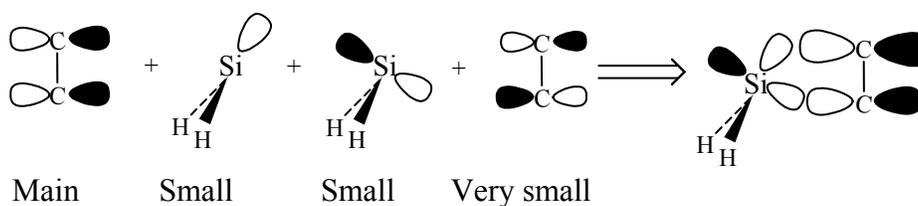
Scheme 1.4

sp^2 lone pair orbital of silylene in a bonding way because the HOMO-6 is the most stable in

energy among the molecular orbitals consisting of the π and π^* orbitals of acetylide and the

sp^2 and p orbitals of silylene. Into this overlap, the empty p orbital of silylene mixes in a

bonding way with the π orbital of acetylide because the empty p orbital is at higher energy

than the π orbital. The π^* orbital of acetylide also slightly mixes into this orbital in a bonding

way with the sp^2 lone pair orbital of silylene. These orbital mixings lead to bonding overlap of

the deformed π orbital of acetylide with the empty p and sp^2 lone pair orbitals of silylene, as

shown in Scheme 1.4(B). In other words, the HOMO-6 involves CT from the π orbital of

acetylide to the empty p orbital of silylene.

Comparison of **1** with **2** provides us information of the W-Si and W-C1 bonding nature of **1**. In **2**, the SiH_2 moiety is bound to the W center through donation from the sp^2 lone pair orbital to the empty d orbital of W, which is observed in the HOMO-6 of **2**, as shown in Figure 1.3B. In **1**, on the other hand, there is no clear bonding overlap but a deformed bonding overlap between W and Si centers is observed in the HOMO-2, as shown in Figure 1.3A. This deformed overlap can be easily understood in terms that the bonding orbital between the sp^2 lone pair orbital of silylene and the empty p orbital of acetylide (Scheme 1.4(A)) interacts with the empty d orbital of W. Although silacyclopropene is formed from silylene and acetylene in the absence of $Cp(CO)_2W$, SiH_2 cannot completely change its orientation toward the C1-C2 bond in the presence of $Cp(CO)_2W$. This is because the bonding overlap between the sp^2 lone pair of SiH_2 and the empty d orbital of W suppresses the complete change of the SiH_2 orientation. Also, the occupied d_z^2 orbital overlaps well with the empty p orbital of SiH_2 in **2**, to form the d_π-p back donating interaction, which is observed in the HOMO-1 of **2**. However, the d_z^2 orbital does not form such interaction in **1**, as shown by the HOMO of **1**. These results indicate that **1** does not involve a pure silylene group unlike **2**, which is consistent with the discussion based on the geometrical features. In **2**, the HOMO-3 involves the bonding overlap between the π orbital of acetylide and the unoccupied d_{xy} orbital of W (Figure 1.3). Its anti-bonding counter part is the HOMO. The similar orbitals are observed in the HOMO-5 and the HOMO of **1**, respectively. The HOMO-8 of **1** and **2** involves bonding interaction between the unoccupied d_{xz} orbital of W and the sp lone pair of acetylide. These results suggest that the interaction between acetylide and W in **1** is similar to that of the normal acetylide ligand, which is consistent with the similar W-C1 distance between **1** and **2**.

From all these results, it should be clearly concluded that the CCH(SiH$_2$) moiety of **1** is considered neither to be a pure silacyclopropenyl group nor to be the sum of pure silylene and acetylide groups. In **1**, the acetylide group strongly interacts with silylene through the CT from the π orbital of acetylide to the empty p orbital of silylene and the CT from the sp^2 lone pair of silylene to the π^* orbital of acetylide. Despite these strong CT interactions, the CCH(SiH$_2$) moiety does not change to a pure silacyclopropenyl group because of the presence of bonding interaction between the sp^2 lone pair orbital of silylene and the empty d orbital of W. Thus, the CCH(SiH$_2$) moiety of **1** is understood to be an interesting intermediate species which is trapped by the W center in the formation reaction of silacyclopropene from acetylene and silylene.

1.3.3 Substituent Effects on the Bonding Nature of Cp(CO)$_2$W(C≡CR^1)(SiR$^2_2$)

Significant substituent effects on the Si-C and W-Si distances were observed when Me and ^{t}Bu groups were introduced on the C2 atom, as described above. These substituent effects are interpreted in terms of the π and π^* orbitals of the acetylide group. Their orbital energy become higher by introduction of electron-donating substituent, as shown in Table 1.2. Both the bonding interaction of the acetylide π orbital with the silylene empty p orbital and the anti-bonding interaction of the acetylide π orbital with the silylene sp^2 lone pair orbitals become stronger, as the π orbital of acetylide rises in energy. Considering that the introduction of Me and ^{t}Bu groups on C2 increases the Si-C2 distance, it is concluded that the anti-bonding interaction increases than does the bonding interaction. In other words, the repulsive interaction between the sp^2 lone pair orbital of silylene and the π orbital of acetylide is still

Table 1.2. The π and π^* orbital energies of acetylene and sp^2 lone pair and empty p orbital energies of silylene.

orbital	[H−C≡C−R^1][b] orbital energy[a] (eV)		
	R^1 = H	R^1 = Me	R^1 = ^{t}Bu
π	−7.78	−7.15	−7.02
	(−10.6)	(−9.99)	(−9.85)
π^*	−0.67	0.14	0.09
	(3.57)	(4.38)	(4.31)

orbital	SiR$^2_2$[c] orbital energy[a] (eV)	
	R^2 = H	R^2 = Me
sp^2 lone pair	−6.01	−5.19
	(−8.47)	(−7.68)
p	−3.28	−2.19
	(0.26)	(1.29)

[a] The DFT/BS-II calculation. In parentheses are Hartree-Fock orbital energies (BS-II). [b] Orbitals of free HCCR^1 are presented, where the geometry was taken to be the same as that in Cp(CO)$_2$W(C≡CR^1)(SiR$^2_2$) (R^1 = H or Me or ^{t}Bu and R^2 = H or Me) (see Appendix A.1.2). [c] Orbitals of free silylene are presented. Geometries are optimized with the DFT/BS-I method.

strong in **1**. This repulsive interaction shifts the direction of the lone pair orbital of silylene toward the W center from the C1 atom in **1-Mea** and **1-^{t}Bu**. As a result, the electron-donating substituent on C2 strengthens the coordinate bond of silylene with the W center, which shortens the W-Si distance in **1-Mea** and **1-^{t}Bu** than that in **1**.

Introduction of Me on Si raises the energy of the sp^2 lone pair orbital and the empty p orbital of the silylene (Table 1.2). As the sp^2 lone pair orbital becomes higher in energy, both the bonding and anti-bonding interactions of the sp^2 lone pair of silylene with the π^* and π orbitals of acetylide, respectively, become stronger. However, the bonding interaction

between the empty p orbital of silylene and the π orbital of acetylide becomes weaker. Because these effects compensate each other, the Si-C1, Si-C2 and W-C1 distances change little in **1-Meb**. However, the W-Si distance becomes moderately longer in **1-Meb** than in **1**. This is interpreted, as follows: The electron-donating group on Si decreases the participation of the empty p orbital in the bonding interaction with the π orbital of acetylide but increases the participation of the sp^2 lone pair in the bonding interaction with the π^* orbital of acetylide. As a result, the direction of the lone pair orbital of SiH$_2$ shifts toward C1, which weakens the W-Si interaction and thereby increase the W-Si distance.

1.3.4 Conversion from Cp(CO)$_2$W(Me)(SiH$_3$C≡CH) to Cp(CO)$_2$W(Si(H)$_2$C≡CH)

We wished to investigate the reaction from Cp(CO)$_2$W(Me)(SiH$_3$C≡CH) **5** to Cp(CO)$_2$W(Si(H)$_2$C≡CH) because interesting elementary steps and intermediates are involved in the reaction. This conversion reaction takes place through two steps; in the first step, **5** converts to Cp(CO)$_2$W(Me)(H)(Si(H)$_2$C≡CH) **6** through the Si-H oxidative addition. In the second step, **6** converts to Cp(CO)$_2$W(Si(H)$_2$C≡CH)(CH$_4$) **7** through the reductive elimination of methane.

The conversion reaction of **5** to **6** takes place without any barrier, as shown in Figure 1.4. The geometry optimization of **5** smoothly leads to **6**, where the geometry of **5** was optimized with the Si-H distance fixed to be the same as that of the free HCCSiH$_3$ molecule. The Si-H bond gradually lengthens and the W-Si and W-H distances gradually shorten upon going to **6** from **5**. In **6**, the Si-H distance is 2.320 Å, and the W-H and W-Si distances are 1.735 Å and 2.579 Å, respectively. These geometrical features indicate that the Si-H σ-bond is completely
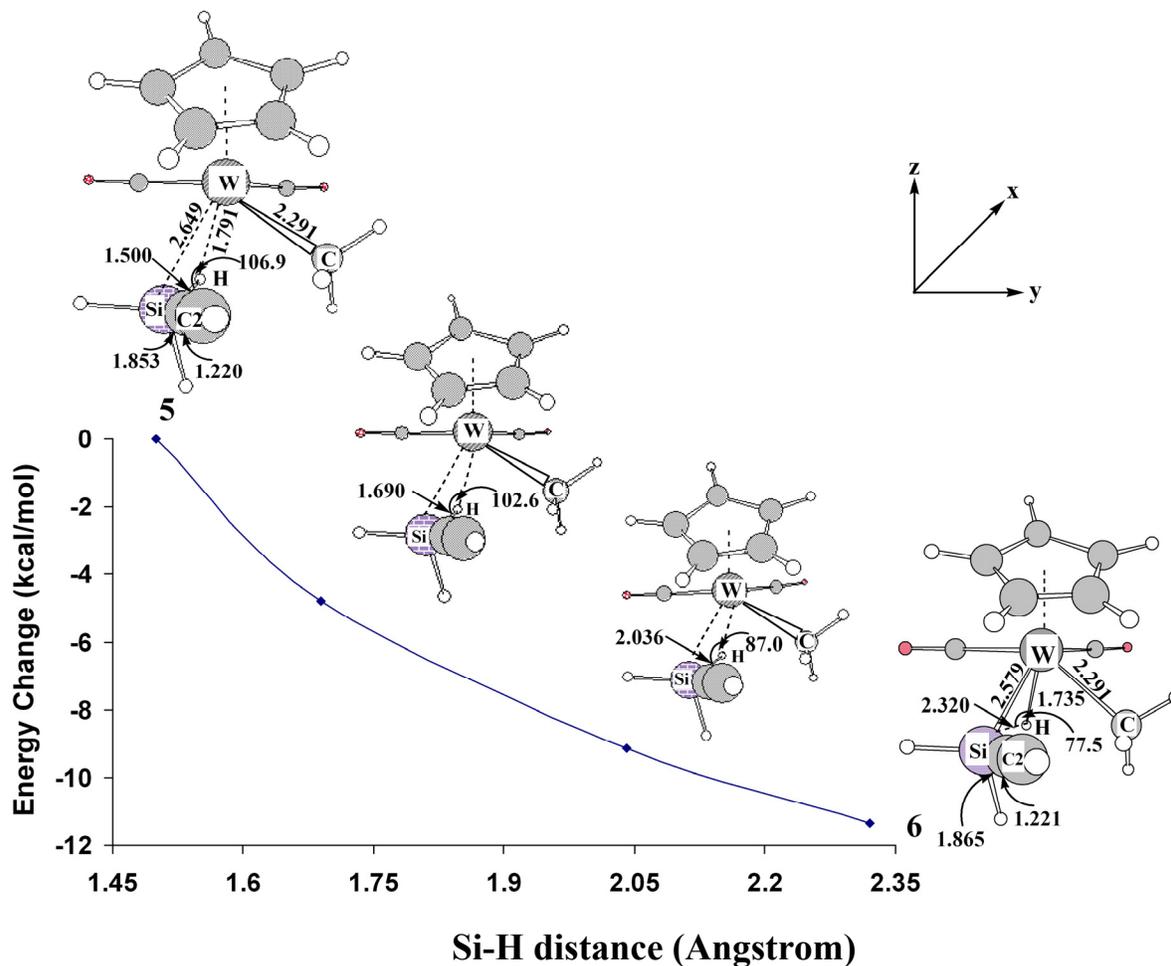
Figure 1.4. Geometry[a] and energy[b] changes by the conversion reaction of Cp(CO)$_2$W(CH$_3$)(H$_3$SiC≡CH) **5** to Cp(CO)$_2$W(CH$_3$)(H)(H$_2$SiC≡CH) **6**.
[a] DFT/ BS-I optimization was carried out. Bond lengths are in angstrom and bond angles are in degree. [b] DFT/BS-II calculation (in kcal/mol).

broken, and the W-Si and the W-H bonds are formed in **6**. This conversion reaction is considerably exothermic, as shown in Table 1.3. Though the DFT-calculated reaction energy (ΔE) value is moderately different from the MP4(SDTQ)-calculated value, the ΔE value fluctuates little upon going to MP4(SDTQ) from MP2, suggesting that the MP4(SDTQ) value is reliable.

To understand this conversion reaction, we examined several important molecular orbitals. In **5**, the HOMO and HOMO-1 mainly consist of a d orbital, while the other three d

Table 1.3: Activation barrier (E_a),[a,b] reaction energy (ΔE),[a,b] and destabilization energy (DE)[a,b] in the conversion reactions from $Cp(CO)_2W(Me)(H_3SiC\equiv CH)$ **5** to $Cp(CO)_2W(Me)(H)(Si(H)_2C\equiv CH)$ **6**, from **6** to $Cp(CO)_2W(CH_4)(Si(H)_2C\equiv CH)$ **7**, and from $Cp(CO)_2W(Si(H)_2C\equiv CH)$ **8** to $Cp(CO)_2W(Si(H)_2C\equiv CH)$ **9**.

Method	Conversion of **5** to **6**	Conversion of **6** to **7**		Methane dissociation from **7** (**7**→ **8**)	Conversion of **8** to **9**
	ΔE	E_a	ΔE	DE	ΔE
	(kcal/mol)	(kcal/mol)	(kcal/mol)	(kcal/mol)	(kcal/mol)
DFT	-11.4	10.7	-0.6	8.2	-31.2
MP2	-13.0	10.0	2.9	18.4	-45.8
MP3	-14.7	16.0	2.6	10.2	-26.6
MP4(DQ)	-15.4	14.4	3.9	13.4	-34.9
MP4(SDQ)	-15.5	14.8	3.7	13.9	-34.5
MP4(SDTQ)	-14.2	11.8	2.6	17.5	-43.3

(a) E_a is energy difference between transition state and reactant, ΔE is energy difference between product and reactant, and DE is the destabilization energy induced by methane dissociation. (b) The BS-II was employed.

orbitals are involved in unoccupied space (see Appendix A.1.3.(A)). These results indicate that the W center takes +2 oxidation state in **5**. In **6**, it is noted that only one d orbital of W is in occupied space and the remaining four d orbitals are in unoccupied space, which clearly shows that the doubly occupied d_z^2 orbital becomes unoccupied and the W center takes +4 oxidation state in **6**; see Figure 1.4 for coordinate system. The HOMO-4 involves the bonding overlap between the 1s orbital of H and the empty d_z^2 orbital of W and the HOMO-1 involves the bonding overlap between the sp^3 lone pair of Si and the empty d orbital of W (see Appendix A.1.3.(B)). All these results are consistent with our understanding that the Si-H oxidative addition takes place in this process.
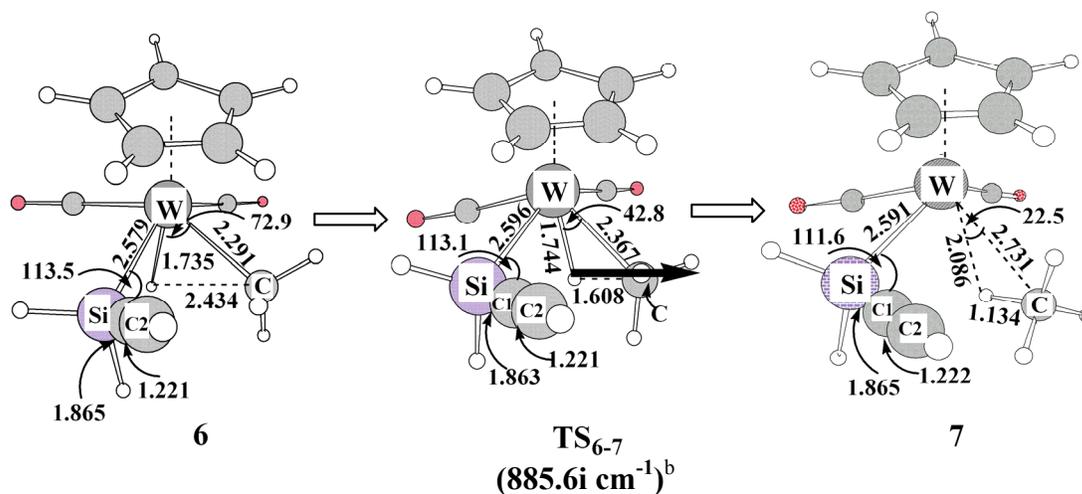
Figure 1.5. Geometry changes[a] in the reductive elimination of methane from Cp(CO)$_2$W(Me)(H)(Si(H)$_2$C≡CH) **6** to afford Cp(CO)$_2$W(CH$_4$)(Si(H)$_2$C≡CH) **7**.
[a] DFT/BS-I optimization was carried out. Bond lengths are in angstrom and bond angles are in degree. [b] Arrow in **TS$_{6\text{-}7}$** represents important movement of atom in imaginary frequency. Imaginary frequency is given in parentheses. DFT/BS-I calculation.

The intermediate **6** converts to Cp(CO)$_2$W(Si(H)$_2$C≡CH)(CH$_4$) **7** through transition state

TS$_{6\text{-}7}$, as shown in Figure 1.5. In **TS$_{6\text{-}7}$**, only one imaginary frequency (885.6i cm^{-1}) mainly

involves the movement of the hydride ligand toward the Me ligand. In this transition state, the

W-C distance moderately lengthens to 2.367 Å by 0.076 Å and the W-H distance becomes

slightly longer. The C-H distance is still long. These geometrical features indicate that the W-

H and W-C bonds are still kept and the C-H bond is not effectively formed yet in **TS$_{6\text{-}7}$**; in

other words, this transition state is reactant-like. In **7**, the C-H distance is 1.134 Å, which

clearly shows that methane is completely formed in **7** and interacts with the W center through

the weak interaction similar to the agostic interaction because its C-H distance is somewhat

longer than the usual C-H bond. This reaction takes place easily with a moderate activation

barrier and either very small exothermicity (DFT/BS-II) or small endothermicity

(MP4(SDTQ)/BS-II) (see Table 1.3); the activation barrier somewhat fluctuates at MP3 but converges upon going to MP4(SDTQ) from MP2. Also, the MP4(SDTQ)-calculated value is almost the same as the DFT-calculated value. The moderate activation barrier is consistent with the reactant-like TS_{6-7}. Though the reaction energy is slightly different between DFT and MP4(SDTQ) methods, the difference is not large, indicating that this reaction is almost thermoneutral. The orbital changes observed in this reductive elimination are the reverse of those observed in the oxidative addition of the Si-H bond. We omitted detailed discussion here; see Appendix A.1.3 for orbital changes and A.1.4. for the corresponding discussion.

As shown in Figure 1.6, methane dissociation from **7** leads to a coordinatively unsaturated complex, $Cp(CO)_2W(Si(H)_2C\equiv CH)$ **8**, with moderate destabilization energy, where the geometry of **8** was taken to be the same as that of **7** except for the absence of methane moiety. The destabilization energy (DE) is evaluated to be 8.2 and 17.5 kcal/mol with the DFT and MP4(SDTQ) methods, respectively (Table 1.3). Because the DFT method does not incorporate well the dispersion interaction which participates considerably in the interaction of methane with the metal center, the MP4(SDTQ)-calculated value is more reliable here than the DFT-calculated value. In **8**, the $C\equiv C$ triple bond does not interact with the W center. The geometry optimization of **8** smoothly leads to $Cp(CO)_2W(Si(H)_2C\equiv CH)$ **9** in which the $C\equiv C$ triple bond coordinates with the W center, as shown in Figure 1.6. The $C\equiv C$ triple bond gradually approaches the W center in the reaction. Consistent with this geometry change, one of the π orbitals of the $C\equiv C$ triple bond becomes considerably lower in energy (see Appendix A.1.5). The approach of the $C\equiv C$ triple bond to the W center induces the direction change of the sp^3 orbital on Si, which interacts substantially with the W center in **8**, to increase the sp^3 orbital energy. However, its energy does not rise so much because this sp^3 orbital changes to
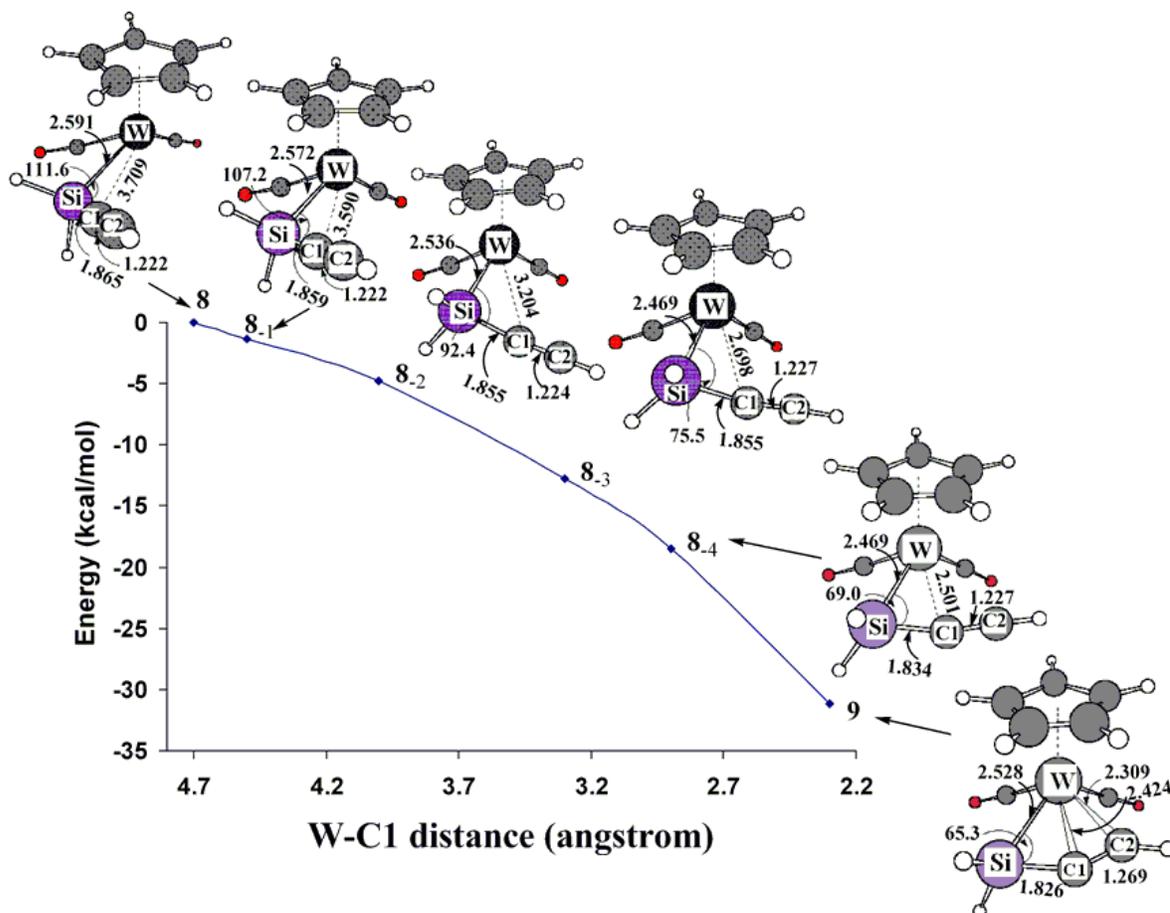
Figure 1.6. Geometry[a] and energy[b] changes by the conversion reaction of $Cp(CO)_2W(Si(H)_2C\equiv CH)$ **8** to $Cp(CO)_2W(Si(H)_2C\equiv CH)$ **9**.
[a] DFT/ BS-I optimization was carried out. Bond lengths are in angstrom and bond angles are in degree. [b] DFT/BS-II calculation (in kcal/mol).

the HOMO of a silapropargyl-type $Si(H)_2C\equiv CH$ species, which will be discussed below in detail. As a result, the conversion of **8** to **9** easily takes place with no barrier and considerably large exothermicity, as shown in Table 1.3. The DFT-calculated exothermicity (31.2 kcal/mol) is similar to the MP4(SDQ)-calculated value (34.5 kcal/mol) but somewhat smaller than the MP4(SDTQ)-calculated value (43.3 kcal/mol), suggesting that the exothermicity is between 31 to 43 kcal/mol. Thus, it can be considered that this process is considerably exothermic.

47

1.3.5 Geometry and Bonding Nature of Cp(CO)₂W̅(Si(H)₂C≡C-H) 9

Here, we wish to discuss the bonding nature of **9** because this species is of considerable interest, as follows: This is considered to be Si analogue of transition-metal propargyl complex and such a species has not been reported yet. To clarify the characteristic feature of **9**, we optimized the model propargyl complex **9C**, Cp(CO)₂W̅(C(H)₂C≡CH). As shown in Figure 1.7, the C1-C2 distance of **9** is almost the same as that of **9C**. The Si-C1 (1.826 Å) and C1-C2 (1.269 Å) bond distances of **9** are intermediate between the Si-C single and the Si=C double bonds and between C=C double and C≡C triple bonds, respectively; R(Si-C)=1.895 Å and 1.717 Å in H₃Si-CH₃ and H₂Si=CH₂, respectively, and R(C-C)=1.334 Å and 1.209 Å in H₂C=CH₂ and HC≡CH, respectively, where the DFT/BS-I optimized values are presented. The Si-C1-C2 angle of the [Si(H)₂CCH]⁻ ligand in **9** is 140º, which is similar to that of **9C**.

Figure 1.7. Geometry[a] of Cp(CO)₂W(C(H)₂C≡CH) **9C** and geometry[a] changes by the conversion reaction of Cp(CO)₂W(Si(H)₂C≡CH) **9** to Cp(CO)₂W(C≡CH)(SiH₂) **1**.
[a] DFT/BS-I optimization was carried out. Bond lengths are in angstrom and bond angles are in degree.   [b] Arrows in **TS₉₋₁** represent important movement of atoms in imaginary frequency. Imaginary frequency is given in parentheses.

HOMO-2   **HOMO-6**   **HOMO-8**

(-7.2)   (-9.7)   (-10.8)

(A) Cp(CO)$_2$W(Si(H)$_2$C≡CH) 9

HOMO-2   **HOMO-6**   **HOMO-19**

(-7.6)   (-10.2)   (-12.7)

(B) Cp(CO)$_2$W(C(H)$_2$C≡CH) 9C

LUMO   **HOMO (SOMO)**   **HOMO-2**

(-1.0)   (-6.0)   (-8.9)

(C) ·Si(H)$_2$CCH

LUMO   **HOMO (SOMO)**   **HOMO-2**

(0.0)   (-6.5)   (-9.5)

(D) ·C(H)$_2$CCH

Figure 1.8. Several important Kohn-Sham orbitals observed in Cp(CO)$_2$W(Si(H)$_2$C≡CH) **9**, Cp(CO)$_2$W(C(H)$_2$C≡CH) **9C** and their fragments ·Si(H)$_2$CCH and ·C(H)$_2$CCH. In parentheses are orbital energies (eV unit).

All these geometrical features suggest that the [SiH$_2$CCH]$^-$ ligand in **9** can be considered as a silicon analogue of the η^3-propargyl/allenyl group. Of course, some differences between **9** and **9C** are observed; for instance, the W-C2 distance is somewhat longer in **9** than in **9C**, while the W-C1 distance of **9** is much longer than that of **9C**. These are not surprising, as follows: Because of the larger size of Si than that of C, the W-Si distance of **9** is longer than the W-C3 distance of **9C**, which leads to the longer W-C1 and W-C2 distances in **9** than in **9C**.

To investigate the coordinate bond of the [Si(H)$_2$CCH]$^-$ ligand, we examined several important molecular orbitals of **9** and **9C**, as shown in Figures 1.8(A) and (B). The HOMO and HOMO-1 of **9** mainly consist of a d orbital, which are similar to the HOMO and HOMO-1 of **1**. The remaining three d orbitals are in unoccupied molecular orbitals in both complexes. These results are consistent with the fact that the W center takes +2 oxidation state in **9** and **9C**. There are two important molecular orbitals for the interaction; one is HOMO-2 and the other is HOMO-6. Because these orbitals involve the bonding interaction between the Si(H)$_2$CCH moiety and W, we first discuss frontier orbitals of ·Si(H)$_2$CCH and the usual propargyl groups. The HOMO of both ·Si(H)$_2$CCH and ·C(H)$_2$CCH is non-bonding π orbital ($\varphi_{n\pi}$) which consists of p orbitals of terminal C and Si (or C) atoms, as shown in Figures 1.8(C) and 1.8(D). Although two p orbitals of terminal C atoms contribute to the HOMO in almost the same extent in ·C(H)$_2$CCH, the p orbital of Si contributes more to the HOMO than that of C in ·Si(H)$_2$CCH. This is because the p orbital of Si is at higher energy than that of C; for instance, the p orbital of ·SiH$_3$ is at -5.39 eV and that of ·CH$_3$ is at -6.41 eV, where orbital energies calculated with DFT/BS-II method are presented (Hartree-Fock orbital provides similar energy difference between them) [49]. The HOMO-2 is, however, considerably different between ·C(H)$_2$CCH and ·Si(H)$_2$CCH; it is the usual π orbital in ·C(H)$_2$CCH, which

(A) ... + ... + ... $\Longrightarrow$ ... **non-bonding π-orbital**

Large

(B) ... + ... + ... $\Longrightarrow$ ... **π-orbital**

Large   Large   Small

(C) ... + ... + ... $\Longrightarrow$ ... **π-orbital**

Small   Large   Small
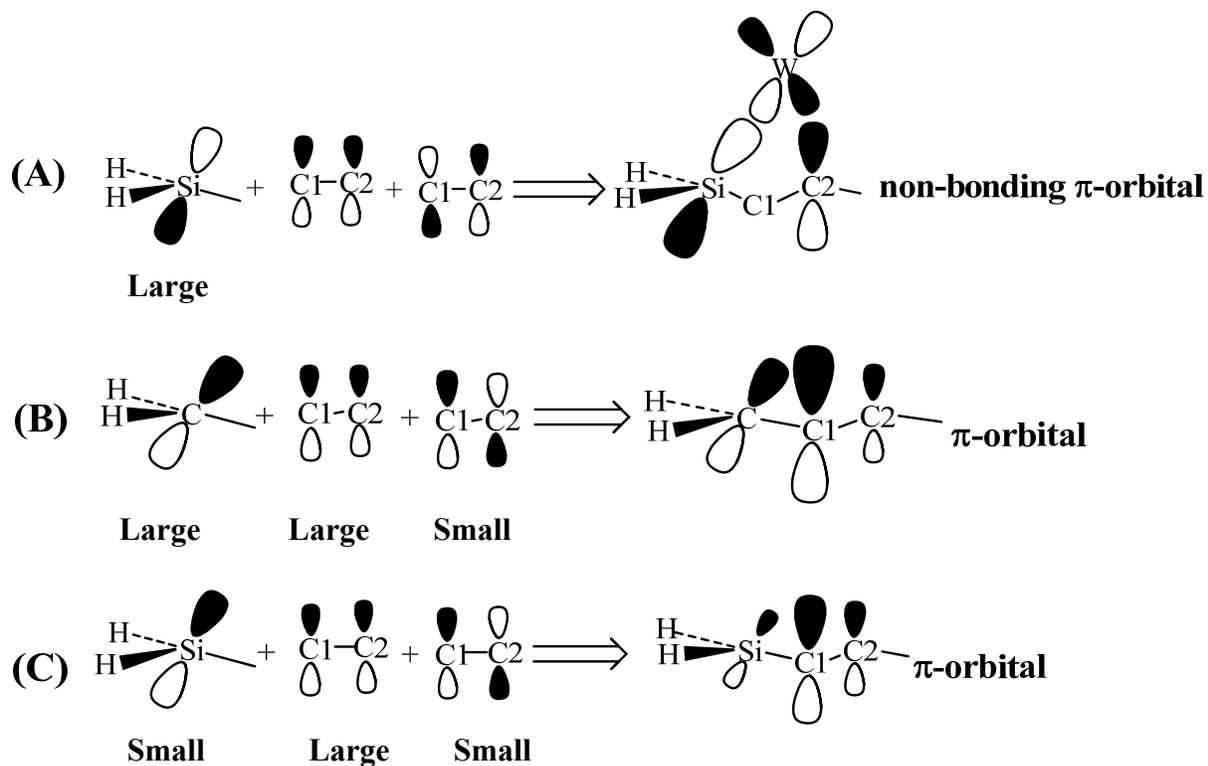
Scheme 1.5

is similar to the π orbital of π-allyl group. In $\cdot$Si(H)$_2$CCH, on the other hand, it is similar to the π orbital of the C=C double bond to which the p orbital of Si moderately contributes. The shape of the HOMO is easily understood in terms of allyl-type orbital mixing, as follows: The p orbital of Si overlaps with the π orbital of acetylide in an anti-bonding way, as shown in Scheme 1.5(A), because the p orbital is at higher energy than the π orbital. The π^* orbital of acetylide mixes into this orbital in a bonding way with the p orbital of Si, to weaken the anti-bonding overlap between the p orbital of Si and the π orbital. This mixing significantly decreases the contribution of C1 p orbital and increases very much that of C2 p orbital to afford $\varphi_{n\pi}$. This $\varphi_{n\pi}$ orbital overlaps with the empty d orbital of W in a bonding way to form the HOMO-2 of **9**. In $\cdot$C(H)$_2$CCH, the p orbitals of three C atoms overlap with each other in a bonding way, to form the HOMO-2 (φ_{π}), as shown in Scheme 1.5(B). Thus, the φ_{π} orbital

51

delocalizes to the terminal C atom. This φ_π orbital overlaps with the acceptor orbital of W in a bonding way to afford the HOMO-6, as shown in Figure 1.8(B). The different shape of the HOMO-2 of $\cdot$Si(H)$_2$CCH is interpreted in terms of the higher energy of Si p orbital, as follows: Because the p orbital of Si is at much higher energy than that of C, as described above, the former orbital much less contributes to the HOMO-6 than the latter orbital, as shown in Scheme 1.5(C). As a result, the φ_π orbital moderately delocalizes onto the Si atom, as shown in Figure 1.8(C). Because of the rather localized φ_π orbital of $\cdot$Si(H)$_2$CCH, the HOMO-6 of **9** is considerably different from that of **9C**, as shown in Figures 1.8(A) and (B).

From all these results, it should be concluded that although **9** is considered to be the Si analogue of propargyl/allenyl complex and the non-bonding π orbital is similar to that of the propargyl/allenyl group, the conjugation between Si and C atoms is very weak in the π-orbital unlike the π-orbital of the usual propargyl/allenyl group in which the considerable conjugation is clearly observed.

1.3.6   Conversion   reaction   of   Cp(CO)$_2$W(Si(H)$_2$C≡C-H)   **9**   to Cp(CO)$_2$W(C≡C-H)(SiH$_2$) 1

Because **Form-A** is correct understanding of Cp(CO)$_2$W(SiH$_2$)(C≡CH) **1**, as discussed above, the conversion reaction of **9** to **1** involves the α-Si-C σ-bond activation via the interesting 1,2-alkynyl shift, which takes place through the transition state **TS$_{9-1}$**, as shown in Figure 1.8. In the imaginary frequency of **TS$_{9-1}$**, the direction of the sp orbital of the C≡C-H group is changing toward the W center. As a result, the W-C1 distance shortens to 2.369 Å and the W-C2 distance considerably lengthens to 3.278 Å in **TS$_{9-1}$**. At the same time, the Si-C1 distance lengthens to 1.915 Å in **TS$_{9-1}$**, while it is still shorter than that of **1** by 0.053 Å.

Table 1.4: Activation barrier $(E_a)^{a,b}$ and reaction energy $(\Delta E)^{a,b}$ in the conversion reaction of $Cp(CO)_2W(Si(R^2)_2C\equiv CH)$ **9** to $Cp(CO)_2W(C\equiv CH)(SiH_2)$ **1**.

Method	E_a (kcal/mol)	ΔE (kcal/mol)
DFT	15.3	-4.9
MP2	20.7	0.4
MP3	14.0	-1.4
MP4(DQ)	15.5	-0.1
MP4(SDQ)	14.8	-0.9
MP4(SDTQ)	18.8	-0.6
CCSD(T)	15.8	-0.7

[a] E_a is energy difference between transition state and reactant and ΔE is energy difference between product and reactant. [b] The BS-II was employed.

All these results indicate that the Si-C1 σ-bond and the W-C2 bond of **9** are going to be broken and the W-C1 bond is going to be formed in **TS$_{9-1}$**. Interestingly, the W-Si distance of **TS$_{9-1}$** is shorter than those of **9** and **1** by 0.089 Å and 0.177 Å, respectively. The C1-C2 distance of **TS$_{9-1}$** is shorter than those of **9** and **1**, too. These interesting geometry changes relate to the interaction between $[Si(H)_2CCH]^-$ and the W center, which will be discussed below.

This conversion reaction easily takes place with a moderate activation barrier of 15.3 (15.8) kcal/mol and a small exothermicity of 4.9 (0.7) kcal/mol, as shown in Table 1.4, where the DFT- and CCSD(T)-calculated energies are given without and in parenthesis, respectively. The CCSD(T) and DFT methods present a similar activation barrier but the MP4(SDTQ) method presents a moderately larger value. On the other hand, the DFT-calculated exothermicity is moderately larger than the others. It is likely that the DFT- and CCSD(T)-calculated activation barriers and the MP4(SDTQ)- and CCSD(T)-calculated exothermicities are reliable.
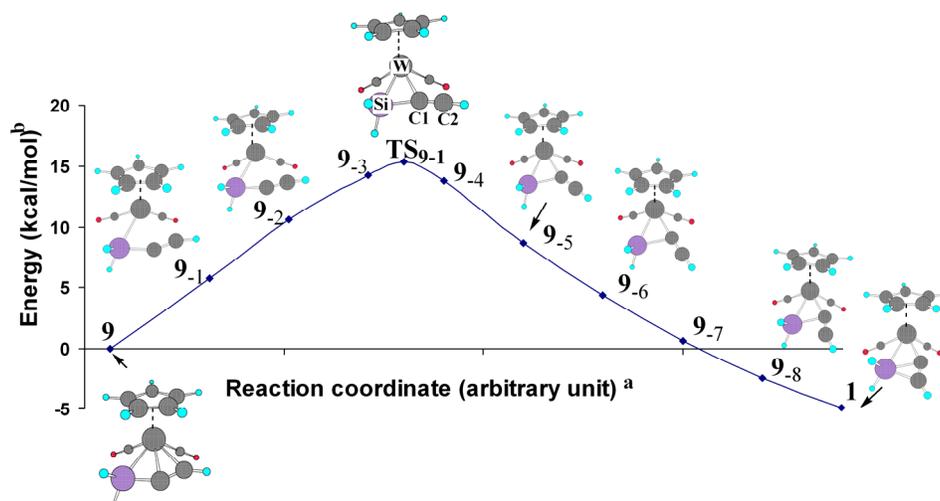
(A) Potential energy Changes
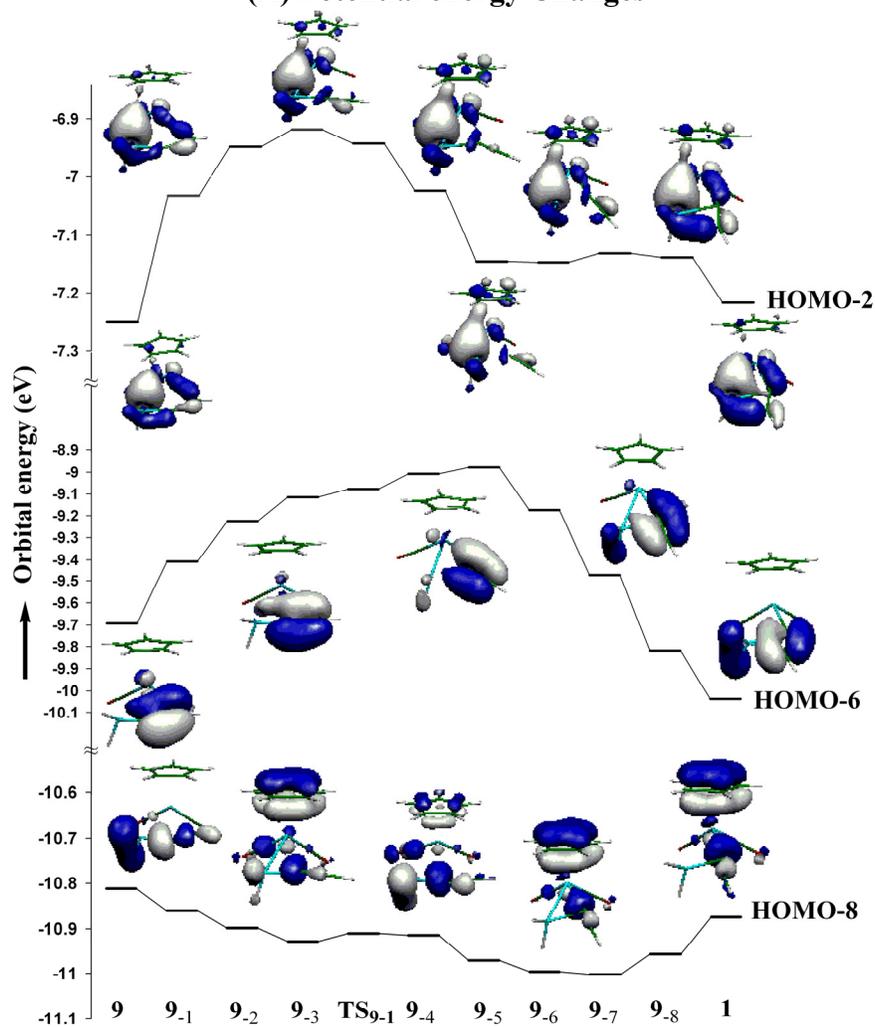
(B) Orbital energy changes[b]

Figure 1.9. Changes in potential energy and orbital energies in conversion reaction of Cp(CO)$_2$W(Si(H)$_2$C≡CH) **9** to Cp(CO)$_2$W(C≡CH)(SiH$_2$) **1**.
[a] Reaction coordinates from IRC calculation. [b] The DFT/BS-II calculation.

The d orbital population of W changes little upon going to **1** (5.77e) from **9** (5.77e) but it is moderately larger in **TS$_{9-1}$** (5.85e) than in **9** and **1**, where the DFT/BS-II calculated values are given in parentheses. We found above that W has a +2 oxidation state in both **9** and **1**. This is consistent with almost the same d orbital population in **9** and **1**. These results indicate that the conversion reaction from **9** to **1** takes place without changing the oxidation state of W. The moderate increase in W d orbital population in **TS$_{9-1}$** relates to the interactions in the transition state, as will be discussed below.

It is of considerable interest to clarify the reason why the α-Si-C σ-bond activation easily takes place with the moderate activation barrier. To clearly understand this α-Si-C σ-bond activation, we carried out an IRC (Intrinsic Reaction Coordinate) calculation and examined the molecular orbitals along the reaction coordinate, as shown in Figure 1.9, where Kohn-Sham energies of three important orbitals are plotted against the reaction coordinate (see Figure 1.9(B)). In Hartree-Fock orbitals, essentially the same energy changes are observed (see Appendix A.1.6). One is HOMO-8, which mainly consists of the Si-C1 bonding orbital in **9**. This orbital energy does not change very much in the reaction in spite of the fact that the Si-C bond is broken in the reaction. This is because the sp lone pair orbital of acetylide decreases the bonding overlap with the sp^3 orbital of silyl group by changing its orientation from the Si atom toward the W center, but it starts to overlap with the acceptor orbital of W, as shown in Scheme 1.6. On the other hand, the HOMO-6 rises considerably in energy upon going to **9$_{-5}$** from **9** and then becomes considerably lower in energy upon going to **1** from **9$_{-5}$**; see Figure 1.9 for **9$_{-1}$** to **9$_{-8}$**. These changes are easily understood in terms of the interaction of the acetylide π orbital with either the acceptor orbital of W or the empty p orbital of the silylene, as follows: The HOMO-6 of **9** mainly consists of the bonding interaction between the π

55
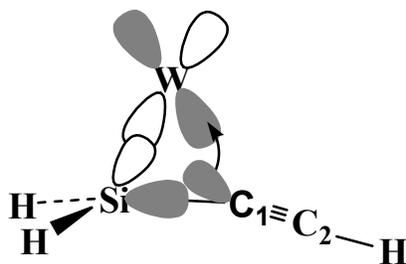
Scheme 1.6

orbital of acetylide and the acceptor orbital of W, as shown in Figure 1.8(A). Because the acetylide moiety changes its orientation upon going to **TS$_{9-1}$** from **9**, the bonding overlap between the acetylide π orbital and the acceptor orbital of W decreases, as shown in Figure 1.9, which increases the HOMO-6 energy. However, the acetylide π orbital starts to overlap with the empty p orbital of silylene upon going to **1** from **9$_{-5}$**, to stabilize the HOMO-6 in energy.

The HOMO-2 energy changes in a complicated manner; it first rises in energy and reaches the maximum before **TS$_{9-1}$**. Then, it lowers in energy upon going to **9$_{-5}$** from **9$_{-3}$**. At **TS$_{9-1}$**, it is decreasing in energy. After **9$_{-5}$**, its energy changes little. The HOMO-2 of **9** mainly consists of the bonding overlap between the empty d orbital of W and the $\varphi_{n\pi}$ orbital, as shown in Figure 1.8(A). The energy rise in the early stage of the reaction is easily understood in terms that the bonding overlap between the p orbital of C2 and the empty d orbital of W becomes small upon going to **9$_{-3}$** from **9**, as clearly observed in Figure 1.9. Upon going from **9$_{-3}$** to **9$_{-5}$** through **TS$_{9-1}$**, silylene is gradually formed. Its lone pair orbital overlaps with the W center in a bonding way around **TS$_{9-1}$**, which lowers the HOMO-2 in energy, as shown in Figure 1.9. This is consistent with the shorter W-Si distance and the larger W d orbital population at **TS$_{9-1}$** than in **9** and **1**. In the later half of this reaction from **9$_{-5}$** to **1**, silylene changes its direction toward the C1 atom, which decreases the overlap between the lone pair

orbital and the acceptor orbital of W, to increase the energy of HOMO-2. However, the π^* orbital of acetylide starts to overlap with the lone pair orbital of silylene in a bonding way upon going to **1** from **9-5**, which lowers the HOMO-2 in energy. Because these two effects compensate each other, the HOMO-2 energy little changes in the later half of the reaction.

From these results, three important conclusions are extracted, as follows: (1) The origin of the activation barrier is the weakening of the bonding interaction between the $\varphi_{n\pi}$ orbital of the silapropargyl group and the acceptor orbital of W, (2) the π orbital of acetylide is stabilized in energy by the interaction with the empty p orbital of silylene, and (3) the lone pair of silylene is stabilized in energy by the interaction with the π^* orbital of acetylide. In other words, the driving force for the 1,2-alkynyl shift is the CT interactions between the π orbital of acetylide and the empty p orbital of silylene and between the lone pair orbital of silylene and the π^* orbital of acetylide.

1.4   Conclusions

The geometry and bonding nature of $Cp^*(CO)_2W(C{\equiv}C^tBu)(SiPh_2)$ and all steps of its formation reaction from $Cp^*(CO)_2W(Me)(HSi(Ph)_2C{\equiv}C^tBu)$ were theoretically investigated with the DFT, MP2 to MP4(SDTQ), and CCSD(T) methods, where $Cp(CO)_2W(C{\equiv}CH)(SiH_2)$ **1** and $Cp(CO)_2W(Me)(Si(H)_3C{\equiv}CH)$ **5** were adopted as their models, respectively. The geometrical features and the bonding nature indicate that **1** is neither a pure silacyclopropenyl complex of W nor a pure silylene acetylide complex of W. Although pure silacyclopropenyl group is not formed in **1**, the orbitals of **1** resemble well those observed in the formation reaction of silacyclopropene from silylene and acetylene. Those orbitals are formed through interactions of the π and π^* orbitals of acetylide with the lone pair and empty p orbitals of

silylene. In **1**, CT occurs from the π orbital of the acetylide moiety to the empty p orbital of silylene and simultaneously the other CT occurs from the sp^2 lone pair orbital of silylene to the π^* orbital of acetylide. From these frontier orbitals, as well as the geometry of **1**, it should be concluded that the CCH(SiH$_2$) moiety of **1** is an intermediate species trapped by the W center in the formation reaction of silacyclopropene from silylene and acetylene. The substituent on the acetylide group considerably influences the geometry of **1**.

Complex **1** is formed from **5** through several steps, as follows: Cp(CO)$_2$W(Me)(Si(H)$_3$C≡CH) **5** first converts to Cp(CO)$_2$W(H)(Me)(Si(H)$_2$C≡CH) **6** with no barrier and considerable exothermicity through Si-H oxidative addition. Then, **6** converts to Cp(CO)$_2$W(CH$_4$)(Si(H)$_2$C≡CH) **7** through the reductive elimination of methane with a moderate activation barrier of 10.7 (11.8) kcal/mol, where the DFT- and MP4(SDTQ)-calculated energies are given without parentheses and in parentheses, respectively. This reductive elimination is almost thermoneutral. After methane dissociation from **7**, the coordination of the C≡C triple bond to W takes place with no barrier and large exothermicity of 31.2 (43.3) kcal/mol, to afford Cp(CO)$_2$W(Si(H)$_2$C≡CH) **9**. Finally, **9** converts to Cp(CO)$_2$W(C≡CH)(SiH$_2$) **1** through the α-Si-C σ-bond activation with moderate activation barrier of 15.3, 18.8, and 15.8 kcal/mol and exothermicity of 4.9, 0.6, and 0.7 kcal/mol, which are calculated with the DFT, MP4(SDTQ), and CCSD(T) methods, respectively. This moderate activation barrier arises from the stabilization of the π orbital of acetylide by the bonding interaction with the empty p orbital of silylene and that of the lone pair of silylene by the bonding interaction with the π^* orbital of acetylide. In other words, the α-Si-C σ-bond activation easily occurs via the 1,2-alkynyl shift because of these bonding interactions.

Complex **9** is a silicon analogue of η^3-propargyl/allenyl complex of W, while the delocalization in [H$_2$SiCCH]$^-$ is much less than in [H$_2$CCCH]$^-$. The non-bonding π-orbital of the H$_2$SiCCH moiety is essentially the same as that of the propargyl group but the π conjugation between Si and C atoms is very weak in the π orbital unlike the sufficient π conjugation in the propargyl complex. Thus, **9** is understood in terms of 50% of the Si analogue of a tungsten η^3-propargyl complex and 50% of a tungsten alkynylsilyl complex.

Bibliography

[1]   Tilley, T. D. In *The Silicon-Heteroatom Bond*; Patai, S., Rappoprt, Z., Eds.; Wiley: New York, **1991**; Chapters 9 and 10, pp 245, 309. (b) Eisen, M. S. In *The Chemistry of Organic Silicon Compounds*; Rappoport, Z., Apeloig, Y., Eds.; Wiley: New York, **1998**; vol.2, chapter 35, p2037.

[2]   Sharma, H. K.; Pannell, K. H. *Chem. Rev.* **1995**, *95*, 1351.

[3]   (a) Braunstein, P.; Knorr, M. *J. Organomet. Chem.* **1995**, *500*, 21. (b) Braunstein, P.; Boag, N. M. *Angew. Chem. Int. Ed. Engl.* **2001**, *40*, 2427.

[4]   (a) Ogino, H.; Tobita, H. *Ad. Organomet. Chem.* **1998**, *42*, 223. (b) Ogino, H. *The Chem. Record* **2002**, *2*, 291. (c) Okazaki, M.; Tobita, H.; Ogino, H. *Dalton Trans.* **2003**, 493.

[5]   Corey, J. Y.; Braddock-Wilking, J. *Chem. Rev.* **1999**, *99*, 175.

[6]   Schmidt, G.; Welz, E. *Angew. Chem. Int. Ed. Engl.* **1977**, *16*, 785.

[7]   Zybill, C.; Müller, G. *Angew. Chem. Int. Ed. Engl.* **1987***, 26*, 669.

[8]   (a) Tobita, H.; Ueno, K.; Ogino, H. *Chem. Lett.* **1986**, 1777. (b) Tobita, H.; Ueno, K.; Ogino, H. *Bull. Chem. Soc. Jpn.* **1988**, *61*, 2797. (c) Ueno, K.; Tobita, H.; Shimoi, M.; Ogino, H. *J. Am. Chem. Soc.* **1988**, *110,* 4092. (d) Tobita, H.; Ueno, K.; Shimoi, M.; Ogino, H. *J. Am. Chem. Soc.* **1990**, *112*, 3415. (e) Ueno, K.; Tobita, H.; Ogino, H. *Chem. Lett.* **1990**, 369. (f) Takeuti, T.; Tobita, H.; Ogino, H. *Organometallics* **1991**, *10,* 835. (g) Ueno, K.; Ito, S.; Endo, K.; Tobita, H.; Inomata, S.; Ogino, H. *Organometallics* **1994**, *13*, 3309. (h) Tobita, H.; Wada, H.; Ueno, K.; Ogino, H. *Organometallics* **1994**, *13*, 2545. (i) Ueno, K.; Nakano, K.; Ogino, H. *Chem. Lett.*

1996, 459. (j) Ueno, K.; Masuko, A.; Ogino, H. *Organometallics* **1997**, *16*, 5026. (k) Okazaki, M.; Tobita, H.; Ogino, H. *Chem. Lett.* **1997**, 437. (l) Wada, H.; Tobita, H.; Ogino, H. *Chem. Lett.* **1998**, 993. (m) Ueno, K.; Sakai, M.; Ogino, H. *Organometallics* **1998**, *17*, 2138. (n) Ueno, K.; Masuko, A.; Ogino, H. *Organometallics* **1999**, *18,* 2694. (o) Tobita, H.; Sato, T.; Okazaki, M.; Ogino, H. *J. Organomet. Chem.* **2000**, *611*, 314. (p) Minglana, J. J. G.; Okazaki, M.; Tobita, H.; Ogino, H. *Chem. Lett.* **2002**, 406.

[9] (a) Pannell, K. H.; Cervantes, J.; Hernandez, C.; Cassias, J.; Vincenti, S. *Organometallics* **1986**, *5*, 1056. (b) Jones, K. L.; Pannell, K. H. *J. Am. Chem. Soc.* **1993**, *115*, 11336. (c) Jones, K. L.; Pannell, K. H. *Organometallics* **2001**, *20*, 7.

[10] Straus, D. A.; Tilley, T. D.; Rheingold, A. L.; Geib, J. S. *J. Am. Chem. Soc.* **1987**, *109*, 5872.

[11] (a) Grumbine, S. D.; Tilley, T. D.; Rheingold, A. L. *J. Am. Chem. Soc.* **1993***, 115*, 358. (b) Grumbine, S. D.; Tilley, T. D.; Arnold, F. P.; Rheingold, A. L. *J. Am. Chem. Soc.* **1993**, *115*, 7884.

[12] (a) Corriu, R. J. P.; Lanneau, G. F.; Chauhan, B. P. S. *Organometallics* **1993**, *12*, 2001. (b) Corriu, R. J. P.; Chauhan, B. P. S.; Lanneau, G. F. *Organometallics* **1995**, *14*, 1646. (c) Chauhan, B. P. S.; Corriu, R. J. P.; Lanneau, G. F.; Priou, C.; Auner, N.; Handwerker, H.; Herdtweck, E. *Organometallics* **1995**, *14*, 1657.

[13] Bodensieck, U.; Braunstein, P.; Dech, W.; Faure, T.; Knorr, M.; Stern, C. *Angew. Chem. Int. Ed. Engl.* **1994**, *33*, 2440.

[14] Chen, W.; Edwards, A. J.; Esteruelas, M. A.; Lahoz, F. J.; Olivan, M.; Oro, L. A. *Organometallics* **1996**, *15*, 2185.

[15] (a) Michell, G. P.; Tilley, T. D. *Angew. Chem. Int. Ed. Engl.* **1998**, *37*, 2524. (b) Michell, G. P.; Tilley, T. D. *J. Am. Chem. Soc*. **1998**, *120*, 7635. (c) Peters, J. C.; Feldman, J. D.; Tilley, T. D. *J. Am. Chem. Soc.* **1999**, *121*, 9871.

[16] Sakaba, H.; Tsukamoto, M.; Hirata, T.; Kabuto, C.; Horino, H. *J. Am. Chem. Soc.* **2000**, *122*, 11511.

[17] Denk, M.; Hayashi, R. K.; West, R. *J. Chem. Soc. Chem. Commun.* **1994**, 33.

[18] Gehrhus, B.; Hitchcock, P. B.; Lappert, M. F.; Maciejewski, H. *Organometallics* **1998**, *17*, 5599.

[19] Petri, S. H. E.; Eikenberg, D.; Neumann, B.; Stammler, H. G.; Jutzi, P. *Organometallics* **1999**, *18*, 2615.

[20] Woo, L. K.; Smith, D. A.; Young, Jr. V. G. *Organometallics* **1991**, *10*, 3977.

[21] Feldman, J. D.; Mitchell, G. P.; Notle, J. O.; Tilley, T. D. *J. Am. Chem. Soc*. **1998**, *120*, 11184.

[22] Cundari, T. R.; Gordon, M. S.; *J. Phys. Chem*. **1992**, *96*, 631.

[23] Marquez, A.; Sanz, J. F. *J. Am. Chem. Soc*. **1992**, *114*, 2903.

[24] Jacobsen, H.; Ziegler, T. *Organomettallics* **1995**, *14*, 224.

[25] Boheme, C.; Frenking, G. *Organometallics* **1998**, *17*, 5801.

[26] Beddie, C.; Hall, M. B.; *J. Am. Chem. Soc*. **2004**, *126*, 13564.

[27] Sakaba, H.; Yoshida, M.; Kabuto, C.; Kabuto, K. *J. Am. Chem. Soc*. **2005**, *127*, 7276.

[28] (a) Burger, P.; Bergman, R. G. *J. Am. Chem. Soc*. **1993**, *115*, 10462. (b) Klei, S. R.; Tilley, T. D.; Bergman, R. G. *Organometallics* **2001**, *20*, 3220. (c) Klei, S. R.; Tilley, T. D.; Bergman, R. G. *Organometallics* **2002**, *21*, 4648. (d) Okazaki, M.; Suzuki, E.; Miyajima, N.; Tobita, H.; Ogino, H. *Organometallics* **2003**, *22*, 4633. (e) Suzuki, E.;

Okazaki, M.; Tobita, H. *Chem. Lett*. **2005**, *34*, 1026.

[29]   Sakaba, H.; Watanabe, S.; Kabuto, C.; Kabuto, K.   *J. Am. Chem. Soc*. **2003**, *125*, 2842.

[30]   (a) Becke, A. D. *Phys Rev. A*. **1988**, *38*, 3098. (b) Becke, A. D. *J. Chem. Phys*. **1993**, *98*, 5648.

[31]   (a) Perdew, J. P. *In Electronic Structure of Solids*`91, Ziesche, P.; Eschrig, H., Ed.; Akademic Verlag, Berlin, **1991**; p 11. (b) Perdew, J. P.; Chevary, J. A.; Vosko, S. H.; Jackson, K. A.; Pederson, M. R.; Singh, D. J.; Fiolhais, C. *Phys. Rev. B*. **1992**, *46*, 6671. (c) Perdew, J. P.; Chevary, J. A.; Vosko, S. H.; Jackson, K. A.; Pederson, M. R.; Singh, D. J.; Fiolhais, C. *Phys. Rev. B*. **1993**, *48*, 4978. (d) Perdew, J. P.; Burke, K.; Wang, Y. *Phys Rev. B*. **1996**, *54*, 16533.

[32]   Lee, C.; Yang, W.; Parr, R. G. *Phys. Rev. B*. **1988**, *37*, 785.

[33]   Adamo, C.; Barone, V. *J. Chem. Phys*. **1998**, *108*, 664.

[34]   Hay, P. J.; Wadt, W. R.   *J. Chem. Phys*. **1985**, *82*, 299.

[35]   (a) Dunning Jr, T. H. *J. Chem. Phys*. **1989**, *90*, 1007. (b) Woon, D. E.; Dunning Jr, T. H. *J. Chem. Phys*. **1993**, *98*, 1358.

[36]   Ditchfield, R.; Hehre, W. J.; Pople, J. A. *J. Chem. Phys*. **1971**, *54*, 724.

[37]   (a) Hehre, W. J.; Ditchfield, R.; Pople, J. A. *J. Chem. Phys*. **1972**, *56*, 2257. (b) Hariharan, P. C.; Pople, J. A. *Theor. Chim. Acta* **1973**, *28*, 213. (b) Francl, M. M.; Petro, W. J.; Hehre, W. J.; Binkley, J. S.; Gordon, M. S.; Defrees, D. J.; Pople, J. A. *J. Chem. Phys* **1982**, *77*, 3654.

[38]   Dunning Jr, T. H. *In Modern Theoretical Chemistry, Vol. 3*, Schaefer III, H. F., Ed.; Plenum: New York, **1976**: p 1-28. The d polarization function (ζ=0.3247)

implemented in Gaussian 03 program package (Revision C.02) was used for Si.

[39]   Couty, M.; Hall, M. B. *J. Comput. Chem*. **1996**, *17*, 1359.

[40]   Ehlers, A. W.; Bohme, D. S.; Gobbi, A.; Hollwarth, A.; Jonas, V.; Kohler, K. F.; Stegmann, R.; Veldkamp, A.; Frenking, G. *Chem. Phys. Lett*. **1993**, *208*, 111.

[41]   Pople, J. A.; et al. *Gaussian 03,* Revision C.02, Gaussian Inc.: Wallingford, CT, **2004**.

[42]   Glendening, E. D.; Reed, A. E.; Carpenter, J. E.; Weinhold, F. NBO Version, 3.1.

[43]   (a) Flükiger, P.; Lüthi, H. P.; Portmann, S.; Weber, J. *MOLEKEL 4.3*, Swiss Center for Scientific Computing, Manno (Switzerland), **2000-2002**. (b) Portmann, S.; Lüthi, H. P. *MOLEKEL*, An Interactive Molecular Graphics Tool, *CHIMIA*, **2000**, *54*, 766-770.

[44]   Pin, Chin-Wei.; Peng, Jiun-Jang.; Shiu, Chin-Wei.; Chi, Yun.; Peng, Shie-Ming.; Lee, Gene-Hsiang. *Organometallics* **1998**, *17*, 438.

[45]   Tutsui, S.; Sakamoto, K.; Kabuto, C.; Kira, M. *Organometallics* **1998**, *17,* 3819.

[46]   Sakaba, H.; Tsukamoto, M.; Hirata, T.; Kabuto, C.; Horino, H. *J. Am. Chem. Soc*. **2000**, *122*, 11511.

[47]   Chung, G.; Gordon, M. S. *Organomettalics* **1999**, *18*, 4881.

[48]   Koch, R.; Bruhn, T.; Weidenbruch, M. *Organometallics* **2004**, *23*, 1570.

[49]   The HF-calculated p orbital of $\cdot SiH_3$ is at -7.85 eV and that of $\cdot CH_3$ is at -10.47 eV.

Appendix

A.1.1 Selected optimized parameters of $Cp(CO)_2W(C\equiv CH)(SiH_2)$ **1**

Table A.1.1. Basis set[a] effects on the optimized parameters[b] of $Cp(CO)_2W(C\equiv CH)(SiH_2)$ **1**

	B3LYP				B3PW91				MPWPW91				Expt.[c]
	BS-I	BS-III	BS-IV	BS-V	BS-I	BS-III	BS-IV	BS-V	BS-I	BS-III	BS-IV	BS-V	
W-Si	2.656	2.649	2.665	2.662	2.616	2.612	2.624	2.620	2.630	2.626	2.635	2.634	2.567
W-C1	2.020	2.023	2.012	2.018	2.014	2.017	2.007	2.013	2.017	2.018	2.010	2.014	2.050
Si-C1	1.978	1.979	1.964	1.972	1.968	1.968	1.955	1.962	1.978	1.978	1.963	1.972	1.937
Si-C2	1.952	1.958	1.918	1.936	1.957	1.962	1.924	1.942	1.960	1.963	1.929	1.944	2.009
C1-C2	1.300	1.294	1.299	1.297	1.299	1.293	1.298	1.295	1.311	1.307	1.311	1.309	1.270
W-Si-C1	49.1	49.3	48.7	48.9	49.7	49.9	49.4	49.6	49.4	49.6	49.2	49.3	51.9
C1-Si-C2	38.6	38.4	39.1	38.8	39.0	38.4	39.1	38.8	38.9	38.7	39.3	39.1	37.5

[a] In BS-III, 6-31G* basis sets were employed for C and O, while for Si, H and W, the same basis sets as those of BS-I were used. In BS-IV, 6-31G* basis set was employed for Si, while for C, O, H, and W the same basis sets as those of BS-III were used. In BS-V, D95(d) basis set was employed for Si, while for C,O, H, and W the same basis sets as those of BS-III were used.
[b] Bond lengths and angles are in angstrom and degree, respectively. [c] Reference 27.

A.1.2   Geometry of HCCR[1].
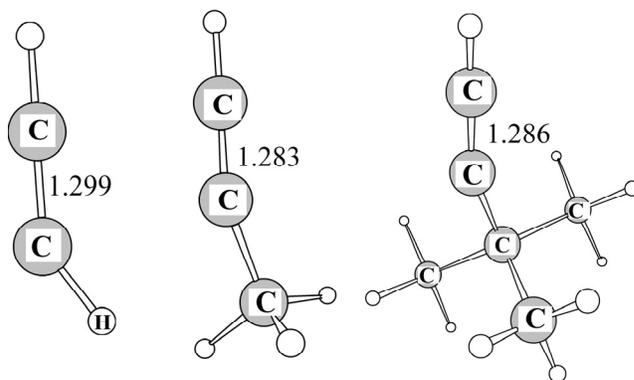
$\angle$**CCR[1]=145.7°** (R[1]=H)
             =154.7° (R[1]=CH$_3$)
             =152.9° (R[1]=[t]Bu)

Figure A.1.1.   Geometries[a] of HCCR[1] (R[1] = H, Me, or [t]Bu).
[a] Bond lengths are in angstrom and bond angles are in degree.
Geometry of -C≡CR[1] is similar to that in Cp(CO)$_2$W(C≡CR[1])(SiR[2]$_2$)
(R[1] = H, Me, or [t]Bu and R[2] = H or Me).

A.1.3 Kohn-Sham MOs in the conversion reaction of Cp(CO)$_2$W(Me)(H$_3$SiC≡CH) **5** to Cp(CO)$_2$W(CH$_4$)(Si(H)$_2$C≡CH) **7**.

HOMO   **HOMO-1**

(A) Cp(CO)$_2$W(Me)(H$_3$SiC≡CH) 5

HOMO   **HOMO-1**   **HOMO-3**   **HOMO-4**

(B) Cp(CO)$_2$W(Me)(H)(Si(H)$_2$C≡CH) 6

HOMO   **HOMO-1**   **HOMO-8**

(C) Cp(CO)$_2$W(Me)(H)(Si(H)$_2$C≡CH) TS$_{6-7}$

HOMO   **HOMO-1**   **HOMO-13**

(D) Cp(CO)$_2$W(CH$_4$)(Si(H)$_2$C≡CH) 7
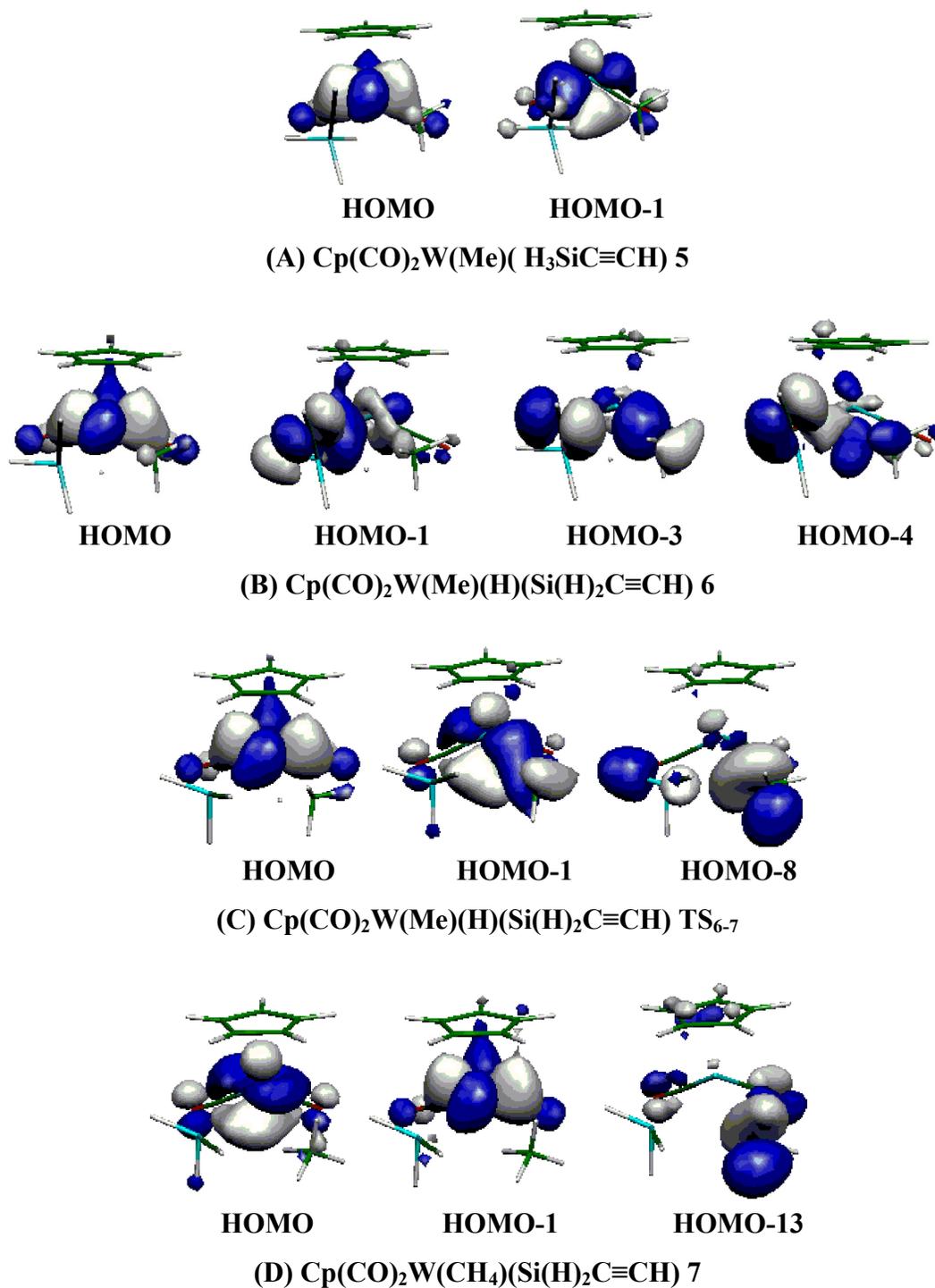
Figure A.1.2. Several important Kohn-Sham MOs observed in the conversion reaction of Cp(CO)$_2$W(Me)(H$_3$SiC≡CH) **5** to Cp(CO)$_2$W(CH$_4$)(Si(H)$_2$C≡CH) **7**.

A.1.4 Discussion on the conversion reaction of Cp(CO)$_2$W(Me)(H$_3$SiC≡CH) **5** to Cp(CO)$_2$W(CH$_4$)(Si(H)$_2$C≡CH) **7**.

For clear understanding of the conversion reaction of **6** to **7**, we examined several important molecular orbitals. In **6**, only one d orbital of W is doubly occupied, which is the HOMO, as shown in A.1.3(C). This result indicates that the W center takes +4 oxidation state. In the HOMO-3, the sp^3 orbital of CH$_3$ overlaps with the empty d$_{xz}$ orbital of the W center in a bonding way, and in the HOMO-4, the 1s orbital of H overlaps with the empty d$_z{}^2$ orbital of the W center in a bonding way. In **TS$_{6-7}$**, the shape of the HOMO little changes (see A.1.3(C)), while the d orbital contribution considerably increases in the HOMO-1, in which the 1s orbital of H and the sp^3 orbital of CH$_3$ overlap with the d orbital in a bonding way. The 1s orbital of H and the sp^3 orbital of CH$_3$ possess different phase from each other, which means that the approach of H to Me increases their anti-bonding overlap but the increment in d orbital contribution weakens the anti-bonding overlap. This feature corresponds to the increase in the charge transfer from the H 1s and CH$_3$ sp^3 orbitals to the d orbital of the W center. The HOMO-8 involves the charge transfer from the C-H σ-bond to the d$_{xz}$ orbital of W center. In **7**, two occupied d orbitals are observed in HOMO and HOMO-1 (see A.1.3(D)), and the remaining three d orbitals are unoccupied. These results clearly show that the W center takes a +2 oxidation state. HOMO-13 of **7** represents that the C-H σ-bond is completely formed. These orbital changes are consistent with the reductive elimination.
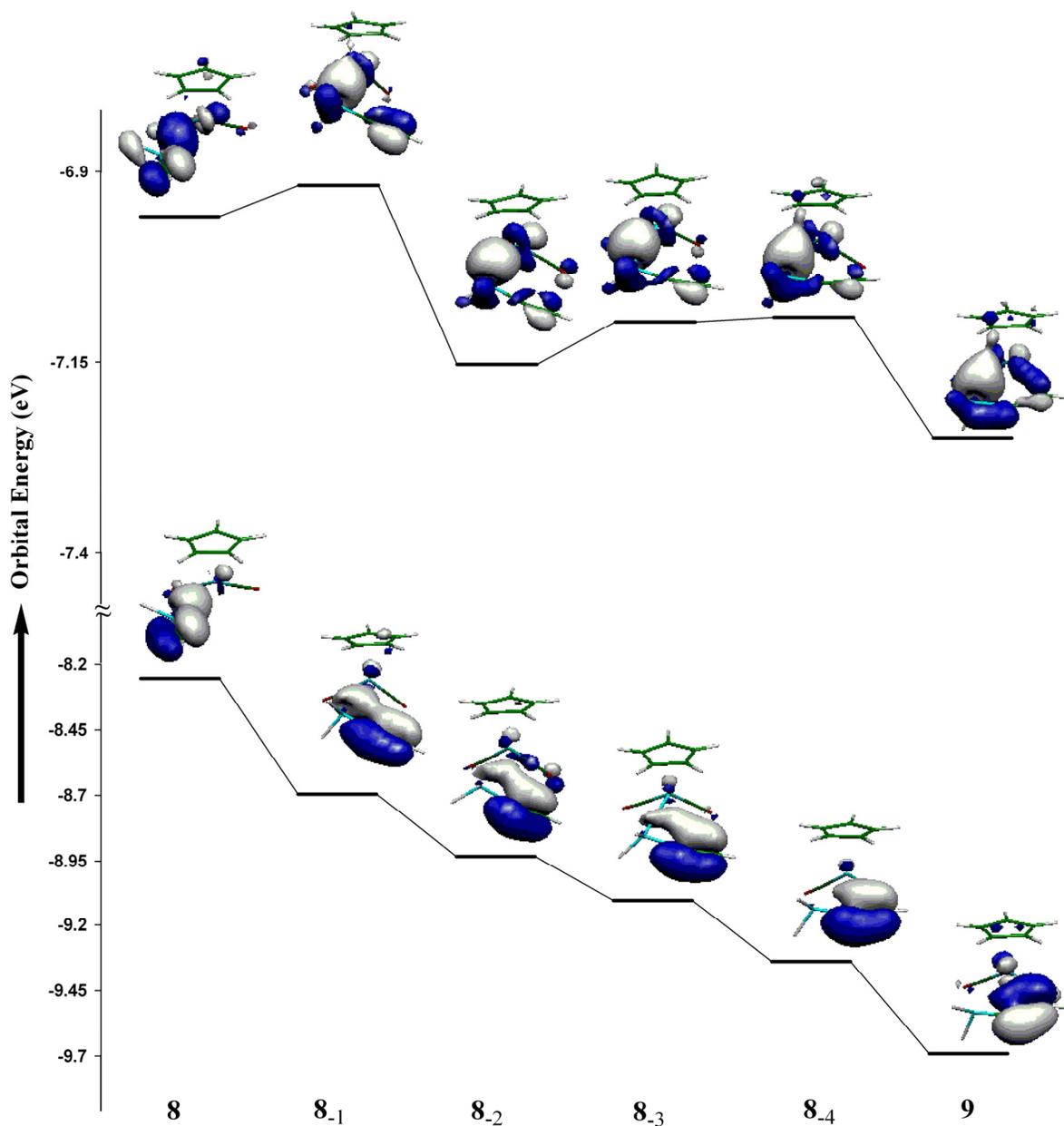
Figure A.1.3. Changes in orbital energies[a] (in eV unit) in the conversion reaction of Cp(CO)$_2$W(Si(H)$_2$C≡CH) **8** to Cp(CO)$_2$W(Si(H)$_2$C≡CH) **9**.
[a] The DFT/BS-II method.

A.1.6 Changes in HF orbital energies in the conversion reaction of $Cp(CO)_2W(Si(H)_2C \equiv CH)$ **9** to $Cp(CO)_2W(C \equiv CH)(SiH_2)$ **1**.
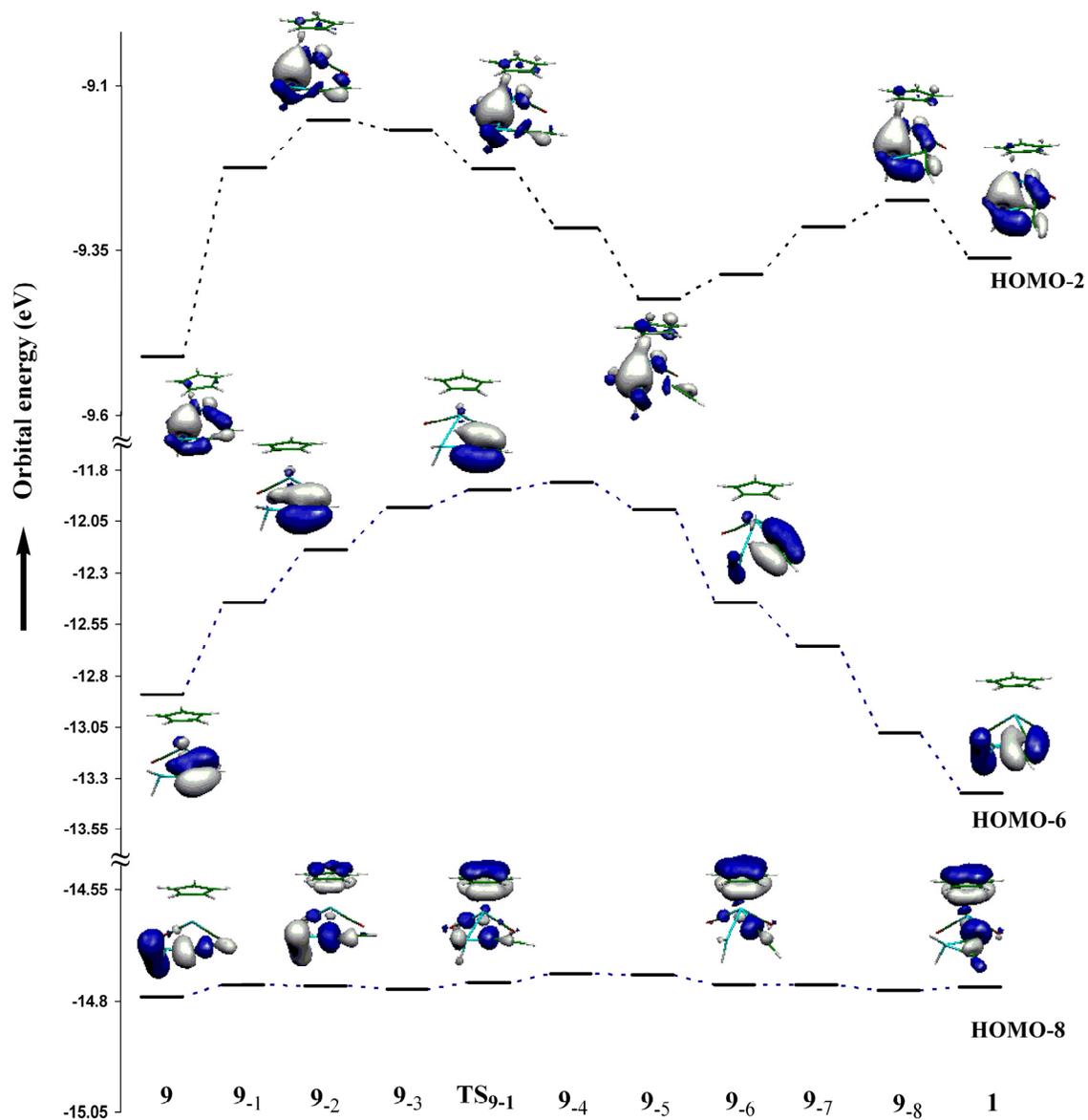
Figure A.1.4. Changes in orbital energies[a] (in eV unit) in the conversion reaction of $Cp(CO)_2W(Si(H)_2C \equiv CH)$ **9** to $Cp(CO)_2W(C \equiv CH)(SiH_2)$ **1**.

[a] The HF/BS-II method.

Chapter 2

Theoretical Study of Tungsten η^3-Silaallyl/η^3-Vinylsilyl and Vinyl Silylene Complexes: Their Interesting Bonding Nature and Relative Stability

2.1   Introduction

Silaallyl species is of considerable interest because it is the simplest of all conjugate systems including Si element. Unfortunately, silaallyl species would not be stable and a free silaallyl species has not been isolated yet, to our knowledge [1-3]. However, the interaction with a transition metal complex is expected to stabilize the silaallyl species. In this regard, transition metal complex of η^3-1-silaallyl (η^3-H$_2$SiCHCH$_2$) is one of the interesting compounds in coordination chemistry, organometallic chemistry, and synthetic chemistry [1-4]. Many efforts were made to isolate the transition metal η^3-silaallyl complex, as follows: In 1976, Sakurai and his collaborators reported the preparation of η^3-1-silapropenyl complexes of iron(II) [1a]. However, the same authors corrected that the compound synthesized was actually the η^2-vinyldisilane complex of iron [1b]. The η^3-1-silaallyl complex, Cp*(PMe$_3$)Ru(η^3-Ph$_2$SiCHCH$_2$), was synthesized by thermolysis of Cp*(PMe$_3$)$_2$Ru{Si(CH=CH$_2$)Ph$_2$} but details were not presented [4]. Recently, a stable tungsten η^3-1-silaallyl complex Cp*(CO)$_2$W(η^3-Me$_2$SiCHCMe$_2$) **A1** was successfully isolated via Si-H σ-bond activation of dimethylvinylsilane HMe$_2$Si(CH=CMe$_2$) with

Cp*(CO)$_2$W(MeCN)Me, as shown in Scheme 2.1 [5]. The η^3-coordination of Me$_2$SiCHCMe$_2$

was clearly seen in its X-ray structure. In the reaction of Cp*(CO)$_2$W(MeCN)Me with similar
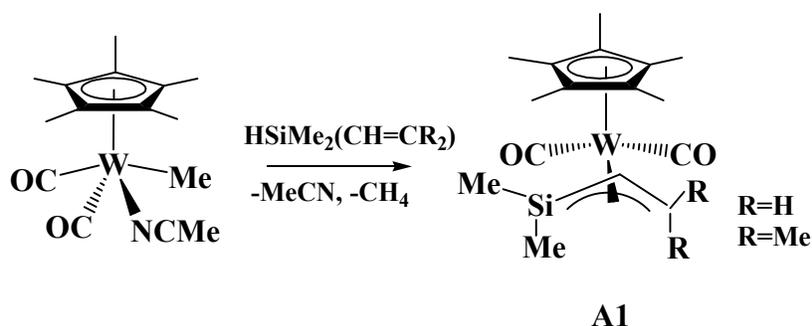
Scheme 2.1. Formation of Cp*(CO)$_2$W(η^3-Me$_2$SiCHCR$_2$) **A1**

diphenylalkynylsilane HPh$_2$Si(C≡C^{t}Bu), on the other hand, not a similar tungsten η^3-1-

silaalkynyl complex Cp*(CO)$_2$W(η^3-Ph$_2$SiCC^{t}Bu) **B1** but a tungsten acetylide silylene

complex Cp*(CO)$_2$W(CC^{t}Bu)(Ph$_2$Si) **B2** was isolated, while **B1** was proposed as an

intermediate in the formation reaction of **B2**, as shown in Scheme 2.2 [6]. We also

theoretically investigated **B1** and **B2** and found that their bonding nature and electronic

structures were very interesting [7]. Thus, it is worth investigating the bonding nature of the

similar η^3-1-silaallyl complex **A1** in comparison with the η^3-1-silapropargyl and the usual η^3-
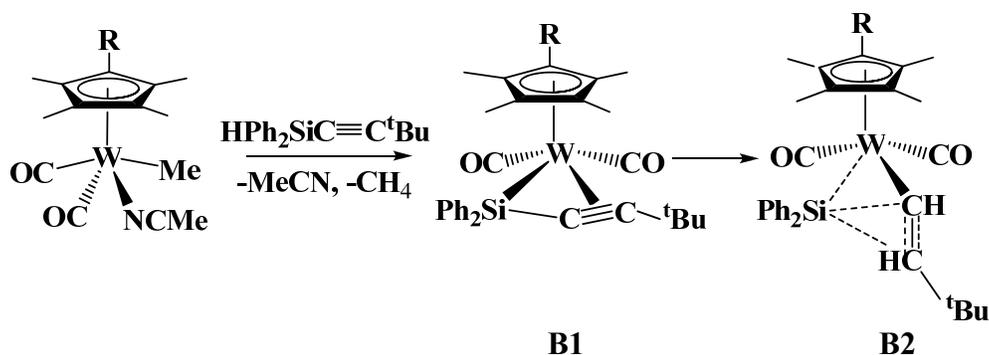
Scheme 2.2. Formation of Cp*(CO)$_2$W(CC^{t}Bu)(SiPh$_2$) **B2**

allyl complexes and to clarify the reasons why **A1** was isolated but **B1** was not, and why **B2** was isolated but the similar vinyl silylene complex Cp*(CO)$_2$W(CHCMe$_2$)(SiMe$_2$) **A2** was not.

In the present work, we theoretically investigated the geometries and bonding nature of Cp(CO)$_2$W(η^3-H$_2$SiCHCH$_2$) **1** and Cp(CO)$_2$W(CHCH$_2$)(SiH$_2$) **2**, and the conversion reaction of **1** to **2** with the DFT, MP2 to MP4(SDTQ), and CCSD(T) methods, where **1** and **2** were adopted as models of **A1** and **A2**, respectively. Our main purposes here are (1) to clarify characteristic features of the geometry and bonding nature of **1** in comparison with its carbon analogue, Cp(CO)$_2$W(η^3-H$_2$CCHCH$_2$) **1C** and η^3-1-silapropargyl analogue, Cp(CO)$_2$W(η^3-H$_2$SiCCH) **3**, where **3** was adopted as a model of **B1**, (2) to evaluate the relative stabilities of **1** and **2**, and (3) to clarify the reasons why Cp(CO)$_2$W(η^3-H$_2$SiCHCH$_2$) **1** was isolated but the similar tungsten η^3-silapropargyl complex Cp(CO)$_2$W(η^3-H$_2$SiCCH) **3** was not and why the tungsten vinyl silylene complex Cp(CO)$_2$W(CHCH$_2$)(SiH$_2$) **2** was not isolated but the similar tungsten acetylide silylene complex Cp(CO)$_2$W(CCH)(SiH$_2$) **4** was isolated, where **4** was investigated as a model of **B2**.

2.2   Computational Details

Geometries were optimized with the density functional theory (DFT), where the B3PW91 [8, 9] functional was adopted for the exchange-correlation terms. This is because the optimized geometry of the similar complex Cp(CO)$_2$W(CCR)(SiR$_2$) by the B3PW91 functional agrees well with the experimental one [6] but the geometry optimized by the B3LYP functional [8, 10] is somewhat different from the experimental one, as we reported recently [7]. We ascertained that each equilibrium geometry did not exhibit any imaginary frequency and each transition state exhibited only one imaginary frequency. Energy was

evaluated with the DFT, MP2 to MP4(SDTQ), and CCSD(T) methods, where the DFT-optimized geometries were adopted.

Two kinds of basis set systems, BS-I and BS-II, were used in this work. In BS-I, usual LANL2DZ [11] basis set was used for W, the cc-pVDZ basis sets [12] were used for Si, C, and O atoms, and the 6-31G basis set was used for H [13] This BS-I system was employed for geometry optimization. In BS-II, valence electrons of W were represented with the (541/541/111/1) basis set [11, 14, 15] with the same effective core potentials as those of LANL2DZ. The same basis sets as those of BS-I were used for the other atoms. This BS-II system was employed to evaluate energy changes.

Gaussian 03 program package [16] was used for all these computations. Laplacian of electron density was evaluated with MOLDEN program package (version 4.6) [17] and molecular orbitals were drawn with MOLEKEL program package (version 4.3) [18].

2.3   Results and Discussion

In this chapter, we wish to discuss first the geometries and bonding nature of $Cp(CO)_2W(\eta^3\text{-}H_2SiCHCH_2)$ **1** and $Cp(CO)_2W(CHCH_2)(SiH_2)$ **2**, and then discuss the conversion reaction of **1** to **2** in comparison with the conversion of $Cp(CO)_2W(\eta^3\text{-}H_2SiCCH)$ **3** to $Cp(CO)_2W(CCH)(SiH_2)$ **4**. Finally, we will discuss the reasons why **1** was isolated but **3** was not.

2.3.1   Geometry and Bonding Nature of $Cp(CO)_2W(\eta^3\text{-}H_2SiCHCH_2)$ 1

The optimized geometry of $Cp(CO)_2W(\eta^3\text{-}H_2SiCHCH_2)$ **1** agrees with the experimental one [5] where the W-Si and W-C2 distances are moderately shorter and the W-C1, Si-C1, and
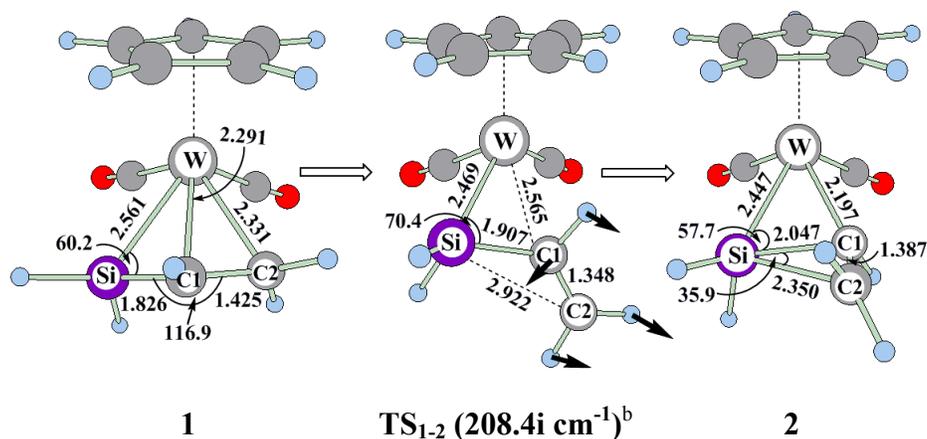
Figure 2.1. Geometry[a] changes by the conversion reaction of $Cp(CO)_2W(\eta^3\text{-}H_2SiCHCH_2)$ **1** to $Cp(CO)_2W(CHCH_2)(SiH_2)$ **2**.
[a] The DFT/BS-I method was used. Bond lengths are in angstroms and bond angles are in degree. [b] Imaginary frequency is given in parenthesis. Arrows in **TS$_{1-2}$** represent important movements of atoms in imaginary frequency.

C1-C2 distances are moderately longer than the corresponding experimental values; see Figure 2.1 and Table 2.1 for important geometrical parameters. Introduction of Me groups on the C2 and Si atoms leads to excellent agreement of the optimized geometry with the experimental one (see Table 2.1). The W-Si and W-C2 distances in **1** are moderately longer than those of **3** by 0.033 Å and 0.022 Å, respectively, and the W-C1 distance of **1** is

Table 2.1. Selected optimized parameters[a] of $Cp(CO)_2W(\eta^3\text{-}R^2_2SiCHCR^1_2)$ (R^1=H or Me; R^2=H or Me)

	1 (R^1=H, R^2=H)	**1-Mea** (R^1=Me, R^2=H)	**1-Meb** (R^1=Me, R^2=Me)	Expt.[b] (R^1=Me, R^2=Me)
W-Si	2.561	2.549	2.581	2.571
W-C1	2.291	2.303	2.293	2.281
W-C2	2.331	2.454	2.427	2.419
Si-C1	1.826	1.833	1.835	1.801
C1-C2	1.425	1.424	1.427	1.410
<SiC1C2	116.9	120.9	123.9	122.0

[a] DFT(B3PW91)/BS-I method was used. Bond lengths are in angstroms, and bond angles are in degrees. [b] Ref. 5.
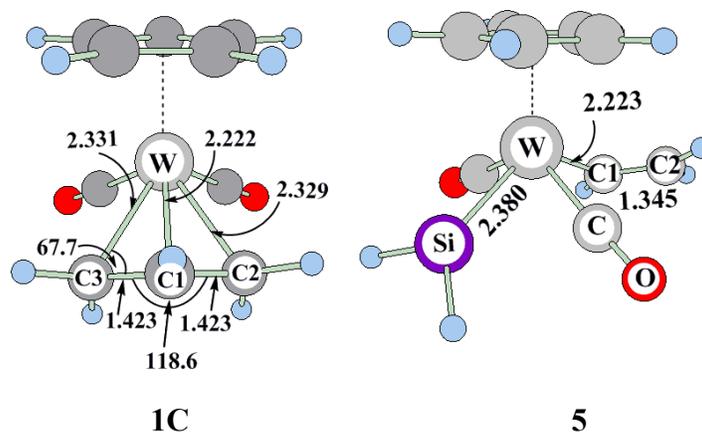
Figure 2.2. Geometries[a] of Cp(CO)$_2$W(η^3-H$_2$CCHCH$_2$) **1C** and Cp(CO)$_2$W(CHCH$_2$)(SiH$_2$) **5**.

[a] The DFT/BS-I method was used. Bond lengths are in angstroms and bond angles are in degrees.

considerably shorter than that of **3** by 0.133 Å (see Ref. 7 for the optimized geometry of **3**). This significantly shorter W-C1 distance in **1** suggests that the W-C1 interaction is stronger in **1** than in **3**. The SiC1C2 angle of **1** is smaller than that of **3** by 23.1°, because the C1 atom takes sp^2-hybridization in **1** but sp-hybridization in **3**.

For a better understanding of the geometry and bonding nature of **1**, we optimized tungsten η^3-allyl complex, Cp(CO)$_2$W(η^3-H$_2$CCHCH$_2$) **1C**, as shown in Figure 2.2. The C1-C2, W-C1, and W-C2 distances and the SiC1C2 angle of **1** are almost the same as those of **1C**.

Laplacian of electron density provides clear information of the bonding characteristics [19-22]. The Laplacian plot on the Si-C1-C2 plane of **1** indicates accumulation of electron density between C1 and C2 atoms but little accumulation of electron density between Si and C1 atoms, as shown in Figure 2.3(A), where red lines represent accumulation of electron density and blue lines represent depletion of electron density. On the other hand, the Laplacian plot on the C1-C2-C3 plane of **1C** represents accumulation of electron density between C1 and C2 atoms and between C1 and C3 atoms (Figure 2.3(B)). These results

indicate that the Si-C1 interaction in **1** is much weaker than the C3-C1 one in **1C** and that the
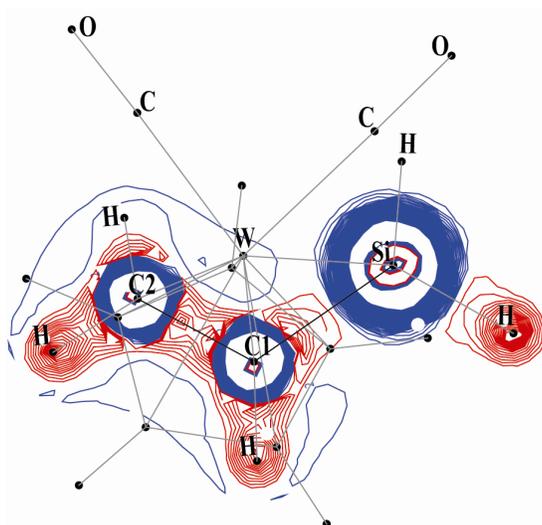
Si-C1-C2 plane

(A) Cp(CO)$_2$W(η^3-H$_2$SiCHCH$_2$) 1
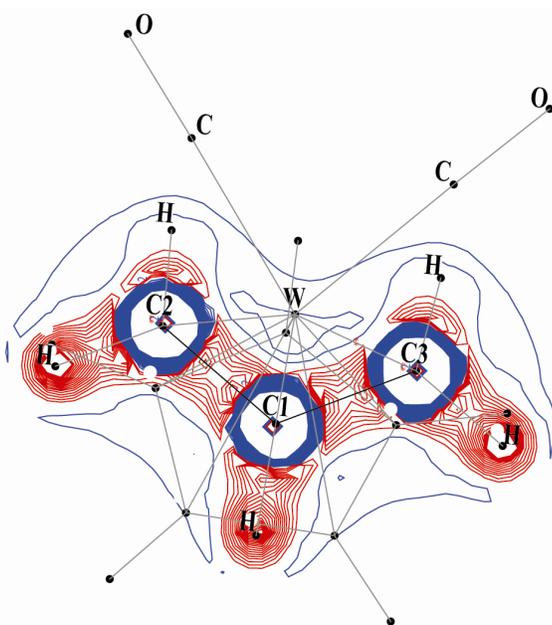
C3-C1-C2 plane

(B) Cp(CO)$_2$W(η^3-H$_2$CCHCH$_2$) 1C

Figure 2.3. Laplacian of electron density on the Si-C1-C2 plane in Cp(CO)$_2$W(η^3-H$_2$SiCHCH$_2$) **1** and on the C3-C1-C2 plane in Cp(CO)$_2$W(η^3-H$_2$CCHCH$_2$) **1C**. Contour values are 0.0, ±0.1, ±0.2,…. Red and blue lines represent accumulation of electron density and depletion of electron density, respectively.

W-Si-C1 plane   **W-C1-C2 plane**

(A) Cp(CO)$_2$W(η^3-H$_2$SiCHCH$_2$) 1

W-C1-C3 plane   **W-C1-C2 plane**

(B) Cp(CO)$_2$W(η^3-H$_2$CCHCH$_2$) 1C
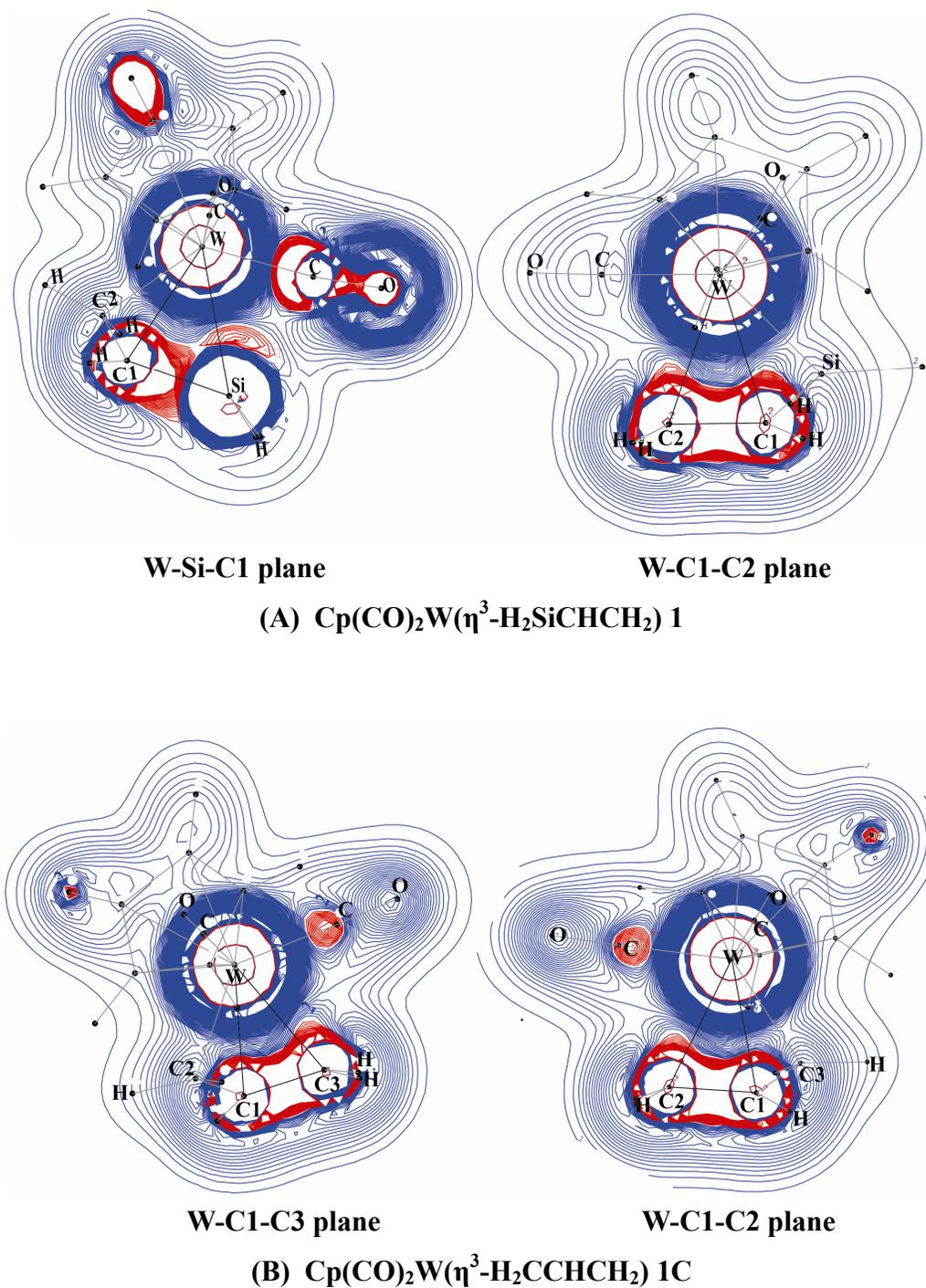
Figure 2.4. Laplacian of electron density on the W-Si-C1 and W-C1-C2 planes of Cp(CO)$_2$W(η^3-H$_2$SiCHCH$_2$) **1** and on the W-C3-C1 and W-C1-C2 planes of Cp(CO)$_2$W(η^3-H$_2$CCHCH$_2$) **1C**. Contour values are 0.0, ±0.01, ±0.02,….. Red and blue lines represent accumulation of electron density and depletion of electron density, respectively.

η^3-allyl moiety is well conjugated but the η^3-silaallyl is not. In **1**, the Laplacian plots of the W-C1-Si and W-C1-C2 planes exhibit that electron accumulation occurs in the separated regions; one is the region between W and the C1-C2 moiety and the other is the region between W and Si atoms, as shown in Figure 2.4(A). In **1C**, on the other hand, electron accumulation occurs in the region between W and the C1-C2-C3 moiety (Figure 2.4(B)); note that the electron accumulation between W and the C1-C2 moiety is combined with that between W and the C1-C3 moiety at the C1 atom. From these results, it is concluded that the interaction between W and η^3-H_2CCHCH_2 is delocalized over three C atoms in **1C** but the interaction between W and η^3-$H_2SiCHCH_2$ is not delocalized but separated into two interactions in **1**; one is the interaction between W and the silyl group and the other is that between W and the vinyl group. In other words, **1** is not a pure tungsten η^3-silaallyl complex but it is a species between η^3-silaallyl and η^3-silylvinyl complexes.

These features presented by the Laplacian plots should be reflected in molecular orbitals. As shown in Figures 2.5(A) and 2.5(B), the HOMO and HOMO-1 of **1** mainly consist of d orbitals like those of **1C**. The remaining three d-orbitals are unoccupied in both **1** and **1C**, which is consistent with the +2 oxidation state of W (d^4 system) in **1** and **1C**. The HOMO-2 and HOMO-5 are important in **1** because these two orbitals include the bonding interaction between the $H_2SiCHCH_2$ moiety and the W center. To discuss these bonding orbitals, we will first examine frontier orbitals of the 1-silaallyl group $\cdot H_2SiCHCH_2$ and the usual allyl group, $\cdot H_2CCHCH_2$ (see Figures 2.6(A) and 2.6(B)). The SOMO of both $\cdot H_2SiCHCH_2$ and $\cdot H_2CCHCH_2$ is a non-bonding π orbital ($\varphi_{n\pi}$), which consists of p orbitals of terminal C2 and Si (or C3) atoms. It is noted that the $\varphi_{n\pi}$ of $\cdot H_2SiCHCH_2$ is much different from that of $\cdot H_2CCHCH_2$, as follows: The $\varphi_{n\pi}$ of $\cdot H_2CCHCH_2$ is symmetrical; in other words, the p
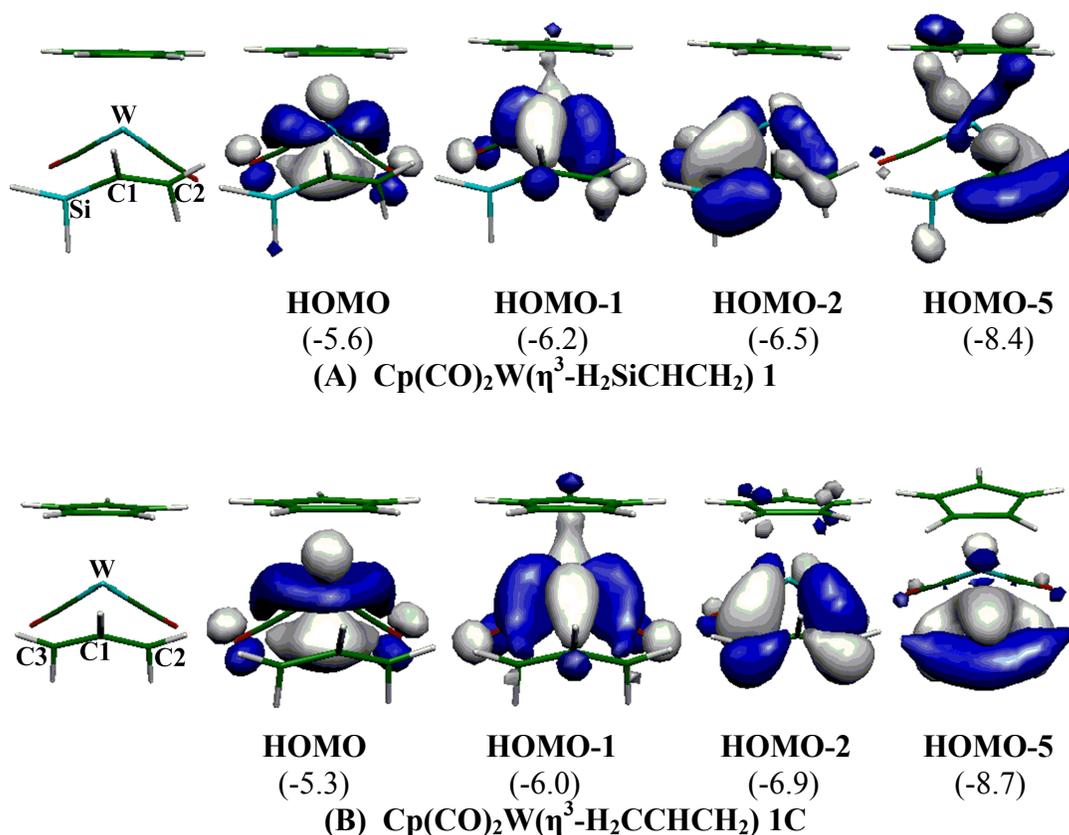
Figure 2.5. Several important Kohn-Sham orbitals in $Cp(CO)_2W(\eta^3-H_2SiCHCH_2)$ **1** and $Cp(CO)_2W(\eta^3-H_2CCHCH_2)$ **1C**. Kohn-Sham orbital energies (in eV unit) are given in parentheses.

orbitals of terminal C atoms contribute to the $\varphi_{n\pi}$ to the same extent (Figure 2.6(A)). On the other hand, the p orbital of Si more contributes to the $\varphi_{n\pi}$ than that of terminal C2 in $\cdot H_2SiCHCH_2$ (Figure 2.6(B)). This is because the p orbital of $\cdot SiH_3$ is at much higher energy (-5.39 eV) than that of $\cdot CH_3$ (-6.41 eV), where orbital energies are calculated with the DFT/BS-II method; note that Hartree-Fock orbitals show similar energy difference between them [23]. The $\varphi_{n\pi}$ orbitals of $\cdot H_2SiCHCH_2$ and $\cdot H_2CCHCH_2$ overlap with the SOMO of $\cdot Cp(CO)_2W$ (Figure 2.6D) in a bonding way to form the HOMO-2 of **1** and **1C**. Because the Si p orbital more contributes to the $\varphi_{n\pi}$ than the C p orbital, the W-Si overlap is much larger
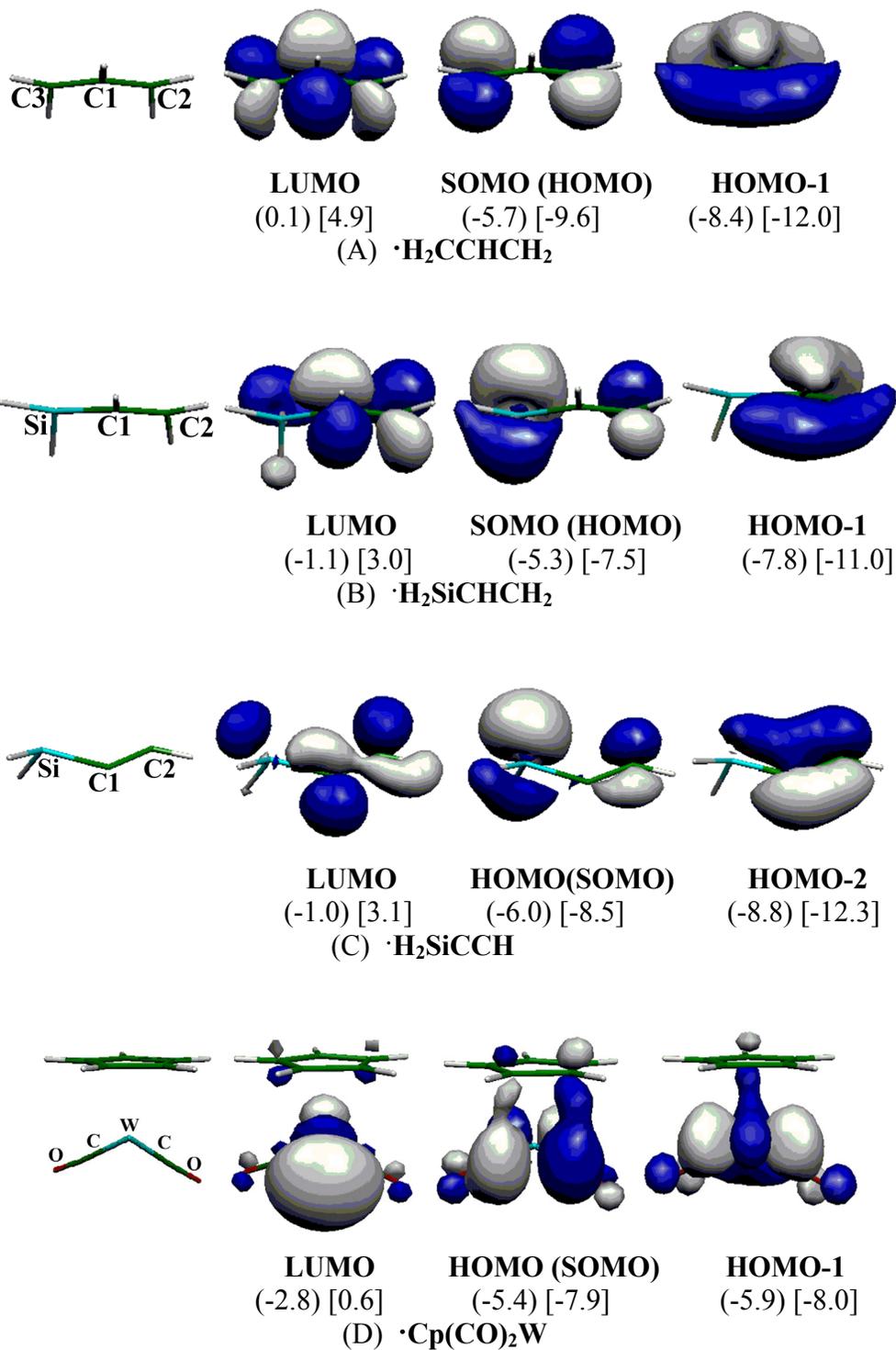
Figure 2.6. Several important Kohn-Sham orbitals in the fragments $\cdot H_2CCHCH_2$, $\cdot H_2SiCHCH_2$, $\cdot H_2SiCCH$, and $\cdot Cp(CO)_2W$. Kohn-Sham and HF orbital energies (in eV unit) are given in parentheses and brackets, respectively.

81

than the W-C2 overlap in the HOMO-2 of **1**. On the other hand, the W-C2 overlap is the same as the W-C3 overlap in the HOMO-2 of **1C**.

The HOMO-1 of both $\cdot$H$_2$SiCHCH$_2$ and $\cdot$H$_2$CCHCH$_2$ is a bonding π orbital (φ_π) but significantly large difference is observed between them, as follows: The p orbitals of all three C atoms contribute to the φ_π, and therefore, the φ_π is well delocalized in $\cdot$H$_2$CCHCH$_2$ (Figure 2.6(A)). On the other hand, the p-orbital of Si contributes much less to the φ_π than that of C3 (Figure 2.6(B)). As a result, the conjugation between Si and C atoms is very weak in the φ_π of $\cdot$H$_2$SiCHCH$_2$. This is interpreted in terms of orbital energy and orbital overlap; because the $\varphi_{n\pi}$ is at much higher energy than the φ_π and the Si p orbital is at much higher energy than that of C, as described above, the Si p orbital contributes much more to the $\varphi_{n\pi}$ but much less to the φ_π than that of C. Also, the longer Si-C bond distance than the C-C distance leads to smaller overlap between the Si p and C p orbitals. Certainly, the Laplacian of electron density shows much smaller conjugation between Si and C1 atoms in **1** than that between C1 and C3 atoms in **1C**, as discussed above. This φ_π orbital of $\cdot$H$_2$SiCHCH$_2$ and $\cdot$H$_2$CCHCH$_2$ overlaps with the acceptor orbital (LUMO) of $\cdot$Cp(CO)$_2$W (Figure 2.6(D)) in a bonding way to form the HOMO-5 of **1** and **1C**. Because the π orbital of the C=C double bond much more contributes to the φ_π of $\cdot$H$_2$SiCHCH$_2$ than the Si p orbital, the HOMO-5 of **1** is considerably different from that of **1C**, as shown in Figures 2.5(A) and 2.5(B). Apparently, the HOMO-5 of **1** mainly contains the coordinate bond of the C=C double bond with the empty d orbital of W. On the other hand, the φ_π of $\cdot$H$_2$CCHCH$_2$ interacts with the empty d orbital of W in **1C** to form the delocalized bonding interaction between the W center and three C atoms. In conclusion, the η^3-H$_2$SiCHCH$_2$ interacts with the W center through the coordinate bonds of the C=C π orbital and Si p orbital with the LUMO of Cp(CO)$_2$W in **1**, while the η^3-

H$_2$CCHCH$_2$ interacts with the W center through the coordinate bonds of delocalized $\varphi_{n\pi}$ and φ_π orbitals with the LUMO of Cp(CO)$_2$W in **1C**. These results are consistent with the Laplacian plots of **1** and **1C**, as discussed above.

The HOMO-1 of **1C** consists of the bonding overlap between the π^* orbital (φ_{π^*}) of η^3-allyl group and the HOMO-1 of ·Cp(CO)$_2$W. This is typical π-back donation interaction. On the other hand, the π-back donation of **1** is much different from that of **1C**, as follows: The Si p orbital little contributes to the HOMO-1 of **1**. This is because the Si p orbital largely contributes to the $\varphi_{n\pi}$ of ·H$_2$SiCHCH$_2$ but little to the φ_{π^*} of ·H$_2$SiCHCH$_2$ (Figure 2.6(B)). Thus, the HOMO-1 of **1** is understood in terms of the π-back donation from the occupied d orbital of W to the π^* orbital of the C=C double bond.

These features relate to the geometry of **1** as follows: The Si-C1 (1.826 Å) and C1-C2 (1.425 Å) bond distances in **1** are intermediate between the Si-C single and the Si=C double bonds and between the C-C single and C=C double bonds, respectively; R(Si-C) = 1.895 Å, R(Si=C) = 1.717 Å, R(C-C) = 1.542 Å, and R(C=C) = 1.334 Å, where the DFT/BS-I optimized values are presented [24].

From these results, the following conclusions are presented; (1) The Si p orbital more contributes to the $\varphi_{n\pi}$ than the C p orbital. (2) The Si p orbital little contributes to the φ_π, indicating that the φ_π is understood in terms of the π orbital between two C atoms. (3) As a result, the π-conjugation between Si and C atoms is much smaller than that of the η^3-allyl group. (4) Complex **1** is understood to be a species between η^3-vinylsilyl and η^3-1-silaallyl complexes. And, (5) these features arise from the fact that the p orbital of Si is at higher energy than that of C and the Si-C distance is longer than the C-C distance.

2.3.2 Geometry and Bonding Nature of Cp(CO)$_2$W(CHCH$_2$)(SiH$_2$) 2

Cp(CO)$_2$W(CCH)(SiH$_2$) **4** is understood to be a tungsten acetylide silylene complex in which charge transfer (CT) occurs from the π orbital of the acetylide moiety to the empty p orbital of the silylene and simultaneously the reverse CT occurs from the sp^2 lone-pair orbital of the silylene to the π* orbital of the acetylide [7]. Though the similar bonding interactions are expected in **2**, several differences are observed between **2** and **4**, as follows: W-C1, Si-C1, and Si-C2 distances in **2** are significantly longer than those of **4** by 0.183 Å, 0.079 Å, and 0.393 Å, respectively (see Figure 2.1 and Ref. 7 for the optimized geometries of **2** and **4**, respectively). The longer W-C1 bond of **2** suggests that the W-vinyl bond in **2** is weaker than the W-acetylide bond in **4**. The significantly longer Si-C1 and Si-C2 distances of **2** suggest that the interaction between the silylene and vinyl groups is much weaker in **2** than that between the silylene and acetylide groups in **4**. On the other hand, the W-Si distance in **2** is significantly shorter than that of **4**, indicating that the W-silylene interaction is stronger in **2** than in **4**. Consistent with these geometrical features, the sp^2 lone pair orbital of silylene expands toward the W center at a small angle of 7.5º with the W-Si bond and at a large angle of 50.2º with the Si-C1 bond in **2**. On the other hand, its direction considerably shifts toward the C1 atom from the W center in **4**; the lone pair orbital makes considerably large angle of 35.4º with the W-Si bond and considerably small angle of 14.3º with the Si-C1 bond. It is worth investigating the reasons why the geometry of **2** is much different from that of **4**, because these features deeply relate to the reason why **2** cannot be isolated.

The Laplacian plots on the Si-C1-C2 plane clearly show that the electron accumulation between silylene and vinyl groups in **2** is smaller than that between silylene and acetylide groups in **4** (Figure 2.7). These results indicate that the interaction between the silylene and

84

Si-C1-C2 plane

(A) Cp(CO)$_2$W(CHCH$_2$)(SiH$_2$) 2

Si-C1-C2 plane
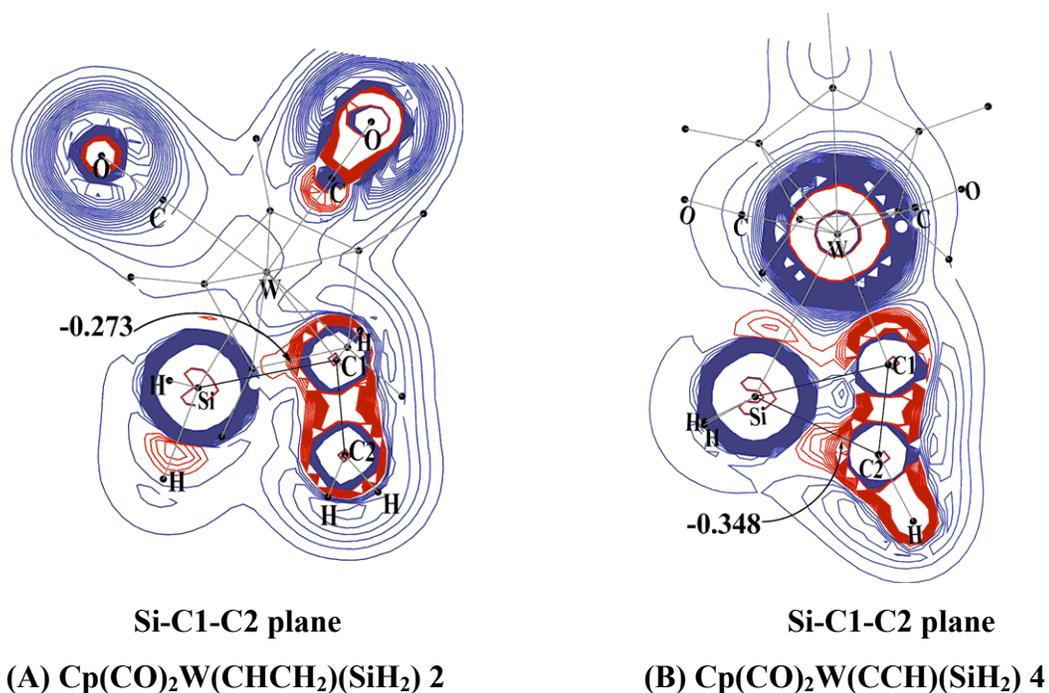
(B) Cp(CO)$_2$W(CCH)(SiH$_2$) 4

Figure 2.7. Laplacian of electron density on the Si-C1-C2 plane of Cp(CO)$_2$W(CHCH$_2$)(SiH$_2$) **2** and Cp(CO)$_2$W(CCH)(SiH$_2$) **4**. Contour values are 0.0, ±0.025, ±0.05,…… Red and blue lines represent accumulation of electron density and depletion of electron density, respectively. Values (in a.u) in negative region are given in parentheses.

vinyl groups in **2** is weaker than that between silylene and acetylide groups in **4**. The Laplacian plot on the W-Si-C1 plane (Figure 2.8A and B) shows that the electron accumulation between the W center and silylene is larger in **2** than in **4**, indicating that the W-silylene bond is stronger in **2** than in **4**. Also, the electron accumulation between the W center and the acetylide group in **4** is larger than that between the W center and the vinyl group in **2** (Figure 2.8A and B). This result suggests that the W-acetylide interaction in **4** is stronger than the W-vinyl one in **2**.

The HOMO and HOMO-1 of **2** mainly consist of a W d orbital. The presence of these two doubly occupied d orbitals is consistent with the +2 oxidation state of W (d^4 system).

W-Si-C1 plane   **W-C1-C2 plane**

(A) Cp(CO)$_2$W(CHCH$_2$)(SiH$_2$) 2

W-Si-C1 plane   **W-C1-C2 plane**

(B) Cp(CO)$_2$W(CHCH$_2$)(SiH$_2$) 4
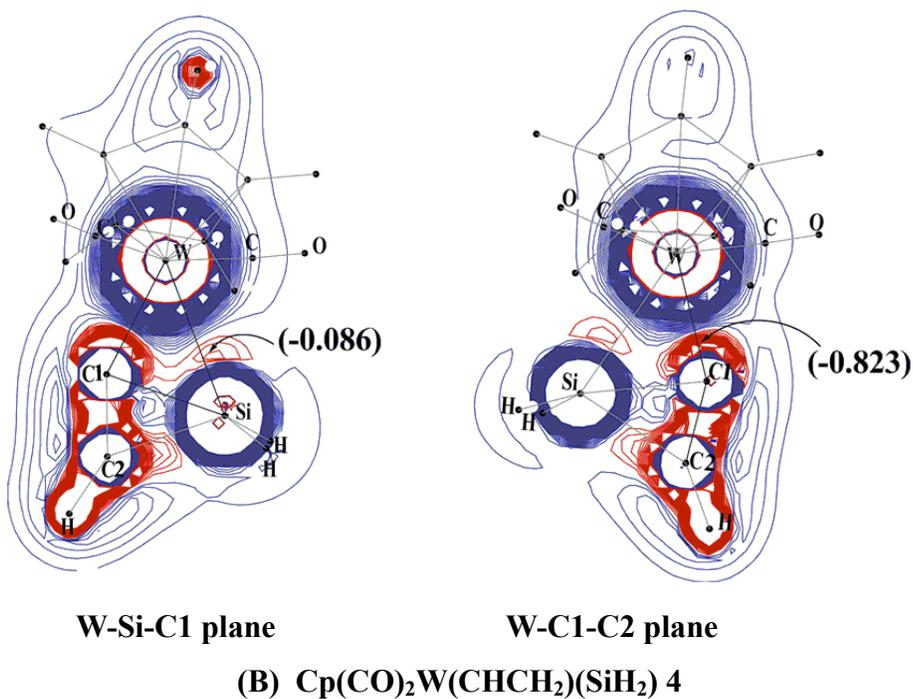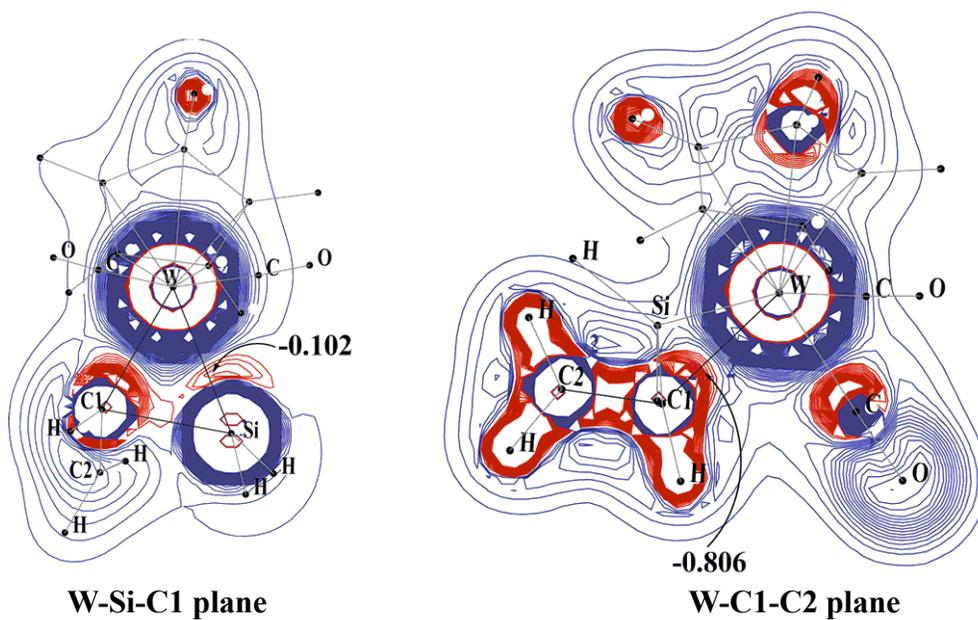
Figure 2.8. Laplacian of electron density on the W-Si-C1 and W-C1-C2 planes of Cp(CO)$_2$W(CHCH$_2$)(SiH$_2$) **2** and Cp(CO)$_2$W(CCH)(SiH$_2$) **4**. Contour values are 0.0, ±0.025, ±0.050,….Red and blue lines represent accumulation of electron density and depletion of electron density, respectively. Values (in a.u) in negative region are given in parentheses.
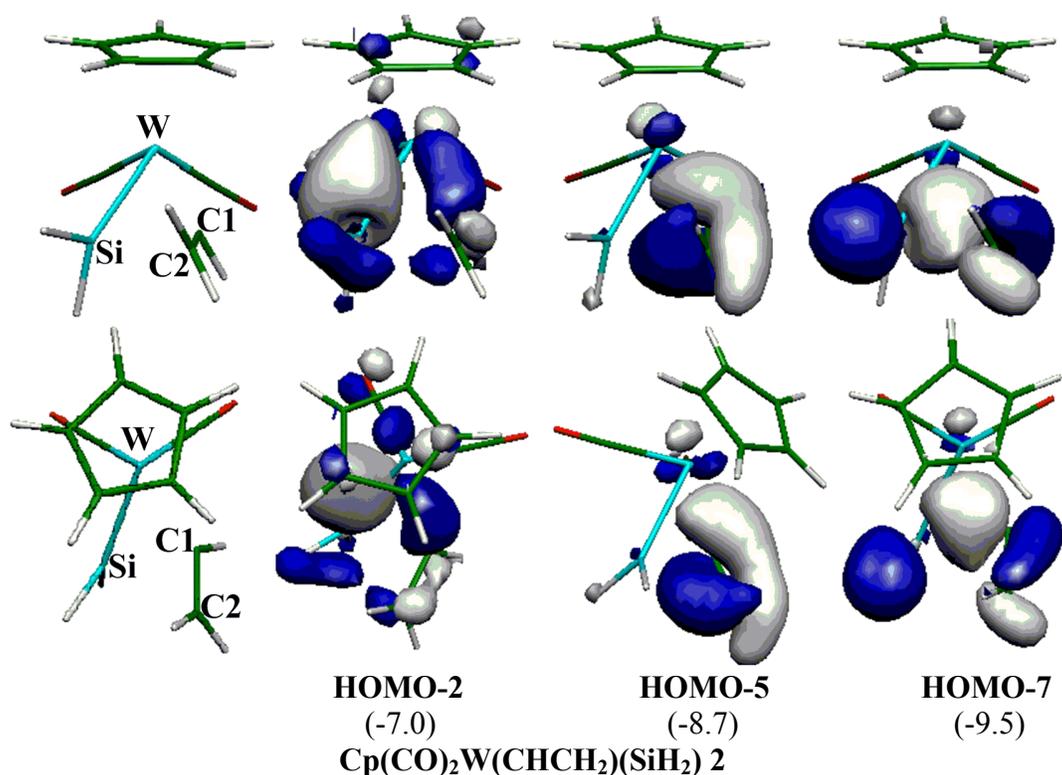
Figure 2.9. Several important Kohn-Sham orbitals in Cp(CO)$_2$W(CHCH$_2$)(SiH$_2$) **2**. In parentheses are orbital energies (in eV unit).

The HOMO-2 and HOMO-7 include the bonding interactions of the W center with the silylene and vinyl groups, as shown in Figure 2.9. Both are somewhat different from the corresponding HOMO-2 and HOMO-6 of **4** (see Ref. 7 for the orbital pictures of **4**). The HOMO-2 of **2** mainly consists of the bonding overlap between the empty d orbital of W and the sp^2 lone pair orbital of silylene. However, bonding interaction is little observed between silylene and vinyl groups in this HOMO-2, while the considerably large bonding overlap between silylene and acetylide groups is observed in the HOMO-2 of **4**. This significant difference in HOMO-2 between **2** and **4** is consistent with the much smaller accumulation of electron density between silylene and vinyl groups in **2** than that between silylene and acetylide groups in **4**, as described above and in Figure 2.7. Moreover, the sp^2 lone pair
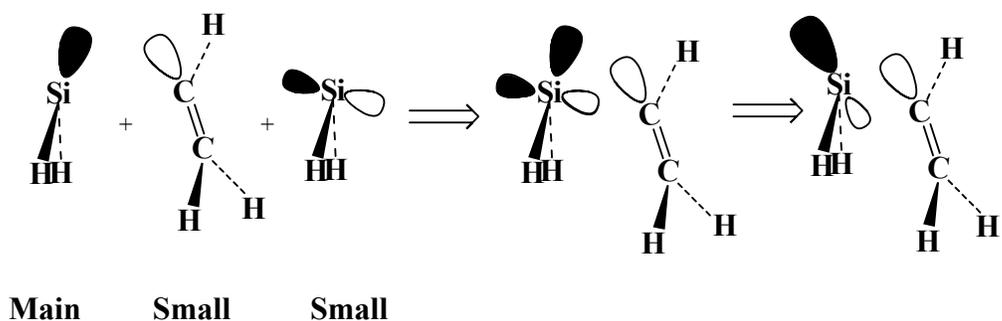
(A) HOMO-2
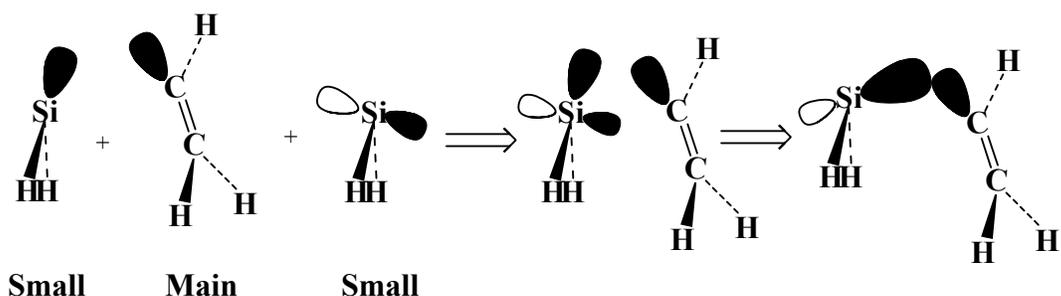
(B) HOMO-7

Scheme 2.3

orbital of silylene expands outside the W-Si-C1 triangle in **2** unlike that of **4**. In the HOMO-7

of **2**, the bonding overlap is observed between Si and C1 atoms, while its position is different

from both the sp^2 lone pair and empty p orbitals of silylene. These features of the HOMO-2

and HOMO-7 are interpreted in terms of orbital interactions among the sp^2 lone pair and

empty p orbitals of the silylene group and the sp^2 lone pair orbital of the vinyl group as

follows: The sp^2 lone pair orbital of the silylene overlaps with the sp^2 lone pair orbital of the

vinyl group in an anti-bonding way. Into this anti-bonding overlap, the empty p orbital of the

silylene mixes in a bonding way with the sp^2 lone pair orbital of the vinyl group, as shown in

Scheme 2.3(A), because the empty p orbital of the silylene is at higher energy than the anti-

bonding overlap; the sp^2 lone pair and empty p orbitals of SiH_2 are at -6.2 eV and -3.2 eV,

respectively, and the sp^2 lone pair of $\cdot CHCH_2$ is at -7.9 eV, where the Kohn-Sham orbital

88

energies are presented [25]. These orbital mixings lead to formation of the HOMO-2. In the bonding counterpart of the HOMO-2, the sp^2 lone pair orbital of the vinyl group overlaps with the sp^2 lone pair orbital of the silylene in a bonding way, into which the empty p orbital of the silylene mixes in a bonding way, as shown in Scheme 2.3(B), because the empty p orbital of silylene is at higher energy than the sp^2 lone pair orbitals of the vinyl and silylene groups. These orbital mixings lead to formation of the HOMO-7. In other words, in **2**, the sp^2 lone pair orbital of the vinyl group participates in the CT interaction with the silylene group, whereas the π orbital of the vinyl group little participates in the CT with the silylene. In **4**, on the other hand, both π and π^* orbitals of the acetylide group participate in CT interaction with the silylene group, as discussed previously [7]. The reason of these significant differences between **2** and **4** can be understood in terms of the differences in geometry between the vinyl and acetylide groups, which will be discussed below.

From above discussed geometrical features, Laplacian of electron density, and orbital pictures, it is clearly concluded that **2** can be understood as a tungsten vinyl silylene complex in which the CT interaction between the vinyl and silylene groups is weak.

2.3.3 Relative Stabilities of Cp(CO)$_2$W(η^3-H$_2$SiCHCH$_2$) 1 and Cp(CO)$_2$W(CHCH$_2$)(SiH$_2$) 2 and Conversion Reaction of 1 to 2

Before starting to discuss the relative stabilities and the activation barrier of the conversion reaction of **1** to **2**, we wish to examine briefly what computational method presents reliable results of energy change. The CCSD(T) and DFT methods present similar activation barrier, as shown in Table 2.2, while the MP4(SDTQ) method presents moderately larger activation barrier than the CCSD(T) and DFT methods; see Table 2.2. Moreover, the

Table 2.2. Activation barriers $(E_a)^a$ and reaction energies $(\Delta E)^a$ of the conversion reactions of $Cp(CO)_2W(\eta^3\text{-}H_2SiCHCH_2)$ **1** to $Cp(CO)_2W(CHCH_2)(SiH_2)$ **2** and of $Cp(CO)_2W(\eta^3\text{-}H_2SiCCH)$ **3** to $Cp(CO)_2W(CCH)(SiH_2)$ **4**.[b]

Method	Conversion reaction of **1** to **2**		Conversion reaction of **3** to **4**[b]	
	E_a^a (kcal/mol)	ΔE^a (kcal/mol)	E_a^a (kcal/mol)	ΔE^a (kcal/mol)
DFT	33.2	20.9	15.3	-4.9
MP2	45.1	26.3	20.7	0.4
MP3	30.8	19.9	14.0	-1.4
MP4(DQ)	35.9	22.6	15.5	-0.1
MP4(SDQ)	35.1	22.2	14.8	-0.9
MP4(SDTQ)	40.6	24.1	18.8	-0.6
CCSD(T)	34.2	21.0	15.8	-0.7

[a] E_a is energy difference between transition state and reactant, and ΔE is energy difference between product and reactant. The BS-II was employed. [b] Ref. 7.

barrier moderately fluctuates around MP2 and MP3 levels and somewhat increases upon going to MP4(SDTQ) level from MP4(SDQ) level. The reaction energy much less depends on the computational methods, while the MP4(SDTQ) method presents larger reaction energy than the CCSD(T) and DFT methods. In the conversion reaction of **3** to **4**, the MP4(SDQ), MP4(SDTQ), and CCSD(T) methods presented similar reaction energy, while the DFT method presented moderately larger exothermicity than the others [7]. From these results, it is concluded that the CCSD(T) method presents reliable results. Here, we present discussion based on the CCSD(T)- and DFT-calculated values.

Complex **1** converts to **2** with a large endothermicity of 21.0 (20.9) kcal/mol (see Table 2.2), where the CCSD(T)- and DFT-calculated values are given without and in parentheses, respectively, hereafter. On the other hand, **3** converts to **4** with a moderate exothermicity of 0.7 (4.9) kcal/mol (Table 2.2). These results clearly indicate that **1** is much more stable than **2** but **3** is moderately less stable than **4**. Consistent with these results of relative stabilities,

tungsten η^3-1-silaallyl/η^3-vinylsilyl complex was isolated experimentally but similar tungsten η^3-1-silapropargyl/η^3-alkynylsilyl complex was not, while tungsten acetylide silylene complex was isolated experimentally but similar tungsten vinyl silylene complex was not.

It is very important to clarify whether **1** easily converts to **2** or not. This reaction takes place via α-Si-C σ-bond activation like the conversion reaction of **3** to **4** [7]. Apparently, the geometry changes by the conversion reaction of **1** to **2** are similar to those of **3** to **4** [7], as shown in Figure 2.1. Thus, we mention only important geometrical changes, here. Upon going to the transition state **TS$_{1-2}$** from **1**, the Si-C1 distance moderately lengthens to 1.907 Å by 0.081 Å and the C1-C2 distance moderately shortens to 1.348 Å by 0.077 Å. The significantly large changes are observed in the orientation of the C1-C2 bond and the W-C2 distance. The direction of the sp^2 orbital of the CH=CH$_2$ group much more changes toward the W center in **TS$_{1-2}$** than that of the sp orbital of C≡CH group in **TS$_{3-4}$**; the WC1C2 angle more increases by 77.7º upon going to **TS$_{1-2}$** from **1**, but it increases by 58.9º upon going to **TS$_{3-4}$** from **3**. This direction change induces the considerably large lengthening of the W-C2 bond in **TS$_{1-2}$**. Also, the W-C1 bond considerably lengthens by 0.274 Å upon going to **TS$_{1-2}$** from **1**, which is in contrast with slight decrease of the W-C1 bond by 0.055 Å upon going to **TS$_{3-4}$** from **3**.

The activation barrier of the conversion reaction of **1** to **2** is calculated to be 34.2 (33.2) kcal/mol (see Table 2.2), while that of the conversion reaction of **3** to **4** is moderate, being 15.8 (15.3) kcal/mol [7]. These results indicate that the tungsten η^3-silaallyl/η^3-vinylsilyl complex **1** is stable unlike the tungsten η^3-silapropargyl/η^3-alkynylsilyl complex **3**. The origin of the large activation barrier of the conversion reaction of **1** to **2** is easily understood by inspecting the geometry changes in **TS$_{1-2}$** and the bonding interactions of **1**. The C=C

double bond coordinates with the W center in **1**, as discussed above, and the coordinate bond is much stronger in **1** than in **3**, which will be discussed below. We already found that the W-C2 bond much more lengthens and the W-C1 bond moderately more lengthens in **TS$_{1-2}$** than in **TS$_{3-4}$**. These geometry changes suggest that the coordinate bond of the C=C double bond with the W center is almost broken in **TS$_{1-2}$**. This bond breaking induces larger energy loss in **TS$_{1-2}$** than in **TS$_{3-4}$**. As a result, the conversion reaction of **1** to **2** needs larger activation barrier than that of **3** to **4**.

2.3.4 Reasons why Cp(CO)$_2$W(η^3-H$_2$SiCHCH$_2$) 1 is Isolated but Cp(CO)$_2$W(η^3-H$_2$SiCCH) 3 is not and why Cp(CO)$_2$W(CCH)(SiH$_2$) 4 is Isolated but Cp(CO)$_2$W(CHCH$_2$)(SiH$_2$) 2 is not

In the conversion reaction of **1** to **2**, the bonding interaction between Cp(CO)$_2$W and η^3-silaallyl/η^3-vinylsily groups and the Si-C bond are broken. The interaction energy between Cp(CO)$_2$W and H$_2$SiCHCH$_2$ moieties is calculated with various methods, as shown in Table

Table 2.3. Interaction energies (INT) calculated between H$_2$SiCHCH$_2$ and Cp(CO)$_2$W moieties in **1** and between H$_2$SiCCH and Cp(CO)$_2$W moieties in **3**.

Method	INT[a] (kcal/mol)	
	1	**3**
DFT	110.3	102.0
MP2	157.5	145.3
MP3	116.8	109.4
MP4(DQ)	131.8	123.3
MP4(SDQ)	131.4	121.8
MP4(SDTQ)	148.7	138.3
CCSD(T)	122.1	112.7

(a) INT = E$_t$ (**1** or **3**) - E$_t$ [·Cp(CO)$_2$W] − E$_t$ [·H$_2$SiCHCH$_2$ or ·H$_2$SiCCH]. The BS-II was employed.

2.3. Though the MP4(SDQ)- and MP4(SDTQ)-calculated values are considerably larger than the DFT- and CCSD(T)-calculated values (see Table 2.3), the CCSD(T)-calculated value is moderately larger than the DFT-calculated value. However, their differences between **1** and **3** are similar in DFT and CCSD(T) methods. Thus, we believe that the reliable discussion can be presented based on DFT- and CCSD(T)-calculated values. This interaction energy in **1** is larger than the interaction energy between $Cp(CO)_2W$ and H_2SiCCH moieties in **3** by 9.4 (8.3) kcal/mol (see Table 2.3). The reason is easily understood, as follows: The SOMOs of $\cdot H_2SiCHCH_2$ and $\cdot H_2SiCCH$ are the $\varphi_{n\pi}$ orbital, which overlaps with the d orbital (SOMO) of W to form the HOMO-2 of both **1** and **3** (see Figure 2.5A and Figure 2.10 for orbital pictures

| HOMO | HOMO-1 | HOMO-2 | HOMO-6 |
| (-5.3) | (-6.1) | (-7.2) | (-9.7) |
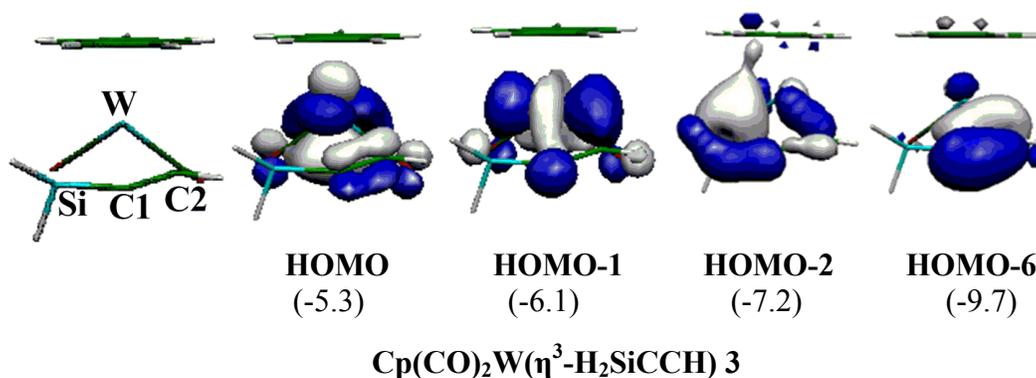
$Cp(CO)_2W(\eta^3\text{-}H_2SiCCH)$ **3**

Figure 2.10. Several important Kohn-Sham orbitals in $Cp(CO)_2W(\eta^3\text{-}H_2SiCCH)$ **3**. In parentheses are the Kohn-Sham orbital energies (in eV unit). Ref. 7.

of **1** and **3**, respectively). The SOMO (-5.3 eV) of $\cdot H_2SiCHCH_2$ is at moderately higher energy than that (-6.0 eV) of $\cdot H_2SiCCH$, where the Kohn-Sham orbital energies are presented (see Figure 2.6B and C). The SOMO of $\cdot Cp(CO)_2W$ is at energy of -5.4 eV, which is between

SOMO energies of $\cdot H_2SiCHCH_2$ and $\cdot H_2SiCCH$ (see Figure 2.6D). The covalent bond energy ΔE_{cov} is approximately represented by eq 2.1, where ε_A and ε_B are orbital energies of the SOMOs and β is resonance integral. This eq 2.1 indicates that the covalent bond energy

$$\Delta E_{cov} = \left| \varepsilon_B - \varepsilon_A \right| + \beta^2 / \left| \varepsilon_B - \varepsilon_A \right| \qquad (2.1)$$

increases with increase in the energy difference between two SOMOs. Because the energy difference between the SOMOs of $\cdot H_2SiCHCH_2$ and $\cdot Cp(CO)_2W$ is not different very much from that between the SOMOs of $\cdot H_2SiCCH$ and $\cdot Cp(CO)_2W$, it is likely that the W-Si bond energy is similar in **1** and **3**. The HOMO-1 of $\cdot H_2SiCHCH_2$ and the HOMO-2 of $\cdot H_2SiCCH$ are the φ_π orbital, which overlaps with the empty d orbital (LUMO) of $\cdot Cp(CO)_2W$ in a bonding way to form HOMO-5 of **1** and HOMO-7 of **3**, as discussed above. Because this is CT interaction and the φ_π orbital (-7.8 eV) of $\cdot H_2SiCHCH_2$ is at higher energy than that of $\cdot H_2SiCCH$ (-8.8 eV), the W-(C=C) coordinate bond of **1** is stronger than the W-(C≡C) coordinate bond of **3**. The HOMO-1 mainly includes the π back-donation interaction in **1** and **3**. This is formed by CT from the doubly occupied d orbitals (HOMO-1) of $\cdot Cp(CO)_2W$ to the π^* orbital of $\cdot H_2SiCHCH_2$ and $\cdot H_2SiCCH$. The LUMO (-1.1 eV) of $\cdot H_2SiCHCH_2$ is at similar energy to that (-1.0 eV) of $\cdot H_2SiCCH$ (see Figure 2.6B and C). Thus, the π back-donation contributes similarly to the coordinate bonds of **1** and **3**. From these results, it is concluded that the stronger CT from the π orbital of vinyl to the d orbital of W is responsible for the stronger interaction between $Cp(CO)_2W$ and $H_2SiCHCH_2$ moieties than that between $Cp(CO)_2W$ and H_2SiCCH moieties.

Table 2.4. Si-C bond energies (E_{Si-C}) in $H_3SiCHCH_2$ and H_3SiCCH.[a]

Method	E_{Si-C}[b] (kcal/mol)	
	$H_3SiCHCH_2$	H_3SiCCH
DFT	50.6	86.4
MP2	60.6	101.9
MP3	54.5	90.4
MP4(DQ)	52.9	89.2
MP4(SDQ)	52.8	89.6
MP4(SDTQ)	57.4	95.6
CCSD(T)	46.8	83.3

[a] Geometry is the same as that in **1** and **3** (see Appendix A.2.1 for the geometries).
[b] $E_{Si-C} = E_t$ ($H_3SiCHCH_2$ or H_3SiCCH)- E_t (·SiH_3)- E_t (·$CHCH_2$ or ·CCH).

On the other hand, the Si-C bond is considerably stronger in H_3SiCCH by 36.5 (35.8) kcal/mol than in $H_3SiCHCH_2$ (see Table 2.4), where the geometries of H_3SiCCH and $H_3SiCHCH_2$ were taken to be the same as those of **1** and **3** [26]. This is easily interpreted in terms of the SOMO energies of ·$CHCH_2$ (sp^2 lone pair orbital) and ·CCH (sp lone pair orbital). The SOMO (-7.7 eV) of ·$CHCH_2$ is at much higher energy than that (-10.1 eV) of ·CCH, where the Kohn-Sham orbital energies are presented [27]. The SOMO of ·SiH_3 is at -5.5 eV [27]. Because the energy difference in SOMO between ·$CHCH_2$ and ·SiH_3 is considerably smaller than that between ·CCH and ·SiH_3, the Si-C bond is considerably weaker in $H_3SiCHCH_2$ than that of H_3SiCCH; see eq 2.1.

The W-silylene and the W-acetylide interactions in **4** are different very much from the usual W-silylene and W-acetylide bonds, because considerably strong silylene-acetylide interaction is formed in **4**. Thus, we evaluated the W-silylene, W-vinyl, and silylene-vinyl interaction energies in **2** and the W-silylene, W-acetylide, and silylene-acetylide interaction energies in **4** in an approximate manner, as shown in Scheme 2.4; for instance, when the vinyl
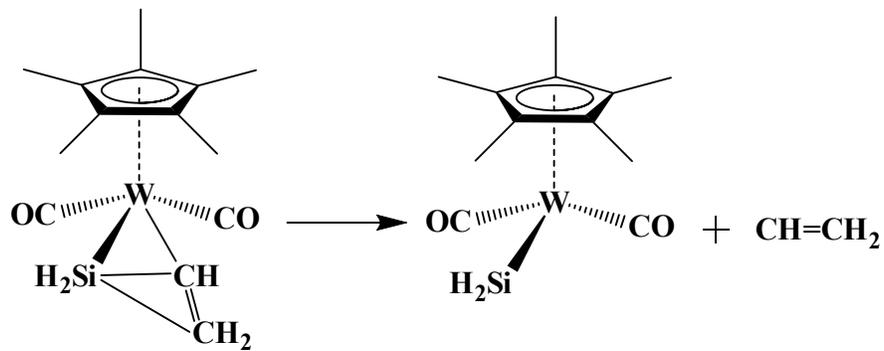
(A) ΔE = DE (W-CH=CH₂) + DE (SiH₂-CH=CH₂)
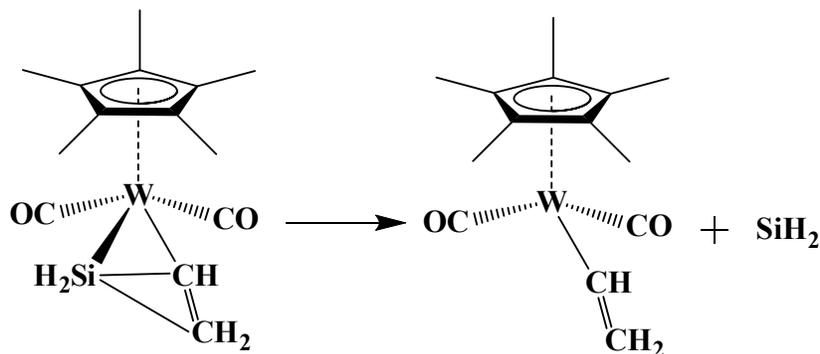
(B) ΔE = DE (W-SiH₂) + DE (SiH₂-CH=CH₂)
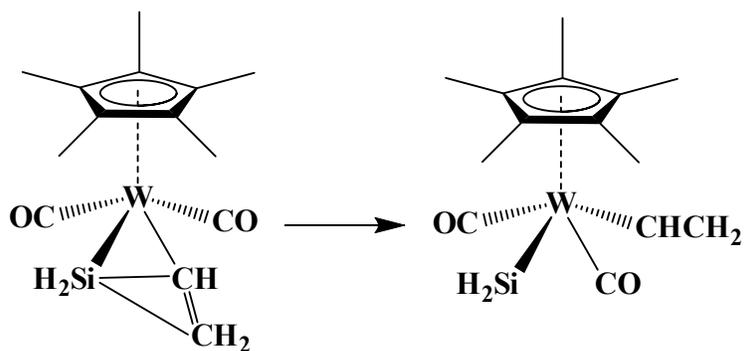
2 **2'**
(C) ΔE = DE (SiH₂-CH=CH₂) = E(2) – E(2')

Scheme 2.4

moiety is eliminated from **2**, the W-vinyl and the silylene-vinyl interactions are broken. Thus, the energy loss corresponds to the sum of the W-vinyl and the silylene-vinyl bonding interactions, as shown in Scheme 2.4(A). The silylene-vinyl interaction was evaluated as the

Table 2.5. W-silylene, W-vinyl, and silylene-vinyl bond energies $(\Delta E)^a$ in $Cp(CO)_2W(CHCH_2)(SiH_2)$ **2** and W-silylene, W-acetylide, and silylene-acetylide bond energies $(\Delta E)^a$ in $Cp(CO)_2W(CCH)(SiH_2)$ **4**.

Method	ΔE^a (kcal/mol) in **2**			ΔE^a (kcal/mol) in **4**		
	$W-SiH_2$	$W-CHCH_2$	SiH_2-CHCH_2	$W-SiH_2$	$W-CCH$	SiH_2-CCH
DFT	39.9	43.6	47.4	34.0	88.8	74.6
MP2	61.1	74.5	43.1	50.3	102.3	69.7
MP3	29.9	48.2	49.0	21.3	67.4	77.0
MP4(DQ)	41.7	55.3	45.1	33.2	80.4	71.0
MP4(SDQ)	43.0	56.0	43.6	35.5	80.3	68.4
MP4(SDTQ)	56.0	70.4	39.4	48.5	97.1	63.5
CCSD(T)	42.0	50.2	43.0	37.0	77.0	64.9

^{a} See Scheme 2.4 for the ΔE calculation method. The BS-II was employed.

energy difference between **2** and **2'**, as shown in Scheme 2.4(C), where the geometry of **2'** was taken to be the same as that of **2** except for the positions of the CO and $CHCH_2$ groups; their positions were exchanged with each other so as not to allow the $CHCH_2$ group interact with the SiH_2 group. The energy difference between **2** and **2'** corresponds to the silylene-vinyl interaction. These values are summarized in Table 2.5.

The W-silylene bond of **2** is stronger than that of **4** by 5.0 (5.9) kcal/mol, which is consistent with the above discussion based on Laplacian of electron density. This is because the sp^2 lone pair orbital of silylene expands towards the W center in **2** but its direction changes towards the C1 atom in **4**, as we discussed previously [7]; in other words, the sp^2 lone pair of the silylene overlaps better with the empty d orbital of W in **2** than in **4**. The W-vinyl bond of **2** is considerably weaker than the W-acetylide bond of **4** by 26.8 (45.2) kcal/mol. The silylene-acetylide interaction is much stronger than the silylene-vinyl interaction by 21.9 (27.2) kcal/mol. These results are also consistent with results of the Laplacian of electron density. The reason will be discussed below in more detail. As shown in Scheme 2.5, the

Cp(CO)$_2$W(η^3–H$_2$SiCHCH$_2$) **1** $\longrightarrow$ Cp(CO)$_2$W(CHCH$_2$)(SiH$_2$) **2**

		W-vinyl:	50.2 (43.6)
W-(η^3–H$_2$SiCHCH$_2$):	122.1 (110.3)	W-silylene:	42.0 (39.9)
Si-C:	46.8 (50.6)	Silylene-vinyl:	43.0 (47.4)
Total:	168.9 (160.9)	Total:	135.2 (130.9)

Difference = + 33.7 (30.0)

Cp(CO)$_2$W(η^3–H$_2$SiCCH) **3** $\longrightarrow$ Cp(CO)$_2$W(CCH)(SiH$_2$) **4**

		W-acetylide:	77.0 (88.8)
W-(η^3–H$_2$SiCCH):	112.7 (102.0)	W-silylene:	37.0 (34.0)
Si-C:	83.3 (86.4)	Silylene-acetylide:	64.9 (74.6)
Total:	196.0 (188.4)	Total:	178.9 (197.4)

Difference = + 17.1 (-9.0)

CCSD(T)/BS-II and DFT/BS-II-calculated values (in kcal/mol unit) are presented without and in parenthesis, respectively.

Scheme 2.5

sum of W-(η^3-H$_2$SiCHCH$_2$) and Si-C bond energies in **1** are larger than that of W-vinyl, W-silylene, and silylene-vinyl interaction energies in **2** by 33.7 (30.0) kcal/mol. Interestingly, this energy difference is similar to the endothermicity of the conversion reaction of **1** to **2**, suggesting that the bond energies evaluated here are reliable. On the other hand, the sum of W-(η^3-H$_2$SiCCH) and Si-C bond energies in **3** are smaller than that of W-acetylide, W-silylene, and silylene-acetylide interaction energies in **4** by 9.0 kcal/mol, where the DFT-calculated values were adopted. In the CCSD(T) calculations, the sum of W-(η^3-H$_2$SiCCH) and Si-C bond energies in **3** is larger than that of W-acetylide, W-silylene, and silylene-acetylide interaction energies in **4** by 17.1 kcal/mol. Though this energy difference is reverse to the relative stabilities of **3** and **4**, the CCSD(T)-calculated energy difference between **3** and **4** is much smaller than that between **1** and **2**. Thus, it is concluded that **3** is less easily isolated

than **1** even if we take the CCSD(T)-calculated energy changes.

From these results, we can easily understand the reasons why **1** was isolated but **2** was not. Though the Si-C bond is weak in **1**, the W-(η^3-H$_2$SiCHCH$_2$) interaction is considerably strong. Moreover, the W-vinyl and the silylene-vinyl interactions are very weak in **2**. As a result, **1** was isolated but **2** was not. On the other hand, the Si-C bond is strong in **3** but the W-(η^3-H$_2$SiCCH) interaction is weak. Moreover, the W-acetylide and the silylene-acetylide interactions are very strong in **4**. As a result, **4** was isolated, but **3** was not.

2.3.5 Reasons why the W-acetylide bond is Stronger than the W-vinyl bond

It is of considerable interest to clarify the reasons why the W-acetylide bond is stronger than the W-vinyl bond, because this is one of the important factors to stabilize **4** relative to **3**. We also evaluated the W-vinyl bond energy in an ideal complex Cp(CO)$_2$W(CHCH$_2$)(SiH$_2$) **5** (Figure 2.2), in which the vinyl group was placed at the opposite side to silylene to evaluate the pure W-vinyl bond energy. Also, the pure W-acetylide bond energy was calculated from the similar ideal complex Cp(CO)$_2$W(CCH)(SiH$_2$) **6** (see Ref. 7 for the optimized geometry of **6**). The W-vinyl bond of **5** is considerably weaker than the W-acetylide bond of **6** by 31.5 (35.1) kcal/mol (see Appendix A.2.2), which is consistent with the large difference between the W-vinyl and W-acetylide bond energies in **2** and **4**. This reason is interpreted in terms of the energy difference of valence orbital between vinyl and acetylide groups; The sp lone pair orbital of the acetylide is at lower energy (-11.1 eV) than the sp^2 lone pair orbital (-6.6 eV) of the vinyl group, where the Kohn-Sham orbital energies are presented [28]. Because these orbitals are at lower energy than the SOMO of ·Cp(CO)$_2$W(SiH$_2$) which is at -5.2 eV [28], the energy difference between the valence orbitals of the Cp(CO)$_2$W(SiH$_2$) and acetylide groups

is larger than that between the $Cp(CO)_2W(SiH_2)$ and vinyl groups, which leads to the stronger W-acetylide bond than the W-vinyl bond; see eq 2.1.

We also evaluated the W-silylene bond energy in **5** and **6**. The pure W-silylene bond energy is similar in both **5** and **6** (see Appendix A.2.3), as expected. On the other hand, the W-silylene bond of **2** is stronger than that of **4**, as discussed above. This is because the sp^2 lone pair orbital of the silylene expands toward the W center in **2** but it considerably deviates from the W-Si line in **4**; it makes angles of 7.5º and 35.4º with the W-Si bond in **2** and **4**, respectively. This significantly large difference arises from the difference between the silylene-vinyl and silylene-acetylide interactions, which will be discussed below.

2.3.6　Reasons why the Interaction between the Silylene and Vinyl groups is Weaker than that between the Silylene and Acetylide groups

It is also very important to clarify the reason why the silylene-vinyl interaction is much weaker than the silylene-acetylide interaction. The strong CT between the silylene and acetylide moieties is observed in **4**, as discussed previously [7]. Unlike **4**, on the other hand, weak CT is observed between the silylene and vinyl moieties in **2**, as discussed above. First, we examined the π and π^* orbitals of the vinyl and acetylide groups. The π and π^* orbitals are at -7.6 eV and -0.4 eV, respectively, in vinyl group and at -9.1 eV and -1.3 eV, respectively, in acetylide group [29]. These results suggest that the π orbital of vinyl forms stronger CT with the empty p orbital of silylene but the π^* orbital of vinyl forms weaker CT with the sp^2 lone pair orbital of silylene. Usually, silylene is considered to be electron-accepting. Thus, the former CT is more important than the latter one, which leads to expectation that the silylene-vinyl interaction is stronger than the silylene-acetylide one. This is not consistent
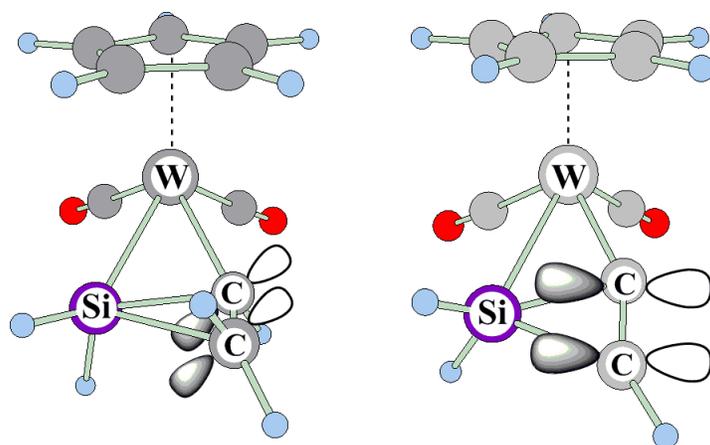
(A) Cp(CO)$_2$W(CHCH$_2$)(SiH$_2$) **2**   (B) Cp(CO)$_2$W(CCH)(SiH$_2$) **4**

Scheme 2.6

with the computational results. Thus, the π and π^* orbital energies of the vinyl group are not responsible for the weak interaction between the silylene and vinyl groups and another factor must be responsible for it.

The π orbital of the vinyl group is perpendicular to the C=C bond and does not well expand toward the empty p orbital of silylene moiety, as shown in Scheme 2.6(A). This is because the sp^2 orbital of the vinyl group must expand toward the W center and therefore, the C=C double bond deviates from the best position to form the CT interaction with the silylene group; in other words, its π orbital cannot overlap well with the empty p orbital of the silylene group and the CT interaction between the silylene and vinyl groups is weak in **2**. On the other hand, the sp orbital of the acetylide group is collinear to the C≡C bond and the π and π^* orbitals of acetylide are cylindrical around the C≡C triple bond, as shown in Scheme 2.6(B). Thus, the C≡C triple bond can form strong CT with the silylene moiety in **4**.

2.4 Conclusions

The geometry and bonding nature of interesting new tungsten η^3-silaallyl/η^3-vinylsilyl complex, $Cp(CO)_2W(\eta^3\text{-}H_2SiCHCH_2)$ **1**, tungsten vinyl silylene complex $Cp(CO)_2W(CHCH_2)(SiH_2)$ **2**, and conversion reaction of **1** to **2** were theoretically investigated with the DFT, MP2 to MP4(SDTQ), and CCSD(T) methods, where **1** was adopted as a model of $Cp^*(CO)_2W(\eta^3\text{-}Me_2SiCHCMe_2)$. The non-bonding π orbital ($\varphi_{n\pi}$) of the $\eta^3\text{-}H_2SiCHCH_2$ moiety of **1** is similar to that of the η^3-allyl group except that the Si p orbital more contributes to the $\varphi_{n\pi}$ than the C p orbital. On the other hand, the π orbital (φ_π) of **1** is considerably different from that of the η^3-allyl group; the π-conjugation between the Si and C atoms is very weak unlike that of the η^3-allyl group in which π-conjugation is considerably strong. Thus, **1** can be understood to be a species between tungsten η^3-vinylsilyl and tungsten η^3-silaallyl complexes.

Because our previous study indicated that similar tungsten η^3-silapropargyl/η^3-alkynylsilyl complex $Cp(CO)_2W(\eta^3\text{-}H_2SiCCH)$ **3** easily converted to tungsten acetylide silylene complex $Cp(CO)_2W(CCH)(SiH_2)$ **4**, we theoretically investigated tungsten vinyl silylene complex $Cp(CO)_2W(CHCH_2)(SiH_2)$ **2** which is similar to **4**. The sp^2 lone pair orbital of silylene group expands towards the W center in **2**, and therefore, strong W-silylene interaction is formed in **2**, while a very weak CT interaction is formed between the vinyl and silylene groups in **2**. From these results, **2** is understood to be a pure tungsten vinyl silylene complex unlike **4** in which a strong CT interaction is formed between the acetylide and silylene groups.

Complex **1** is much more stable than **2** by 21.0 (20.9) kcal/mol, while **3** is less stable than **4** by 0.7 (4.9) kcal/mol. These differences can be interpreted, as follows: Though the Si-C bond is weak in **1**, the W-($\eta^3\text{-}H_2SiCHCH_2$) interaction is considerably strong. Moreover, the

W-vinyl and the silylene-vinyl interactions are very weak in **2**. As a result, **1** is much more stable than **2**. On the other hand, the Si-C bond is strong in **3** but the W-(η^3-H$_2$SiCCH) interaction is weak. Moreover, the W-acetylide and the silylene-acetylide interactions are very strong in **4**. As a result, **3** is less stable than **4**. Thus, **1** can be isolated but **2** cannot, while **4** can be isolated but **3** cannot.

Complex **1** converts to **2** with a large activation barrier of 34.2 (33.2) kcal/mol, while **3** easily converts to **4** with a moderate activation barrier of 15.8 (15.3) kcal/mol. The larger activation barrier of the conversion reaction of **1** to **2** can be interpreted as follows: The coordinate bond of the C=C double bond with the W center is much stronger in **1** than in **3**. This coordinate bond of the C=C double bond is almost broken in the transition state. Thus, this bond breaking induces large energy loss, which is one of the origins of the large activation barrier.

It is worth discussing significantly large differences between **1** and **3** and between **2** and **4**. The φ_π orbital of ·H$_2$SiCHCH$_2$ is at higher energy than that of ·H$_2$SiCCH, which leads to formation of stronger W-(η^3-H$_2$SiCHCH$_2$) interaction of **1** than the similar W-(η^3-H$_2$SiCCH) interaction of **3**. The energy difference between the sp^2 orbital of vinyl and SOMO of Cp(CO)$_2$W(SiH$_2$) is much smaller than that between the sp orbital of acetylide and the SOMO of Cp(CO)$_2$W(SiH$_2$), and therefore, the W-vinyl bond of **2** is considerably weaker than the W-acetylide bond of **4** because the covalent bond energy increases with increase in the energy difference between two orbitals. The vinyl group interacts with the W center using its sp^2 orbital, which leads to very unfavorable orientation of the C=C double bond for the interaction with silylene. On the other hand, the acetylide group interacts with the W center using its sp orbital and the π and π* orbitals surround the C≡C triple bond in a cylindrical way, which are

favorable for the interaction with the silylene. As a result, the silylene-vinyl interaction in **2** is much weaker than the silylene-acetylide interaction of **4**. These results indicate that the tungsten η^3-silaallyl/η^3-vinylsilyl complex **1** can be isolated but the tungsten vinyl silylene complex **2** cannot unlike the tungsten acetylide silylene complex $Cp(CO)_2W(CCH)(SiH_2)$ **4**.

From these results, we wish to emphasize that the isolation of $Cp(CO)_2W(\eta^3-R^1{}_2SiCCR^2)$ is challenging and also predict that a variety of transition metal η^3-silaallyl/η^3-vinylsilyl complexes can be synthesized by a method similar to that of the Sakaba and Tilley groups.

Bibliography

[1]   (a) Sakurai, H.; Kamiyama, Y.; Nakadaira, Y. *J. Am. Chem. Soc*. **1976**, *98*, 7453. (b) Sakurai, H.; Kamiyama, Y.; Mikoda, A.; Kobayashi, T.; Sasaki, K.; Nakadaira, Y. *J. Organomet. Chem.* **1980**, *201*, C14. (c) Sakurai, H.; Kamiyama, Y.; Nakadaira, Y. *J. Organomet. Chem.* **1980**, *184*, 13.

[2]   Radnia, P.; Mckennis, J. S. *J. Am. Chem. Soc*. **1980**, *102*, 6349.

[3]   Dai, X.; Kano, N.; Kako, M.; Nakadaira, Y. *Chem. Lett*. **1999**, 717.

[4]   Dysard, J. M.; Tilley, T. D.; Woo, T. K. *Organometallics* **2001**, *20*, 1195.

[5]   Sakaba, H.; Watanabe, S.; Kabuto, C.; Kabuto, K. *J. Am. Chem. Soc*. **2003**, *125*, 2842.

[6]   Sakaba, H.; Yoshida, M.; Kabuto, C.; Kabuto, K. *J. Am. Chem. Soc*. **2005**, *127*, 7276.

[7]   Ray, M.; Nakao, Y.; Sato, H.; Sakaba, H.; Sakaki, S. *J. Am. Chem. Soc*. **2006**, *128*, 11927.

[8]   (a) Becke, A. D. *Phys Rev. A*. **1988**, *38*, 3098. (b) Becke, A. D. *J. Chem. Phys*. **1993**, *98*, 5648.

[9]   (a) Perdew, J. P. *In Electronic Structure of Solids*`91, Ziesche, P.; Eschrig, H., Ed.; Akademic Verlag, Berlin, **1991**; p 11. (b) Perdew, J. P.; Chevary, J. A.; Vosko, S. H.; Jackson, K. A.; Pederson, M. R.; Singh, D. J.; Fiolhais, C. *Phys. Rev. B*. **1992**, *46*, 6671. (c) Perdew, J. P.; Chevary, J. A.; Vosko, S. H.; Jackson, K. A.; Pederson, M. R.; Singh, D. J.; Fiolhais, C. *Phys. Rev. B*. **1993**, *48*, 4978. (d) Perdew, J. P.; Burke, K.; Wang, Y. *Phys Rev. B*. **1996**, *54*, 16533.

[10]   (a) Lee, C.; Yang, W.; Parr, R. G. *Phys. Rev. B*. **1988**, *37*, 785. (b) Miehlich, B.; Savin, A.; Stoll, H.; Preuss, H. *Chem. Phys. Lett*. **1989**, *157*, 200.

[11]   Hay, P. J.; Wadt, W. R. *J. Chem. Phys*. **1985**, *82*, 299.

[12]   (a) Dunning Jr, T. H. *J. Chem. Phys*. **1989**, *90*, 1007. (b) Woon, D. E.; Dunning Jr, T. H. *J. Chem. Phys*. **1993**, *98*, 1358.

[13]   (a) Ditchfield, R.; Hehre, W. J.; Pople, J. A. *J. Chem. Phys.* **1971**, *54*, 724. (b) Hehre, W.; Ditchfield, R.; Pople, J. A. *J. Chem. Phys.* **1972**, *56*, 2257.

[14]   Couty, M.; Hall, M. B. *J. Comput. Chem*. **1996**, *17*, 1359.

[15]   Ehlers, A. W.; Bohme, D. S.; Gobbi, A.; Hollwarth, A.; Jonas, V.; Kohler, K. F.; Stegmann, R.; Veldkamp, A.; Frenking, G. *Chem. Phys. Lett*. **1993**, *208*, 111.

[16]   Pople, J. A.; et al. *Gaussian 03,* Revision C.02, Gaussian Inc.: Wallingford, CT, **2004**.

[17]   (a) Flükiger, P.; Lüthi, H. P.; Portmann, S.; Weber, J. *MOLEKEL 4.3*, Swiss Center for Scientific Computing, Manno (Switzerland), **2000-2002**. (b) Portmann, S.; Lüthi, H. P. *MOLEKEL*, An Interactive Molecular Graphics Tool, *CHIMIA*, **2000**, *54*, 766-770.

[18]   Schaftenaar, G.; Noordik, J. H. *MOLDEN*, A Pre- and Post-Processing Program for Molecular and Electronic Structures, *J. Comput.-Aided Mol. Design*, **2000**, *14*, 123-134

[19]   (a) Bader, R. F. W. *Atoms in Molecules: a Quantum Theory*; Clarendon: New York, 1990. (b) Bader, R. F. W. *Chem. Rev*. **1991**, *91*, 893.

[20]   Frenking, G.; Fröhlich, N. *Chem. Rev*. **2000**, *100*, 717.

[21]   (a) Fan, M. F.; Lin, Z. *Organometallics* **1998**, *17*, 1092. (b) Liu, D.; Lam, K. C.; Lin, Z. *Organometallics* **2003**, *22*, 2827.

[22]   (a) Sakaki, S.; Yamaguchi, S.; Musashi, Y.; Sugimoto, M. *J. Organomet. Chem*. **2001**, *635*, 173. (b) Tomita, T.; Takahama, T.; Sugimoto, M.; Sakaki, S. *Organometallics*

2002, *21*, 4138. (c) Nakajima, S.; Yokogawa, D.; Nakao, Y.; Sato, H.; Sakaki, S. *Organometallics* **2004**, *23*, 4672. (d) Nakajima, S.; Sumimoto, M.; Nakao, Y.; Sato, H.; Sakaki, S.; Osakada, K. *Organometallics* **2005**, *24*, 4029.

[23]   The HF-calculated p orbital of ·SiH$_3$ is at -7.85 eV and that of ·CH$_3$ is at -10.47 eV.

[24]   DFT(B3PW91)/BS-I optimized geometries of H$_3$Si-CH$_3$, H$_2$Si=CH$_2$, CH$_3$-CH$_3$, and CH$_2$=CH$_2$ were taken, respectively.

[25]   Geometries of silylene and vinyl groups were taken to be the same as that in **2**.

[26]   In both H$_3$SiCHCH$_2$ and H$_3$SiCCH, the third H atom connected with Si was placed on the W-Si bond line of **1** and **3**, respectively, with the usual Si-H distance (1.490 Å); see Appendix A.2.1(A) for the geometries.

[27]   Geometries of ·SiH$_3$, ·CHCH$_2$, and ·CCH were taken to be the same as that in **1** and **3**; see Appendix A.2.1(B) for the geometries.

[28]   Geometries of ·CHCH$_2$, ·CCH, and ·Cp(CO)$_2$W(SiH$_2$) were taken to be the same as that in **5** and **6**.

[29]   Geometries of vinyl and acetylide groups were taken to be the same as that in **2** and **4**, respectively.

Appendix

A.2.1   Geometries of $H_3SiCHCH_2$, H_3SiCCH, ·SiH_3, ·$CHCH_2$, and ·CCH.

(A)   **$H_3SiCHCH_2$**   **H_3SiCCH**

(B)   **·SiH_3**   **·$CHCH_2$**   **·CCH**
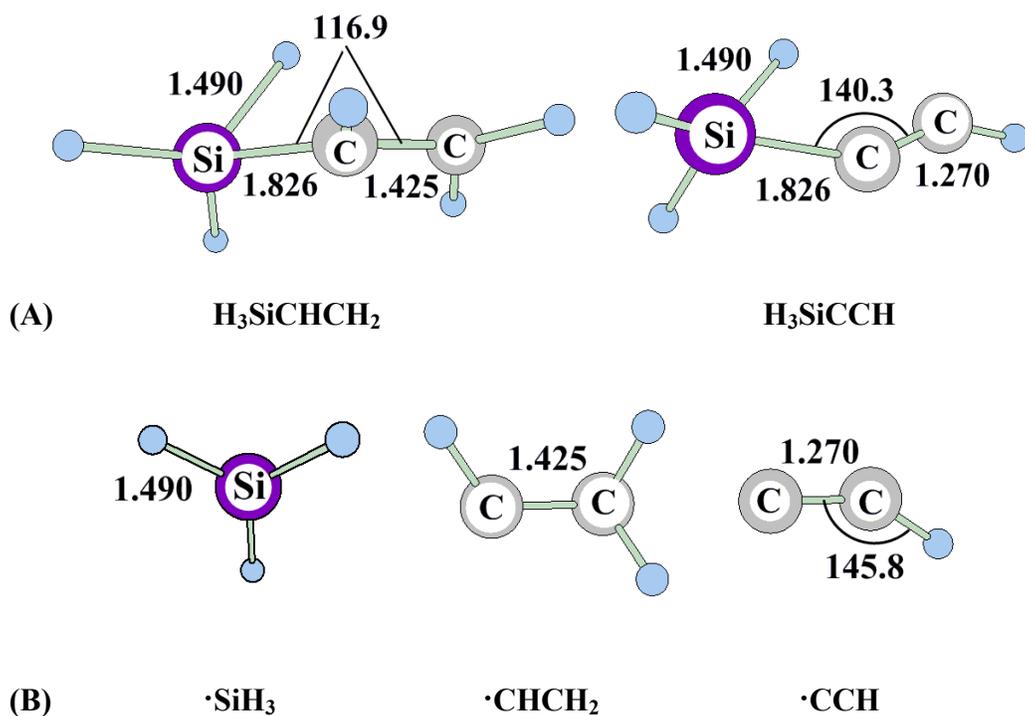
Figure A.2.1.   Geometries of $H_3SiCHCH_2$[a], H_3SiCCH[a], ·SiH_3[b], ·$CHCH_2$[b], and ·CCH[c].
[a] Geometries of $H_2SiCHCH_2$ and H_2SiCCH are taken to be the same as those in **1** and **3**. Third H on Si was placed on the W-Si bond line of **1** and **3** with usual Si-H bond length. Bond lengths are in angstroms and bond angles are in degrees.
[b] Geometry is taken to be the same as that in $H_3SiCHCH_2$.
[c] Geometry is taken to be the same as that in H_3SiCCH.

A.2.2 W-acetylide and W-vinyl bond energies in $Cp(CO)_2W(HCCH_2)(SiH_2)$ **5** and $Cp(CO)_2W(CCH)(SiH_2)$ **6**.

Table A.2.1. W-acetylide and W-vinyl bond energies $(DE)^a$ (in kcal/mol unit) in $Cp(CO)_2W(HCCH_2)(SiH_2)$ **5** and $Cp(CO)_2W(CCH)(SiH_2)$ **6**.

Method	DE (W-CHCH$_2$)	DE (W-CCH)
DFT	72.2	107.3
MP2	97.5	138.8
MP3	83.0	119.4
MP4(DQ)	90.2	128.6
MP4(SDQ)	89.5	126.6
MP4(SDTQ)	100.9	138.8
CCSD(T)	82.7	114.2

^{a} $DE = E_t$ (**5** or **6**) - E_t [·$Cp(CO)_2W(SiH_2)$] - E_t (·$CHCH_2$ or ·CCH). The BS-II was employed.

A.2.3 W-silylene bond energies in $Cp(CO)_2W(HCCH_2)(SiH_2)$ **5** and $Cp(CO)_2W(CCH)(SiH_2)$ **6**.

Table A.2.2. W-silylene bond energies $(DE)^a$ (in kcal/mol unit) in $Cp(CO)_2W(HCCH_2)(SiH_2)$ **5** and $Cp(CO)_2W(CCH)(SiH_2)$ **6**.

Method	5	6
DFT	-81.8	-82.5
MP2	-104.6	-105.0
MP3	-76.1	-76.6
MP4(DQ)	-87.5	-88.3
MP4(SDQ)	-87.9	-88.8
MP4(SDTQ)	-98.3	-99.2
CCSD(T)	-84.9	-85.7

^{a} $DE = E_t$ (**5** or **6**) - E_t [$Cp(CO)_2W(CHCH_2)$ or $Cp(CO)_2W(CCH)$] - E_t (SiH$_2$). The BS-II was employed.

Chapter 3

How to Stabilize η^3-Silapropargyl/Alkynylsilyl Complex of $[CpL_2M]^+$ (L = CO, PMe$_3$, or PF$_3$ and M = W or Mo). Theoretical Prediction

3.1   Introduction

As well known, silicon compounds are much different from carbon analogues even if their compositions are similar to each other; for instance, silicon analogue of acetylene is very reactive and takes trans-bent structure, as reported recently [1-5, 6b-12].   Because of significantly large differences between carbon and silicon compounds, silicon analogues of various carbon compounds have drawn a lot of interests [1-16].

Transition metal η^3-propargyl/allenyl complex has been one of the research targets in recent organometallic chemistry, coordination chemistry, and catalytic chemistry because of its interesting geometry and reactivity [17, 18].   In this regard, many important results have been reported on their syntheses and characterization [17-20].   However, transition metal η^3-silapropargyl/alkynylsilyl complex, which is one of silicon analogues of the η^3-propargyl/allenyl complex, has not been synthesized yet, to our best knowledge, though it is expected to be of considerable interest.

Recently, tungsten η^3-silapropargyl/alkynylsilyl complex Cp*(CO)$_2$W(η^3-Ph$_2$SiCC^{t}Bu) **A** (Cp* = C$_5$Me$_5$) was experimentally proposed as an intermediate in the synthesis of tungsten acetylide-silylene complex Cp*(CO)$_2$W(CC^{t}Bu)(SiPh$_2$) **B**, as shown in Scheme 3.1 [21-23].
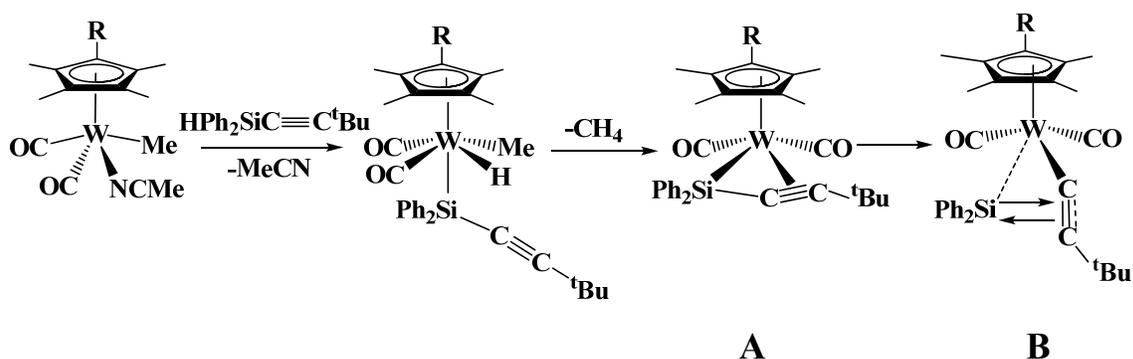
Scheme 3.1. Formation of $Cp^*(CO)_2W(CC^tBu)(SiPh_2)$ **B** via $Cp^*(CO)_2W(\eta^3\text{-}Ph_2SiCC^tBu)$ **A**

However, **A** has not been isolated yet, though the similar tungsten η^3-silaallyl complex $Cp^*(CO)_2W(\eta^3\text{-}Me_2SiCHCMe_2)$, which is silicon analogue of the transition metal η^3-allyl complex, was isolated recently [24]. We also theoretically investigated the geometries and the bonding natures of $Cp(CO)_2W(\eta^3\text{-}H_2SiCCH)$ **1** ($Cp = C_5H_5$) and $Cp(CO)_2W(CCH)(SiH_2)$ **2**, where **1** and **2** were employed as models of **A** and **B**, respectively [22]. In the work, we found that **1** was slightly less stable than **2**. This computational result strongly suggests that one can succeed to synthesize the transition metal η^3-silapropargyl/alkynylsilyl complex with appropriate metal center, ligand, and substituents on Si and C atoms.

Our theoretical studies on the tungsten η^3-silapropargyl/alkynylsilyl complex $Cp(CO)_2W(\eta^3\text{-}H_2SiCCH)$ **1** [22] and tungsten η^3-silaallyl/vinylsilyl complex $Cp(CO)_2W(\eta^3\text{-}H_2SiCHCH_2)$ [25] demonstrated their interesting bonding natures; for instance, the non-bonding π-orbitals ($\varphi_{n\pi}$) of $\eta^3\text{-}H_2SiCCH$ and $\eta^3\text{-}H_2SiCHCH_2$ groups are similar to those of the η^3-propargyl and η^3-allyl groups, respectively, but their π-orbitals (φ_π) are significantly different from those of the η^3-propargyl and η^3-allyl groups; in other words, the electronic structure of $\eta^3\text{-}H_2SiCCH$ group is intermediate between those of η^3-silapropargyl and alkynylsilyl groups and that of $\eta^3\text{-}H_2SiCHCH_2$ group is intermediate between those of η^3-

silaallyl and vinylsilyl groups. These theoretical results indicate that the transition metal η^3-silapropargyl/alkynylsilyl complex provides new interesting category of transition metal silicon compounds. Thus, its synthesis is challenging and its experimental characterization is interesting.

In this work, we theoretically investigated the η^3-silapropargyl/alkynylsilyl complex $CpL_2M(\eta^3-R^2{}_2SiCCR^1)$ (**1** for M = W and **3** for M = Mo; L = CO, PMe$_3$, or PF$_3$; Cp = C$_5$H$_5$, R^1 = H, Me, ^{t}Bu, or CF$_3$; R^2 = H, Me or F) and the acetylide-silylene complex $CpL_2M(CCR^1)(SiR^2{}_2)$ [23] (**2** for M = W and **4** for M = Mo) with DFT, MP2 to MP4(SDTQ), and CCSD(T) methods. We also investigated the conversion reactions of **1** and **3** to **2** and **4**, respectively. Our main purposes here are to present theoretical prediction how to stabilize the transition metal η^3-silapropargyl/alkynylsilyl complex and to clarify how and why the stabilities, electronic structures, and bonding natures of **1** and **3** depend on the substituents of Si and C, ligands, and metal center.

3.2   Computational Details

$CpL_2M(\eta^3-R^2{}_2SiCCR^1)$ and $CpL_2M(CCR^1)(SiR^2{}_2)$ are neutral and take closed-shell singlet spin state [26]. Their geometries were optimized with the density functional theory (DFT). Here, we employed B3PW91 functional [27, 28] for the exchange-correlation term because the geometry of Cp(CO)$_2$W(CC^{t}Bu)(SiH$_2$) was well optimized with this functional compared to B3LYP functional [27, 29] (see Appendix A.3.1). We ascertained that each equilibrium geometry did not exhibit any imaginary frequency and each transition state possessed only one imaginary frequency in which geometry changes were consistent with the

reaction. Energy was evaluated with DFT, MP2 to MP4(SDTQ), and CCSD(T) methods, where the DFT-optimized geometry was employed.

Three kinds of basis set systems, Basis Set System-I (BS-I), Basis Set System-II (BS-II), and Basis Set System-III (BS-III), were employed in this work. In BS-I, core electrons of W and Mo were replaced with effective core potentials (ECPs) [30] and their valence electrons were represented with (341/321/21) and (341/321/31) basis sets [30], respectively. cc-pVDZ basis sets [31] were used for Si, C, and O, and 6-31G basis set was used for H [32]. This BS-I was employed for geometry optimization. In BS-II, valence electrons of W and Mo were represented with (541/541/111/1) and (541/541/211/1) basis sets [30, 33, 34], respectively, where their core electrons were replaced with the same ECPs as those of BS-I. For the other atoms, the same basis sets as those of BS-I were employed. This BS-II was used to evaluate energy changes. In BS-III, valence electrons of W and Mo were represented by (311111/22111/411/11) basis sets with Stuttgart-Dresden-Bonn (SDB) ECPs [35, 36]. For the other atoms, cc-pVTZ basis sets were used [37], where the f polarization function was excluded to save CPU time. This BS-III was used to check if BS-II presents reliable energy change. Zero-point energy (ZPE), thermal energy, and entropy change were calculated with the DFT/BS-I method at 298 K and 1 atm, where the assumptions of rigid rotator and harmonic oscillator were employed to evaluate partition functions of rotation and vibration movements and the assumption of ideal gas was employed to evaluate partition function of translation movement. Solvation effects (toluene; $\varepsilon = 2.379$) were taken into consideration with polarizable continuum model (PCM) [38], where optimized geometries in gas-phase were employed.

Gaussian 03 program package (revision C.02) [39] was used for all these computations.

3.3   Results and Discussion

In this article, we wish to investigate first the relative stability of $Cp(CO)_2M(\eta^3$-$H_2SiCCH)$ to $Cp(CO)_2M(CCH)(SiH_2)$, make comparison between molybdenum and tungsten complexes, and then discuss ligand and substituent effects on the relative stabilities of $CpL_2M(\eta^3$-$R^2_2SiCCR^1)$ to $CpL_2M(CCR^1)(SiR^2_2)$.

3.3.1   Geometries and Relative Stabilities of $Cp(CO)_2M(\eta^3$-$H_2SiCCH)$ and $Cp(CO)_2M(CCH)(SiH_2)$ (M = W or Mo)

Because geometries of $Cp(CO)_2W(\eta^3$-$H_2SiCCH)$ **1** and $Cp(CO)_2W(CCH)(SiH_2)$ **2** were previously discussed in our theoretical study [22], we wish to focus on the differences in geometry between the tungsten and molybdenum complexes, here. Several geometrical parameters are moderately different between them (see Figure 3.1 and Appendix A.3.2 for their geometries): For instance, the Mo-Cp (center of the Cp ring) distance is moderately shorter than the W-Cp distance by 0.039 Å in $Cp(CO)_2M(\eta^3$-$H_2SiCCH)$ and by 0.043 Å in $Cp(CO)_2M(CCH)(SiH_2)$, indicating that the Mo-Cp interaction is moderately stronger than the W-Cp interaction probably because the donation from Cp to M becomes stronger upon switching W to Mo, as shown by the smaller electron population of Cp in **3** than in **4** (see Appendix A.3.3). The Mo-C1 and Mo-C2 distances in $Cp(CO)_2Mo(\eta^3$-$H_2SiCCH)$ **3** are moderately longer than the W-C1 and W-C2 distances of the tungsten analogue **1** by 0.017 Å and 0.051 Å, respectively, though atomic radius of molybdenum is smaller than that of tungsten. The Mo-Si distance of $Cp(CO)_2Mo(CCH)(SiH_2)$ **4** is moderately shorter than the W-Si distance of the tungsten analogue **2** by 0.026 Å, while the Mo-C1 and Si-C2 distances,

115
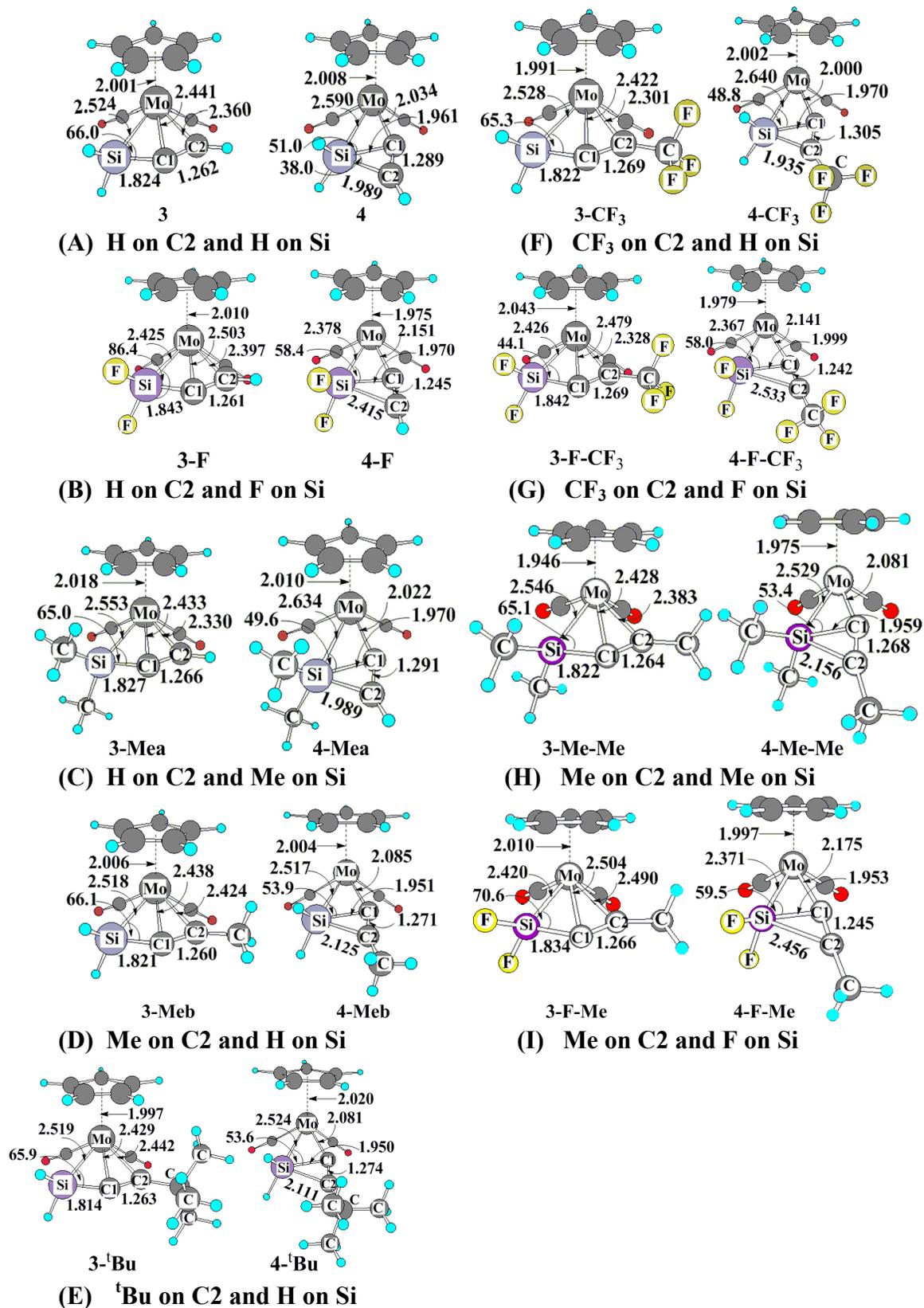
Figure 3.1. DFT(B3PW91)/BS-I optimized geometries of $Cp(CO)_2Mo(\eta^3-R^2{}_2SiCCR^1)$ and $Cp(CO)_2Mo(CCR^1)(SiR^2{}_2)$, where $R^1 = H$, Me, ^tBu, or CF_3 and $R^2 = H$, F, or Me. Bond lengths are in angstroms and bond angles are in degree. See Appendix A.3.2 for geometries of tungsten complexes.

Table 3.1: Relative stability $(\Delta E)^{a)}$ (in kcal/mol unit) of $Cp(CO)_2M(\eta^3\text{-}H_2SiCCH)$ to $Cp(CO)_2M(CCH)(SiH_2)$ (M = W or Mo) calculated with various computational methods.

Method	M = W [b)]	M = Mo
DFT	-4.9 (-4.0)[c)]	-1.9 (-0.9)[c)]
MP2	+0.4	+4.1
MP3	-1.4	+2.5
MP4(DQ)	-0.1	+3.5
MP4(SDQ)	-0.9	+2.7
MP4(SDTQ)	-0.6	+2.9
CCSD(T)	-0.7	+2.9

[a] The ΔE value is energy difference between $Cp(CO)_2M(CCH)(SiH_2)$ and $Cp(CO)_2M(\eta^3\text{-}H_2SiCCH)$. The BS-II was employed. [b] Ref. 22. [c] In parenthesis is the ΔE value between $Cp^*(CO)_2M(\eta^3\text{-}H_2SiCCH)$ and $Cp^*(CO)_2M(CCH)(SiH_2)$.

respectively. These geometrical differences suggest that the Mo-$(\eta^3\text{-}H_2SiCCH)$ bond of **3** and Mo-C1 and Si-C2 bonding interactions of **4** are moderately weaker than the corresponding interactions of the tungsten analogues, respectively. The Wiberg bond indices are consistent with above results; The Mo-C1 and Mo-C2 bond indices of **3** are moderately smaller than the W-C1 and W-C2 bond indices of **1** by 0.041 and 0.052, respectively, and the Mo-C1 and Si-C2 bond indices of **4** are moderately smaller than the W-C1 and Si-C2 bond indices of **2** by 0.081 and 0.049, respectively; see Appendix A.3.4 for details of Wiberg bond index. These differences relate to the relative stabilities of the η^3-silapropargyl/alkynylsilyl and acetylide-silylene forms [23], as will be discussed below.

Relative stability of the η^3-silapropargyl/alkynylsilyl form (**1** for M = W and **3** for M = Mo) to the acetylide-silylene form (**2** for M = W and **4** for M = Mo) is represented by the energy difference (ΔE) between these two forms, as shown in Table 3.1, where a positive ΔE value means that the η^3-silapropargyl/alkynylsilyl form is more stable than the acetylide-silylene form. It is noted that the relative stability of the η^3-silapropargyl/alkynylsilyl form is larger in the Mo complex than in the W complex; for instance, the ΔE value increases

from -4.9 kcal/mol to -1.9 kcal/mol at the DFT level and from -0.7 kcal/mol to 2.9 kcal/mol at the CCSD(T) level upon going from the W complex to the Mo complex. Effect of Cp* on the relative stability of **1** to **2** was investigated because Cp* was used in the experiment; see Appendix A.3.5 for the geometries of the Cp* complexes [21]. The difference of ΔE value between Cp and Cp* complexes is not large (about 1 kcal/mol); the ΔE value is -4.9 (-4.0) kcal/mol in the W complexes and -1.9 (-0.9) kcal/mol in the Mo complexes, as shown in Table 3.1, where in parenthesis and out of parenthesis are ΔE values for Cp* and Cp, respectively. Thus, we employed Cp instead of Cp* to save CPU time.

It is necessary to examine whether or not the DFT method presents reliable results about the relative stability of the η^3-silapropargyl/alkynylsilyl form to the acetylide-silylene form, because only the DFT method can be applied to large complexes bearing ^tBu, CF_3, PMe_3, and PF_3. The MP4(SDQ), MP4(SDTQ), and CCSD(T) methods present similar ΔE values in both W and Mo complexes, as shown in Table 3.1, suggesting that these methods present reliable results here. On the other hand, the DFT method presents more negative ΔE value than the other methods in the W complex. In the Mo complex, the DFT method presents negative ΔE value but the other methods present positive value. In other words, the DFT method underestimates the stability of the η^3-silapropargyl/alkynylsilyl form. However, the change of ΔE value due to switching W to Mo is similar by a shift across such different levels as DFT, MP4(SDTQ), and CCSD(T); for instance, the ΔE value increases by 3.0, 3.5, and 3.6 kcal/mol in the DFT, MP4(SDTQ), and CCSD(T) methods, respectively, upon switching W to Mo. Thus, it is suggested that though the DFT method underestimates the stability of the η^3-silapropargyl/alkynylsilyl form, the DFT method is useful to discuss how and why the

stabilities of the η^3-silapropargyl/alkynylsilyl and acetylide-silylene forms depend on the central metal, ligands, and substituents.

We also examined basis set effects by comparing the ΔE value among the DFT/BS-I, DFT/BS-II, and DFT/BS-III methods. Though the ΔE value is slightly different among these calculations, the difference is not large and the trend is the same in all the calculations with BS-I, BS-II and BS-III, indicating that BS-II is useful to discuss the central metal, ligand, and substituent effects; see Appendix A.3.6 for the DFT/BS-I and DFT/BS-III computational results.

3.3.2 Substituent Effects on Geometries and Relative Stabilities of $Cp(CO)_2M(\eta^3-R^2_2SiCCR^1)$ and $Cp(CO)_2M(CCR^1)(SiR^2_2)$ (M = W or Mo, R^1 = H, Me, ^tBu, or CF_3, and R^2 = H, Me, or F)

Significantly large changes are observed in geometry when σ-electron-withdrawing/π-electron-donating F is introduced on Si, as shown in Figure 3.1: In $Cp(CO)_2Mo(\eta^3-F_2SiCCH)$ **3-F**, the Mo-Si distance becomes moderately shorter than that of **3**, indicating that the Mo-Si bonding interaction becomes stronger in **3-F** than in **3**. In $Cp(CO)_2Mo(CCH)(SiF_2)$ **4-F**, the Si-C2 distance is considerably longer and the Mo-Si distance is somewhat shorter than those of **4**. Also, the direction of SiF_2 considerably shifts toward the Mo center in **4-F** compared to that of **4** in which the lone pair orbital of SiH_2 expands toward the C1 atom. These geometrical differences between **4** and **4-F** suggest that the acetylide-silylene interaction is considerably weaker in **4-F** than in **4**, while the Mo-SiR^2_2 and Mo-CCR^1 interactions become stronger by the introduction of F on Si. The Wiberg bond index supports these suggestions: The Mo-Si bond index of **3-F** is moderately larger than that of **3** by 0.049, while the Mo-Si

119

Table 3.2: Relative stability (ΔE)[a] (in kcal/mol unit) of $CpL_2M(\eta^3\text{-}R^2{}_2SiCCR^1)$ to $CpL_2M(CCR^1)(SiR^2{}_2)$ (M = W or Mo, L = CO, PMe₃, or PF₃).

R^1 on C2	R^2 on Si	L	M = W	M = Mo
^{t}Bu	H	CO	-5.2	-2.3
H	H	CO	-4.9	-1.9
		PMe₃	-14.3	-6.7
		PF₃	-5.6	-2.4
H	Me	CO	-4.2	-0.7
CF₃	H	CO	-4.1	-0.7
Me	F	CO	-4.0	-1.8
Me	H	CO	-3.5	-0.4
Me	Me	CO	-2.5	+0.4
H	F	CO	-2.0	+0.1
CF₃	F	CO	+1.1	+2.6

(a) The ΔE value is energy difference between $CpL_2M(CCR^1)(SiR^2{}_2)$ and $CpL_2M(\eta^3\text{-}R^2{}_2SiCCR^1)$. The DFT(B3PW91)/BS-II method was employed. Its positive value represents that $CpL_2M(\eta^3\text{-}R^2{}_2SiCCR^1)$ is more stable than $CpL_2M(CCR^1)(SiR^2{}_2)$.

bond index is somewhat larger by 0.182 and the Si-C2 bond index is considerably smaller by 0.383 in **4-F** than those of **4**. The Mo-Cp distance slightly lengthens upon going to **3-F** from **3** by 0.009 Å but somewhat shortens upon going to **4-F** from **4** by 0.033 Å, indicating that the Mo-Cp interaction little changes in **3-F** but becomes somewhat stronger in **4-F** by F on Si. This is because the donation of Cp to Mo becomes stronger in **4-F** but slightly in **3-F**. The population changes are consistent with this discussion (see Appendix A.3.3 for population and explanation). The similar geometry changes by the introduction of F on Si are observed in the tungsten analogues (see Appendix A.3.2). The introduction of F on Si somewhat increases the stability of the η^3-silapropargyl/alkynylsilyl form by 2.9 kcal/mol and 2.0 kcal/mol in both of W and Mo complexes, respectively, as shown in Table 3.2, which is consistent with the changes in geometry and Wiberg bond index; remember the considerably longer Si-C2 distance and considerably smaller Si-C2 bond index in **4-F** than in **4**.

However, introduction of Me on Si induces moderate changes in geometries of **3** and **4**. The Mo-Si distance becomes moderately longer but the Mo-C2 distance becomes moderately shorter in **3-Mea** and the Mo-Si distance becomes moderately longer in **4-Mea**. The Wiberg bond indices also support these geometry changes; see Appendix A.3.7. The Mo-Cp distance becomes somewhat longer in **3-Mea** by 0.017 Å but little in **4-Mea**. These results are consistent with population changes; see Appendix A.3.3 for population changes and discussion. Though these geometry changes are not clearly related to the relative stability of the η^3-silapropargyl/alkynylsilyl form, the Me on Si slightly increases the stability of the η^3-silapropargyl/alkynylsilyl form by 0.7 kcal/mol and 1.2 kcal/mol in the W and Mo complexes, respectively.

Introduction of electron-donating Me on C2 moderately increases the Mo-C2 distance in **3-Meb** and the Mo-C1 distance in **4-Meb**, but little changes the Si-C1 distance in **3-Meb** and the Mo-Cp distances in **3-Meb** and **4-Meb**; see Figure 3.1. The similar geometry changes are induced by introduction of bulky ^tBu on C2 except for the Mo-Cp distance which slightly shortens in **3-^tBu** and moderately lengthens in **4-^tBu**; see **3-^tBu** and **4-^tBu** in Figure 3.1; see Appendix A.3.3 for populations and explanation. Introduction of electron-withdrawing CF_3 on C2 moderately decreases the Mo-C2 and Mo-Cp distances in **3-CF$_3$** and the Mo-C1 and Mo-Cp distances in **4-CF$_3$**. These changes are reverse to those induced by Me and ^tBu, as expected. The Wiberg bond indices are consistent with the geometry changes by the introduction of Me, ^tBu, and CF_3 on C2; see Appendix A.3.7. The introduction of Me on C2 moderately and CF_3 on C2 even more moderately increase the stability of the η^3-silapropargyl/alkynylsilyl form by 1.4 (1.5) kcal/mol and 0.8 (1.2) kcal/mol, respectively, but the introduction of the bulky ^tBu on C2 slightly decreases the stability of the η^3-

silapropargyl/alkynylsilyl form by 0.3 (0.4) kcal/mol though both Me and ^{t}Bu on C2 induces similar geometry changes, where values of W and Mo complexes are presented without and with parenthesis, respectively.

The largest stability of the η^3-silapropargyl/alkynylsilyl form is observed in the combination of Mo center, CF_3 on C2, and F on Si (see Table 3.2) [40]. On the other hand, the largest stability of the acetylide-silylene form is observed in the combination of W center, ^{t}Bu on C2, and either H or Me on Si.

We evaluated equilibrium constant (K_p) between the η^3-silapropargyl/alkynylsilyl and acetylide-silylene forms to incorporate the entropy and thermal energy in the discussion. Both of the K_p and ΔE values present the same trend about the relative stability; see Appendix A.3.8. Thus, we wish to discuss the relative stability based on the ΔE value, hereafter.

3.3.3 Why Does the σ-Electron-Withdrawing/π-Electron-Donating F on Si Increase the Stability of the η^3-Silapropargyl/Alkynylsilyl form but the Electron-Donating Me on Si Little Influence it?

Prior to starting discussion on the reason, we wish to summarize the bonding natures of the η^3-silapropargyl/alkynylsilyl and acetylide-silylene forms, which were discussed in our previous work [22]. Several important molecular orbitals of the η^3-silapropargyl/alkynylsilyl group are shown in Figure 3.2 (A). The SOMO is non-bonding π orbital ($\varphi_{n\pi}$) which is somewhat localized on Si. The HOMO-1 is π-bonding orbital (φ_π^1) perpendicular to the SiCC plane. The HOMO-2 is in-plane π-bonding orbital (φ_π^2). Both are largely localized on the CC moiety. The LUMO is anti-bonding π^* orbital (φ_π^*). In Cp(CO)$_2$M, the SOMO (φ_{SOMO}^M) mainly consists of d orbital of M which forms bonding interaction with Cp and CO ligands

(Figure 3.2 (B)). The HOMO-1 and HOMO-2 are non-bonding d orbital of M. The LUMO (φ_{LUMO}^{M}) mainly consists of d orbital of M. The $\varphi_{n\pi}$ mainly participates in covalent interaction

LUMO
($\varphi_{\pi*}$)

SOMO
($\varphi_{n\pi}$)

HOMO-1
(φ_{π}^{1})

HOMO-2
(φ_{π}^{2})

(A) ·R$^{2}_{2}$SiCCR^{1}

LUMO
(φ_{LUMO}^{M})

SOMO
(φ_{SOMO}^{M})

HOMO-1

HOMO-2

(B) Cp(CO)$_2$M·

LUMO
(empty p; φ_{p}^{Si})

HOMO
(lone pair orbital; φ_{lp}^{Si})

(C) SiR$^{2}_{2}$

LUMO+1
($\varphi_{\pi*}^{AC}$)

LUMO
($\varphi_{\pi*}^{AC}$)

HOMO
($\varphi_{\pi1}^{AC}$)

HOMO-1
($\varphi_{\pi2}^{AC}$)

SOMO
(φ_{sp}^{AC})
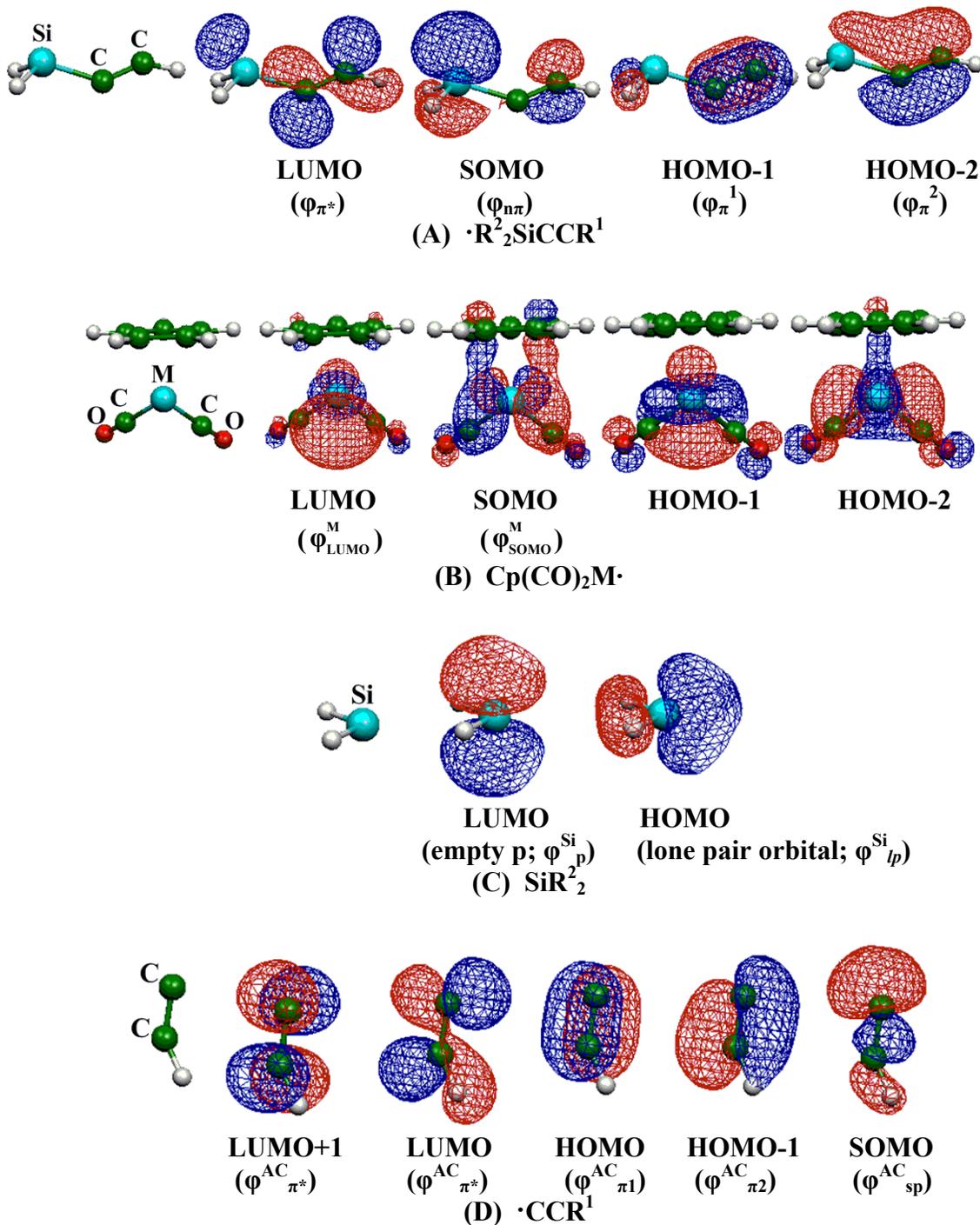
(D) ·CCR^{1}

Figure 3.2. Several important Kohn-Sham orbitals in the fragments, ·R$^{2}_{2}$SiCCR^{1}, Cp(CO)$_2$M·, SiR$^{2}_{2}$ and ·CCR^{1}.

Table 3.3. Orbital energies[a] (in eV unit) of several important orbitals of fragments $\cdot R^2{}_2SiCCR^1$, $\cdot CCR^1$, $SiR^2{}_2$, and $\cdot CpL_2M$.

		·R²₂SiCCR¹			·CCR¹		
R^1	R^2	$\varphi_{\pi*}$	$\varphi_{n\pi}$ (SOMO)	φ_{π}	$\varphi^{AC}_{\pi*}$	φ^{AC}_{π}	φ^{AC}_{sp} (SOMO)
H	H	-0.9 (3.5)	-6.0 (-9.1)	-8.8 (-12.3)	-0.9 (3.5)	-8.9 (-12.0)	-10.3 (-14.0)
Me	H	-0.4 (3.8)	-5.7 (-8.7)	-8.2 (-11.4)	-0.2 (4.0)	-8.2 (-11.1)	-9.3 (-14.9)
ᵗBu	H	-0.5 (3.7)	-5.6 (-8.7)	-8.1 (-11.3)	-0.4 (3.8)	-8.0 (-10.9)	-9.0 (-13.3)
CF₃	H	-1.9 (2.5)	-6.6 (-9.7)	-9.5 (-13.5)	-2.2 (1.9)	-9.7 (-12.9)	-10.9 (-16.4)
H	Me	-0.5 (3.7)	-5.1 (-8.2)	-8.3 (-12.0)	-1.0 (3.3)	-8.9 (-11.8)	-10.2 (-14.0)
H	F	-1.6 (2.5)	-6.8 (-10.6)	-9.4 (-12.9)	-0.8 (3.5)	-8.9 (-11.8)	-10.3 (-13.8)
CF₃	F	-2.7 (1.6)	-7.3 (-11.2)	-10.0 (-14.1)	-2.2 (1.9)	-9.7 (-12.9)	-10.9 (-16.4)

$SiR^2{}_2$		
R^2	φ^{Si}_{lp}	φ^{Si}_{p}
H	-5.9 (-8.4)	-3.2 (0.3)
Me	-5.1 (-7.6)	-2.2 (1.3)
F	-8.1 (-11.2)	-2.4 (0.1)

$Cp(L)_2M\cdot$				
	φ^{M}_{LUMO}	φ^{M}_{SOMO}	HOMO-1	HOMO-2
M = W				
L=CO	-2.8 (0.6)	-5.3 (-7.9)	-5.7 (-8.2)	-5.8 (-8.0)
L=PMe₃	-1.3 (1.5)	-3.2 (-5.2)	-3.6 (-5.9)	-3.9 (-6.1)
L=PF₃	-3.2 (0.2)	-5.9 (-8.8)	-6.1 (-9.0)	-6.4 (-9.1)
M = Mo				
L=CO	-2.5 (0.6)	-5.5 (-8.2)	-5.8 (-8.8)	-6.0 (-8.5)
L=PMe₃	-1.1 (1.6)	-3.6 (-6.0)	-3.8 (-6.5)	-3.9 (-6.7)
L=PF₃	-2.9 (0.2)	-6.1 (-9.0)	-6.3 (-9.4)	-6.6 (-9.6)

[a] BS-II calculation. DFT and HF energies are presented without and in parenthesis, respectively.

with the φ^{M}_{SOMO} of $Cp(CO)_2M\cdot$ and the φ_{π}^{2} mainly participates in charge-transfer (CT) interaction with the φ^{M}_{LUMO} of $Cp(CO)_2M\cdot$. In the acetylide-silylene form, the M-silylene

interaction is not strong very much because the silylene moiety tends to form silacyclopropenyl group by changing its direction toward the acetylide moiety [22]. Though the silacyclopropenyl group is not completely formed [22, 23], two kinds of CT interactions are strongly formed between acetylide and silylene moieties; one is the CT from the lone pair (φ^{Si}_{lp}) of silylene to the π^* $(\varphi^{AC}_{\pi^*})$ of acetylide and the other is the CT from the π (φ^{AC}_{π}) of acetylide to the empty p (φ^{Si}_{p}) of silylene (Figure 3.2 (C) and (D)) [22, 23].

The introduction of F on Si weakens both CT interactions, as follows: The F substituent lowers the φ^{Si}_{lp} energy of silylene by 2.2 eV through its σ-electron-withdrawing nature, as shown in Table 3.3, to weaken the CT from silylene to acetylide, where DFT(B3PW91)/BS-II-calculated orbital energies are presented. Also, the F substituent raises the φ^{Si}_{p} energy of silylene by 0.8 eV through its π-electron-donating nature (see Table 3.3), which weakens the CT from acetylide to silylene. As a result, the acetylide-silylene interaction is considerably weakened by the introduction of F on Si.

The introduction of F on Si, on the other hand, strengthens the M-(η^3-R$^2_2$SiCCR^1) bonding interaction, which is interpreted in terms of the valence orbital energy of the η^3-R$^2_2$SiCCR^1 group. As shown in Table 3.3, the $\varphi_{n\pi}$ energy of ·R$^2_2$SiCCR^1 becomes lower by 0.8 eV by the introduction of F on Si. The M-(η^3-R$^2_2$SiCCR^1) bond energy was successfully discussed with eqs 3.1 and 3.2 [25, 41], where ε_A and ε_B are orbital energies of SOMOs of two fragments and β is resonance integral. The eq 3.1 is derived on the basis of simple

$$\Delta E_{cov} = \sqrt{(\varepsilon_A - \varepsilon_B)^2 + 4\beta^2} \qquad (3.1)$$

$$\Delta E_{cov}^{approx} = \left|\varepsilon_A - \varepsilon_B\right| + \frac{\beta^2}{\left|\varepsilon_A - \varepsilon_B\right|} \qquad (3.2)$$

Hückel MO method and the eq 3.1 is simplified to eq 3.2 when the $\left| \varepsilon_A - \varepsilon_B \right|$ value is much larger than the $\left| \beta \right|$ value. These eqs indicate that the A-B bond energy becomes larger as the SOMO energy difference increases when the β value does not change. Note that the β value is also an important factor to determine the bond strength. The β value between $Cp(CO)_2M\cdot$ and $\cdot R^2{}_2SiCCR^1$ depends on the overlap between the valence orbital of $Cp(CO)_2M\cdot$ and that of $\cdot R^2{}_2SiCCR^1$. Because the valence orbital of $\cdot R^2{}_2SiCCR^1$ is mainly determined by the SiCC flame, it is likely that the β value does not depend very much on the substituents R^1 and R^2. This suggests that the energy difference between the φ^M_{SOMO} and $\varphi_{n\pi}$ must be examined as an important factor to discuss how much the bond energy depends on R^1 and R^2. The φ^M_{SOMO} energy of $Cp(CO)_2M\cdot$ is higher than the $\varphi_{n\pi}$ energy of $\cdot R^2{}_2SiCCR^1$ (see Table 3.3). Thus, the M-$(\eta^3$-$R^2{}_2SiCCR^1)$ bond energy becomes larger as the $\varphi_{n\pi}$ energy of $\cdot R^2{}_2SiCCR^1$ becomes lower. The σ-electron-withdrawing F on Si lowers the $\varphi_{n\pi}$ energy of $\cdot R^2{}_2SiCCR^1$ and increases the energy gap between $\varphi_{n\pi}$ and φ^M_{SOMO}, which leads to strengthening of the M-$(\eta^3$-$R^2{}_2SiCCR^1)$ bonding interaction. From these results, it should be concluded that the F on Si stabilizes the η^3-silapropargyl/alkynylsilyl form and destabilizes the acetylide-silylene form.

Though both Me and F on Si increase the stability of the η^3-silapropargyl/alkynylsilyl form, the effect of the Me is considerably smaller than that by the F. The Me on Si raises the $\varphi_{n\pi}$ energy of $\cdot R^2{}_2SiCCR^1$ by 0.4 eV, which leads to decrease of the energy difference between SOMOs of $Cp(CO)_2M\cdot$ and $\cdot R^2{}_2SiCCR^1$. Thus, the M-$(\eta^3$-$R^2{}_2SiCCR^1)$ bonding interaction becomes weak by introduction of Me on Si. Also, the Me on Si raises the φ^{Si}_{lp} and φ^{Si}_p energies of $SiMe_2$ by 0.8 eV and 1.0 eV, respectively, relative to those of SiH_2 (Table 3.3), which strengthens the CT from silylene to acetylide but weakens the CT from acetylide

to silylene. It is likely that the CT from acetylide to silylene is more important than the CT from silylene to acetylide because singlet silylene is electron-withdrawing. This suggests that the acetylide-silylene interaction becomes weak by the Me on Si. Thus, the Me on Si weakens both of the M-(η^3-$R^2_2SiCCR^1$) and acetylide-silylene interactions. As a result, the Me on Si does not influence very much the relative stability of the η^3-silapropargyl/alkynylsilyl form to the acetylide-silylene form.

3.3.4   Comparison Between W and Mo Centers

We wish to explain the reason why the Mo center favors the η^3-silapropargyl/alkynylsilyl form but the W center favors the acetylide-silylene form. The φ^M_{SOMO} and doubly occupied d orbitals of Cp(CO)$_2$Mo· exsist at lower energies but the φ^M_{LUMO} (-2.5 eV) exsists at higher energy than those of the W analogue (-2.8 eV), as shown in Table 3.3. Because the φ^{AC}_{sp} energy of ·CCR^1 is lower than the φ^M_{SOMO} energy of Cp(CO)$_2$M· (Table 3.3), the SOMO energy difference is larger in the W complex (5.0 eV) than in the Mo complex (4.8 eV). Because, the $\varphi_{n\pi}$ energy of ·$R^2_2SiCCR^1$ is lower than the φ^M_{SOMO} energy of Cp(CO)$_2$M· (Table 3.3), the SOMO energy difference between ·$R^2_2SiCCR^1$ and Cp(CO)$_2$M· is larger in the W complex (0.7 eV) than in the Mo complex (0.5 eV). Moreover, the second term of eq 3.1 more contributes to the M-L bond energy in the third row transition metal complex than in the second row transition metal complex; because the β value becomes larger upon going from the second row transition metal to the third row one. As a result, the W-C1 and W-(η^3-$R^2_2SiCCR^1$) bonding interactions are stronger than the Mo-C1 and Mo-(η^3-$R^2_2SiCCR^1$) bonding interactions, respectively. In the η^3-silapropargyl/alkynylsilyl form, not only the covalent M-(η^3-$R^2_2SiCCR^1$) interaction but also the charge-transfer (CT) from the φ^2_π of

$\cdot R^2_2SiCCR^1$ to the φ^M_{LUMO} of $Cp(CO)_2M\cdot$ participates in energy stabilization. Because the φ_π^2 of $\cdot R^2_2SiCCR^1$ is largely localized in the CC moiety (see Figure 3.2 (A)), the M-(CC) interaction is formed by this CT. Because the φ^M_{LUMO} energy of $Cp(CO)_2W\cdot$ (-2.8 eV) is lower than that of $Cp(CO)_2Mo\cdot$ (-2.5 eV), this CT interaction is stronger in the W complex than in the Mo complex. Thus, both of the $M-CCR^1$ and $M-(\eta^3-R^2_2SiCCR^1)$ bonding interactions are stronger in the W complex than in the Mo complex. The above simple discussion does not present the clear explanation, and therefore, we must inspect the bonding interaction in more detail.

It is noted that the φ^{AC}_{sp} energy of $\cdot CCR^1$ is much lower than the $\varphi_{n\pi}$ energy of $\cdot R^2_2SiCCR^1$ by 4.3 eV (Table 3.3); in other words, the SOMO energy difference between $\cdot CCR^1$ and $Cp(CO)_2M\cdot$ is much larger than that between $\cdot R^2_2SiCCR^1$ and $Cp(CO)_2M\cdot$. Thus, the $M-CCR^1$ bond energy increases upon going from Mo to W because the φ^M_{SOMO} energy of $Cp(CO)_2W\cdot$ (-5.3 eV) is higher than that of $Cp(CO)_2Mo\cdot$ (-5.5 eV), and its increment is almost proportional to the SOMO energy difference between $Cp(CO)_2M\cdot$ and $\cdot CCR^1$, as presented by eq 3.2. On the other hand, the $M-(\eta^3-R^2_2SiCCR^1)$ bond energy increases upon going from Mo to W to a lesser extent than the increment of the SOMO energy difference between $Cp(CO)_2M\cdot$ and $\cdot R^2_2SiCCR^1$. In this case, the second term of eq 3.1 more contributes to the $M-(\eta^3-R^2_2SiCCR^1)$ bond energy than the $M-CCR^1$ bond energy. In other words, the $M-CCR^1$ bond energy increases upon going from Mo to W to a greater extent than does the $M-(\eta^3-R^2_2SiCCR^1)$ bond energy. This means that the Mo center is more favorable for stabilization of the η^3-silapropargyl/alkynylsilyl form than the W center.

3.3.5   Why Do Me, ^{t}Bu, and CF$_3$ on C Influence the Relative Stability of the η^3-Silapropargyl/Alkynylsilyl Form to the Acetylide-Silylene Form?

The frontier orbital energies of ·CCR^1 and ·R$^2_2$SiCCR^1 become higher by introduction of Me on C2 (see Table 3.3), which leads to decrease of the energy difference between their valence orbitals and the φ^M_{SOMO} of Cp(CO)$_2$M·. On the other hand, the frontier orbital energies of ·CCR^1 and ·R$^2_2$SiCCR^1 become lower by introduction of CF$_3$ on C2, which leads to increase of the energy difference between their valence orbitals and the φ^M_{SOMO} of Cp(CO)$_2$M·. Thus, Me on C2 weakens both M-CCR^1 and M-(η^3-R$^2_2$SiCCR^1) bonds but CF$_3$ on C2 strengthens both of them. As a result, Me and CF$_3$ do not change the relative stability of the η^3-silapropargyl/alkynylsilyl form very much. We could not find clear reason why the Me on C2 moderately and the CF$_3$ on C2 even more moderately increase the stability of the η^3-silapropargyl/alkynylsilyl form [42].

Though the electronic effects are similar between Me and ^{t}Bu (Table 3.3), they induce the reverse effect on the stability of the η^3-silapropargyl/alkynylsilyl form (Table 3.2), as discussed above, indicating that not the electronic factor but the steric factor plays important role here. It is likely that the bulky substituent on C2 tends to take a more distant position from the Cp. Thus, the bulky substituent such as ^{t}Bu prefers the acetylide-silylene form to the η^3-silapropargyl/alkynylsilyl form, because the ^{t}Bu on C2 is more distant from the Cp in the acetylide-silylene form than in the η^3-silapropargyl/alkynylsilyl form.

3.3.6 Ligand Effects on Geometries and Relative Stabilities of $CpL_2M(\eta^3\text{-}H_2SiCCH)$ and $CpL_2M(CCH)(SiH_2)$ (M = W or Mo and L = CO, PMe$_3$, or PF$_3$)

Use of electron-donating PMe$_3$ in place of CO moderately decreases the Mo-Si, Mo-C1, and Mo-C2 distances and even more moderately the Mo-Cp distance in **3-PMe$_3$** and moderately decreases the Mo-C1 and Si-C2 distances in **4-PMe$_3$** (Figure 3.3). These results suggest that the M-(η^3-R$^2{}_2$SiCCR^1) bond becomes stronger in **3-PMe$_3$** than in **3** and the Mo-CCR^1 bond and the acetylide-silylene interaction become stronger in **4-PMe$_3$** than in **4**. Electron-withdrawing PF$_3$ induces opposite geometry changes to those of PMe$_3$ except for the Mo-C1 distance in **3-PF$_3$**, as follows: Use of PF$_3$ in place of CO moderately increases the Mo-Si distance but moderately decreases the Mo-C1 and Mo-Cp distances in **3-PF$_3$**, while it moderately increases the Mo-C1 and Si-C2 distances and moderately decreases the Mo-Cp distance in **4-PF$_3$**; see Appendix A.3.3 for the discussion of the M-Cp distance. These results suggest that the M-(η^3-R$^2{}_2$SiCCR^1) bond becomes moderately weaker in **3-PF$_3$** than in **3** and the Mo-CCR^1 bond and the acetylide-silylene interaction become moderately weaker in **4-PF$_3$** than in **4**. These suggestions are also supported by the Wiberg bond index; see Appendix A.3.7.

PMe$_3$ considerably decreases the stability of the η^3-silapropargyl/alkynylsilyl form by 9.4 and 4.8 kcal/mol in the W and Mo complexes, respectively, as shown in Table 3.2, and PF$_3$ slightly decreases it in both W and Mo complexes, in contrast to the opposite geometry changes to those of PMe$_3$.

PMe$_3$ considerably destabilizes the φ^M_{SOMO} energy of CpL$_2$M· (M = W or Mo; L = CO, PMe$_3$, or PF$_3$) by about 2.0 eV compared to CO (Table 3.3). On the other hand, PF$_3$

(A) PMe₃ ligand systems

3-PMe₃
< PMoP = 86

4-PMe₃
< PMoP = 88

(B) PF₃ ligand systems

3-PF₃
< PMoP = 83

4-PF₃
< PMoP = 85
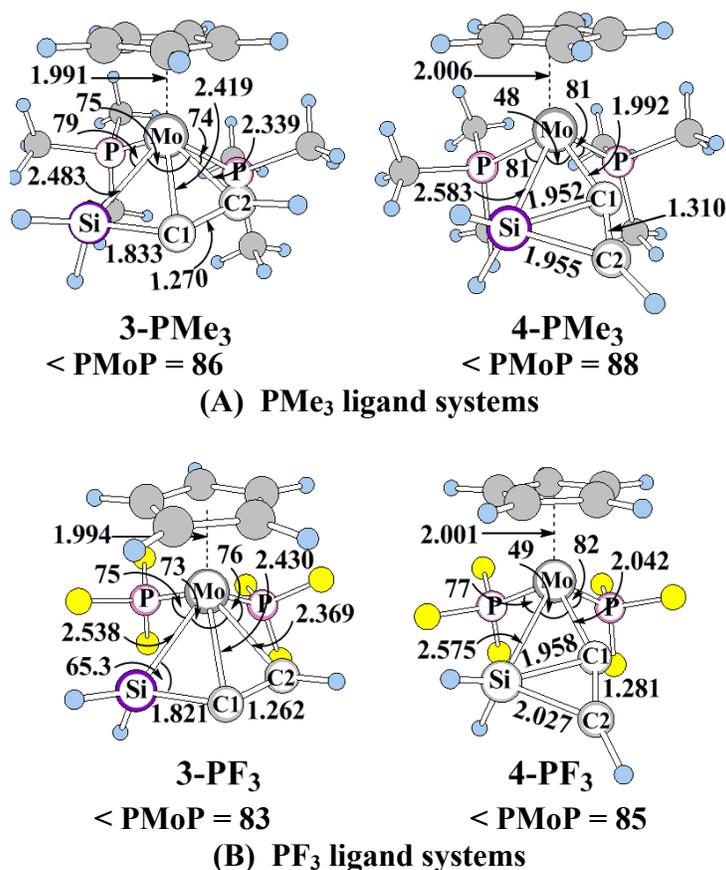
Figure 3.3. DFT(B3PW91)/BS-I optimized geometries of $CpL_2Mo(\eta^3-H_2SiCCH)$ and $CpL_2Mo(CCH)(SiH_2)$, where L = PMe₃ or PF₃. See Appendix A.3.9 for geometries of the tungsten analogues. Bond lengths are in angstroms and bond angles are in degree.

moderately stabilizes the φ_{SOMO}^M energy by 0.6 eV. Though PMe₃ and PF₃ induce opposite electronic effects to each other, both of them increase the stability of the acetylide-silylene form. This result suggests that not electronic factor but steric factor plays important role here, as follows: Because PF₃ and PMe₃ are larger than CO, the coordination structure around metal center becomes more congested by coordination of PMe₃ and PF₃. Also, the coordination structure of the η^3-silapropargyl/alkynylsilyl complex is more congested than that of the acetylide-silylene complex; for instance, the SiMC2 angle is about 75° in the η^3-

silapropargyl/alkynylsilyl form but the SiMC1 angle is about 50° in the acetylide-silylene form. Thus, PF_3 and PMe_3 prefer the less congested acetylide-silylene form.

From these results, it is concluded that among these three ligands, CO should be used to stabilize the η^3-silapropargyl/alkynylsilyl form and PMe_3 should be used to stabilize the acetylide-silylene form.

3.3.7   Conversion   Reaction   of $Cp(CO)_2Mo(\eta^3\text{-}H_2SiCCH)$ to $Cp(CO)_2Mo(CCH)(SiH_2)$

We wish to mention the conversion reaction of $Cp(CO)_2Mo(\eta^3\text{-}H_2SiCCH)$ **3** to $Cp(CO)_2Mo(CCH)(SiH_2)$ **4** because the experimental conditions to isolate **3** depend on the activation barrier of this conversion reaction. This reaction occurs through the transition state **TS$_{3\text{-}4}$**, as shown in Figure 3.4. In **TS$_{3\text{-}4}$**, the Si-C1 and Mo-C2 bonds of **3** are going to be broken like those of the tungsten analogue [22]. The geometry changes in the imaginary frequency, which are displayed by arrows in Figure 3.4, are consistent with this conversion reaction.

The CCSD(T) and DFT methods present similar activation barrier (E_a) but the MP4(SDTQ) method presents larger barrier than the CCSD(T) and DFT methods; see Appendix A.3.10. The barrier moderately fluctuates around MP2 and MP3, and somewhat increases upon going to MP4(SDTQ) from MP4(SDQ).   Thus, it is concluded that the DFT- and CCSD(T)- calculated activation barriers are reliable for both W and Mo complexes. The activation barrier of the conversion reaction of **3** to **4** is 13.2 (14.1) kcal/mol, where values without parenthesis and with parenthesis are DFT- and CCSD(T)-calculated Ea values, respectively. This activation barrier is moderately smaller than that of the tungsten complex,
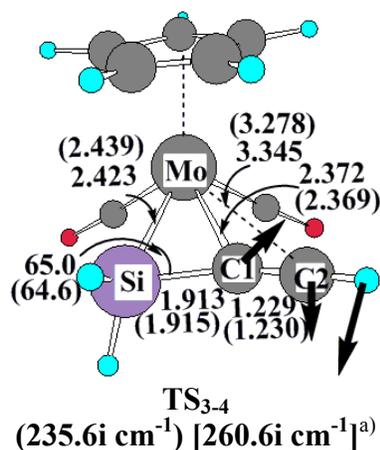
Figure 3.4. DFT(B3PW91)/BS-I optimized geometry of transition state in conversion reaction of $Cp(CO)_2Mo(\eta^3\text{-}H_2SiCCH)$ **3** to $Cp(CO)_2Mo(CCH)(SiH_2)$ **4**. Bond lengths are in angstrom and bond angles are in degree. In parentheses are parameters for tungsten analogue.

[a] Imaginary frequencies for molybdenum and tungsten analogues are given in parenthesis and bracket, respectively. Arrows represent important movement of atoms in imaginary frequency.

which is 15.3 (15.8) kcal/mol [22]. This difference is interpreted in terms of the M-(η^3-$R^2_2SiCCR^1$) bond, as follows: In the transition state, the Si-C1 bond is being broken and the C2 is moving away from the Mo center, as shown in Figure 3.4. The origin of the activation barrier is the weakening of the Si-C1 bond and the Mo-(C1-C2) coordinate bond. Because the Si-C1 bond weakening occurs in both W and Mo complexes, the difference in E_a between W and Mo complexes arises from the weakening of the M-(C1-C2) coordinate bond. Because the φ_π of $\cdot R^2_2SiCCR^1$ is largely localized on the C1C2 moiety (Figure 3.2), as discussed above, the C1C2 moiety forms the CT with the φ^M_{LUMO} of $Cp(CO)_2M\cdot$. The Mo-(C1-C2) coordinate bond is moderately weaker than the W-(C1-C2) bond because the φ^M_{LUMO} energy of $Cp(CO)_2Mo\cdot$ (-2.5 eV) is higher than that of the W analogue (-2.8 eV). As a result, the Mo-C2 bond breaking induces smaller energy loss than the W-C2 bond breaking in the transition state.

These moderate activation barriers suggest that the isolation of the η^3-silapropargyl/alkynylsilyl form should be tried at low temperature in both of Mo and W complexes.

3.4   Conclusions

The relative stability of the η^3-silapropargyl/alkynylsilyl complex $CpL_2M(\eta^3$-$R^2_2SiCCR^1)$ (**1** for M = W and **3** for M = Mo; L = CO, PMe$_3$, or PF$_3$; Cp = C$_5$H$_5$, R^1 = H, Me, ^{t}Bu, or CF$_3$, R^2 = H, Me or F) to the acetylide-silylene complex $CpL_2M(CCR^1)(SiR^2_2)$ (**2** for M = W and **4** for M = Mo) was theoretically investigated.   Computational results are summarized in Scheme 3.2. From these computational results, we wish to predict that the combination of electron-withdrawing CF$_3$ on C, σ-electron-withdrawing/π-electron-donating F on Si, Mo center, and CO is the best to stabilize the η^3-silapropargyl/alkynylsilyl form and the combination of bulky ^{t}Bu on C, either H or Me on Si, W center, and PMe$_3$ is the best to stabilize the acetylide-silylene form.

The conversion reaction of Cp(CO)$_2$Mo(η^3-H$_2$SiCCH) **3** to Cp(CO)$_2$Mo(CCH)(SiH$_2$) **4** occurs with moderate activation barrier, suggesting that the isolation of the η^3-silapropargyl/alkynylsilyl form should be tried at low temperature.
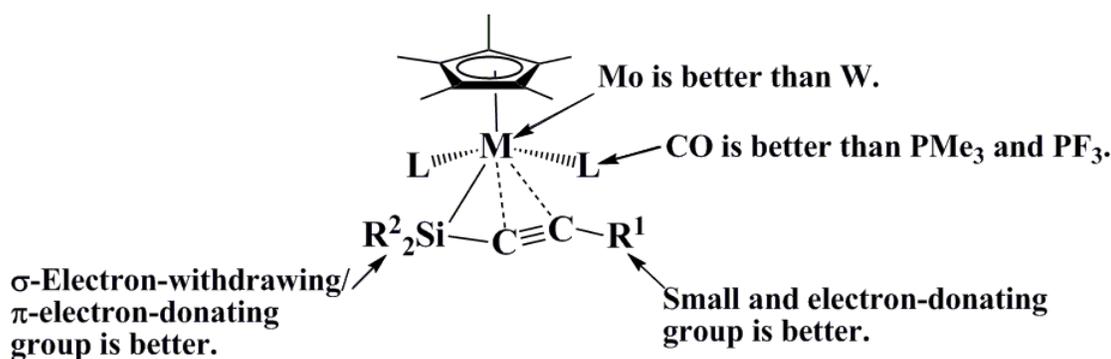
Scheme 3.2. How to stabilize $CpL_2M(\eta^3$-$R^2_2SiCCR^1)$

From this theoretical study, we wish to predict that the synthesis of the η^3-silapropargyl/alkynylsilyl complex will be succeeded in a near future by employing Mo as the metal center with Cp and CO ligands and introducing σ-electron-withdrawing/π-electron-donating group on Si and σ-electron-withdrawing group on C [43].

Bibliography

[1]   (a) Sekiguchi, A.; Ichinohe, M.; Kinjo, R. *Bull. Chem. Soc. Jpn*. **2006**, *6*, 825. (b) Frenking, G.; Krapp, A.; Nagase, S.; Takagi, N.; Sekiguchi, A. *Chemphyschem* **2006**, *7*, 799. (c) Sekiguchi, A.; Rei, K.; Masaaki, I. *Science* **2004**, *305*, 1755. (d) Sekiguchi, A.; Zigler, S.; Robert, W.; Josef, M. *J. Am. Chem. Soc*. **1986**, *108*, 4241.

[2]   (a) Weidenbruch, M. *Angew. Chem., Int. Ed*. **2005**, *44*, 514. (b) Weidenbruch, M. *J. Organomet. Chem*. **2002**, *646*, 39.

[3]   Jutzi, P. *Angew. Chem. Int. Ed*. **2000**, *39*, 3797.

[4]   (a) Power, P. P. *Chem. Comm*. **2003**, *17*, 2091 and references therein. (b) Power, P. P. *Organometallics* **2007**, *26*, 4362.

[5]   (a) Takagi, N.; Nagase, S. *Eur. J. Inorg. Chem*. **2002**, *11*, 2775. (b) Takagi, N.; Nagase, S. *Chem. Lett*. **2001**, *10*, 966. (c) Kobayashi, K.; Takagi, N.; Nagase, S. *Organometallics* **2001**, *20*, 234. (d) Takagi, N.; Nagase, S. *Organometallics* **2001**, *20*, 5498. (e) Nagase, S.; Kobayashi, K.; Takagi, N. *J. Organomet. Chem*. **2000**, *611*, 264. (f) Kobayashi, K.; Nagase, S. *Organometallics* **1997**, *16*, 2489.

[6]   (a) Clabo, D. A.; Schaefer, H. F. *J. Chem. Phys*. **1986**, *84*, 1664. (b) Thies, B. S.; Grev, R. S.; Schaefer, H. F. *Chem. Phys. Lett*. **1987**, *140*, 355. (c) Colegrove, B. T.; Schaefer, H. F. *J. Phys. Chem*. **1990**, *94*, 5593. (d) Colegrove, B. T.; Schaefer, H. F. *J. Am. Chem. Soc*. **1991**, *113*, 1557. (e) Grev, R. S. *Adv. Organomet. Chem*. **1991**, *33*, 125. (f) Grev, R. S.; Schaefer, K. F. *J. Chem. Phys*. **1992**, *97*, 7990.

[7]   (a) Cordonnier, M.; Bogey, M.; Demuynck, C.; Destombes, J.-L. *J. Chem. Phys.* **1992**, *97*, 7984. (b) Bogey, M.; Bolvin, H.; Demuynck, C.; Destombes, J. L. *Phys. Rev. Lett.* **1991**, *66*, 413.

[8]   (a) Koseki, S.; Gordon, M. S. *J. Phys. Chem.* **1988**, *92*, 364. (b) Koseki, S.; Gordon, M. S. *J. Phys. Chem.* **1989**, *93*, 118.

[9]   Lischka, H.; Kohler, H.-J. *J. Am. Chem. Soc.* **1983**, *105*, 6646.

[10]   Binkley, J. S. *J. Am. Chem. Soc.* **1984**, *106*, 603.

[11]   Kalcher,J.; Sax, A.; Olbrich, G. *Int. J. Quantum Chem.* **1984**, *25*, 543.

[12]   Kohler, H.-J.; Lischka, H. *Chem. Phys. Lett.* **1984**, *112*, 33.

[13]   Wiberg, N.; Niedermayer, W.; Fischer, G.; Nöth, H.; Suter, M. *Eur. J. Inorg. Chem.* **2002**, 1066.

[14]   Kutzelning, W. *Angew. Chem. Int. Ed. Engl.* **1984**, *23*, 272.

[15]   Coolidge, M. B.; Hrovat, D. A.; Borden, W. T. *J. Am. Chem. Soc.* **1992**, *114*, 2354.

[16]   Doherty, S.; Corrigan, G. F.; Carty, A. G.; Sappa, E. *Adv. Organomet. Chem.* **1995**, *37*, 39.

[17]   Tsuji, J.; Mandai, T. *Angew. Chem., Int. Ed. Engl.* **1995**, *34*, 2589.

[18]   (a) Casey, C. P.; Yi, C. S. *J. Am. Chem. Soc.* **1992**, *114*, 6597. (b) Casey, C. P.; Selmeczy, A. D.; Nash, J. R.; Yi, C. S.; Powell, D. R.; Hayashi, R. K. *J. Am. Chem. Soc.* **1996**, *118*, 6698. (c) Casey, C. P.; Nash, J. R.; Yi, C. S.; Selmeczy, A. D.; Chung, S.; Powell, D. R.; Hayashi, R. K. *J. Am. Chem. Soc.* **1996**, *118*, 6698. (d) Casey, C. P.; Boller, T. M.; Kraft, S.; Guzei, I. A. *J. Am. Chem. Soc.* **2002**, *124*, 13215.

[19]   Chen, J. T. *Coord. Chem. Rev.* **1999**, *190/192*, 1143 and references therein.

[20]   (a) Shuchart, C. E.; Richard, W. R.; Wojcicki, A. *J. Organomet. Chem*. **1992**, *424*, 185.

(b) Blosser, P. W.; Gallucci, J. C.; Wojcicki, A. *J. Am. Chem. Soc*. **1993**, *115*, 2994. (c) Blosser, P. W.; Schimpff, D. G.; Gallucci, J. C.; Wojcicki, A. *Organometallics* **1993**, *12*, 1993. (d) Graham, J. P.; Wojcicki, A.; Bursten, B. E. *Organometallics* **1999**, *18*, 837. (e) Wojcicki, A. *Inorg. Chem. Comm*. **2002**, *5*, 82 and references therein.

[21]   Sakaba, H.; Yoshida, M.; Kabuto, C.; Kabuto, K. *J. Am. Chem. Soc*. **2005**, *127*, 7276.

[22]   Ray, M.; Nakao, Y.; Sato, H.; Sakaba, H.; Sakaki, S. *J. Am. Chem. Soc*. **2006**, *128*, 11927.

[23]   The complex **B** of Scheme 1 contains strong charge transfer interactions between acetylide and silylene moieties, as discussed previously in our work.[22] As a result, the silylene moiety considerably changes its direction toward the acetylide moiety and the bonding interaction between metal and silylene becomes weak. These features indicate that the bonding nature of this complex is intermediate between those of pure acetylide silylene complex and pure silacyclopropenyl complex. Here, we use the name of "acetylide-silylene complex" because there is no appropriate name for such species, where we placed a hyphen "-" between words of acetylide and silylene to represent the presence of bonding interaction between them.

[24]   Sakaba, H.; Watanabe, S.; Kabuto, C.; Kabuto, K. *J. Am. Chem. Soc*. **2003**, *125*, 2842.

[25]   Ray, M.; Nakao, Y.; Sato, H.; Sakaki, S. *Organometallics* **2007**, *26*, 4413.

[26]   The proton NMR chemical shifts and spectrum shape indicate that $Cp^*(CO)_2W(CC^tBu)(SiPh_2)$ takes closed shell singlet state.[21] Though $Cp^*(CO)_2W(\eta^3\text{-}R^2{}_2SiCCR^1)$ has not been synthesized, proton NMR chemical shifts and spectrum shape

of the similar $Cp^*(CO)_2W(\eta^3\text{-}Me_2SiCHCMe_2)$ indicate that this complex takes closed-shell singlet state, too.[24]

[27]   (a) Becke, A. D. *Phys Rev. A*. **1988**, *38*, 3098. (b) Becke, A. D. *J. Chem. Phys*. **1993**, *98*, 5648.

[28]   (a) Perdew, J. P. *In Electronic Structure of Solids`91, Ziesche, P.; Eschrig, H., Ed.; Akademic Verlag, Berlin, 1991; p 11. (b) Perdew, J. P.; Chevary, J. A.; Vosko, S. H.; Jackson, K. A.; Pederson, M. R.; Singh, D. J.; Fiolhais, C. *Phys. Rev. B*. **1992**, *46*, 6671. (c) Perdew, J. P.; Chevary, J. A.; Vosko, S. H.; Jackson, K. A.; Pederson, M. R.; Singh, D. J.; Fiolhais, C. *Phys. Rev. B*. **1993**, *48*, 4978. (d) Perdew, J. P.; Burke, K.; Wang, Y. *Phys Rev. B*. **1996**, *54*, 16533.

[29]   (a) Lee, C.; Yang, W.; Parr, R. G. *Phys. Rev. B*. **1988**, *37*, 785. (b) Miehlich, B.; Savin, A.; Stoll, H.; Preuss, H. *Chem. Phys. Lett*. **1989**, *157*, 200.

[30]   Hay, P. J.; Wadt, W. R. *J. Chem. Phys*. **1985**, *82*, 299.

[31]   (a) Dunning Jr, T. H. *J. Chem. Phys*. **1989**, *90*, 1007. (b) Woon, D. E.; Dunning Jr, T. H. *J. Chem. Phys*. **1993**, *98*, 1358.

[32]   (a) Ditchfield, R.; Hehre, W. J.; Pople, J. A. *J. Chem. Phys*. **1971**, *54*, 724. (b) Hehre, W.; Ditchfield, R.; Pople, J. A. *J. Chem. Phys*. **1972**, *56*, 2257.

[33]   Couty, M.; Hall, M. B. *J. Comput. Chem*. **1996**, *17*, 1359.

[34]   Ehlers, A. W.; Böhme, D. S.; Gobbi, A.; Höllwarth, A.; Jonas, V.; Köhler, K. F.; Stegmann, R.; Veldkamp, A.; Frenking, G. *Chem. Phys. Lett*. **1993**, *208*, 111.

[35]   Andrae, D.; Haeussermann, U.; Dolg, M.; Stoll, H.; Preuss, H. *Theor. Chim. Acta* **1990**, *77*, 123.

[36]   Martin, J. M. L.; Sundermann, A. *J. Chem. Phys*. **2001**, *114*, 3408.

[37] (a) Dunning Jr., T. H. *J. Chem. Phys*. **1989**, *90*, 1007. (b) Woon, D. E.; Dunning Jr., T. H. *J. Chem. Phys*. **1993**, *98*, 1358.

[38] (a) Miertuš, S.; Scrocco, E.; Tomasi, J. *Chem. Phys*. **1981**, *55*, 117. (b) Miertuš, S.; Tomasi, J. *Chem. Phys*. **1982**, *65*, 239. (c) Cossi, M.; Barone, V.; Cammi, R.; Tomasi, J. *Chem. Phys. Lett*. **1996**, *255*, 327.

[39] Pople, J. A.; et al. *Gaussian 03,* Revision C.02, Gaussian Inc.: Wallingford, CT, **2004**.

[40] Introduction of Me on C2 more increases the stability of the η^3-silapropargyl/alkynylsilyl form than that of CF_3, when H is bound with Si. However, introduction of CF_3 more increases the stability than that of Me, when F is bound with Si. We could not find the clear reason.

[41] (a) Sakaki, S.; Biswas, B.; Sugimoto, M. *Organometallics* **1998**, *17*, 1278. (b) Biswas, B.; Sugimoto, M.; Sakaki, S. *Organometallics* **1999**, *18*, 4015. (c) Sakaki, S.; Kai, S.; Sugimoto, M. *Organometallics* **1999**, *18*, 4825. (d) Sumimoto, M.; Iwane, N.; Takahama, T, Sakaki, S. *J. Am. Chem. Soc*. **2004**, *126*, 10457.

[42] The small energy gap between the frontier orbital of $Cp(CO)_2M\cdot$ and those of $\cdot CCR^1$ and $\cdot R^2{}_2SiCCR^1$ leads to the large stability of the η^3-silapropargyl/alkynylsilyl form; see discussion of Mo and W centers. Thus, Me on C2 increases the stability of the η^3-silapropargyl/alkynylsilyl form.   However, CF_3 on C2 moderately increases the stability of the η^3-silapropargyl/alkynylsilyl form, against the above expectation. It is likely that the CT from acetylide to silylene becomes weak by CF_3 on C2, which moderately increases the stability of the η^3-silapropargyl/alkynylsilyl form.

[43] In the synthesis of $Cp^*(CO)_2W(CC^tBu)(SiPh_2)$, NMR spectra indicate that at low temperature several monomeric species are equilibrated with a dimer complex

$[Cp^*(CO)_2W(Me_2SiCC^tBu)]_2$. $Cp^*(CO)_2W(\eta^3\text{-}Me_2SiCC^tBu)$ is one of the plausible candidates of such monomeric species. This result strongly suggests that the η^3-silapropargyl/alkynylsilyl form can be synthesized by reasonable choices of metal center and substituents. See footnote 4 of ref. 21.

Appendix

A.3.1   Optimized Parameters of Cp(CO)$_2$W(CC^{t}Bu)(SiH$_2$) **2-^{t}Bu**.

Table A.3.1.   Selected Optimized Parameters[a] of Cp(CO)$_2$W(CC^{t}Bu)(SiH$_2$) **2-^{t}Bu.**

	B3LYP	B3PW91[b]	Expt[c]
W-Si	2.576	2.564	2.567
W-C1	2.065	2.047	2.050
Si-C1	1.967	1.957	1.937
Si-C2	2.072	2.038	2.009
C1-C2	1.281	1.286	1.270
∠WSiC1	52.0	51.7	51.9
∠C1SiC2	36.9	37.5	37.5

[a] The BS-I was employed. Bond lengths are in angstroms and bond angles are in degrees.
[b] Ref. 22.
[c] Ref. 21.

A.3.2 Optimized geometries of $Cp(CO)_2W(\eta^3-R^2_2SiCCR^1)$ and $Cp(CO)_2W(CCR^1)(SiR^2_2)$.
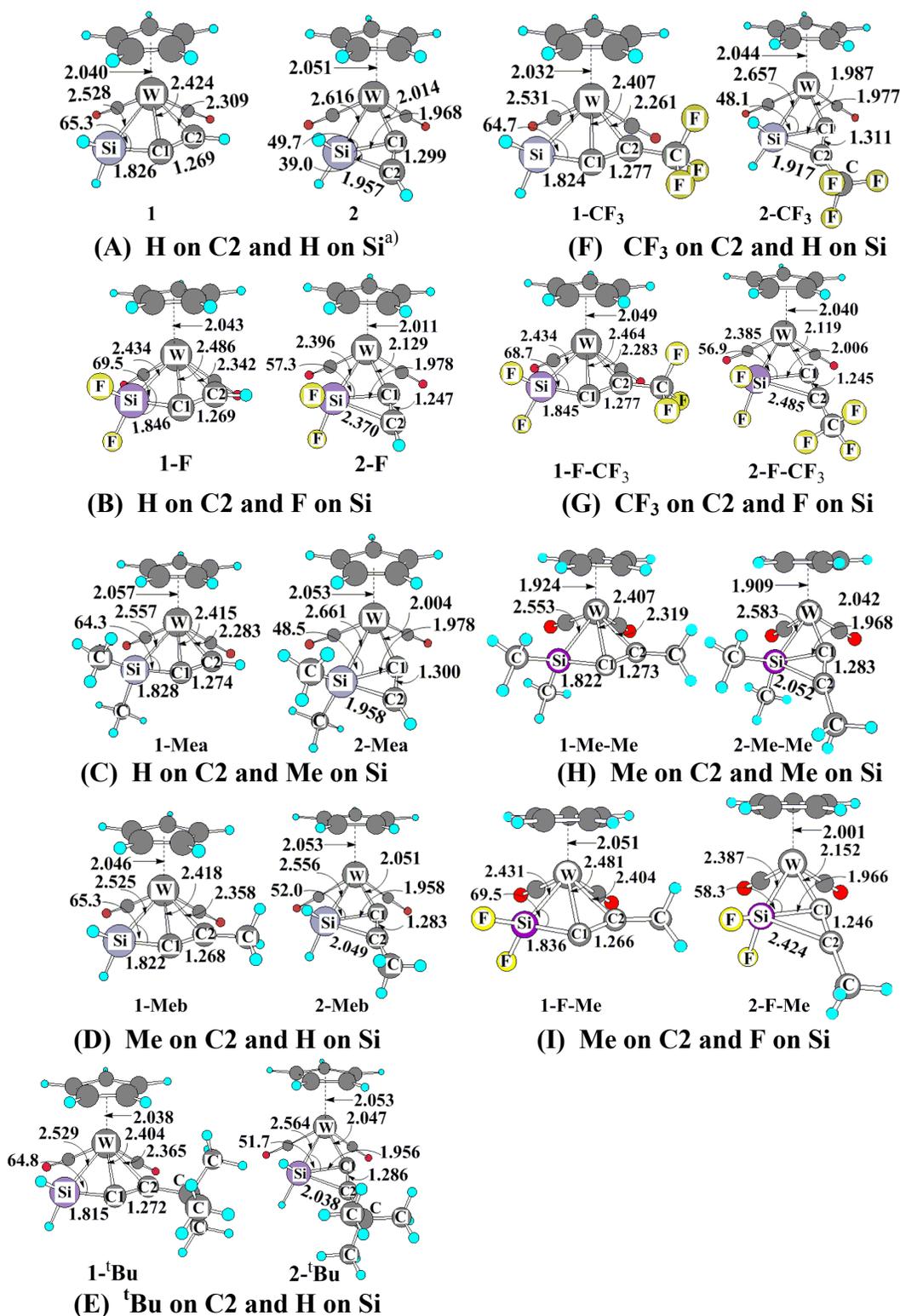
Figure A.3.1 DFT/BS-I optimized geometries of $Cp(CO)_2W(\eta^3-R^2_2SiCCR^1)$ and $Cp(CO)_2W(CCR^1)(SiR^2_2)$, where R^1= H, Me, ^tBu, or CF_3 and R^2= H, F, or Me. Bond lengths are in angstrom and bond angles are in degree. [a] Reference 22.

A.3.3 Population changes of Cp and M in $Cp(CO)_2M(\eta^3\text{-}R^2_2SiCCR^1)$ and $Cp(CO)_2M(CCR^1)(SiR^2_2)$.

Table A.3.2 Population[a] changes of Cp and M in $Cp(CO)_2M(\eta^3\text{-}R^2_2SiCCR^1)$ (**1** for M = W and **3** for M = Mo) and $Cp(CO)_2M(CCR^1)(SiR^2_2)$ (**2** for M = W and **4** for M = Mo).

R^1 on C2	R^2 on Si	Mo	Cp	W	Cp
η^3-Silapropargyl/alkynylsilyl form (**1** and **3**)					
H	H	42.404	35.042	74.081	35.115
		(42.742)[b]	(35.091)	(74.444)	(35.202)
		[42.953][b]	[34.981]	[74.691]	[35.062]
H	F	42.489	35.023	74.200	35.094
Me	H	42.399	35.056	74.072	35.124
^tBu	H	42.381	35.050	74.063	35.117
CF_3	H	42.393	35.004	74.069	35.078
H	Me	42.391	35.086	74.072	35.140
Acetylide-silylene form (**2** and **4**)					
H	H	42.415	35.086	74.091	35.151
		(42.677)[b]	(35.153)	(74.424)	(35.228)
		[42.958][b]	[35.023]	[74.697]	[35.101]
H	F	42.588	35.056	74.116	35.117
Me	H	42.466	35.093	74.121	35.158
^tBu	H	42.457	35.095	74.129	35.159
CF_3	H	42.372	35.061	74.057	35.127
H	Me	42.404	35.117	74.083	35.175

[a] DFT(B3PW91)/BS-II NBO calculation.
[b] Values for PMe_3 and PF_3 are presented in parenthesis and in bracket, respectively.

(A)   The effect of F introduced to Si

The F on Si considerably lowers the lone pair orbital energy of SiR^2_2, which weakens the charge-transfer (CT) from SiF_2 to M to strengthen the charge-transfer (CT) from Cp to M. Thus, the M-Cp distance becomes shorter in the acetylide-silylene form.   In the η^3-silapropargyl/alkynylsilyl form, the situation is different, as follows: The F on Si moderately lowers the HOMO (non-bonding π) of the η^3-silapropargyl/alkynylsilyl group because the F lowers the HOMO energy by σ-electron-withdrawing nature but raises it by π-electron-donating nature.   Because the HOMO energy of the η^3-silapropargyl/alkynylsilyl group becomes moderately lower by the F on Si, the CT from the η^3-silapropargyl/alkynylsilyl group to Mo becomes moderately weaker, which moderately increases the CT from Cp to Mo in **3-F** compared to **3**. It is also likely that the larger size of F than H sterically induces the lengthening of the Mo-Cp distance.   Probably because the steric effect is larger than the electronic one, the Mo-Cp distance becomes moderately longer by the F on Si in **3-F** than in **3**. The same discussion can be presented for the W analogues.

(B)   The effect of Me introduced to Si

The Me on Si raises the orbital energy of the η^3-silapropargyl/alkynylsilyl group to suppress the CT from Cp to Mo. Thus, the Me on Si increases the Mo-Cp distance in **3-Mea**. In **4-Mea**, the Mo-Cp interaction is little influenced by the Me on Si because $SiMe_2$ mainly interacts with CCH in **4-Mea** unlike SiF_2 in **4-F** in which SiF_2 mainly interacts with the Mo center.

(C)   The effects of Me, ^tBu, and CF_3 introduced to C2

The CF_3 on C2 weakens the CT from η^3-$R^2_2SiCCR^1$ to Mo in **3-CF$_3$** and the CT from CCR^1 to Mo in **4-CF$_3$**. Thus, the Mo-Cp interaction becomes stronger and the Mo-Cp distance becomes shorter in both **3-CF$_3$** and **4-CF$_3$** than those of **3** and **4**.

The ^tBu on C2 moderately lengthens the Mo-Cp distance in **4-^{t}Bu**, as discussed in the text. This is because the ^tBu strengthens the donation of CCR^1 to weaken the CT from Cp to Mo. However, the ^tBu slightly shortens the Mo-Cp distance in **3-^{t}Bu**. Also, the Me on C2 moderately decreases the Mo-Cp distance in both **3-Meb** and **4-Meb**. The reasons for these results can not be found at this moment. Because the Mo-Cp distance does not deeply relate to the relative stability of the η^3-silapropargyl/alkynylsilyl form, we wish to stop the discussion.

(D)   The effects of PMe$_3$ and PF$_3$

In both of the PMe$_3$ and PF$_3$ complexes, the Mo-Cp distance becomes shorter than that in the CO complex. The electron population of Cp is larger in the PMe$_3$ complex than in the CO complex, and smaller in the PF$_3$ complex than in the CO complex, as expected from strongly electron-donating nature of PMe$_3$ and weakly electron-donating nature of PF$_3$ (see Appendix A.3.3). Thus, the change in the Mo-Cp distance is not consistent with the population change here. One plausible reason is that the PMe$_3$ and PF$_3$ can not take the best position to form an octahedral-like geometry due to the steric bulk and therefore their coordinate bonds with the metal become weaker than that of the CO, leading to the strengthening of the Mo-Cp interaction. However, this is speculation and we wish to stop the discussion here, too.

A.3.4   Wiberg bond indices in $CpL_2M(\eta^3-R^2{}_2SiCCR^1)$ and $CpL_2M(CCR^1)(SiR^2{}_2)$.

Table A.3.3   Wiberg bond indices[a] of several important bonds in $CpL_2M(\eta^3-R^2{}_2SiCCR^1)$ and $CpL_2M(CCR^1)(SiR^2{}_2)$ (M = W or Mo, L = CO, PMe_3, or PF_3).

R^1 on C2	R^2 on Si	L	M-Si	M-C1	M-C2	Si-C1	Si-C2
η^3-Silapropargyl/alkynylsilyl form (1 and 3)							
H	H	CO	0.519	0.297	0.389	0.926	-
			$(0.543)^{b)}$	(0.338)	(0.441)	(0.930)	
		PMe_3	0.615	0.359	0.447	0.919	-
			(0.662)	(0.463)	((0.659)	(0.852)	
		PF_3	0.509	0.311	0.389	0.918	-
			(0.535)	(0.352)	(0.435)	(0.918)	
H	F	CO	0.568	0.304	0.362	0.741	-
			(0.601)	(0.346)	(0.417)	(0.741)	
Me	H	CO	0.528	0.284	0.337	0.914	-
			(0.550)	(0.328)	(0.392)	(0.922)	
^tBu	H	CO	0.514	0.288	0.340	0.922	-
			(0.535)	(0.335)	(0.398)	(0.930)	
CF_3	H	CO	0.492	0.331	0.418	0.943	-
			(0.520)	(0.375)	(0.463)	(0.942)	
H	Me	CO	0.458	0.311	0.410	0.873	-
			(0.483)	(0.353)	(0.463)	(0.879)	
Acetylide-silylene form (2 and 4)							
H	H	CO	0.455	0.891	-	0.452	0.561
			(0.454)	(0.972)		(0.441)	(0.610)
		PMe_3	0.493	1.053	-	0.453	0.617
			(0.501)	(1.127)		(0.441)	(0.649)
		PF_3	0.475	0.849	-	0.453	0.505
			(0.481)	(0.933)		(0.439)	(0.558)
H	F	CO	0.637	0.636	-	0.418	0.178
			(0.664)	(0.690)		(0.400)	(0.199)
Me	H	CO	0.520	0.755	-	0.461	0.401
			(0.511)	(0.858)		(0.444)	(0.481)
^tBu	H	CO	0.512	0.766	-	0.457	0.416
			(0.502)	(0.869)		(0.441)	(0.494)
CF_3	H	CO	0.402	0.999	-	0.443	0.597
			(0.408)	(1.068)		(0.434)	(0.627)
H	Me	CO	0.407	0.916	-	0.437	0.524
			(0.407)	(0.994)		(0.427)	(0.570)

[a] DFT(B3PW91)/BS-II NBO calculation.
[b] Values in the W complexes are presented in parenthesis.

A.3.5 Optimized geometries of Cp*(CO)$_2$M(η^3-H$_2$SiCCH) and Cp(CO)$_2$M(CCH)(SiH$_2$).

1-Cp*   **2-Cp***

3-Cp*   **4-Cp***
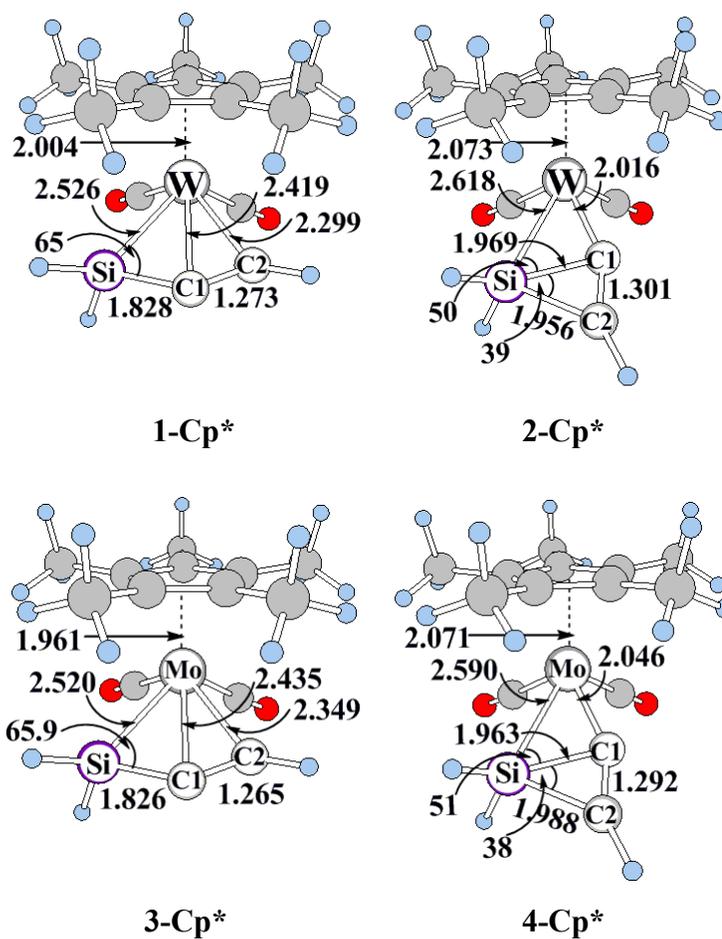
Figure A.3.2 DFT/BS-I optimized geometries of Cp*(CO)$_2$M(η^3-H$_2$SiCCH) and Cp(CO)$_2$M(CCH)(SiH$_2$), where M = W or Mo.

Bond lengths are in angstrom and bond angles are in degree.

A.3.6 Relative stability of $CpL_2M(\eta^3-R^2_2SiCCR^1)$ to $CpL_2M(CCR^1)(SiR^2_2)$.

Table A.3.4 Relative stability $(\Delta E)^{a)}$ (in kcal/mol unit) of $CpL_2M(\eta^3-R^2_2SiCCR^1)$ to $CpL_2M(CCR^1)(SiR^2_2)$ (M = W or Mo).

R¹ on C2	R² on Si	L	M = W			M = Mo		
			BS-I	BS-II	BS-III	BS-I	BS-II	BS-III
tBu	H	CO	-5.9	-5.2	-4.8	-2.7	-2.3	-3.1
H	H	CO	-5.5 (-4.8)^b)	-4.9 (-4.0)	-4.2 (-3.3)	-1.8 (-1.0)	-1.9 (-0.9)	-2.1 (-0.9)
		PMe₃	-15.0	-14.3	-15.3	-6.6	-6.7	-7.8
		PF₃	-5.9	-5.6	-5.1	-2.6	-2.4	-3.5
H	Me	CO	-4.8	-4.2	-3.2	-1.0	-0.7	-1.1
CF₃	H	CO	-4.8	-4.1	-4.5	-1.0	-0.7	-2.4
Me	F	CO	-4.7	-4.0	-3.3	-2.2	-1.8	-2.2
Me	H	CO	-4.1	-3.5	-2.7	-0.8	-0.4	-0.9
Me	Me	CO	-3.2	-2.5	-1.4	0.0	+0.4	+0.2
H	F	CO	-2.7	-2.0	-1.4	-0.3	+0.1	-0.4
CF₃	F	CO	+0.2	+1.1	+0.7	+2.1	+2.6	+1.3

a The ΔE value is energy difference between $CpL_2M(CCR^1)(SiR^2_2)$ and $CpL_2M(R^2_2SiCCR^1)$. The DFT(B3PW91) method was employed.
b In parenthesis is the ΔE value between $Cp^*(CO)_2M(CCR^1)(SiR^2_2)$ and $Cp^*(CO)_2M(R^2_2SiCCR^1)$.

A.3.7 Wiberg Bond Index Change in Cp(CO)$_2$W(η^3-H$_2$SiCCH) **3** and Cp(CO)$_2$W(CCH)(SiH$_2$) **4** by introduction of substituents on Si and C.

	Bond	**Wiberg Bond Index Change**
3 → 3-Mea	Mo-C2	-0.052
	Si-C1	-0.012
4 → 4-Mea	Mo-C1	-0.136
3 → 3-^{t}Bu	Mo-C2	-0.049
	Si-C1	-0.004
4 → 4-^{t}Bu	Mo-C1	-0.125
3 → 3-CF$_3$	Mo-C2	+0.074
4 → 4-CF$_3$	Mo-C1	+0.108
3 → 3-Meb	Mo-Si	-0.061
	Mo-C2	+0.021
4 → 4-Meb	Mo-Si	-0.048
3 → 3-PMe$_3$	Mo-Si	+0.096
	Mo-C1	+0.062
	Mo-C2	+0.058
4 → 4-PMe$_3$	Mo-C1	+0.162
	Si-C2	+0.056
3 → 3-PF$_3$	Mo-Si	-0.010
	Mo-C1	+0.014
4 → 4-PF$_3$	Mo-C1	-0.042
	Si-C2	-0.056

The positive and negative signs represent the increase and decrease of bond index, respectively.

A.3.8 Free energy change (ΔG^0) and Equilibrium constant (K_p) in conversion reaction of $Cp(CO)_2M(\eta^3\text{-}R^2{}_2SiCCR^1)$ to $Cp(CO)_2M(CCR^1)(SiR^2{}_2)$.

Table A.3.5   Free energy change (ΔG^0) and value of Equilibrium constant (K_p) in conversion reaction of $Cp(CO)_2M(\eta^3\text{-}R^2{}_2SiCCR^1)$ to $Cp(CO)_2M(CCR^1)(SiR^2{}_2)$, (M = W or Mo).

R^1 on C2	R^2 on Si	$\Delta G^0{}_{gas}$ [a) kcal/mol	$\Delta G^0{}_{sol}$ [b) kcal/mol	ΔG^{0} [c) kcal/mol	K_p
M = W					
^tBu	H	-7.2	1.2	-6.0	2.4×10^4
H	H	-5.2	0.6	-4.6	2.3×10^3
H	Me	-4.4	0.4	-4.0	8.8×10^2
CF_3	H	-4.1	0.2	-3.9	7.0×10^2
Me	F	-4.9	0.9	-4.0	7.8×10^2
Me	H	-4.3	0.8	-3.5	3.8×10^2
Me	Me	-3.2	0.2	-3.0	1.9×10^2
H	F	-2.6	0.7	-1.9	3.0×10^1
CF_3	F	-0.6	0.7	0.1	8.2×10^{-1}
M = Mo					
^tBu	H	-3.2	1.0	-2.2	4.0×10^1
H	H	-1.9	0.6	-1.3	9.3
Me	F	-3.0	1.2	-1.8	2.1
H	Me	-0.9	0.2	-0.7	3.2
CF_3	H	-1.0	0.3	-0.7	3.0
Me	H	-1.3	0.7	-0.7	3.2
H	F	-0.5	0.6	+0.1	7.0×10^{-1}
Me	Me	4.3×10^{-2}	-0.1	-6.0×10^{-2}	1.1
CF_3	F	0.8	0.8	+1.7	6.0×10^{-2}

(a) DFT(B3PW91)/BS-II.
(b) PCM-DFT(B3PW91)/BS-II.
(c) $\Delta G^0 = \Delta G^0{}_{gas} + \Delta G^0{}_{sol}$.

We evaluated equilibrium constant (K_p) between the η^3-silapropargyl/alkynylsilyl and acetylide-silylene forms to incorporate the entropy and thermal energy in the discussion. First, Gibbs free energy change ΔG^0_{gas} was calculated in gas phase and then the free energy change ΔG^0_{sol} by solvation (toluene) was added to ΔG^0_{gas}, to afford total free energy change ΔG^0, as shown in Appendix A.3.8, where ΔG^0 is the difference in free energy change from the right-hand side to the left-hand side of eq 3.1; in other words, the negative ΔG^0 value represents that the acetylide-silylene form is more stable than the η^3-silapropargyl/alkynylsilyl

$$\text{Cp(CO)}_2\text{M}(\eta^3\text{-R}^2_2\text{SiCCR}^1) \quad \underset{}{\overset{K_p}{\rightleftharpoons}} \quad \text{Cp(CO)}_2\text{M}(\text{CCR}^1)(\text{SiR}^2_2) \qquad (3.1)$$

form and K_p is larger than 1.0. The equilibrium constant (K_p) was evaluated with these ΔG^0 values. Both of the K_p and ΔE values present the same trend about the relative stability; see Table 3.2 for ΔE values. Apparently, the K_p values of the molybdenum complexes are much smaller than that of the tungsten complexes. In both tungsten and molybdenum complexes, the K_p value is the largest for the combination of ^{t}Bu on C2 and H on Si and the smallest for the combination of CF_3 on C2 and F on Si. This means that the acetylide-silylene form can be isolated easily in the tungsten complex when the bulky ^{t}Bu is introduced on C2. On the other hand, the η^3-silapropargyl/alkynylsilyl form can be isolated in the molybdenum complex, when the CF_3 and F are introduced on C2 and Si, respectively. These conclusions are the same as those presented by the potential energy changes. Thus, we wish to discuss the relative stability based on the ΔE value, hereafter.

A.3.9   Optimized geometries of CpL$_2$W(η^3-H$_2$SiCCH) and CpL$_2$W(CCH)(SiH$_2$).

1-PMe$_3$
< PMoP = 88

2-PMe$_3$
< PMoP = 87

(A) PMe$_3$ ligand systems

1-PF$_3$
< PMoP = 83

2-PF$_3$
< PMoP = 85
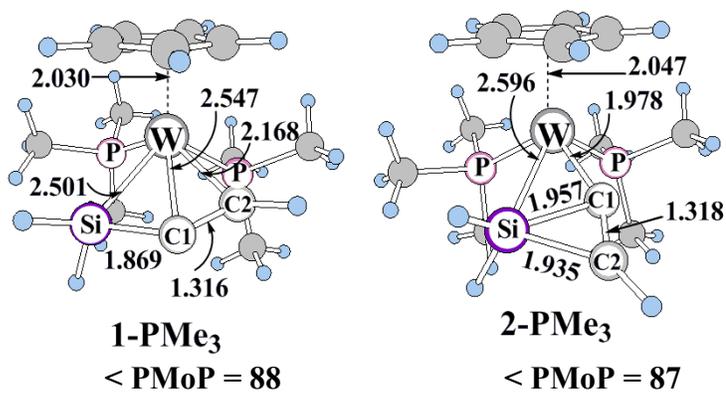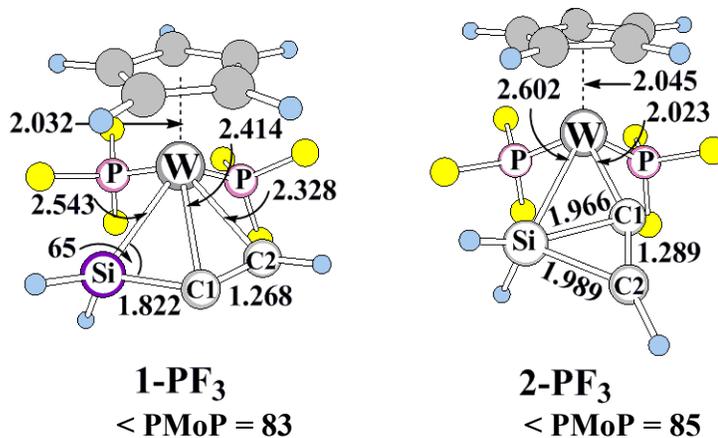
(B) PMe$_3$ ligand systems

Figure A.3.3 DFT/BS-I optimized geometries of CpL$_2$W(η^3-H$_2$SiCCH) and CpL$_2$W(CCH)(SiH$_2$), where L = PMe$_3$ or PF$_3$.
Bond lengths are in angstrom and bond angles are in degree.

A.3.10 Activation barriers calculated with various computational methods in the conversion reaction of $Cp(CO)_2M(\eta^3\text{-}H_2SiCCH)$ to $Cp(CO)_2M(CCH)(SiH_2)$ (M= W or Mo).

Table A.3.6 Activation barriers $(E_a)^a$ calculated with various computational methods in the conversion reaction of $Cp(CO)_2M(\eta^3\text{-}H_2SiCCH)$ to $Cp(CO)_2M(CCH)(SiH_2)$.

Method	M = W [b]	M = Mo
DFT	15.3	13.2
MP2	20.7	19.4
MP3	14.0	11.4
MP4(DQ)	15.5	14.1
MP4(SDQ)	14.8	13.6
MP4(SDTQ)	18.8	18.2
CCSD(T)	15.8	14.1

[a] E_a is energy difference between transition state and $Cp(CO)_2M(\eta^3\text{-}R^2{}_2SiCCR^1)$. The BS-II was employed. [b] Ref. 22.

Chapter 4

Theoretical Study of New Ethynediyl-Bridged Bis(Silylene) Dinuclear Tungsten Complex: Novel Bonding Nature and Electronic Structure

4.1   Introduction

Ethynediyl (C_2^{2-})-bridged dinuclear transition metal complexes have received much interest because of their characteristic geometries, bonding natures, electronic structures, and physicochemical properties [1-18]. Also, they are building block for the synthesis of bare carbon chain stabilized by the transition metal complexes [2, 3, 18]. In this regard, various ethynediyl-bridged dinuclear transition metal complexes have been synthesized and investigated in many experimental [1-17] and theoretical works [16b, 17, 18].

Three possible bonding modes have been proposed, as shown in Schemes 4.1(A) to (C); namely acetylenic M-C≡C-M, cumulenic M=C=C=M, and dimetalla-1,3-butadiyne M≡C-C≡M [2, 17, 18]. Among these three valence bond descriptions, most of the synthesized complexes contain an acetylenic M-C≡C-M structure [3, 6b, 9, 14, 15, 16, 18]. The cumulenic structure was found in a few titanium [2] and tantalum [2, 5] complexes and the dimetalla-1,3-butadiyne structure was reported only in a tungsten complex $(^tBuO)_3W≡C-C≡W(O^tBu)_3$ [4, 17].

Recently,   a   dinuclear   tungsten   complex $Cp^*(CO)_2(SiPh_2)W-CC-W(SiPh_2)(CO)_2Cp^*$ **R1** ($Cp^* = C_5Me_5$) was synthesized by Sakaba and his coworkers [19]. Its mononuclear complex $Cp^*(CO)_2W(SiPh_2)(CC^tBu)$ **R2**
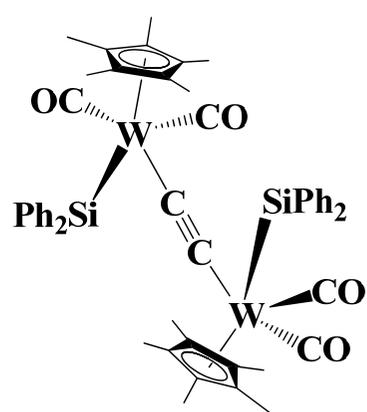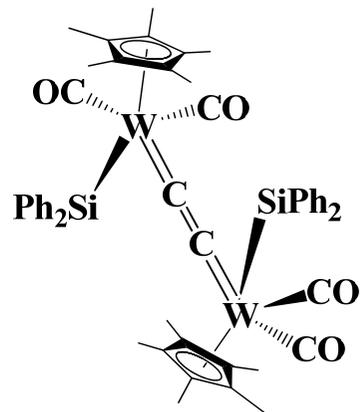
(A) Acetylenic form   (B) Cumulenic form   (C) Dimetalla butadiyne form   (D) Disilabutadiyne form
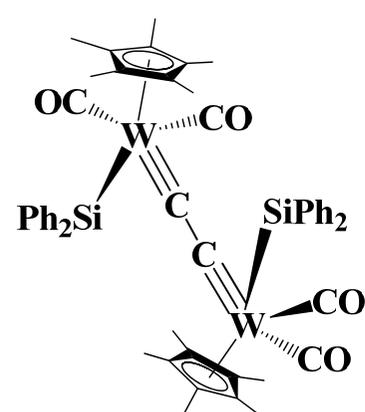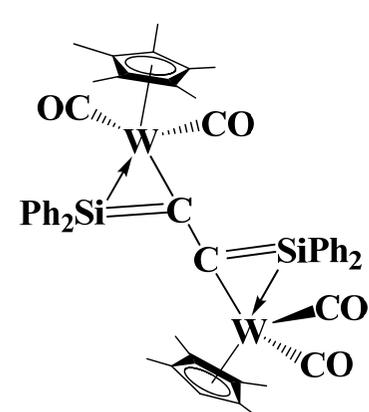
Four Possible Bonding Modes of Cp*(CO)$_2$(SiPh$_2$)W-CC-W(SiPh$_2$)(CO)$_2$Cp* R1

Scheme 4.1

was also synthesized, recently [20]. Our theoretical study of the model mononuclear complex $Cp(CO)_2W(SiH_2)(CCH)$ disclosed its novel bonding nature [21], as follows: It is a tungsten acetylide silylene complex which involves two kinds of charge transfer (CT) interactions between the silylene and acetylide moieties; one is the CT from the lone pair orbital of the silylene to the π^* orbital of the acetylide and the other is the CT from the π orbital of the acetylide to the empty p orbital of the silylene. However, the geometries of the CC and SiH_2 moieties of **R1** are considerably different from those of **R2**. Thus, it is worthy investigating the bonding nature of **R1**, as follows: (i) which bonding mode of the acetylenic form W-C≡C-W, the cumulenic form W=C=C=W, and the dimetalla-1,3-butadiyne form W≡C-C≡W is involved in **R1**, (ii) whether or not the Si-C-C-Si moiety of **R1** is characterized to be a disilabutadiene ($R_2Si=C-C=SiR_2$) (see Scheme 4.1 (D)), (iii) whether or not the bonding interaction is formed between the Si and C atoms. It is also noted that transition metal silylene complexes are interesting research targets in the coordination chemistry, organometallic chemistry, synthetic chemistry, and theoretical chemistry because of their interesting bonding natures, electronic structures, and important roles as intermediates in various metal-catalyzed transformation reactions of organosilicon compounds [20-40]. In this regard, transition metal silylene complexes have been investigated in many experimental [20, 22-35] and theoretical works [21, 36-40] to understand their structural features, bonding natures, electronic structures, and reaction behavior.

In this work, we theoretically investigated $Cp(CO)_2(SiH_2)W-CC-W(SiH_2)(CO)_2Cp$ **1** ($Cp = C_5H_5$) with the DFT method, where **1** was employed as a model of **R1**. For clear understanding of the bonding nature of **1**, we also investigated a model ethynediyl-bridged bis(silylene) dinuclear tungsten complex $Cp(CO)_2(SiH_2)W-C≡C-W(SiH_2)(CO)_2Cp$ **2**, in which the CC and SiH_2 groups take positions opposite to each other; in other words, no

$$\textbf{2} \qquad\qquad\qquad \textbf{3} \qquad\qquad\qquad \textbf{4}$$
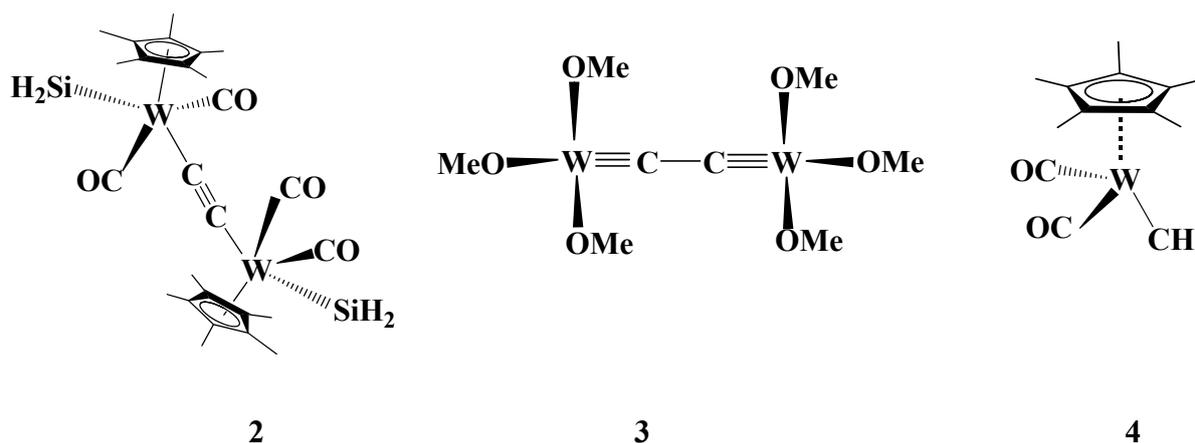
Scheme 4.2

interaction exists between them (see Scheme 4.2). A typical dicarbido dinuclear tungsten complex $(MeO)_3W≡C-C≡W(OMe)_3$ **3** and a mononuclear tungsten carbyne complex $Cp(CO)_2W≡CH$ **4** were also investigated here (see Scheme 4.2) for making comparison of **1** with **3** and **4**. Complex **2** is not unusual because a similar ethynediyl-bridged dinuclear tungsten complex $Cp(CO)_3W-C≡C-W(CO)_3Cp$ was experimentally isolated [9]; note that the silylene resembles CO because the silylene has the lone pair and empty p orbitals like the CO. Complexes **3** and **4** are models of experimentally isolated $(^tBuO)_3W≡C-C≡W(O^tBu)_3$ [4] and $CpL_2W≡CR$ [L = CO, P(OMe)_3 and R = Ph and Me] [41], respectively. Here, our main purpose is to present correct understanding of the bonding nature and electronic structure of **1**.

4.2   Computational Details

Geometry of $Cp(CO)_2(SiH_2)W-CC-W(SiH_2)(CO)_2Cp$ **1** was optimized with the density functional theory (DFT), where the B3PW91 functional [42, 43] was employed for the exchange-correlation term because this functional presented better agreement of the optimized geometry of the model mononuclear complex $Cp(CO)_2W(CCH)(SiH_2)$ **5** [21] with the experimental one $Cp^*(CO)_2W(CC^tBu)(SiPh_2)$ **R2** [20] than does the

158

B3LYP-functional [42, 44]. We ascertained that none of the equilibrium geometries exhibited any imaginary frequency.

Two kinds of basis set systems, BS-I and BS-II, were mainly used in this work. In BS-I, core electrons of W were replaced with effective core potentials (ECPs) [45] and their valence electrons were represented by (341/321/21) basis sets [45]. Usual cc-pVDZ [46] basis sets were employed for Si, C, and O and usual 6-31G [47] basis set was used for H. This BS-I system was used for geometry optimization. In BS-II, the core electrons of W were replaced with Stuttgart-Dresden-Bonn (SDB) ECPs and their valence electrons were represented by (311111/22111/411/11) basis sets [48, 49]. For the other atoms, the cc-pVTZ basis sets [50] were employed, where the f polarization function was excluded to save the computational time. This BS-II system was used to evaluate Wiberg bond index [51] and population changes. Another basis set system BS-III was employed to check the reliability of the Mulliken population analysis with the BS-II system because a very diffuse function tends to present unreasonable Mulliken population in several cases. In BS-III, the valence electrons of W were represented by (541/541/111/1) basis set [45, 52, 53], where its core electrons were replaced with the same ECPs as those of BS-I. For the other atoms, the same basis sets as those of the BS-I were employed. The BS-III-calculated Mulliken populations are similar to the BS-II-calculated values; see Appendix A.4.1. We present BS-II-calculated populations in the discussion.

Gaussian 03 program package (revision C.02) [54] was used for all these computations. Population analysis was carried out with the method proposed by Weinhold et al [55]. Molecular orbitals were drawn with MOLEKEL program package (version 4.3) [56].

4.3   Results and Discussion

4.3.1 Optimized Geometries of Cp(CO)₂(SiH₂)W-CC-W(SiH₂)(CO)₂Cp

4.3.1   Optimized Geometries of Cp(CO)$_2$(SiH$_2$)W-CC-W(SiH$_2$)(CO)$_2$Cp 1, Ethynediyl-Bridged Bis(Silylene) Dinuclear Tungsten Complex Cp(CO)$_2$(SiH$_2$)W-C≡C-W(SiH$_2$)(CO)$_2$Cp 2, Dicarbido-Bridged Dinuclear Tungsten Complex (MeO)$_3$W≡C-C≡W(OMe)$_3$ 3, and Tungsten Carbyne Complex Cp(CO)$_2$W(CH) 4
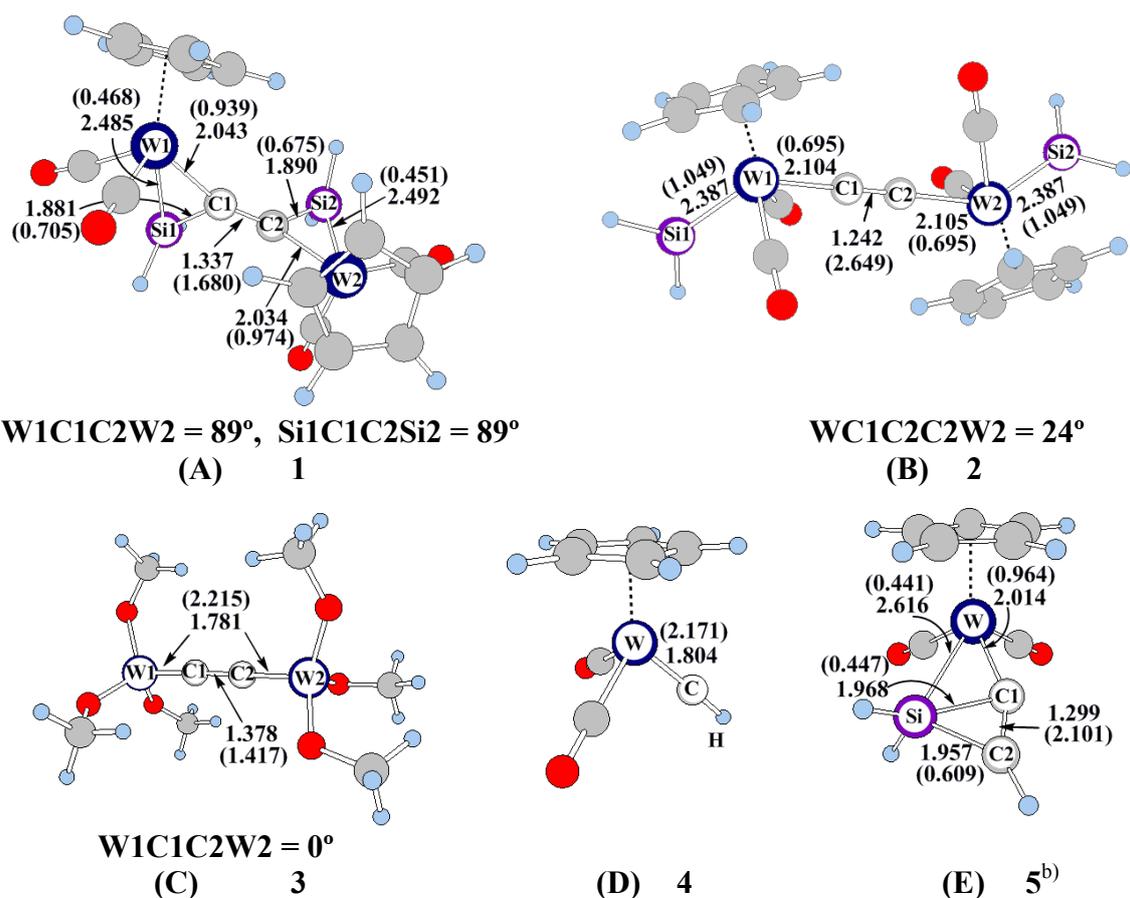
Figure 4.1. Optimized[a)] geometries of (A) Cp(CO)$_2$(SiH$_2$)W-CC-W(SiH$_2$)(CO)$_2$Cp **1**, (B) Cp(CO)$_2$(SiH$_2$)W-C≡C-W(SiH$_2$)(CO)$_2$Cp **2**, (C) (MeO)$_3$W≡C-C≡W(OMe$_3$) **3**, (D) Cp(CO)$_2$W(CH) **4**, and (E) Cp(CO)$_2$W(CCH)(SiH$_2$) **5**. In parentheses are the Wiberg bond indices[c)] and without parentheses are the bond lengths (in Å).
[a)] DFT(B3PW91)/BS-I method was employed.   [b)] Ref. 21 (a).   [c)] DFT(B3PW91)/BS-II NBO calculation.

The optimized geometry of **1** (see Figure 4.1) agrees well with the experimental one, as shown in Table 4.1. The W-Si distances (2.489 Å) in **1** are moderately longer than the usual W-silylene distance (~2.45 Å) [35] but somewhat shorter than that (2.616 Å) of

Table 4.1. Selected optimized parameters[a)] of Cp(CO)$_2$(SiH$_2$)W-CC-W(SiH$_2$)(CO)$_2$Cp **1**, Cp(CO)$_2$(SiH$_2$)W-C≡C-W(SiH$_2$)(CO)$_2$Cp **2**, (MeO)$_3$W≡C-C≡W(MeO)$_3$ **3**, Cp(CO)$_2$W(CH) **4**, and Cp(CO)$_2$W(CCH)(SiH$_2$) **5**.

	1		2	3	4	5[c)]
	Calcd.	**Expt.**[b)]				
M1-Si1	2.492	2.477	2.387	-	-	2.616
M2-Si2	2.485	2.480	2.387	-	-	-
M1-C1	2.034	2.068	2.104	1.781	1.804	2.014
M2-C2	2.043	2.089	2.105	1.781	-	-
Si1-C1	1.890	1.898	-	-	-	1.968
Si2-C2	1.881	1.876	-	-	-	-
Si1-C2	2.908	-	-	-	-	1.957
Si2-C1	2.827	-	-	-	-	-
C1-C2	1.337	1.343	1.242	1.378	-	1.299
M1-Si1-C1	53.0	54.5	-	-	-	49.7
M2-Si2-C2	54.0	55.2	-	-	-	-
M1-C1-C2	159.0	165.1	179.0	180.0	-	152.1
M2-C2-C1	152.0	151.0	179.2	179.8	-	-

Bond lengths are in angstrom and bond angles are in degree.
[a)] DFT (B3PW91)/BS-I method was employed. [b)] Ref. 19. [c)] Ref. 21(a).

Cp(CO)$_2$W(CCH)(SiH$_2$) **5** [21]; see Figure 4.1 and Table 4.1. The angle α between the lone pair of the SiH$_2$ group and the W-Si bond is 11° in **1**, which is much smaller than that (35°) of **5**; see Scheme 4.3 for the definition of the angle α. This small angle represents that the lone pair of the SiH$_2$ does not deviate very much from the W-Si axis. Also, the W-Si bond index (0.460) is moderately larger in **1** than that (0.441) of **5**; see Figure 4.1 for the Wiberg bond indices. In **2**, the SiH$_2$ moiety takes the position trans to the CC moiety (see Figure 4.1). The W-Si distance of **2** is somewhat shorter than that of **1** by 0.11 Å and the W-Si bond index (1.049) is about two times as large as that of **1**. All these results indicate that the W-Si bonding interaction is somewhat stronger in **1** than in **5** but considerably weaker than in **2** and that the silylene interacts with both of the W and the

CC moiety in **1**. The weaker W-Si bond of **1** than in **2** suggests the presence of the bonding interaction between the SiH$_2$ and CC moieties in **1**, as will be discussed below; note that such interaction is absent in **2**.

2

5

Angles are in degree
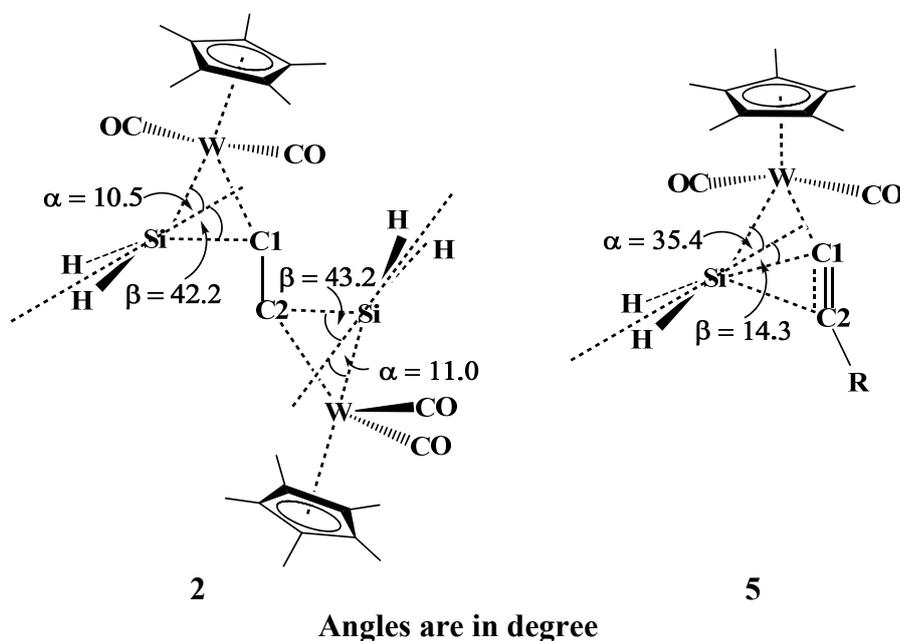
Scheme 4.3

The W-C (2.039 Å) distance in **1** is in the range of the usual W-C single bond distance (~2.05 Å) [57, 58], somewhat shorter than that (2.104 Å) of **2**, and moderately longer than that (2.014 Å) of **5**. However, it is considerably longer than the W-C double bond distance (~1.9 Å) [59] and much longer than the W-C triple bond distances of **3** (1.781 Å) and **4** (1.804 Å). Also, the W-C bond index is somewhat larger in **1** (0.957) than in **2** (0.695), similar to that of **5** (0.964), and much smaller than in **3** (2.190) and **4** (2.171). All these results rule out the possibility that **1** involves a W-C multiple bond. The WCC angle is 156° in **1**, while it is about 180° in **2** including a typical W-ethynediyl bond. Also, the WCCW dihedral angle is 89° in **1**, while it is 24° in **2**. These results suggest that the W-C bond of **1** is much different from that of the pure ethynediyl complex.
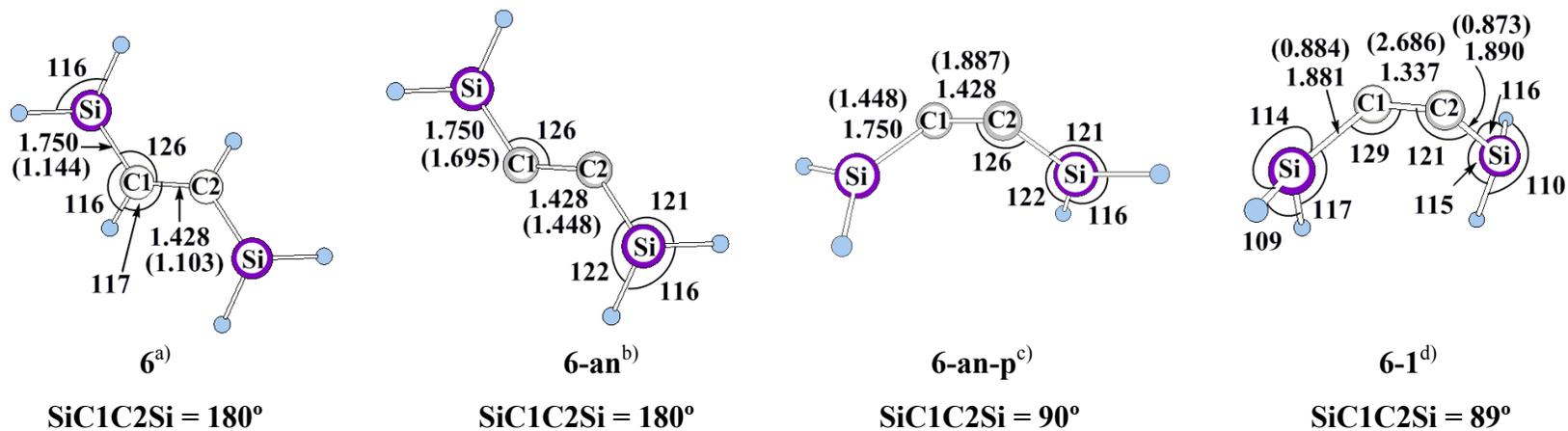
Figure 4.2. Geometries of $H_2Si=CH-CH=SiH_2$ **6** and $[H_2SiCCSiH_2]^{2-}$ **6-an, 6-an-p**, and **6-1**. Bond lengths are in angstrom and bond angles are in degree. In parentheses are the Wiberg bond indices.[e)]
[a)] $H_2SiCHCHSiH_2$ was optimized with the DFT(B3PW91)/BS-I method.   [b)] Geometry was taken to be the same as that of **6**.
[c)] Geometry was taken to be the same as that of **6-an** except the SiCCSi dihedral angle was changed to 90°.   [d)] Geometry was taken to be the same as that in **1**.   [e)] DFT(B3PW91)/BS-II NBO calculation.

The C1-C2 distance (1.337 Å) of **1** is considerably longer than that of **2** by 0.095 Å, somewhat longer than that of **5** by 0.038 Å, and somewhat shorter than that of **3** by 0.041 Å. Consistent with these bond distances, the C1-C2 bond index (1.680) is considerably smaller in **1** than in **5** (2.101) and much smaller than in **2** (2.649), but moderately larger than in **3** (1.417). This C1-C2 distance of **1** is similar to that (1.210 Å) of the C-C double bond and considerably shorter than that (1.428 Å) of a disilabutadiene $H_2Si=CH-CH=SiH_2$ **6**, which is a silicon analogue of 1,3-butadiene $H_2C=CH-CH=CH_2$ (see Figure 4.2) [60]. Its bond index is between those of the C-C single (1.043) and C=C double (2.052) bonds and much larger than that (1.103) of **6** (see Figure 4.2) [60]. From all these results, it is concluded that the C1-C2 bond of **1** is much weaker than that of the pure ethynediyl complex **2**, but the π-conjugation in the CC moiety is much stronger than in disilabutadiene **6**.

The Si1-C1 and Si2-C2 distances (1.885 Å) are considerably shorter in **1** than the Si-C1 distance (1.968 Å) of **5**, but the Si1-C2 and Si2-C1 distances (2.850 Å) are much longer in **1** than the Si-C2 distance (1.957 Å) of **5**; see Figure 4.1. The Si1-C1 and Si2-C2 bond indices are 0.705 and 0.675, respectively, in **1**, which are somewhat larger than the Si-C1 and Si-C2 bond indices (0.447 and 0.609) of **5**. On the other hand, the Si1-C2 and Si2-C1 bond indices (0.065 and 0.075, respectively) are very small in **1**, as expected from the geometry of **1**. These Si1-C1 and Si2-C2 distances of **1** are similar to the Si-C single bond (1.895 Å) but considerably longer than the Si-C distance (1.750 Å) of **6** (see Figure 4.2) [61]. Their bond indices are somewhat smaller than that (0.884) of the Si-C single bond but considerably smaller than that (1.144) of **6** [61]. It is worthy comparing the bond distances and bond indices between the $H_2SiCCSiH_2$ moiety of **1** and a deprotonated disilabutadiene $(H_2SiCCSiH_2)^{2-}$ **6-an** (see Figure 4.2), where the geometry of **6-an** was taken to be the same as the corresponding moiety of **6** because the geometry optimization

of **6-an** leads to the linear Si-C-C-Si geometry, as shown in Appendix A.4.2. The Si1-C1 and C1-C2 bond indices of **6-an** are much larger than those of **6**. Thus, the Si1-C1 and Si2-C2 bonds of **1** are much weaker and the C1-C2 bond is somewhat weaker than those of **6-an**. All these results indicate that the Si1-C1 and Si2-C2 bonding interactions correspond to the Si-C single bond and the C1-C2 bond is similar to the double bond in **1**. It should be noted that the SiCCSi moiety is not planar in **1** but the SiCCSi dihedral angle is 89°, while it is 180° in **6**, indicating the SiCCSi moiety of **1** is not characterized to be a disilabutadiene. Because the Si-C-C-Si dihedral angle is about 90° in **1**, we calculated $[H_2SiCCSiH_2]^{2-}$ **6-an-p** in which the geometry was taken to be the same as that of **6-an** except that the Si-C-C-Si dihedral angle was changed to 90° and also another $[H_2SiCCSiH_2]^{2-}$ **6-1** where the geometry was taken to be the same as that in **1**; see Figure 4.2. Apparently, the C1-C2 bond index is much larger in **6-an-p** and **6-1** than in **1** and the Si-C bond index is somewhat larger in **6-an-p** and **6-1** than in **1**. These results suggest that the $[H_2SiCCSiH_2]^{2-}$ moiety of **1** is much different from **6-an-p** and **6-1** and that various CT interactions are formed between the SiH_2, CC, and W moieties in **1** to induce significantly large change in the $H_2SiCCSiH_2$ moiety of **1**, which will be discussed below in detail.

4.3.2 Population and MO Analyses

W atomic and its d orbital populations in **1** are similar to those of **5** but somewhat smaller than in **2** by 0.159e and 0.079e, respectively; see Table 4.2. The population of the SiH_2 moiety is moderately smaller in **1** than in **5** by 0.028e but much smaller than in **2** by 0.254e, indicating that the SiH_2 moiety of **1** is much different from those of the pure silylene complex **2**. The population of the CC moiety is considerably larger in **1** than in **2**, **5**, and $H_2C≡CH_2$ by 0.397e, 0.208e, and 0.490e, respectively, and considerably smaller

than in **6** by 0.604e. These results indicate that the CC moiety of **1** is different from those

of the pure ethynediyl complex **2**, the acetylide complex **5**, and disilabutadiene **6**. It is

noted that the population of the CC moiety (12.957e) of **1** is moderately larger than that of

6-1 (12.929e) but much smaller than that of **6-an** (13.849e). The population (15.322e) of

Table 4.2. NBO[a] populations of several important atoms and groups in
$Cp(CO)_2(SiH_2)W\text{-}CC\text{-}W(SiH_2)(CO)_2Cp$ **1**, $Cp(CO)_2(SiH_2)W\text{-}C{\equiv}C\text{-}W(SiH_2)(CO)_2Cp$
2, and $Cp(CO)_2W(CCH)(SiH_2)$ **5**.

	1	2	5
W	74.214	74.373	74.240
d	5.879	5.958	5.874
Si	13.022	13.207	13.070
SiH$_2$	15.322	15.564	15.350
C	6.493	6.265	6.186
C	6.464	6.296	6.563
CC	12.957	12.560	12.749

[a] DFT(B3PW91)/BS-II NBO calculation.

the SiH$_2$ moiety of **1** is considerably smaller than in **6** (15.448e), **6-1** (16.551e), and **6-an**

(16.076e). From these results, it is concluded that the H$_2$Si-C-C-SiH$_2$ moiety of **1** is not a

disilabutadiene dianion.

Also, these results suggest that the CT interactions in **1** are different from those of

5 which was discussed previously [21]. To get clear pictures about the CT interactions,

we inspected the MOs of **1**; see Figure 4.3. Also, we analyzed the MOs by representing

them with a linear combination of the MOs of fragments, using eq 4.1 [62, 63], where **1** is

considered to consist of five moieties, as shown in Scheme 4.4;

$$\psi_i(ABCDE) = \sum_j a_{ij}\varphi_j(A) + \sum_k b_{ik}\varphi_k(B) + \sum_l c_{il}\varphi_l(C) + \sum_m d_{im}\varphi_m(D) + \sum_n e_{in}\varphi_n(E) \qquad (4.1)$$

The $\psi_i(ABCDE)$ represents the i-th MO of the total system ABCDE, the $\varphi_j(A)$ is the j-th

MO of fragment A $[Cp(CO)_2W]_A{}^+$, the $\varphi_k(B)$ is the k-th MO of fragment B $(SiH_2)_B$, the

HOMOa (-5.7) **HOMOb (-5.8)**

HOMO-1a (-5.9) **HOMO-1b (-6.0)** **HOMO-2a (-7.0)** **HOMO-2b (-7.1)**

HOMO-3a (-8.2) **HOMO-3b (-8.3)** **HOMO-4 (-9.1)** **HOMO-6 (-10.1)**
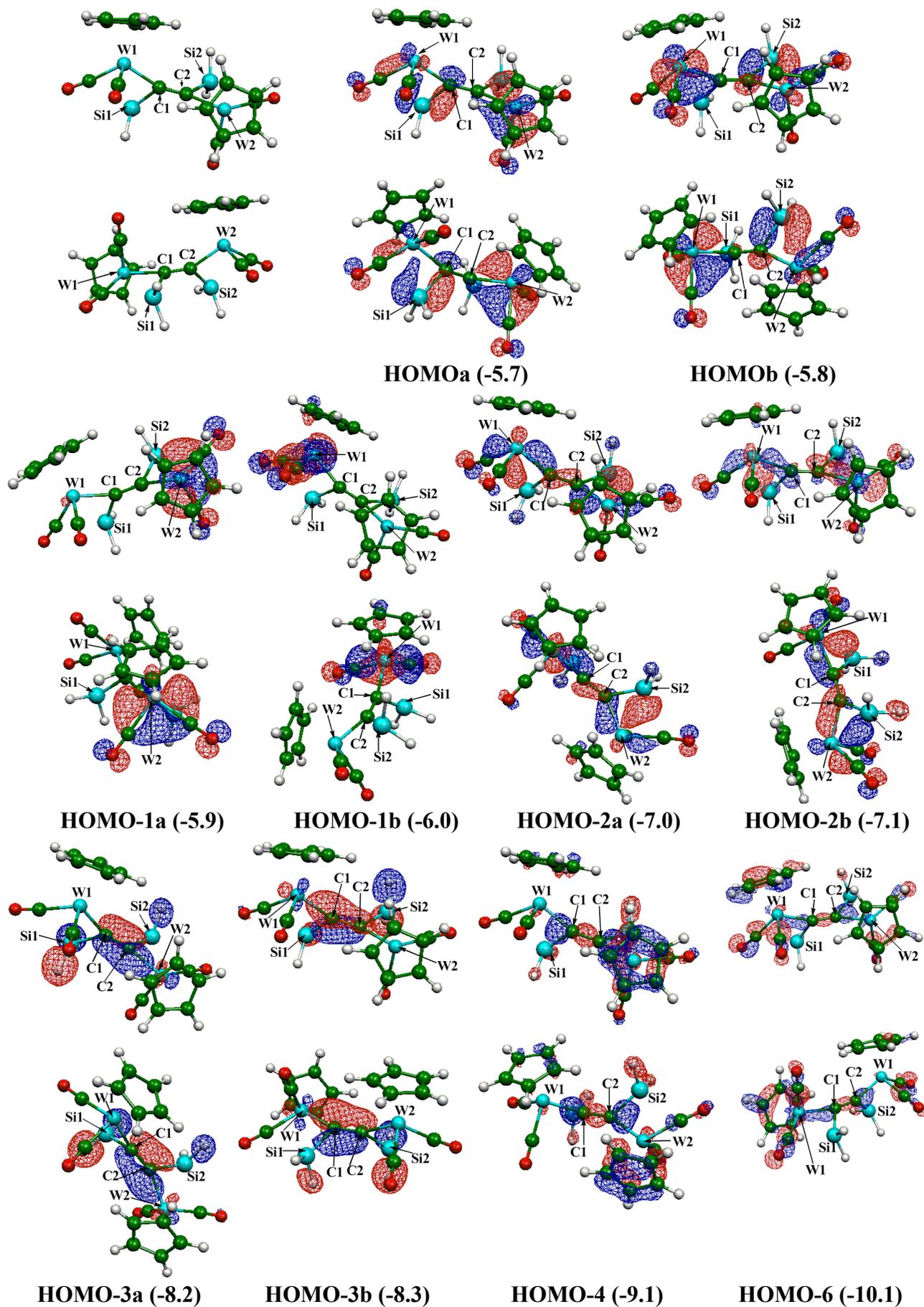
Figure 4.3.   Several important Kohn-Sham MOs in Cp(CO)$_2$(SiH$_2$)W-CC-W(CO)$_2$Cp **1**.   In parentheses are the orbital energies (in eV).

167
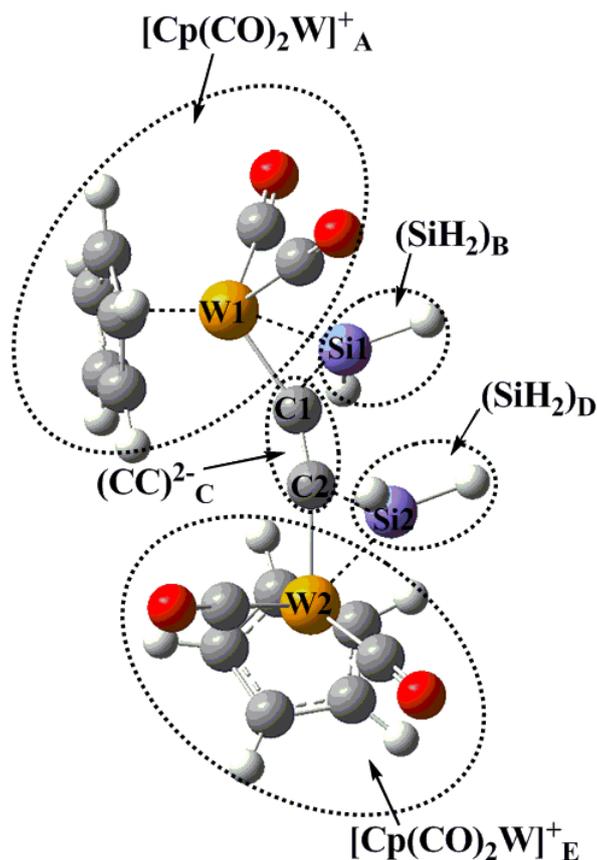
Scheme 4.4

$\varphi_l(C)$ is the l-th MO of fragment C $(CC)_C^{2-}$, the $\varphi_m(D)$ is the m-th MO of fragment D $(SiH_2)_D$, and the $\varphi_n(E)$ is the n-th MO of fragment E $[Cp(CO)_2W]_E^+$. The a_{ij}, b_{ik}, c_{il}, d_{im}, and e_{in} are the expansion coefficients of the $\varphi_j(A)$, $\varphi_k(B)$, $\varphi_l(C)$, $\varphi_m(D)$, and $\varphi_n(E)$, respectively. Important MOs of the $[Cp(CO)_2W]^+$ are LUMO+2, LUMO+1, LUMO, HOMO, and HOMO-1, which mainly consist of the d orbitals of the W center. They are named $\varphi_{LUMO+2}(W)$ etc. hereafter; see Figure 4.4(A) for these MOs. In the SiH_2, HOMO and LUMO play important roles in **1**. The LUMO mainly consists of the empty p orbital and the HOMO is the lone pair orbital; see Figure 4.4(B). These LUMO and HOMO are named φ^{Si}_p and φ^{Si}_{lp}, respectively. In the $(CC)^{2-}$, π^*, π, and lone pair orbitals play important roles in **1**. The degenerate LUMOs are two π^* orbitals which are perpendicular to each other. They are named $\varphi^{CC}_{\pi 1*}$ and $\varphi^{CC}_{\pi 2*}$, respectively; see Figure 4.4(C). The HOMO and HOMO-2 are two lone pair orbitals, which are named φ^{CC}_{lp1} and φ^{CC}_{lp2}

LUMO+2   **LUMO+1**   **LUMO**   **HOMO**   **HOMO-1**

$\varphi_{LUMO+2}(W)$ $\varphi_{LUMO+1}(W)$ $\varphi_{LUMO}(W)$ $\varphi_{HOMO}(W)$ $\varphi_{HOMO-1}(W)$

(A) $[Cp(CO)_2W]^+$

LUMO   **HOMO**

(φ^{Si}_{P}) (φ^{Si}_{lp})

(B) SiH_2

LUMO[a]   **HOMO**   **HOMO-1**[a]   **HOMO-3**

$(\varphi^{CC}_{\pi*})$ (φ^{CC}_{lp1}) (φ^{CC}_{π}) (φ^{CC}_{lp2})

(C) $[CC]^{2-}$
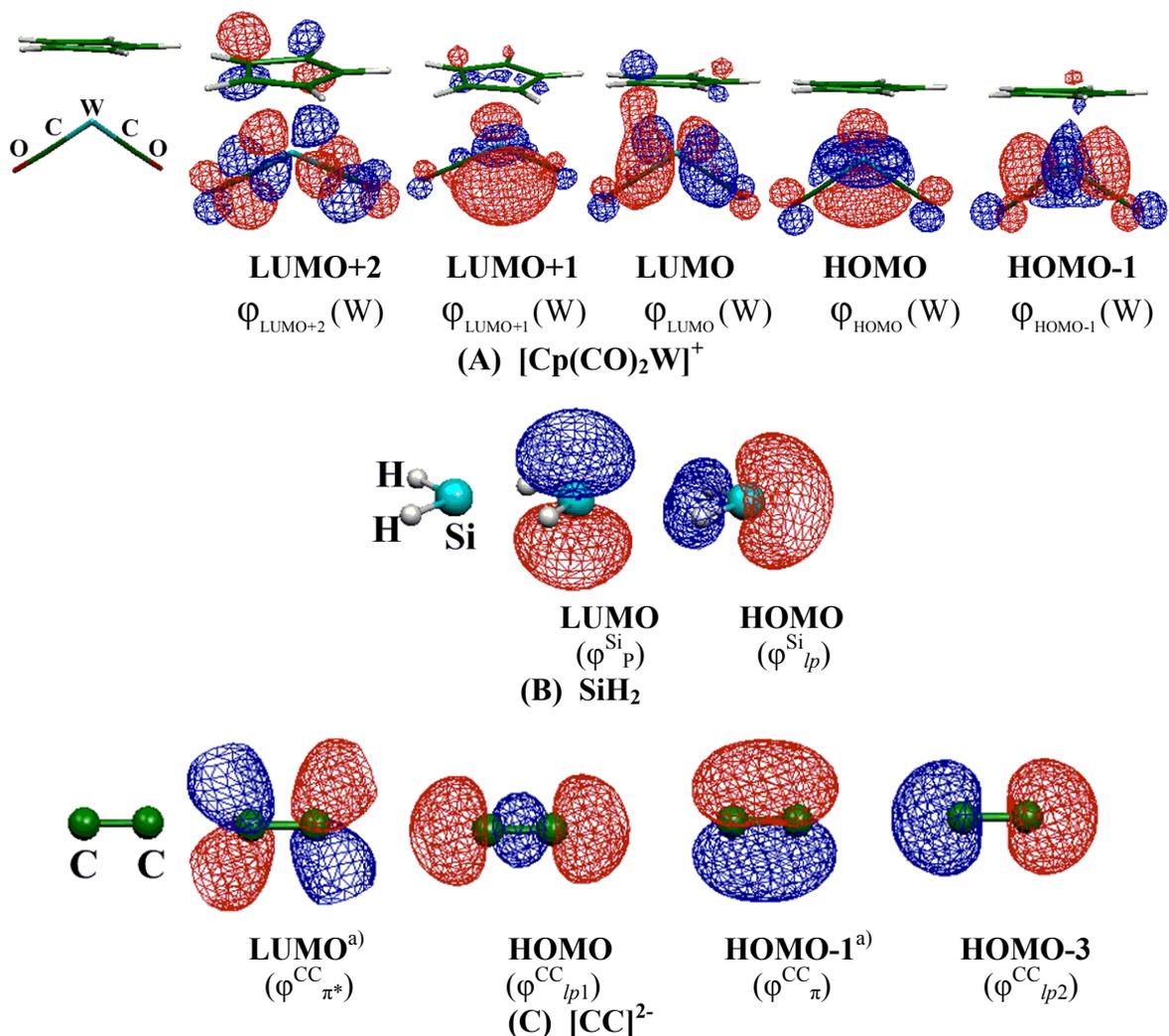
Figure 4.4. Several important Kohn-Sham MOs in $[Cp(CO)_2W]^+$, SiH_2, and $(CC)^{2-}$.
[a] LUMO and HOMO-1 are doubly degenerate. The other orbital perpendicular to this picture exists beside this orbital.

respectively. The degenerate HOMO-1s are two π orbitals, which are named $\varphi^{CC}_{\pi1}$ and $\varphi^{CC}_{\pi2}$, respectively.

As shown in Figure 4.3, the degenerate HOMOs of **1** mainly consist of the occupied d orbital of the W2 (d^{W}_{occ}), which overlaps with the $\varphi^{CC}_{\pi*}$ in a bonding way. This is the π-back-donation from the W2 to the CC moiety. Also, another back-donation interaction between the d^{W}_{occ} of the W1 and the φ^{Si}_{p} is involved in this HOMO. These results are supported by the analysis of MOs with the eq 4.1; see Scheme 4.5(A) for the expansion coefficients of the d^{W}_{occ}, $\varphi^{CC}_{\pi*}$, and φ^{Si}_{p}. The degenerate HOMO-1s mainly

d_{occ} [a)]: **10**   **12**   **2**   **10** d_{occ}: **30**   **HOMO**
d_{unoc} [b)]: **4** d_{unoc}: **17**

(A) HOMO

d_{occ}: **29**   **5**   **3**   **5**   **6**   **3** d_{occ}: **2**   **6**   **3**   **HOMO-4**
d_{unoc}: **4** d_{unoc}: **22**

(B) HOMO-2

28   **5** d_{unoc}: **8**   **HOMO-6**
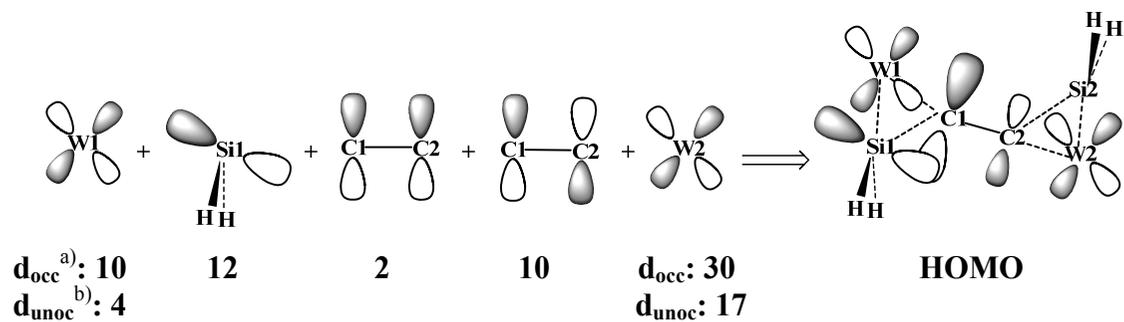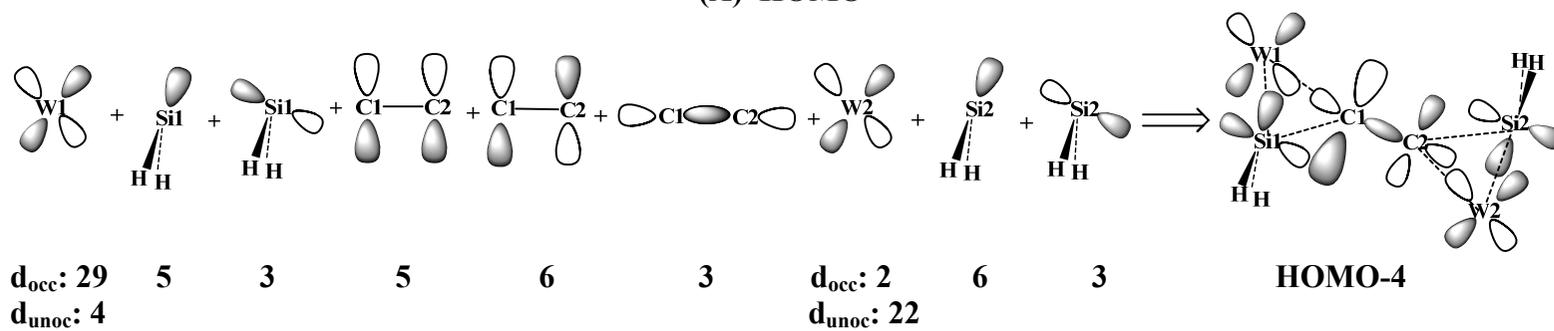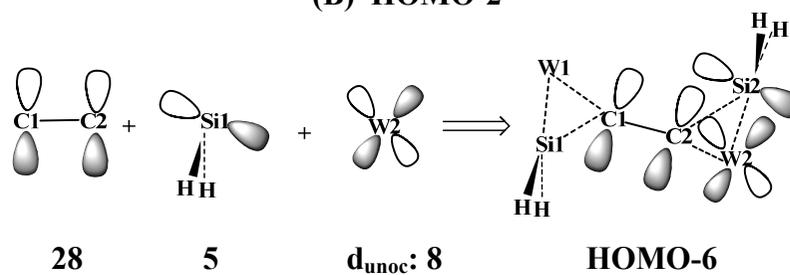
(C) HOMO-3

[a)] Occupied d orbital of W.   [b)] Unoccupied d orbital of W

Scheme 4.5: Weights (in %) of fragment MOs
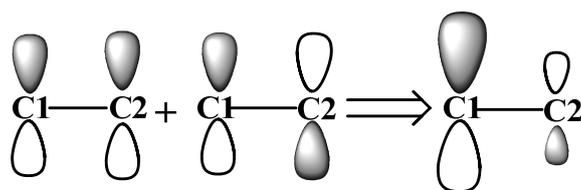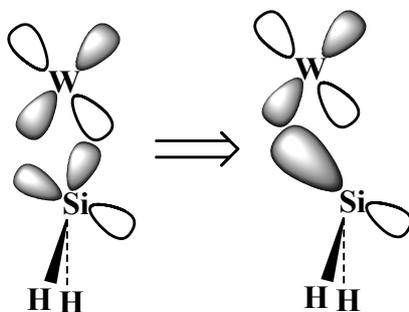
Scheme 4.6

consist of the d^W_{occ}. The degenerate HOMO-2s involve several kinds of CT interactions which are formed between the W, CC, and SiH_2, as follows: The d^W_{occ} of W1 largely participates in this HOMO-2, into which the unoccupied $\varphi^{CC}_{\pi*}$ and φ^{Si}_p mix in a bonding way but the φ^{Si}_{lp} mixes in an anti-bonding way. Also, the d^W_{unoc} of the W2 largely participates in this HOMO-2, into which the occupied φ^{Si}_{lp}, φ^{CC}_{lp}, and φ^{CC}_{π} moderately mix in a bonding way. These orbital interactions are supported by their expansion coefficients; see Scheme 4.5(B). However, the presences of the φ^{CC}_{π} and $\varphi^{CC}_{\pi*}$ are not clearly observed in this HOMO-2 (Figure 4.3). This result is interpreted in terms of the π orbital polarization of the CC moiety, as follows: As shown in Scheme 4.6(A), the mixing of the $\varphi^{CC}_{\pi*}$ into the φ^{CC}_{π} considerably increases the p orbital of C1 but considerably decreases the p orbital of C2. This polarized π_1 bonding orbital is observed in the HOMO-2. In the π_2 space perpendicular to the π_1, the reverse polarization occurs to increase the p orbital of C2 and decrease the p orbital of C1. These polarizations lead to the equivalent atomic populations of C1 and C2 and also the weakening of the π bonding nature. Also, the φ^{Si}_p is not clearly observed in the HOMO-2. This is because the bonding

mixing of the φ^{Si}_{p} and the anti-bonding mixing of the φ^{Si}_{lp} with the d^{W}_{occ} of the W1 lead to the distorted bonding orbital, as shown in Scheme 4.6(B). The degenerate HOMO-3s mainly involve the φ^{CC}_{π}, which overlaps with the φ^{Si}_{p} and the d^{W}_{unoc} in a bonding way; see Scheme 4.5(C) for their expansion coefficients. The HOMO-4 and HOMO-6 involve the bonding interaction between the φ^{CC}_{lp} and the d^{W}_{unoc}. Though the CT from the φ^{CC}_{π} to the φ^{Si}_{p} is found, the CT from the φ^{Si}_{lp} to the $\varphi^{CC}_{\pi*}$ is not clearly observed in the MOs of **1** unlike in **5**. This is because the φ^{Si}_{lp} expands toward the W center in **1** but toward the CC moiety in **5**.

4.3.3   Mulliken Population in Fragment MOs

We evaluated the electron population of the fragment MOs by eq 4.2;

$$\rho_j(A) = \sum_{i}^{occ} [a_{ij}^2 + \sum_{k} a_{ij} b_{ik} S_{jk} + \sum_{l} a_{ij} c_{il} S_{jl} + \sum_{m} a_{ij} d_{im} S_{jm} + \sum_{n} a_{ij} e_{in} S_{jn}] \qquad (4.2)$$

where the $\rho_j(A)$ represents how much electron population the $\varphi_j(A)$ possesses in the total system ABCDE and the S_{jk} is the overlap integral between the $\varphi_j(A)$ and the $\varphi_k(B)$. The sum of the populations of all MOs of the fragment A is the same as the sum of the Mulliken atomic populations in the fragment A.

As shown in Table 4.3, the population (1.863e) of the $\varphi_{HOMO\,-1}(W)$ is close to 2.0e in **1** and that (1.489e) of the $\varphi_{HOMO}(W)$ is similar to that (1.454e) of **2** but considerably smaller than that of **5** (1.778e). Because **2** has an acetylenic structure (W-C≡C-W), **2** is a d^4 complex. The population of the $\varphi_{HOMO}(W)$ in **1** is similar to that of **2**, indicating that **1** is understood to be a d^4 complex (+II oxidation state), too. The considerably smaller population of the $\varphi_{HOMO}(W)$ in **1** and **2** than in **5** arises from the larger CT from the $\varphi_{HOMO}(W)$ to the φ^{Si}_{p} [64], which will be discussed below.

Table 4.3. Mulliken Populations[a] of Fragment MOs in Cp(CO)$_2$(SiH$_2$)W-CC-W(SiH$_2$)(CO)$_2$Cp **1**, Cp(CO)$_2$(SiH$_2$)W-C≡C-W(SiH$_2$)(CO)$_2$Cp] **2**, and Cp(CO)$_2$W(CCH)(SiH$_2$) **5**.

	1	2	5
[Cp(CO)$_2$W]$^+$			
$\varphi_{LUMO+2}(W)$	0.013	0.015	0.011
$\varphi_{LUMO+1}(W)$	0.376	0.638	0.411
$\varphi_{LUMO}(W)$	1.157	0.794	0.835
$\varphi_{HOMO}(W)$	1.489	1.454	1.778
$\varphi_{HOMO-1}(W)$	1.863	1.910	1.844
SiH$_2$			
φ^{Si}_{P}	0.575	0.540	0.665
φ^{Si}_{lp}	0.941	1.256	0.793
[C$_2$]$^{2-}$ or [CCH]$^-$			
$\varphi^{CC}_{\pi*}$	0.453	0.097	0.397
φ^{CC}_{lp1}	1.277	1.276	1.264
φ^{CC}_{π}	1.492	1.812	1.469
φ^{CC}_{lp2}	1.472	1.635	-

[a] DFT(B3PW91)/BS-II calculation. See Appendix A.4.1 for BS-III calculation.

The population (0.575e) of the φ^{Si}_{p} is moderately larger in **1** than in **2** (0.540e) but somewhat smaller than in **5** (0.665e), while that (0.941e) of the φ^{Si}_{lp} is considerably larger in **1** than in **5** (0.793e) but considerably smaller than in **2** (1.256e); see Table 4.3. The population (0.453e) of the $\varphi^{CC}_{\pi*}$ is somewhat larger in **1** than in **5** (0.397e) but considerably larger than in **2** (0.097e), though the φ^{Si}_{lp} does not overlap well with the $\varphi^{CC}_{\pi*}$. The population (1.492e) of the φ^{CC}_{π} in **1** is similar to that (1.469e) of **5** but considerably smaller than that (1.812e) of **2**. The population (1.277e) of the φ^{CC}_{lp1} in **1** is

similar to that (1.276e) of **2** but moderately larger than that (1.264e) of **5** and that (1.472e) of the φ^{CC}_{lp2} is somewhat smaller in **1** than that (1.635e) of **2**.

From the above results, the CT interactions involved in **1** are summerized, as follows: (1) The CT from the CC moiety to the empty d orbital of the W is moderately weaker in **1** than in **5** but somewhat stronger than in **2**. (2) The CT from the φ^{CC}_{π} to the φ^{Si}_{p} occurs to a similar extent to that of **5** but this CT cannot occur in **2**, leading to the considerably large population of the φ^{CC}_{π} in **2** than in **1**. (3) The CT from the φ^{Si}_{lp} to the $\varphi^{CC}_{\pi*}$ is considerably weaker in **1** than in **5** because of the poor overlap between them, which is consistent with the larger population of the φ^{Si}_{lp} in **1** than in **5**. (4) Nevertheless, the population of the $\varphi^{CC}_{\pi*}$ is large, indicating the CT from the d^{W}_{occ} to the $\varphi^{CC}_{\pi*}$ is stronger in **1** than in **5**.

4.3.4   Summary of Bonding Nature of 1

The above-discussed CT interactions are schematically shown in Scheme 4.7. As discussed above, the C-C bond in **1** is weaker than the C-C triple bond but its strength corresponds to the C-C double bond. One reason is the CT from the d^{W}_{occ} to the $\varphi^{CC}_{\pi*}$, which is consistent with the smaller population of the $\varphi_{HOMO}(W)$ and the larger population of the $\varphi^{CC}_{\pi*}$ in **1** than in **5**; see above. Also, the CTs are formed between the φ^{Si}_{lp} and d^{W}_{unoc} and between the d^{W}_{occ} and the φ^{Si}_{p} in **1**. Because the SiH_2 points its direction toward the W, these CTs are strong in **1**, and hence, the W-Si bond of **1** is somewhat stronger than that of **5**. Because the CT from the φ^{Si}_{lp} to the $\varphi^{CC}_{\pi*}$ is considerably weak due to poor overlap between them, only the CT from the φ^{CC}_{π} to the φ^{Si}_{p} contributes to the Si-C bonding interaction in **1**. The Si1-C1 bond index of **1** is somewhat larger than the Si-C1 bond index of **5** but the Si1-C2 bond index is much smaller than the Si-C2 bond index of **5**. This is because the p_{π} orbital of C1 overlaps with the φ^{Si}_{p} in **1** but that of C2 cannot

overlap with the φ^{Si}_p in **1**; see Figure 1 for orientation of the SiH$_2$. The CTs from the φ^{CC}_π of the CC moiety to the φ^{Si}_p of the two SiH$_2$ moieties considerably weaken the C-C bond of **1**. The mixing of the φ^{CC}_π with the $\varphi^{CC}_\pi*$ leads to the polarization of the π orbital. These are other reasons of the much weaker C-C bond in **1** than in **5**.

The above results lead to the conclusions, as follows: (1) The H$_2$SiCCSiH$_2$ moiety is not understood to be a metal-substituted disilabutadiene. (2) The CC moiety is understood as an ethynediyl dianion and the SiH$_2$ moiety as a silylene. (3) The bonding nature should be understood in terms of the various CT interactions between the W, SiH$_2$, and CC moieties.
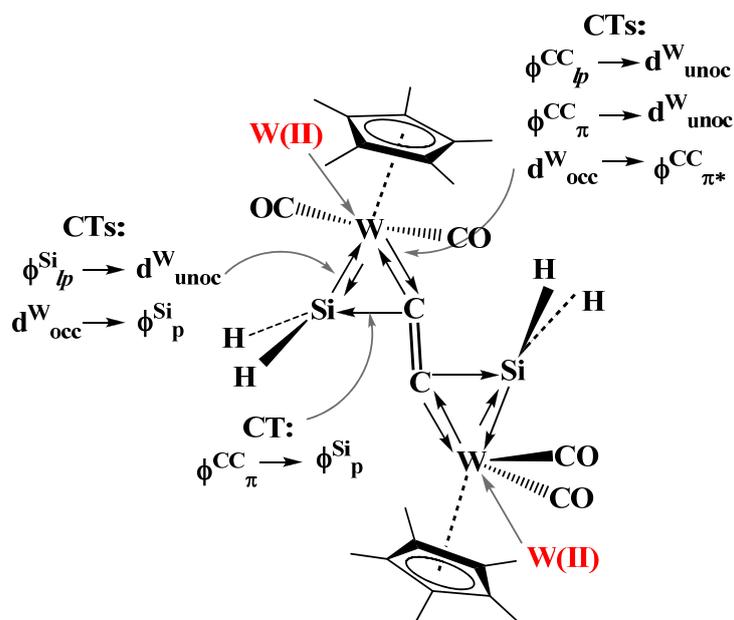
Scheme 4.7

4.4   Conclusions

Bonding nature and electronic structure of Cp(CO)$_2$(SiH$_2$)W-CC-W(SiH$_2$)(CO)$_2$Cp **1** were theoretically investigated with the DFT method, where **1** was employed as a model

of recently synthesized dinuclear tungsten complex Cp*(CO)$_2$(SiPh$_2$)W-CC-W(SiPh$_2$)(CO)$_2$Cp* **R1**.

Computational results clearly indicate that **1** is understood not to be a disilabutadiene-bridged dinuclear tungsten complex and a cumulenic (W=C=C=W) complex but to be an ethynediyl-bridged bis(silylene) dinuclear tungsten complex which contains various charge transfer (CT) interactions between the tungsten center, silylene, and ethynediyl, as shown in Scheme 4.7; the CT occurs from the lone pairs (φ^{CC}_{lp}) of the CC to the empty d orbital (d^{W}_{unoc}) of the W. Also, the CT occurs from the occupied d orbital (d^{W}_{occ}) of the W to the π* orbital ($\varphi^{CC}_{\pi*}$) of the CC. Other CT occurs from the lone pair orbital (φ^{Si}_{lp}) of the SiH$_2$ to the d^{W}_{unoc}, while the CT from the φ^{Si}_{lp} to the $\varphi^{CC}_{\pi*}$ does not occur in **1** unlike that in the mononuclear tungsten acetylide silylene complex Cp(CO)$_2$W(CCH)(SiH$_2$) **5**. This is because the φ^{Si}_{lp} expands toward the W center rather than the CC moiety in **1** but expands toward the CC moiety in **5**. The CT occurs from the d^{W}_{occ} to the empty p orbital (φ^{Si}_{p}) of the SiH$_2$. Also, the CT occurs from the φ^{CC}_{π} to the φ^{Si}_{p}. These CT interactions lead to the considerably strong Si-C bonding interactions. As a result, the Si-C bond strength is rather similar to the Si-C single bond, though it is much weaker than that of a disilabutadiene. The C-C distance is much longer than the typical C≡C triple bond distance and similar to the typical C=C distance. This result is easily interpreted in terms of the back-donation from the d^{W}_{occ} to the $\varphi^{CC}_{\pi*}$ and the CT from the φ^{CC}_{π} to the φ^{Si}_{p}. The mixing of the φ^{CC}_{π} into the $\varphi^{CC}_{\pi*}$ induces the π orbital polarization of the CC moiety in one plane and the reverse π orbital polarization in the perpendicular plane. These polarizations lead to the presence of two equivalent C atoms and the considerable weakening of the CC bond. Thus, **1** is understood to be a new category of ethynediyl-bridged bis(silylene) dinuclear tungsten complex including interesting CT interactions and polarizations.

Bibliography

[1]   Diederich, F.; Rubin, Y. *Angew. Chem., Int. Ed. Engl.* **1992**, *31*, 1101.

[2]   Beck, W.; Niemer, B.; Wieser, M. *Angew. Chem., Int. Ed. Engl.* **1993**, *32*, 923, and references therein.

[3]   Lang, H. *Angew. Chem., Int. Ed. Engl.* **1994**, *33*, 547.

[4]   Listemann, M. L.; Schrock, R. R. *Organometallics* **1985**, *4*, 74-83.

[5]   (a) LaPointe, R. E.; Wolczanski, P. T.; Mitchell, J. F. *J. Am. Chem. Soc.* **1986**, *108*, 6382. (b) Neithamer, D. R.; LaPointe, R. E.; Wheeler, R. A.; Richeson, D. S.; Van Duyne, G. D.; Wolczanski, P. T. *J. Am. Chem. Soc.* **1989**, *111*, 9056.

[6]   (a) Frank, K. G.; Selegue, J. P. *J. Am. Chem. Soc.* **1990**, *112*, 6414. (b) Koutsantonis, G. A.; Selegue, J. P. *J. Am. Chem. Soc.* **1991**, *113*, 2316.

[7]   Davies, J. A.; El-Ghanam, M.; Pinkerton, A. A.; Smith, D. A. *J. Organomet. Chem.* **1991**, *409*, 367.

[8]   Lemke, F. R.; Szalda, D. J.; Bullock, R. M. *J. Am. Chem. Soc.* **1991**, *113*, 8466.

[9]   Chen, M. C.; Tsai, Y. J.; Lin, Y. C.; Tseng, T. W.; Lee, G. H.; Wang, Y. *Organometallics* **1991**, *10*, 378.

[10]   Binger, P.; Müller, P.; Philipps, P.; Gabor, B.; Mynott, R.; Herrmann, A. T.; Langhauser, F.; Krüger, C. *Chem. Ber.* **1992**, *125*, 2209.

[11]   Ramsden, J. A.; Weng, W.; Arif, A. M.; Gladysz, J. A. *J. Am. Chem. Soc.* **1992**, *114*, 5890-5891.

[12]   De Angelis, S.; Solari, E.; Floriani, C.; Chiesi-Villa, A.; Rizzoli, R. *Angew. Chem., Int. Ed. Engl.* **1995**, *34*, 1092.

[13]   Sünkel, K.; Birk, U.; Robl, C. *Organometallics* **1994**, *13*, 1679-1687.

[14] (a) Akita, M.; Takabuchi, A.; Terada, M.; Ishii, N.; Tanaka, M.; Morooka, Y. *Organometallics* **1994**, *13*, 2516-2520. (b) Akita, M.; Moro-oka, Y. *Bull. Soc. Jpn.* **1995**, *68*, 420-432. (c) Akita, M.; Chung, M. C.; Sakurai, A.; Sugimoto, S.; Terada, M.; Tanaka, M.; Morooka, Y. *Organometallics* **1997**, *16*, 4882.

[15] Long, N. J.; Williams, C. K. *Angew. Chem., Int. Ed. Engl.* **2003**, *42*, 2586 and references therein.

[16] (a) Appel, M.; Heidrich, J.; Beck, W. *Chem. Ber.* **1987**, *120*, 1087. (b) Heidrich, J.; Stelman, M.; Appel, M.; Beck, W.; Phillips, J. R.; Trogler, W. C. *Organometallics* **1990**, *9*, 1296.

[17] Caulton, K. G.; Cayton, R. H.; Chisholm, R. H.; Huffman, J. C.; Lobkovsky, E. B.; Xue, Z. *Organometallics* **1992**, *11*, 321.

[18] (a) Belanzoni, P.; Nazzareno, Re.; Rosi, M.; Sgamellotti, A.; Floriani, C. *Organometallics* **1996**, *15*, 4264. (b) Angelis, F. D.; Nazzareno, Re.; Rosi, M.; Sgamellotti, A.; Floriani, C. *J. Chem. Soc. Dalton Trans*. **1997**, 3841. (c) Belanzoni, P.; Nazzareno, Re.; Sgamellotti, A.; Floriani, C. *J. Chem. Soc. Dalton Trans*. **1997**, 4773. (d) Belanzoni, P.; Sgamellotti, A.; Nazzareno, Re.; Floriani, C. *Inorg. Chem.* **2000**, *39*, 1147.

[19] Oike, H.; Kawai, M.; kabuto, C.; Sakaba, H. *55th Symposium on Organometallic Chemistry, Japan,* **2008***, 147.

[20] Sakaba, H.; Yoshida, M.; Kabuto, C.; Kabuto, K. *J. Am. Chem. Soc.* **2005**, *127*, 7226.

[21] (a) Ray, M.; Nakao, Y.; Sato, H.; Sakaba, H.; Sakaki, S. *J. Am. Chem. Soc*. **2006**, *128*, 11927. (b) Ray, M.; Nakao, Y.; Sato, H.; Sakaki, S. *Organometallics* **2007**, *26*, 4413. (c) Ray, M.; Nakao, Y.; Sato, H.; Sakaba, H.; Sakaki, S. *Organometallics* **2009**, *28*, 65.

[22] Schmidt, G.; Welz, E. *Angew. Chem. Int. Ed. Engl*. **1977**, *16*, 785.

[23] (a) Pannell, K. H.; Cervantes, J.; Hernandez, C.; Cassias, J.; Vincenti, S. *Organometallics* **1986**, *5*, 1056. (b) Jones, K. L.; Pannell, K. H. *J. Am. Chem. Soc*. **1993**, *115*, 11336. (c) Sharma, H. K.; Pannell, K. H. *Chem. Rev*. **1995**, *95*, 1351. (d) Jones, K. L.; Pannell, K. H. *Organometallics* **2001**, *20*, 7.

[24] (a) Tobita, H.; Ueno, K.; Ogino, H. *Chem. Lett*. **1986**, 1777. (b) Tobita, H.; Ueno, K.; Ogino, H. *Bull. Chem. Soc. Jpn*. **1988**, *61*, 2797. (c) Ueno, K.; Tobita, H.; Shimoi, M.; Ogino, H. *J. Am. Chem. Soc*. **1988**, *110*, 4092. (d) Tobita, H.; Ueno, K.; Shimoi, M.; Ogino, H. *J. Am. Chem. Soc*. **1990**, *112*, 3415. (e) Ueno, K.; Tobita, H.; Ogino, H. *Chem. Lett*. **1990**, 369. (f) Takeuti, T.; Tobita, H.; Ogino, H. *Organometallics* **1991**, *10*, 835. (g) Ueno, K.; Ito, S.; Endo, K.; Tobita, H.; Inomata, S.; Ogino, H. *Organometallics* **1994**, *13*, 3309. (h) Tobita, H.; Wada, H.; Ueno, K.; Ogino, H. *Organometallics* **1994**, *13*, 2545. (i) Ueno, K.; Nakano, K.; Ogino, H. *Chem. Lett.* **1996**, 459. (j) Ueno, K.; Masuko, A.; Ogino, H. *Organometallics* **1997**, *16*, 5026. (k) Okazaki, M.; Tobita, H.; Ogino, H. *Chem. Lett.* **1997**, 437. (l) Wada, H.; Tobita, H.; Ogino, H. *Chem. Lett.* **1998**, 993. (m) Ueno, K.; Sakai, M.; Ogino, H. *Organometallics* **1998**, *17*, 2138. (n) Ogino, H.; Tobita, H. *Ad. Organomet. Chem.* **1998**, *42*, 223. (o) Ueno, K.; Masuko, A.; Ogino, H. *Organometallics* **1999**, *18*, 2694. (p) Tobita, H.; Sato, T.; Okazaki, M.; Ogino, H. *J. Organomet. Chem.* **2000**, *611*, 314. (q) Minglana, J. J. G.; Okazaki, M.; Tobita, H.; Ogino, H. *Chem. Lett.* **2002**, 406. (r) Ogino, H. *The Chem. Record* **2002**, *2*, 291. (s) Okazaki, M.; Tobita, H.; Ogino, H. *Dalton Trans*. **2003**, 493.

[25] Zybill, C.; Müller, G. *Angew. Chem. Int. Ed. Engl.* **1987***, 26*, 669.

[26] Woo, L. K.; Smith, D. A.; Young, Jr. V. G. *Organometallics* **1991**, *10*, 3977.

[27] (a) Straus, D. A.; Tilley, T. D.; Rheingold, A. L.; Geib, J. S. *J. Am. Chem. Soc.*

1987, *109*, 5872. (b) Tilley, T. D. In *The Silicon-Heteroatom Bond*; Patai, S., Rappoprt, Z., Eds.; Wiley: New York, **1991**; Chapters 9 and 10, pp 245, 309. (c) Grumbine, S. D.; Tilley, T. D.; Rheingold, A. L. *J. Am. Chem. Soc.* **1993**, *115*, 358. (d) Grumbine, S. D.; Tilley, T. D.; Arnold, F. P.; Rheingold, A. L. *J. Am. Chem. Soc.* **1993**, *115*, 7884. (e) Michell, G. P.; Tilley, T. D. *Angew. Chem. Int. Ed. Engl.* **1998**, *37*, 2524. (f) Michell, G. P.; Tilley, T. D. *J. Am. Chem. Soc.* **1998**, *120*, 7635. (g) Feldman, J. D.; Mitchell, G. P.; Notle, J. O.; Tilley, T. D. *J. Am. Chem. Soc.* **1998**, *120*, 11184. (h) Peters, J. C.; Feldman, J. D.; Tilley, T. D. *J. Am. Chem. Soc.* **1999**, *121*, 9871.

[28] (a) Corriu, R. J. P.; Lanneau, G. F.; Chauhan, B. P. S. *Organometallics* **1993**, *12*, 2001. (b) Corriu, R. J. P.; Chauhan, B. P. S.; Lanneau, G. F. *Organometallics* **1995**, *14*, 1646. (c) Chauhan, B. P. S.; Corriu, R. J. P.; Lanneau, G. F.; Priou, C.; Auner, N.; Handwerker, H.; Herdtweck, E. *Organometallics* **1995**, *14*, 1657. (d) Corey, J. Y.; Braddock-Wilking, J. *Chem. Rev.* **1999**, *99*, 175.

[29] (a) Bodensieck, U.; Braunstein, P.; Dech, W.; Faure, T.; Knorr, M.; Stern, C. *Angew. Chem. Int. Ed. Engl.* **1994**, *33*, 2440. (b) Braunstein, P.; Knorr, M. *J. Organomet. Chem.* **1995**, *500*, 21. (c) Braunstein, P.; Boag, N. M. *Angew. Chem. Int. Ed. Engl.* **2001**, *40*, 2427.

[30] Denk, M.; Hayashi, R. K.; West, R. *J. Chem. Soc. Chem. Commun.* **1994**, 33.

[31] Chen, W.; Edwards, A. J.; Esteruelas, M. A.; Lahoz, F. J.; Olivan, M.; Oro, L. A. *Organometallics* **1996**, *15*, 2185.

[32] Eisen, M. S. In *The Chemistry of Organic Silicon Compounds*; Rappoport, Z., Apeloig, Y., Eds.; Wiley: New York, **1998**; vol.2, chapter 35, p2037.

[33] Gehrhus, B.; Hitchcock, P. B.; Lappert, M. F.; Maciejewski, H. *Organometallics* **1998**, *17*, 5599.

[34] Petri, S. H. E.; Eikenberg, D.; Neumann, B.; Stammler, H. G.; Jutzi, P. *Organometallics* **1999**, *18*, 2615.

[35] Sakaba, H.; Tsukamoto, M.; Hirata, T.; Kabuto, C.; Horino, H. *J. Am. Chem. Soc.* **2000**, *122*, 11511 and references therein.

[36] Cundari, T. R.; Gordon, M. S.; *J. Phys. Chem.* **1992**, *96*, 631.

[37] Marquez, A.; Sanz, J. F. *J. Am. Chem. Soc*. **1992**, *114*, 2903.

[38] Jacobsen, H.; Ziegler, T. *Organomettallics* **1995**, *14*, 224.

[39] Boheme, C.; Frenking, G. *Organometallics* **1998**, *17*, 5801.

[40] Beddie, C.; Hall, M. B.; *J. Am. Chem. Soc*. **2004**, *126*, 13564.

[41] Carter, J. D.; Kingsbury, K. B.; Wilde, A.; Schoch, T. K.; Carolyn, J. L.; Pham, E. K.; McElwee-White, L. *J. Am. Chem. Soc*. **1991**, *113*, 2947.

[42] (a) Becke, A. D. *Phys Rev. A*. **1988**, *38*, 3098. (b) Becke, A. D. *J. Chem. Phys*. **1993**, *98*, 5648.

[43] (a) Perdew, J. P. *In Electronic Structure of Solids*`91, Ziesche, P.; Eschrig, H., Ed.; Akademic Verlag, Berlin, **1991**; p 11. (b) Perdew, J. P.; Chevary, J. A.; Vosko, S. H.; Jackson, K. A.; Pederson, M. R.; Singh, D. J.; Fiolhais, C. *Phys. Rev. B*. **1992**, *46*, 6671. (c) Perdew, J. P.; Chevary, J. A.; Vosko, S. H.; Jackson, K. A.; Pederson, M. R.; Singh, D. J.; Fiolhais, C. *Phys. Rev. B*. **1993**, *48*, 4978. (d) Perdew, J. P.; Burke, K.; Wang, Y. *Phys Rev. B*. **1996**, *54*, 16533.

[44] (a) Lee, C.; Yang, W.; Parr, R. G. *Phys. Rev. B*. **1988**, *37*, 785. (b) Miehlich, B.; Savin, A.; Stoll, H.; Preuss, H. *Chem. Phys. Lett*. **1989**, *157*, 200.

[45] Hay, P. J.; Wadt, W. R. *J. Chem. Phys*. **1985**, *82*, 299.

[46] (a) Dunning Jr, T. H. *J. Chem. Phys*. **1989**, *90*, 1007. (b) Woon, D. E.; Dunning Jr, T. H. *J. Chem. Phys*. **1993**, *98*, 1358.

[47] (a) Ditchfield, R.; Hehre, W. J.; Pople, J. A. *J. Chem. Phys.* **1971**, *54*, 724. (b) Hehre, W.; Ditchfield, R.; Pople, J. A. *J. Chem. Phys.* **1972**, *56*, 2257.

[48] Andrae, D.; Haeussermann, U.; Dolg, M.; Stoll, H.; Preuss, H. *Theor. Chim. Acta* **1990**, *77*, 123.

[49] Martin, J. M. L.; Sundermann, A. *J. Chem. Phys.* **2001**, *114*, 3408.

[50] (a) Dunning Jr., T. H. *J. Chem. Phys.* **1989**, *90*, 1007. (b) Woon, D. E.; Dunning Jr., T. H. *J. Chem. Phys.* **1993**, *98*, 1358.

[51] Wiberg, K. B. *Tetrahedron* **1968**, *24*, 1083.

[52] Couty, M.; Hall, M. B. *J. Comput. Chem.* **1996**, *17*, 1359.

[53] Ehlers, A. W.; Bohme, D. S.; Gobbi, A.; Hollwarth, A.; Jonas, V.; Kohler, K. F.; Stegmann, R.; Veldkamp, A.; Frenking, G. *Chem. Phys. Lett.* **1993**, *208*, 111.

[54] Pople, J. A.; et al. *Gaussian 03,* Revision C.02, Gaussian Inc.: Wallingford, CT, **2004**.

[55] Glendening, E. D.; Reed, A. E.; Carpenter, J. E.; Weinhold, F. NBO Version, 3.1.

[56] (a) Flükiger, P.; Lüthi, H. P.; Portmann, S.; Weber, J. *MOLEKEL 4.3*, Swiss Center for Scientific Computing, Manno (Switzerland), **2000-2002**. (b) Portmann, S.; Lüthi, H. P. *MOLEKEL*, An Interactive Molecular Graphics Tool, *CHIMIA*, **2000**, *54*, 766-770.

[57] Pin, C. W.; Peng, J.-J.; Shiu, C.-W.; Chi, Y.; Peng, S.-M.; Lee, G.-H. *Organometallics* **1998**, *17*, 438.

[58] Mathur, P.; Mukhopadhyay, S.; Lahiri, G. K.; Chakraborty, S.; Thöne, C. *Organometallics* **2002**, *21*, 5209.

[59] We optimized a typical W-carbene complex $Cp(CO)_2W(CH_2)(CCH)$ with the DFT(B3PW91)/BS-I method.

[60] The C-C distance is 1.542 Å, 1.334 Å, 1.210 Å, and 1.428 Å and the C-C bond

index is 1.043, 2.052, 3.001, and 1.103 in ethane H_3C-CH_3, ethylene $H_2C=CH_2$, acetylene $HC\equiv CH$, and silabutadiene $H_2Si=CH-CH=SiH_2$, respectively, where the distances were optimized with the DFT/BS-I method and the bond index was evaluated with the DFT/BS-II method.

[61] The Si-C distance is 1.895 Å, 1.717 Å, and 1.750 Å and the Si-C bond index is 0.884, 1.818, and 1.144 in H_3Si-CH_3, $H_2Si=CH_2$, and $H_2Si=CH-CH=SiH_2$, respectively.

[62] Dapprich, S.; Frenking, G. *J. Phys. Chem.* **1995**, *99*, 9352.

[63] Burdett, J. K. *Struct. Bonding (Berlin)* **1976**, *31*, 67.

[64] The population of the $\varphi_{HOMO}(W)$ was calculated to be 1.787e in the typical ethynediyl-bridged dinuclear tungsten complex $Cp(CO)_3W-C\equiv C-W(CO)_3Cp$. This population is considerably larger than that (1.454e) of $Cp(CO)_2(SiH_2)W-C\equiv C-W(SiH_2)(CO)_2Cp$ **2**, indicating that the back-donation from the W to the SiH_2 is considerably larger in **2** than that from the W to the CO in $Cp(CO)_3W-C\equiv C-W(CO)_3Cp$.

Appendix

A.4.1 DFT/BS-III-calculated Mulliken population of Fragment MOs.

Table A.4.1. Mulliken Population[a] of Fragment MOs in $Cp(CO)_2(SiH_2)W-CC-W(SiH_2)(CO)_2Cp$ **1**, $Cp(CO)_2(SiH_2)W-C\equiv C-W(SiH_2)(CO)_2Cp]$ **2**, and $Cp(CO)_2W(CCH)(SiH_2)$ **5**.

	1	2	5
$[Cp(CO)_2W]^+$			
$\varphi_{LUMO+2}(W)$	0.012	0.015	0.023
$\varphi_{LUMO+1}(W)$	0.610	0.841	0.633
$\varphi_{LUMO}(W)$	1.193	0.757	0.863
$\varphi_{HOMO}(W)$	1.511	1.928	1.828
$\varphi_{HOMO-1}(W)$	1.866	1.467	1.854
$\varphi_{TOTAL}(W)$	5.191	5.007	5.201
SiH_2			
φ^{Si}_{P}	0.628	0.528	0.696
φ^{Si}_{lp}	0.839	1.138	0.764
$[C_2]^{2-}$ or $[CCH]^-$			
$\varphi^{CC}_{\pi*}$	0.446	0.089	0.281
φ^{CC}_{lp1}	1.113	1.063	1.264
φ^{CC}_{π}	1.482	1.806	1.661
φ^{CC}_{lp2}	1.295	1.417	-

[a] DFT(B3PW91)/BS-III calculation.

A.4.2 Optimized geometry of a deprotonated disilabutadiene $[H_2SiCCSiH_2]^{2-}$
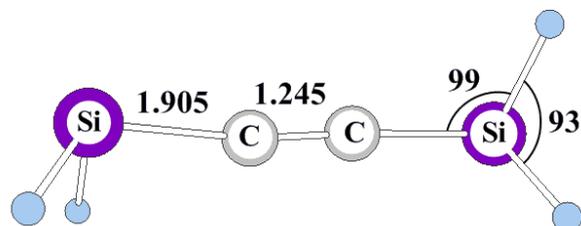
Figure A.4.1. Optimized geometry[a] of $[H_2SiCCSiH_2]^{2-}$ **6-an**. Bond lengths are in angstrom and bond angles are in degree.

[a] DFT/BS-I optimization was carried out.

Chapter 5

Tungsten Dihydride Silyl Complex: New Insight into Their Bonding Nature and Fluxional Behavior

5.1 Introduction

Transition metal hydride silyl complexes have attracted considerable interest during the last two decades because of their importance as possible intermediates in hydrosilation [1-4], varieties in geometry, and interesting bonding features [1-4]. In this regard, many experimental studies have been reported on their syntheses and characterization [1-30]. For instance, Schubert and his coworkers extensively studied the groups 6-8 metal hydride silyl complexes experimentally [1]. Their complexes prefer the structure bearing Si-H interaction relative to the alternative structure bearing separate hydride and silyl ligands. Such hydride silyl complexes bearing the Si-H interaction are often found in mid-transition metal (groups 6-8) [1, 3, 5, 16, 22, 27, 29] and early (group 4-5) transition metal complexes [10, 11, 18-19]. For instance, the Si-H interaction was reported for group 4 metallocene complex such as $Cp_2Ti(PMe_3)(\eta^2\text{-H-SiMe}_3)$ [11b]. However, Zr and Hf analogues do not include such Si-H interaction, suggesting that the structure is sensitive to the central metal [11a]. Another interesting metallocene hydride disilyl complex $Cp_2Ta(SiMe_2H)(H)(SiMe_2H)$ bearing the strong Si-H interaction was reported in the literature [10a]. Nikonov group also recently studied its analogues

Cp$_2$Nb(SiClMe$_2$)(H)(SiClMe$_2$) [18a,b,k] and Cp$_2$Nb(H)$_2$(SiR$_3$) [18c] bearing the Si-H interaction.

Because of their interesting bonding nature, geometry, and important roles in catalytic reactions, the transition metal hydride silyl complexes have drawn considerable theoretical interest [18, 31-35]. For instance, the formation of transition metal hydride silyl complexes and their reactions with alkene and alkyne were investigated by Sakaki and his coworkers [31]. The formation of ruthenium hydride silyl complexes was investigated by the Morokuma group [32]. The Si-H interaction of several transition metal hydride silyl complexes was theoretically studied by Hall [33], Lin [34], and Jacobsen groups [35].

Among transition metal hydride silyl complexes, dihydride silyl complexes of the L$_n$M(H)$_2$SiR$_3$ type have drawn special interest due to their unusual bonding natures and the fluxionalities of their geometries. The bonding natures of such complexes vary among the
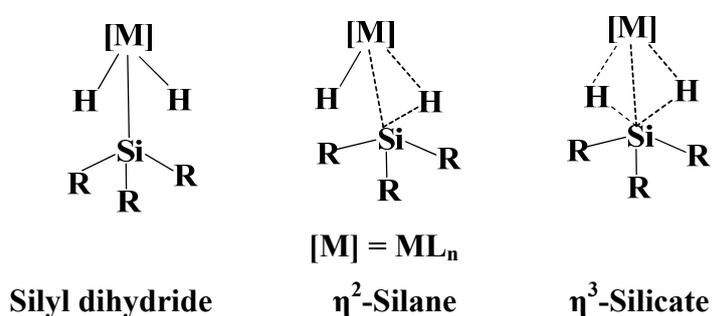
Scheme 5.1

dihydride silyl form, non-classical η^2-silane form [18*l*, 30], and non-classical η^3-silicate form [18m] depending on the strength of the Si-H interligand interaction, as shown in Scheme 5.1; note that the non-classical η^3-silicate form is the rarest among these three bonding modes. Actually, various complexes of the L$_n$M(H)$_2$SiR$_3$ type have been synthesized and characterized for late transition metals such as Fe [18m], Ru [9b, 14, 18d,g, 24, 34d], Os [6b, 9d, 21, 28], Rh [6f, 18*l*, 23, 26b, 30, 32b], and Ir [6a,c,d, 7, 12, 20]. Though this type of complex has been quite rare for the group 6 transition metals,

Cp*(CO)$_2$W(H)$_2$(SiPh$_2$Cl) [27b], Cp*(CO)$_2$W(H)$_2$(SiHPhR) [27c], and

Cp*(CO)$_2$W(H)$_2$(SiHCl$_2$) [27d] (Cp* = C$_5$Me$_5$) were synthesized and characterized,

recently. Experimental evidence for these tungsten complexes showed the presence of the

Si-H interaction [27b,d] as well as the fluxional behavior involving the site exchange of

hydride and silyl ligands [27c] These results suggest that group 6 metals add new features

in the chemistry of transition metal dihydride silyl complexes. In this regard, careful

examination especially detailed theoretical study is necessary to elucidate their interesting

structural features, bonding nature, electronic structure, and mechanism of the unusually

high fluxionality. However, no theoretical study on the mechanism of fluxionality of the

transition metal dihydride silyl complex has yet been reported, to the best of our

knowledge.
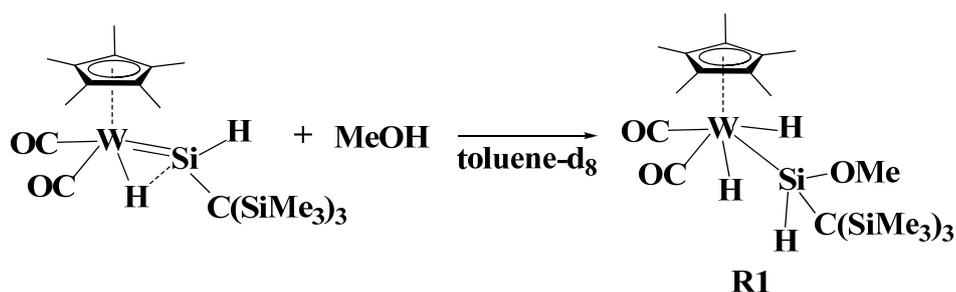
Scheme 5.2. Formation of Cp*(CO)$_2$W(H)$_2$[HSi(OMe){C(SiMe$_3$)$_3$}] **R1**.

In this work, we wish to report the theoretical analyses of the geometry, bonding

nature, electronic structure, and fluxional behavior of

Cp(CO)$_2$W(H)$_2$[SiH(OMe){C(SiH$_3$)$_3$}] **1** (Cp = C$_5$H$_5$) which is a model of the recently

synthesized tungsten dihydride silyl complex Cp*(CO)$_2$W(H)$_2$[SiH(OMe){C(SiMe$_3$)$_3$}] **R1**

(Cp* = C$_5$Me$_5$). Though the reductive elimination is expected to occur in the dihydride

silyl complex, **R1** was successfully synthesized through the reaction of tungsten hydrido

silylene complex Cp*(CO)$_2$(H)W=Si(H)[C(SiMe$_3$)$_3$] with methanol (MeOH) as shown in

Scheme 5.2 [36]. We also theoretically investigated a tungsten dihydride alkyl complex

189

Cp(CO)$_2$W(H)$_2$[CH(OMe){C(CH$_3$)$_3$}] **1C** and a tungsten silyl complex Cp(CO)$_3$W[SiH(OMe)(C(SiH$_3$)$_3$)] **2**, to clearly characterize **1** by making comparison of **1** with these complexes. **1C** is the carbon analogue of **1**. **2** is a typical silyl complex; note that **2** is not unusual because the similar tungsten silyl complex Cp(CO)$_3$W(SiMe$_2$SiMe$_3$) was reported experimentally [37a]. Our purposes here are to present a correct understanding of the bonding nature and the electronic structure of **1**, show novel fluxional behavior of transition metal dihydride silyl complexes.

5.2 Computational Details

The geometry of Cp(CO)$_2$W(H)$_2$[SiH(OMe){C(SiH$_3$)$_3$}] **1** was optimized with the DFT method, where the B3PW91 functional [38, 39] was employed for the exchange-correlation term. We ascertained that none of the equilibrium geometries have an imaginary frequency and each transition state geometry possessed only one imaginary frequency which induced geometry changes consistent with the reaction. Energy was evaluated with the DFT, MP2 to MP4(SDTQ), and CCSD(T) methods, where the DFT-optimized geometry was employed.

Three kinds of basis set systems, BS-I, BS-II, and BS-III, were mainly employed in this work. In BS-I, core electrons of W were replaced with effective core potentials (ECPs) [40] and its valence electrons were represented with a (341/321/21) basis set [40]. Usual 6-31G(d) [41] basis sets were used for the other atoms. This BS-I system was used for the geometry optimization. In BS-II, valence electrons of W were represented with a (541/541/111/1) basis set [40, 42, 43] and its core electrons were replaced with the same ECPs as those of BS-I. For the other atoms, the same basis sets as those of BS-I were employed. This BS-II was used to evaluate energy changes with the MP2 to MP4(SDTQ) and CCSD(T) methods. In BS-III, core electrons of W were replaced with ECPs of the

Stuttgart-Dresden-Bonn (SDB) group and its valence electrons were represented with a (311111/22111/411/11) basis set [44, 45]. Usual 6-311G(d) basis sets [46, 47] were employed for the other atoms. This BS-III of triple-zeta quality was used to evaluate energy, bond index, and population changes with the DFT method. To investigate the basis set effects on the geometry of **1**, we optimized **1** with four kinds of basis set system, BS-I, BS-IV, BS-V, and BS-VI. In BS-IV and BS-V, valence and core electrons of W were represented with the same basis set and ECPs as those of BS-I, respectively. For the other atoms, Huzinaga-Dunning basis sets [48] were used in BS-IV, but usual cc-pVDZ basis sets [49] were used in BS-V. In BS-VI, valence electrons of W were represented with a (5311/5311/111/1) basis set of triple-zeta quality [40, 42, 43] and its core electrons were replaced with the same ECPs as those of BS-I. Usual 6-311G(d) basis sets were employed for the other atoms. The optimized geometry with the BS-I system is little different from those optimized with these better basis set systems, BS-IV, BS-V, and BS-VI, as shown in Appendix A.5.1. Solvation effects (toluene; $\varepsilon = 2.379$) were taken into consideration with a polarizable continuum model (PCM) [50], where optimized geometries in the gas-phase were employed. The DFT/BS-III-calculated energy changes are given without parenthesis throughout this manuscript. In parentheses are the DFT/BS-III-calculated energy changes with solvation effect. The DFT/BS-II, MP4(SDTQ)/BS-II, and CCSD(T)/BS-II-calculated energy changes are given in brackets in this order.

Gaussian 03 program package (revision C.02) [51] was used for all these computations. Population analysis was carried out with the method proposed by Weinhold et al [52] Molecular orbitals were drawn with MOLEKEL program package (version 4.3) [53].

5.3 Results and Discussion

(A) Front view

(B) Side view

1	**1SiH**	**1C**	**2**
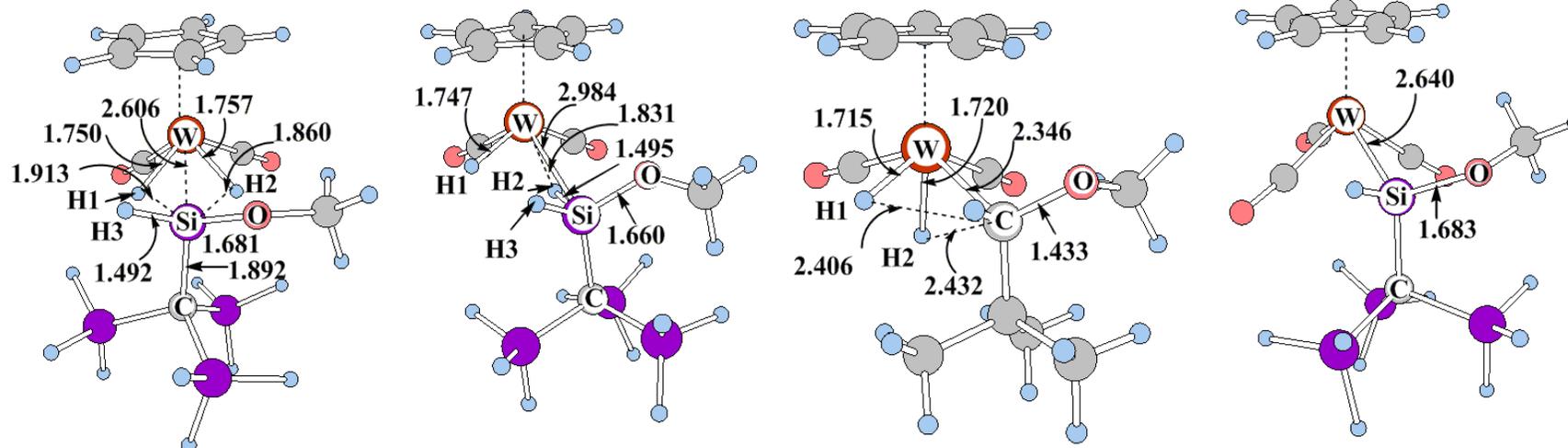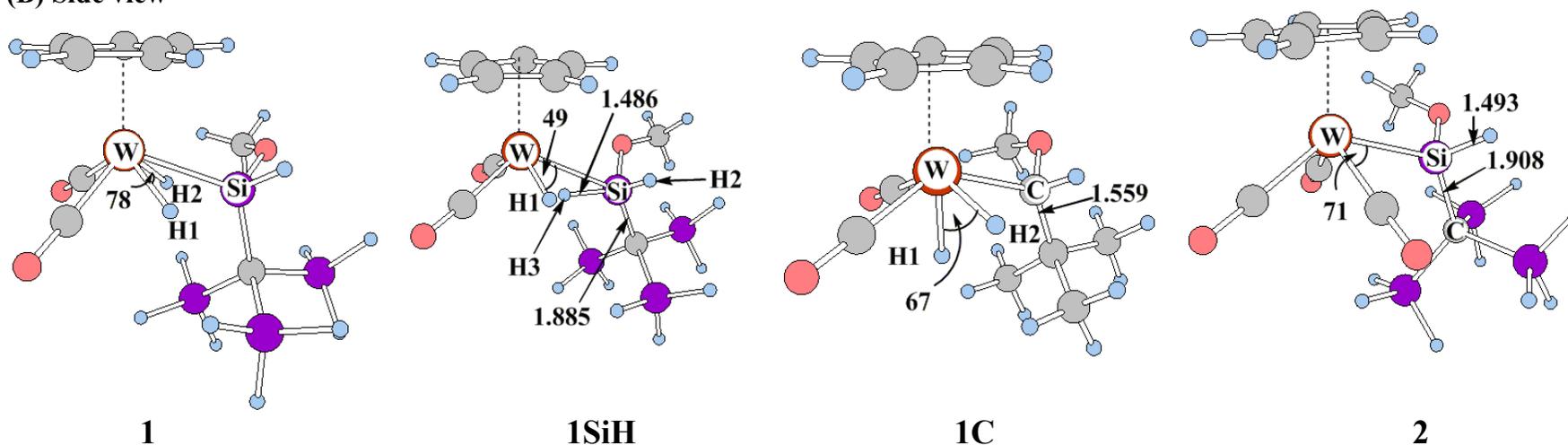
Figure 5.1. DFT(B3PW91)/BS-I optimized geometries of Cp(CO)$_2$W(H)$_2$[SiH(OMe){C(SiH$_3$)$_3$}] **1**, Cp(CO)$_2$W(H)[SiH$_2$(OMe){C(SiH$_3$)$_3$}] **1SiH**, Cp(CO)$_2$W(H)$_2$[CH(OMe){C(CH$_3$)$_3$}] **1C**, and Cp(CO)$_3$W[SiH(OMe){C(SiH$_3$)$_3$}] **2**. Bond lengths are in angstroms and bond angles are in degree.

In this chapter, we wish to discuss first the optimized geometry, bonding nature, and electronic structure of $Cp(CO)_2W(H)_2[SiH(OMe)\{C(SiH_3)_3\}]$ **1** and then the fluxional behavior of **1**.

5.3.1 Optimized Geometries of $Cp(CO)_2W(H)_2[SiH(OMe)\{C(SiH_3)_3\}]$ **1**, Its Carbon Analogue $Cp(CO)_2W(H)_2[CH(OMe)\{C(CH_3)_3\}]$ **1C**, and Typical Tungsten(II) Silyl Complex $Cp(CO)_3W[SiH(OMe)\{C(SiH_3)_3\}]$ **2**

The optimized geometry of **1** agrees well with the experimental one; see Figure 5.1 and Table 5.1. Because significant differences were not found between the optimized geometries of **1** and $Cp^*(CO)_2W(H)_2[SiH(OMe)\{C(SiH_3)_3\}]$ **1-Cp***, Cp was employed for further calculations to save the computational time; see Appendix A.4.1 for the geometry of **1-Cp***.

Table 5.1: Important optimized parameters[a] of $Cp(CO)_2(H)_2W[SiH(OMe)\{C(SiH_3)_3\}]$ **1**, $Cp(CO)_2(H)_2W[CH(OMe)\{C(CH_3)_3\}]$ **1C**, $Cp(CO)_3W[SiH(OMe)\{C(SiH_3)_3\}]$ **2**, and $Cp(CO)_2W(F)_3$ **3**.

| | **1** | | **1C** | **2** | **3** |
	calc.	**expt.**			
W-E[b]	2.606	2.620	2.324	2.640	1.912
W-H1	1.750	-	1.717	-	-
W-H2	1.757	-	1.725	-	-
Si-O	1.681	1.652	-	-	-
Si-C	1.891	1.831	-	1.908	-
Si-H1 (or C-H1)	1.913	-	2.358	-	-
Si-H2 (or C-H2)	1.860	-	2.444	-	-
Si-H3	1.492		-	1.495	-
WSiO (WCO)	112	110.7	115	112	-
WSiC (WCC)	120	126.2	122	124	-

[a] The DFT/BS-I method was employed for geometry optimization. Bond lengths are in angstrom and bond angles are in degree.
[b] E=Si in complexes **1**, and **2**, E=C in **1C**, and E = F in **3**.

As shown in Figure 5.1, the W-Si distances in **1** and Cp(CO)₂W[SiH(OMe){C(SiH₃)₃}] **2** are in the range of the usual W-silyl bond distance (2.354-2.708 Å) but closed to the longer end of the W-silyl distance [54]. The W-Si Wiberg bond index (0.393) is somewhat smaller in **1** than in **2** (0.482), suggesting that the W-Si bond in **1** is somewhat weaker than in **2** but certainly exists; see Appendix A.5.2 for the Wiberg bond indices. The W-H1 and W-H2 distances of **1** are in the range of usual W-H(hydride) bond distance [27c, 37b, 55]. The carbon analogue of **1**, Cp(CO)₂W(H)₂[CH(OMe){C(CH₃)₃}] **1C** (see Figure 5.1), is understood to be a tungsten(IV) dihydride alkyl complex because the C-H inter-ligand interaction is not formed between the hydride and alkyl ligands in general: actually, the C-H1 and C-H2 distances are very long (2.406 Å and 2.432 Å, respectively) and their bond indices are very small (0.048 and 0.056, respectively). This means that strong W-H bonds are involved in **1C**. However, the W-H1 and W-H2 distances of **1** are not different very much from those of **1C**. Though the Wiberg bond indices of the W-H1 and W-H2 bonds are moderately smaller in **1** than in **1C**, they are still considerably large in **1**; they are 0.501 and 0.474, respectively, in **1** and 0.629 and 0.557, respectively, in **1C**. Long H1-H2 distance (2.213 Å) and very small bond index (0.002) between the H1 and H2 in **1** indicate that the η^2-H₂ coordination form is completely ruled out. These results suggest that the H1 and H2 are characterized to be a hydride in **1**, which is also consistent with the proton NMR chemical shifts of **R1** [36]. In **1**, the Si-H1 and Si-H2 distances are 1.913 Å and 1.860 Å, respectively, which are about 0.4 Å longer (25% longer) than the usual Si-H covalent bond. Also, the Si-H1 and Si-H2 bond indices are 0.241 and 0.281, respectively, in **1**. These values are about 35% of the Si-H bond index in the usual silane [56] and about 30% of that of the usual silicate but much larger than that of the C-H bond index of **1C**.

These results suggest that the Si---H1 and Si---H2 bonding interactions are somewhat weaker in **1** than in a normal silane and a normal silicate but certainly exist in **1**. To examine the possibility of a tungsten(II) hydride silane complex, we optimized a model complex Cp(CO)$_2$W(H)[SiH$_2$(OMe){C(SiH$_3$)$_3$}] **1SiH** in which the Si-H2 distance was taken to be the same as that (1.495 Å) of a normal silane [SiH$_2$(OMe){C(SiH$_3$)$_3$}]. The geometry of **1SiH** is considerably different from that of **1**; see Figure 5.1. Moreover, **1SiH** is much less stable than **1** by 28.2 kcal/mol. Full geometry optimization of **1SiH** smoothly leads to the geometry of **1**; see Appendix A.5.3. This result indicates that the tungsten hydride silane complex is very unstable.

All these features demonstrate that **1** is not a tungsten(II) hydride silane complex but it contains one W-silyl and two W-H(hydride) bonds with two weak Si---H bonding interactions.

5.3.2 Population and MO Analyses

Table 5.2. NBO population[a] of several important atoms and groups in Cp(CO)$_2$W(H)$_2$[SiH(OMe){C(SiH$_3$)$_3$}] **1**, Cp(CO)$_2$W(H)$_2$(CH(OMe){C(CH$_3$)$_3$}) **1C**, Cp(CO)$_2$W(H)[SiH$_2$(OMe){C(SiH$_3$)$_3$}] **1SiH**, Cp(CO)$_3$W[SiH(OMe){C(SiH$_3$)$_3$}] **2**, and Cp(CO)$_2$W(F)$_3$ **3**.

Atoms/Groups	1	1C	1SiH	2	3
W	74.474	74.348	74.320	74.421	73.004
d	6.077	5.907	5.946	6.017	4.604
H1	0.968	0.968	1.010	-	-
H2	0.977	0.842	1.147[c]	-	-
Si or C	+1.491[d]	-0.012[d]	+1.635[d]	+1.487[d]	-
SiHR^{1}R^2 or CHR^{1}R$^{2\,[b]}$	+0.221[d]	-0.153[d]	+0.388[d]	+0.161[d]	-

a) DFT(B3PW91)/BS-III calculation.
b) R^1=OMe and R^2=C(SiH$_3$)$_3$ in **1** and **2** and R^1=OMe and R^2=C(CH$_3$)$_3$ in **1C**.
c) Si-H2 distance was taken to be 1.495 Å.
d) NBO charge is given.
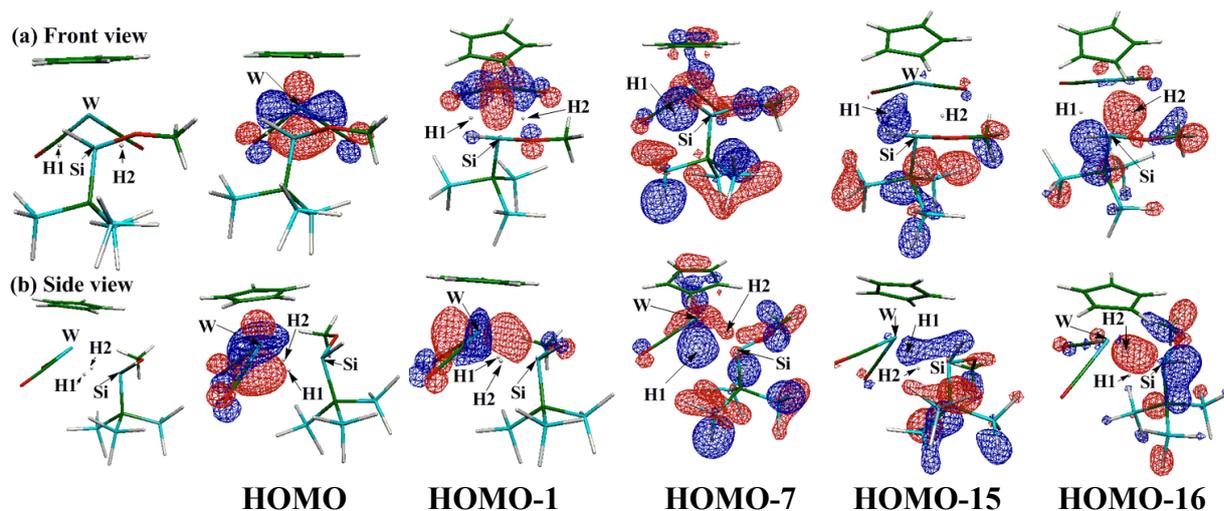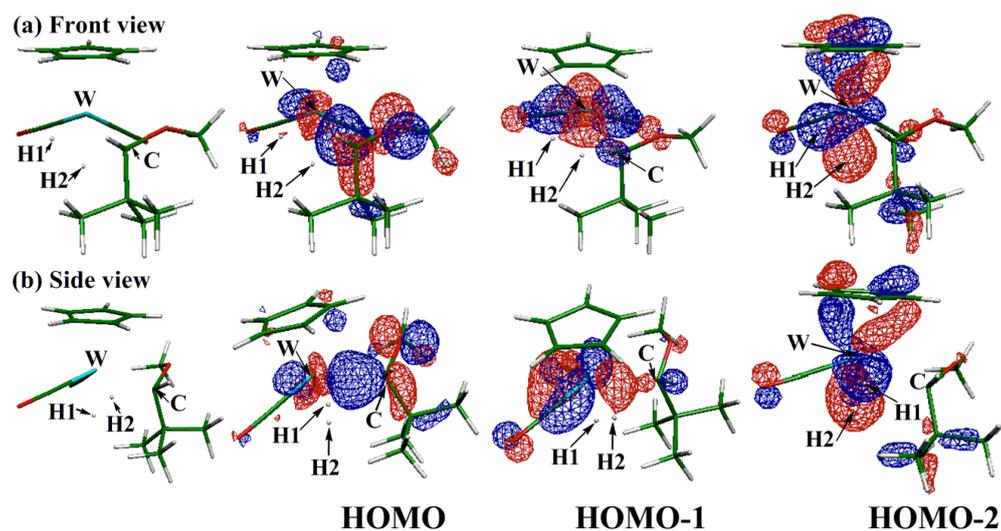
Figure 5.2. Several important Kohn-Sham MOs of $Cp(CO)_2W(H)_2[SiH(OMe)\{C(SiH_3)_3\}]$ **1** and $Cp(CO)_2W(H)_2[CH(OMe)\{(CH_3)_3\}]$ **1C**.

As shown in Table 5.2, W atomic population and its d orbital population are somewhat larger in **1** than in **1C** but considerably larger than in a typical tungsten(IV) complex $Cp(CO)_2W(F)_3$ **3** [57], suggesting that **1** is not a pure tungsten(IV) complex because the W center takes a +IV oxidation state in **1C** and **3**. The H1 atomic population in **1** is similar to that in **1C** and the H2 atomic population is moderately

larger in **1** than in **1C**, indicating that the H1 and H2 atomic populations are almost the same as a hydride. The positive charge of Si is slightly larger in **1** (+1.491) than in **2** (+1.487) but considerably smaller than in **1SiH** (+1.635). The positive charge of the [SiH(OMe){C(SiH$_3$)$_3$}] group is moderately larger in **1** (+0.221) than in **2** (+0.161) but considerably smaller than in **1SiH** (+0.388). These results indicate that the electronic structure of the [SiH(OMe){C(SiH$_3$)$_3$}] group in **1** moderately deviates from that of a pure silyl group and considerably deviates from that of a pure silane group. The considerably large positive charge of the Si center and the presence of two weak Si---H bonding interactions suggest that the Si center takes a hypervalency in **1** and the H1 and H2 are hydrides interacting with both W and Si centers, which will be discussed below in detail. Mulliken population analysis also presents similar results; see Appendix A.5.4.

To understand well the bonding nature of **1**, we inspected Kohn-Sham MOs of **1**. In **1**, the HOMO and HOMO-1 mainly consist of the W d orbitals, as shown in Figure 5.2A, indicating that the W center takes a d^4 electron configuration (+II oxidation state) in **1**. The W-H1 and W-H2 bonding interactions are observed in the HOMO-7 of **1** and a moderately small W-Si bonding interaction is observed in the HOMO-16 of **1**. In contrast to **1**, the W-Si bonding interaction was clearly observed in the HOMO-2 of **2**; see Appendix A.5.5. The Si-H1 and Si-H2 bonding interactions are observed in the HOMO-15 and HOMO-16 of **1**, respectively. In **1C**, on the other hand, only one d orbital of W is clearly observed in the occupied level; see the HOMO-1 in Figure 5.2B. The HOMO involves the W-alkyl bonding interaction and the HOMO-2 involves two W-H(hydride) bonding interactions. No bonding interaction between the alkyl and hydride is observed in any MOs of **1C**, as expected. These results are consistent with our understanding that the alkyl group cannot form a

hypervalent interaction with the H atom, and therefore, the W center takes a d^2 electron configuration (+IV oxidation state) in **1C**. In $Cp(CO)_2W(F)_3$ **3**, only one doubly occupied d orbital of W is observed too, as shown in the HOMO of **3** (see Appendix A.4.5), indicating that **3** is a typical tungsten(IV) complex.

Thus, it is not easy to present a reasonable understanding of the electronic structure and the bonding nature of **1**, as follows: The geometrical features and the Wiberg bond indices indicate the presences of W-silyl and two W-H(hydride) bonds, which is consistent with the +IV oxidation state of the W center (d^2 system). On the other hand, the Kohn-Sham MOs indicate that the W center possesses two doubly occupied d orbitals (d^4 system) in **1**. All these results request us to investigate **1** in much more detail.

5.3.3   Mulliken Population in Fragment MOs

To inspect the bonding nature of **1** more clearly, the Kohn-Sham MOs were analyzed by representing them with a linear combination of MOs of fragments [58, 59], as shown in eq 1;

$$\psi_i(AB) = \sum_j a_{ij} \varphi_j(A) + \sum_k b_{ik} \varphi_k(B) \qquad (1)$$

$$\rho_j(A) = \sum_i^{occ} [a_{ij}^2 + \sum a_{ij} b_{ik} S_{jk}] \qquad (2)$$

where $\psi_i(AB)$ represents the i-th MO of system AB, $\varphi_j(A)$ is the j-th MO of such fragment A as $[Cp(CO)_2W]^+$, $\varphi_k(B)$ is the k-th MO of such fragment B as $[(H)_2SiH(OMe)\{C(SiH_3)_3\}]^-$, and a_{ij} and b_{ik} are the expansion coefficients of $\varphi_j(A)$ and $\varphi_k(B)$, respectively. The $\rho_j(A)$ in eq 2 represents how much electron population the $\varphi_j(A)$ possesses in the total system AB, and S_{jk} is the overlap integral between the

LUMO+2   **LUMO+1**   **LUMO**   **HUMO**   **HOMO-1**

$\varphi_{LUMO+2}(W)$ $\varphi_{LUMO+1}(W)$ $\varphi_{LUMO}(W)$ $\varphi_{HOMO}(W)$ $\varphi_{HOMO-1}(W)$
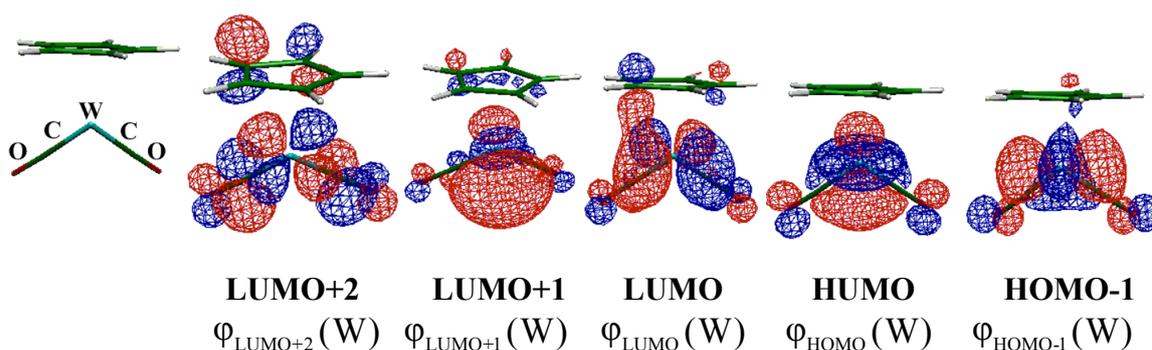
Figure 5.3. Several important Kohn-Sham orbitals of $[Cp(CO)_2W]^+$.

$\varphi_j(A)$ and the $\varphi_k(B)$. The sum of populations of all MOs of the fragment A is the same as the sum of Mulliken atomic populations in the fragment A.

LUMO+2, LUMO+1, LUMO, HOMO, and HOMO-1 of the $[Cp(CO)_2W]^+$ mainly consist of d orbitals of the W center (see Figure 5.3), where they are named $\varphi_{LUMO+2}(W)$ etc. hereafter. In **1C**, the electron population (1.268e) of the $\varphi_{HOMO}(W)$ is considerably smaller than 2.0e and that (0.337e) of **3** is very small, as shown in Table 5.3. The electron population of the $\varphi_{HOMO-1}(W)$ is close to 2.0e in both **1C** and **3**. These results are consistent with our understandings that the W center takes a d^2 electron configuration (+IV oxidation state) in **3** and **1C**, as follows: In **3**, highly electronegative fluoride ligands stabilize the high oxidation state of W, and in **1C**, the W center cannot take a d^4 electron configuration due to the absence of the C---H interligand interactions between the H(hydride) and alkyl ligands. The considerably larger population of the $\varphi_{HOMO}(W)$ in **1C** than in **3** arises from the large charge-transfer (CT) from the alkyl group to the W center in **1C**. In **1SiH**, the populations of the $\varphi_{HOMO}(W)$ and $\varphi_{HOMO-1}(W)$ are 1.903e and 1.931e, respectively, which are closed to 2.0e. In **2**, the population of the $\varphi_{HOMO}(W)$ (1.709) is moderately close to 2.0e, while that of the $\varphi_{HOMO-1}(W)$ (1.802e) is close to 2.0e. These results suggest that the W center takes a +II oxidation state in the hydride silane complex **1SiH** and

Table 5.3. Mulliken Population[a] of Fragment MOs in Cp(CO)$_2$W(H)$_2$[SiH(OMe){C(SiH$_3$)$_3$}] **1** Cp(CO)$_2$W(H)$_2$[CH(OMe){C(CH$_3$)$_3$}] **1C**, Cp(CO)$_2$W(H)[SiH$_2$(OMe){C(SiH$_3$)$_3$}] **1SiH**, Cp(CO)$_3$W[SiH(OMe){C(SiH$_3$)$_3$}] **2**, and Cp(CO)$_2$W(F)$_3$ **3**.

MOs in [Cp(CO)$_2$W]$^+$	1	1C	1SiH	2	3
φ_{LUMO+2}(W)[b]	0.022	0.020	0.015	0.017	0.102
φ_{LUMO+1}(W)	0.682	0.837	0.514	0.563	0.172
φ_{LUMO}(W)	0.836	1.082	0.949	1.036	0.291
φ_{HOMO}(W)	1.882	1.268	1.903	1.709	0.337
φ_{HOMO-1}(W)	1.853	1.948	1.931	1.802	1.966
φ_{Total}(W)	5.275	5.155	5.312	5.127	2.868

[a] DFT(B3PW91)/BS-III calculation.   [b] See Figure 4.3.

the silyl complex **2**. In **1**, populations of the φ_{HOMO}(W) (1.882e) and φ_{HOMO-1}(W) (1.853e) are close to 2.0e. This population of the φ_{HOMO}(W) is considerably larger than that of the typical d^2 complexes **1C** and **3**, moderately larger than and similar to that of the typical d^4 complexes **2** and **1SiH**, respectively. These results are consistent with the MO pictures discussed above. All these results indicate that the W center takes a d^4 electron configuration (+II oxidation state) in **1**.

At the end of this section, we wish to mention that the populations of φ_{LUMO+1}(W) and φ_{LUMO}(W) in **1** are much smaller than 2.0e but considerably larger than zero, as shown in Table 5.3. The similar populations of these MOs are observed in **1C**, **1SiH**, and **2**, except for **3**. These populations indicate that considerably large CT occurs from the silicate-like [(H)$_2${SiH(OMe)(C(SiH$_3$)$_3$)}]$^-$, dihydride alkyl (H$^-$)$_2${CH(OMe)(C(CH$_3$)$_3$)}$^-$, hydride silane (H$^-$){SiH$_2$(OMe)(C(SiH$_3$)$_3$)}, and silyl [SiH(OMe){C(SiH$_3$)$_3$}]$^-$ to the [Cp(CO)$_2$W]$^+$ in **1**, **1C**, **1SiH**, and **2**, respectively.

H1SiH3=95, H1SiC=98, H2SiO=87,   OSiH3=126, OSiH2=123, OSiH1=90,   CSiH2=99,   CSiH3=107,   CSiO=110,
H2SiH1=96, H2SiC=122, H2SiH3=114,   H1SiH3=93, H1SiH2=94, H1SiC=173, H1SiO=154, H1SiH3=89, H1SiH2=72,
OSiH3=87, OSiH1=175, H3SiC=120   H2SiC=91, H3SiC=90, H3SiH2=110   H2SiO=89, H3SiO=99, H3SiH2=148

4-eq[a)]   **4-tbp**[a)]   **4-1**[b)]
(0)   **(0.3)**   **(35.9)**
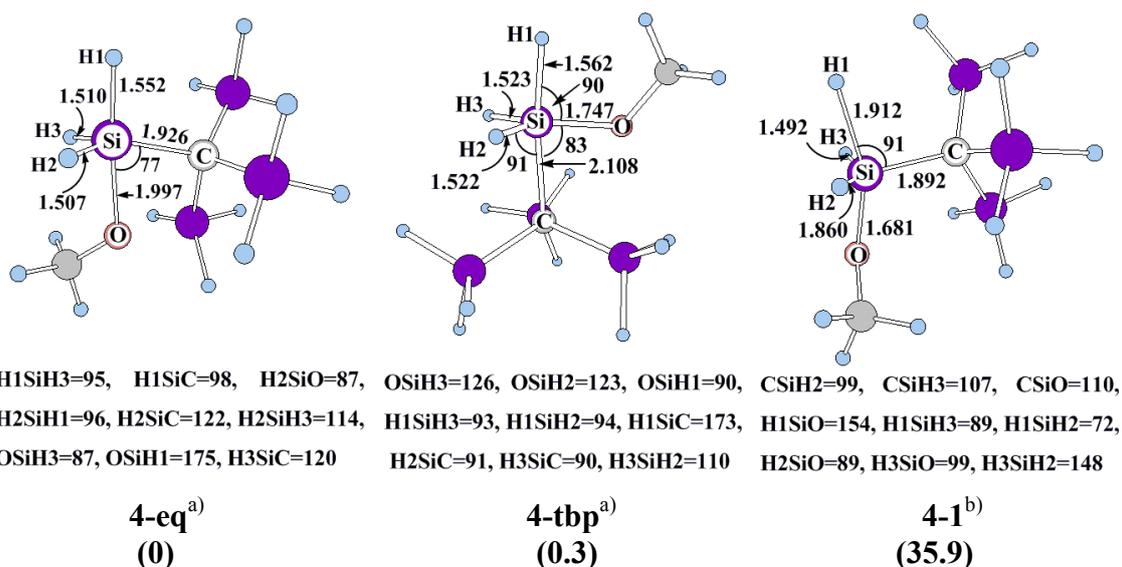
Figure 5.4. Geometries[a)] of silicate $[SiH_3(OMe)(C(SiH_3)_3)]^-$ **4**. Bond lengths are in angstroms and bond angles are in degree. DFT/BS-III-calculated relative energy is presented in parenthesis.
[a)] DFT(B3PW91)/BS-I optimization.
[b)] The geometry was taken to be the same as that in **1**.

5.3.4   Understanding of Bonding Nature of 1

The next issue is to investigate how we can understand the electronic structure of the $(H)_2[SiH(OMe)\{C(SiH_3)_3\}]$ moiety of **1**. Because the W center takes a +II oxidation state in **1**, as discussed above, the $(H)_2[SiH(OMe)\{C(SiH_3)_3\}]$ moiety possesses one negative charge in a formal sense. The five-coordinate silicon compound bearing one negative charge is a silicate anion. Hence, we optimized the geometry of the silicate anion $[SiH_3(OMe)\{C(SiH_3)_3\}]^-$ **4**. As shown in Figure 5.4, **4-eq** is the most stable structure, which adopts a trigonal-bipyramidal structure, as expected. The H1 and OMe are on the pseudo-C_3 axis and the $C(SiH_3)_3$, H2, and H3 are in the equatorial plane. This geometry is consistent with those of the usual penta-coordinated silicate anions [60, 61]. We optimized another trigonal-bipyramidal structure **4-tbp** in which the H and $C(SiH_3)_3$ are on the pseudo-C_3 axis and the OMe is

Table 5.4. Natural population[a] of several important atoms and groups in $[SiH_3(OMe)(C(SiH_3)_3)]^-$ **4**.

Atom/group	4-eq[b]	4-tbp[b]	4-1[c]
Si	13.038	12.906	12.806
H1	1.260	1.295	1.361
H2	1.176	1.224	1.332
H3	1.186	1.224	1.215
OMe	17.634	17.621	17.644
C(SiH$_3$)$_3$	57.705	57.730	58.857

[a] B3PW91/BS-III NBO calculation.   [b] DFT/BS-I optimization.
[c] Geometry was taken to be the same as that in **1**.

in the equatorial plane. This structure is slightly less stable than **4-eq** by only 0.3 [0.7, 1.3, 1.2] kcal/mol. Though the energy difference is very small, **4-tbp** is calculated to be less stable than **4-eq** by all computational methods employed here; see Appendix A.5.6. However, the geometry of (H)$_2$[SiH(OMe){C(SiH$_3$)$_3$}] **4-1**, which is taken to be the same as that in **1**, is considerably less stable than **4-eq** by 35.9 [37.6, 40.6, 39.7] kcal/mol, as presented in Figure 5.4; see also Appendix A.5.6. One of the reasons for the large instability of **4-1** is much elongated Si-H1 and Si-H2 bonds in **4-1**, compared to those of **4-eq**. However, the Si-H1 and Si-H2 bond indices (about 0.7) in **4-1** are not much smaller than those (about 0.9) of **4-eq**; see Appendix A.5.7. The Si atomic population is somewhat smaller by 0.232e and the H1 and H2 atomic populations are somewhat larger by 0.101e and 0.156e, respectively, in **4-1** than those in **4-eq**, indicating that the Si center is more positively and the H1 and H2 atoms are more negatively charged in **4-1**; see Table 5.4. Also, it is noted that the geometry of **4-1** is understood to be a distorted trigonal-bipyramidal like **4-eq**. Significant difference in the Si-H1 and Si-H2 distances between **4-1** and the typical silicate **4-eq** is interpreted in terms of the W-H1 and W-H2 interactions in **1**, as follows: The H1

and H2 atoms, which are more negatively charged in **4-1**, can form a three-center two-electron interaction with the positively charged W and Si centers. Because of the formation of the W-H1 and W-H2 interactions, the Si-H bond becomes weaker in **4-1** than in **4-eq**, leading to the considerable elongation of the Si-H1 and Si-H2 distances. The formulation of the W-H1 and W-H2 bonding interactions overcome the Si-H1 and Si-H2 bond weakening, leading to net stabilization of **1**. Also, the formation of the W-H1 and W-H2 bonds leads to the weakening of the W-Si bond. As a result, the W-Si distance is closed to the longer end of the usual W-silyl bond distance, as discussed above.

In conclusion, the electronic structure and the bonding nature of **1** are understood, as follows: (1) The W center takes a +II oxidation state (d^4 electron configuration). (2) The $(H)_2[SiH(OMe)\{C(SiH_3)_3\}]$ moiety is a distorted silicate anion. This is neither the sum of hydride and silane nor the sum of two hydrides and one silyl group. (3) The H1 and H2 ligands form a non-classical interaction with both the W and Si centers, which leads to the formation of a considerably distorted geometry for the $(H)_2[SiH(OMe)\{C(SiH_3)_3\}]$ moiety from that of **4-eq**. And, (4) the Si center also interacts with the W center, indicating that the Si center takes a six-coordinate structure and the W center adopts an eight-coordinate structure. Both are non-classical, interestingly.

5.3.5   Fluxional Behavior of 1

Because two H ligands were experimentally observed to be equivalent in the NMR time scale despite of the presence of the chiral $[SiH(OMe)\{C(SiH_3)_3\}]$ group, one can expect the fluxional behavior of **1** in which two H ligands easily exchange their positions with each other. We theoretically found two kinds of fluxional

behavior in **1**, (1) position change of [SiH(OMe){C(SiH₃)₃}] and (2) position exchange between two hydrides (H1 and H2). Both are new fluxional behavior.

5.3.5.1   Position Change of the [SiH(OMe){C(SiH₃)₃}]

(A) Front View

(B) Side View

XWSi[a] = 110˚	XWSi = 120˚	XWSi = 143˚
1a	**TS₁ₐ₋₁b (45.5i cm⁻¹)[b]**	**1b**
{0}[c]	{2.9}	{1.5}
[0][d]	[2.7]	[1.5]
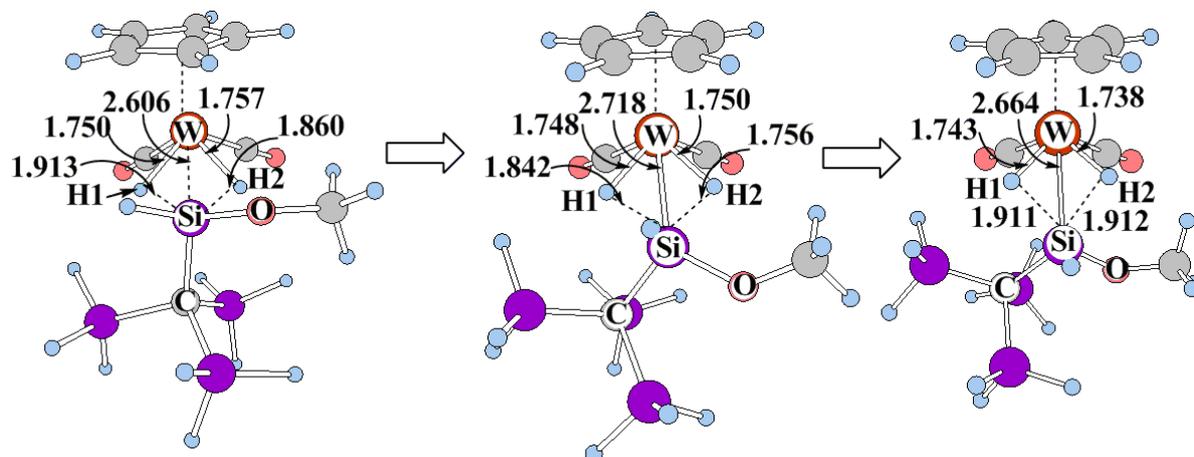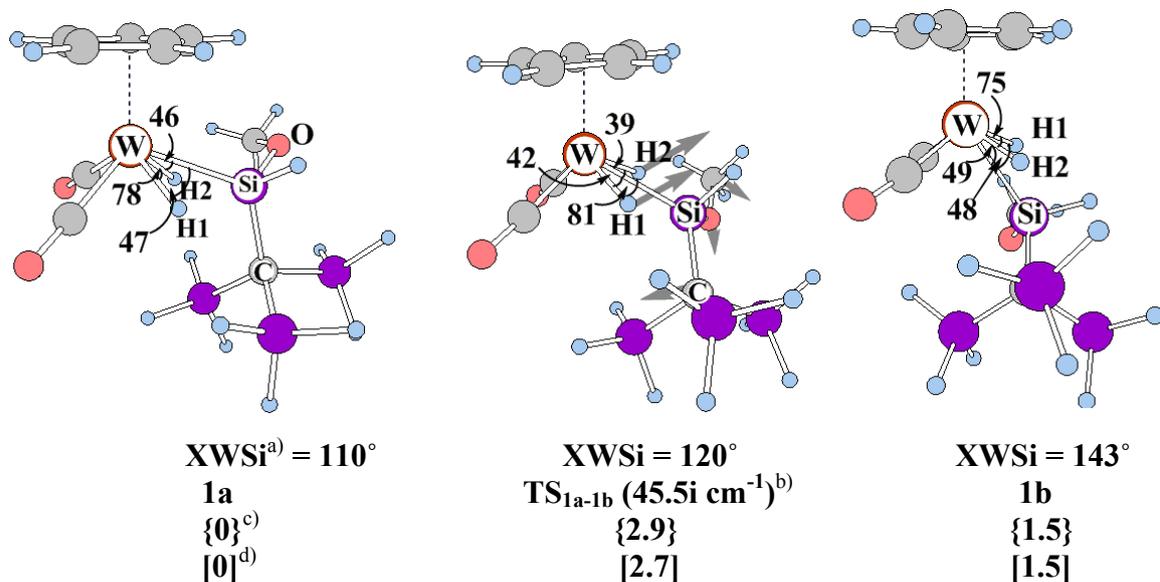
Figure 5.5. Geometry changes upon going from Cp(CO)₂W(H)₂[SiH(OMe){C(SiH₃)₃}] **1a** to Cp(CO)₂W(H)₂[SiH(OMe){C(SiH₃)₃}] **1b**.   Bond lengths are in angstrom and bond angles are in degree. Relative energies (in kcal/mol unit) in gas and solution phases are presented in braces.
[a] X is the center of Cp ring.   [b] The imaginary frequency (in cm⁻¹ unit) is given in parenthesis.   Arrows in **TS₁ₐ₋₁b** represent important movements of atoms in imaginary frequency.   [c] DFT/BS-III-calculated energy change.   d) Solvent effect (toluene) was evaluated with the PCM method.

Besides **1a**, we found another isomer **1b** in which the [SiH(OMe){C(SiH$_3$)$_3$}] takes a down-position with respect to the WH1H2 plane (see Figure 5.5), while the [SiH(OMe){C(SiH$_3$)$_3$}] takes an up-position with respect to the WH1H2 plane in **1a**. Interestingly, the geometry of **1b** is similar to that of Cp*(CO)$_2$W(H)$_2$(SiPh$_2$Cl) reported recently [27b]. This isomer **1b** is slightly less stable than **1a** by 1.5 (1.5) [0.1, 0.1, 0.2] kcal/mol; see also Appendix A.5.8. The (H)$_2$[SiH(OMe){C(SiH$_3$)$_3$}] moiety taking the geometry in **1b** is somewhat more unstable than that in **1a** by 6.6 [6.8, 7.0, 6.7] kcal/mol; see also Appendix A.5.6.
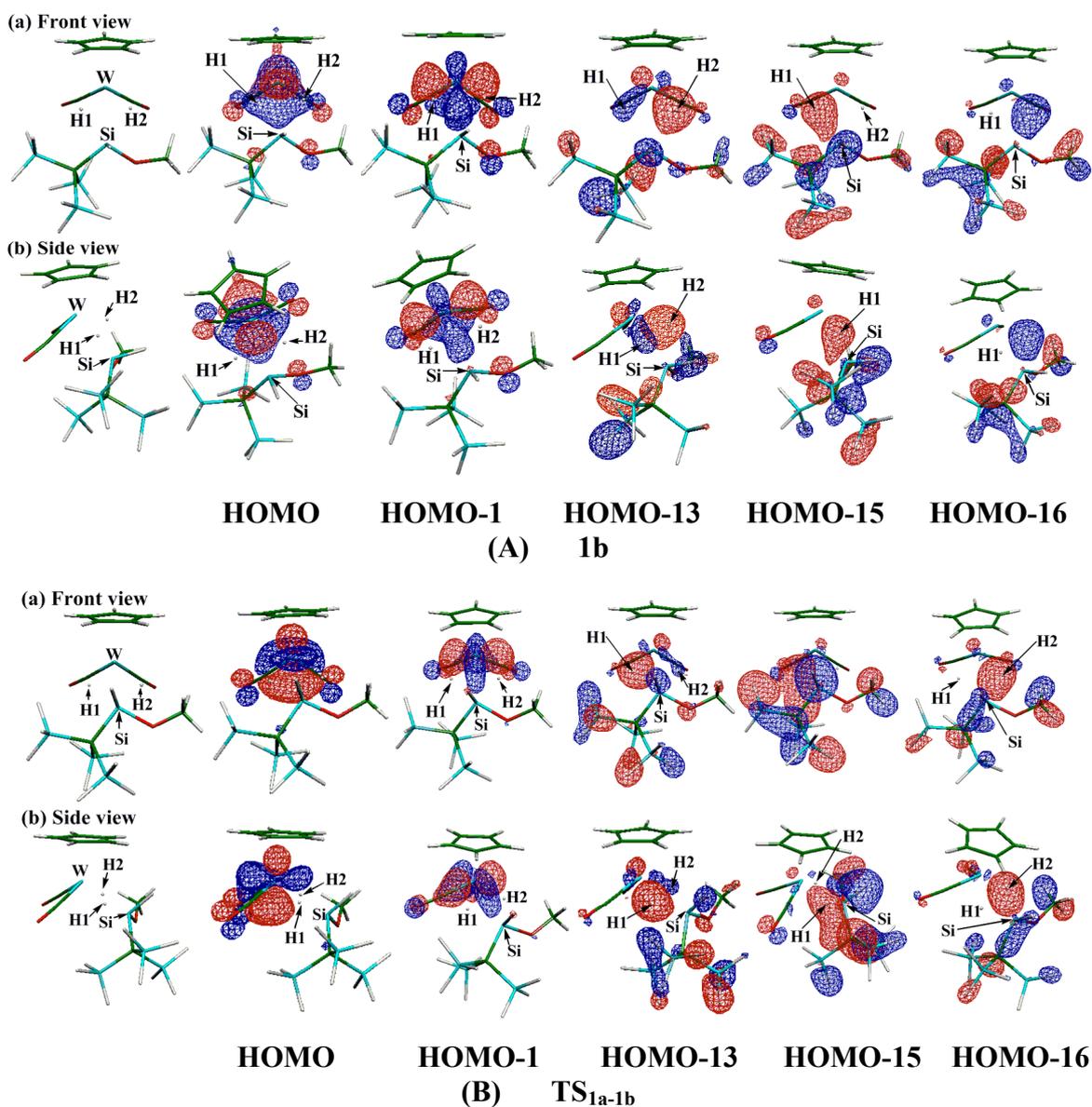
Figure 5.6. Several important Kohn-Sham MOs of **1b** and **TS$_{1a-1b}$** in position change of [SiH(OMe){C(SiH$_3$)$_3$}] of Cp(CO)$_2$W(H)$_2$[SiH(OMe){C(SiH$_3$)$_3$}] **1**.

Table 5.5. Mulliken Population[a] in MOs of $[Cp(CO)_2W]^+$ in the position change of $[SiH(OMe)\{C(SiH_3)\}]$ and H1-H2 exchange reaction of $Cp(CO)_2W(H)_2[SiH(OMe)\{C(SiH_3)\}]$ **1**.

MOs in $[Cp(CO)_2W]^+$	Position Change of $[SiH(OMe)\{C(SiH_3)\}]$		H1-H2 Exchange Reaction		
			Route-I	Route-II	
	1b	**TS$_{1a-1b}$**	**TS$_{1a-1a}$**	**1c**	**TS$_{1c-1d}$**
$\varphi_{LUMO+2}(W)$[b]	0.018	0.020	0.008	0.014	0.007
$\varphi_{LUMO+1}(W)$	0.749	0.668	0.465	1.004	0.860
$\varphi_{LUMO}(W)$	0.826	0.770	1.235	1.227	1.293
$\varphi_{HOMO}(W)$	1.710	1.921	1.899	1.285	1.546
$\varphi_{HOMO-1}(W)$	1.954	1.891	1.863	1.946	1.803
$\varphi_{Total}(W)$	5.257	5.270	5.470	5.476	5.509

[a] DFT(B3PW91)/BS-III calculation.　　[b] See Figure 5.3.

Though the Si-H1 and W-H1 distances are little different in **1a** and **1b**, the Si-H2 distance is moderately longer and the W-H2 distance is slightly shorter in **1b** than in **1a**. Also, the Si-H2 bond index is slightly smaller by 0.025 and the W-H2 bond index is moderately larger by 0.061 in **1b** than in **1a**; see Appendix A.5.9. The Si-H1 and Si-H2 bond indices are 0.239 and 0.256, respectively, in **1b**, indicating that two weak Si---H non-classical interactions are certainly involved in **1b** like in **1a**. The HOMO and HOMO-1 of **1b** mainly consist of W d orbitals, as shown in Figure 5.6(A), indicating that the W center takes a d^4 electron configuration in **1b** like in **1a**. The W-H1 and W-H2 bonding interactions were observed in the HOMO-13 and the W-Si, Si-H1, and Si-H2 bonding interactions were observed in the HOMO-15 and HOMO-16. The W atomic and d orbital populations (74.500e and 6.091e, respectively) are moderately larger in **1b** than those of **1a** (74.474e and 6.077e, respectively). The electron population (1.710e) of the $\varphi_{HOMO}(W)$ is somewhat

smaller than in **1a**, while that (1.954e) of the $\varphi_{HOMO-1}(W)$ is close to 2.0e in **1b**, too; see Table 5.5. This population of the $\varphi_{HOMO}(W)$ in **1b** is considerably larger than that of the d^2 complexes **1C** and **3** (see Table 5.3) and similar to that of the typical d^4 complex **2**. The above results indicate that the electronic structure and bonding nature of **1b** are similar to those of **1a**.

The isomerization from **1a** to **1b** easily occurs via a transition state **TS$_{1a-1b}$**, as shown in Figure 5.5, with a very small activation barrier of 2.9 (2.7) [2.8, 3.9, 3.5] kcal/mol; see also Appendix A.5.8. Intrinsic reaction coordinate (IRC) calculation clearly shows that this transition state is properly connected with **1a** and **1b**; see Appendix A.5.10. The W-H1 and W-H2 distances do not change very much upon going from **1a** to **TS$_{1a-1b}$**. However, the W-Si distance is considerably longer and the Si-H1 and Si-H2 distances are considerably shorter in **TS$_{1a-1b}$** than in **1a**. The Wiberg bond indices are also consistent with these geometry changes; the Si-H1 bond index becomes moderately larger by 0.110 and the W-Si bond index becomes moderately smaller by 0.099 in **TS$_{1a-1b}$** than in **1a**; see Appendix A.5.9. These results suggest that the Si---H1 interaction becomes stronger but the W-Si bond becomes weaker in **TS$_{1a-1b}$** than in **1a**. The HOMO and HOMO-1 of **TS$_{1a-1b}$** mainly consist of W d orbitals, as shown in Figure 5.6(B), indicating that the W center takes a d^4 electron configuration in **TS$_{1a-1b}$** like that in **1a**. The W-H1 and W-H2 bonding interactions were observed in the HOMO-13 and the W-Si, Si-H1, and Si-H2 bonding interactions were observed in the HOMO-15 and HOMO-16 of **TS$_{1a-1b}$**. The W atomic and d orbital populations (74.414e and 6.024e, respectively) are moderately smaller in **TS$_{1a-1b}$** than those of **1a** (74.474e and 6.077e, respectively). The electron population of the $\varphi_{HOMO-1}(W)$ (1.891e) is similar to that in **1a** and that of the $\varphi_{HOMO}(W)$ (1.921e) is considerably larger than in **1a**; see Table 5.5. Because the Si---H1 interaction

becomes moderately stronger in TS_{1a-1b} than in **1a** and the population of the $\varphi_{HOMO}(W)$ is larger in TS_{1a-1b} than in **1a**, it is likely that the silicate character of the $(H)_2[SiH(OMe)\{C(SiH_3)_3\}]$ moiety becomes somewhat stronger in TS_{1a-1b} than in **1a** and **1b**. This is consistent with the fact that the positive charge of the Si center is slightly larger in TS_{1a-1b} (+1.505) than in **1a** (+1.491) and the W-Si distance is considerably longer in TS_{1a-1b} than in **1a**.

The very small activation barrier of this isomerization is understood, as follows: The W-Si interaction becomes weak in TS_{1a-1b}, which is one of the origins of the activation barrier. This destabilization energy is compensated well by the strengthening of the Si-H1 and Si-H2 bonding interactions that reflects in the increase of the silicate anion character.

5.3.5.2   Exchange Processes of H1 and H2

Because the above-discussed position change of the $[SiH(OMe)\{C(SiH_3)_3\}]$ moiety does not lead to the equalization of the diastereotopic H1 and H2 ligands, we need to consider the position changes of the H1 and H2 ligands.

Route-I. In this exchange process, the H1 ligand moves toward the right-hand side (see front view of Figure 5.7) and the H2 ligand moves toward the left-hand side. The geometrical features of the transition state TS_{1a-1a} are summarized, as follows: (1) The H1, H2, and Si atoms are aligned on one line, in which the H1 atom is at a position opposite to the Si atom with respect to the H2 atom, (2) The Si-H2 (1.587 Å) distance is considerably shorter than in **1a**, which is close to that of the silane, (3) the W-Si distance (2.838 Å) is considerably longer than in **1a**, (4) the W-H2 distance (1.820 Å) is moderately longer than in **1a**, and (5) the H1-H2 distance (1.715 Å) is still considerably longer than that (0.75 Å) of dihydrogen molecule [62]. The Wiberg bond indices are consistent with these geometry changes; the Si-H2 bond index is

(A) Front view

(B) Side view

1a   **TS$_{1a-1a}$ (407.2i cm^{-1})$^{a)}$**   **1a**

$\{0\}^{b)}$ $\{25.1\}$ $\{0\}$

$[0]^{c)}$ $[25.4]$ $[0]$
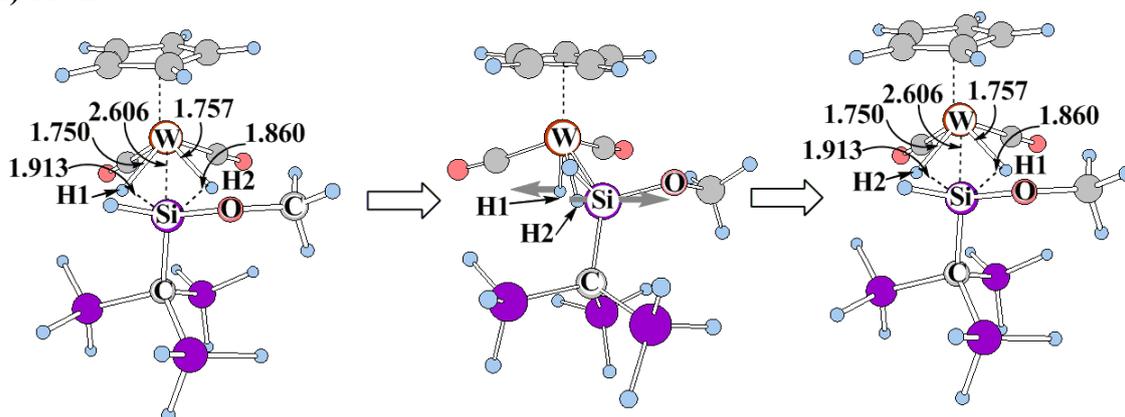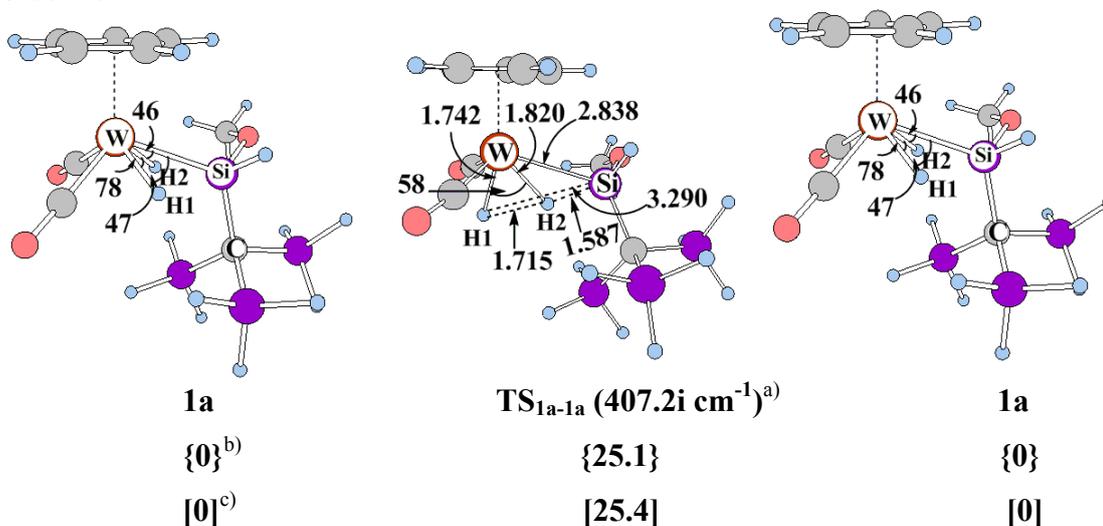
Figure 5.7. Geometry changes in H1-H2 exchange (Route-I) of Cp(CO)$_2$W(H)$_2$[SiH(OMe){C(SiH$_3$)$_3$}] **1**. Bond lengths are in angstroms and bond angles are in degree. Relative energies (in kcal/mol unit) in gas and solution phases are presented in braces.
$^{a)}$ The imaginary frequency is given in parenthesis. Arrows in **TS$_{1a-1a}$** represent important movements of atoms in imaginary frequency.
$^{b)}$ DFT/BS-III-calculated energy change.
$^{c)}$ Solvent effect (Toluene) was evaluated with the PCM method.

0.539, which is somewhat smaller than that of the usual silane [56]. On the other

hand, the W-Si and W-H2 bond indices considerably decrease to 0.226 and 0.297,

respectively, in **TS$_{1a-1a}$** compared to those (0.393 and 0.474, respectively) of **1a**; see

Appendix A.5.9. These results suggest that the W-Si and W-H2 bonds become

considerably weaker than those of **1a**. Very small bond indices between the H1 and

H2 and between the Si and H1 (0.036 and 0.002, respectively) clearly indicate the
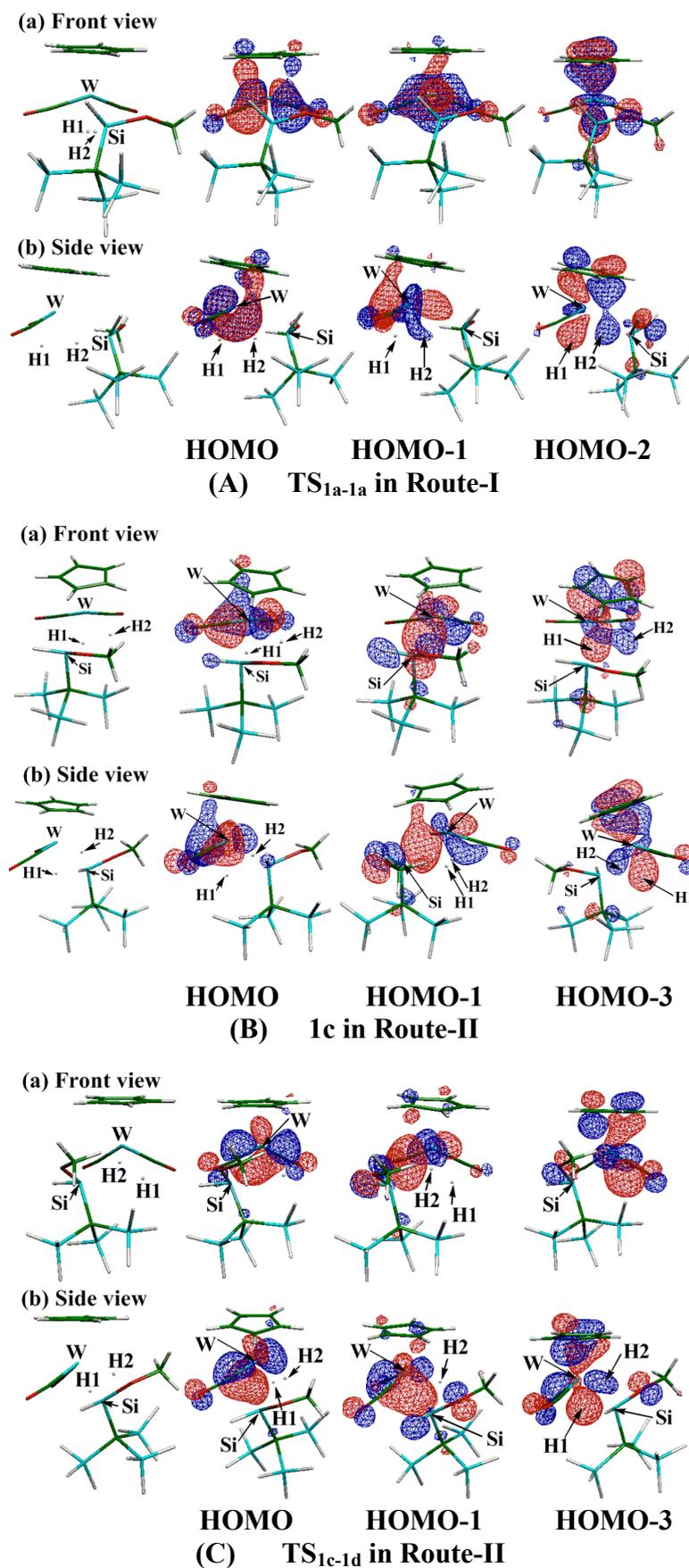
Figure 5.8. Several important Kohn-Sham MOs of transition states **TS$_{1a-1a}$** of **Roue-I** and **1c** and **TS$_{1c-1d}$** of **Route-II** in H1-H2 exchange process of Cp(CO)$_2$W(H)$_2$[SiH(OMe){C(SiH$_3$)$_3$}] **1**.

absence of the H1---H2 and Si---H1 non-classical interactions in $\mathbf{TS_{1a\text{-}1a}}$. Thus, $\mathbf{TS_{1a\text{-}1a}}$ is understood to be a hydride silane complex. The HOMO and HOMO-1 of $\mathbf{TS_{1a\text{-}1a}}$ mainly consist of the W d orbitals, as shown in Figure 5.8(A), and the HOMO-2 involves the W-H1 and W-H2 bonding interactions. Populations of the $\varphi_{HOMO}(W)$ and $\varphi_{HOMO\text{-}1}(W)$ (1.899e and 1.863e, respectively) in $\mathbf{TS_{1a\text{-}1a}}$ (see Table 5.5) are similar to those of $\mathbf{1SiH}$ (Table 5.3). These results suggest that the W center takes a d^4 electron configuration (+II oxidation state) in $\mathbf{TS_{1a\text{-}1a}}$, which is consistent with the above-described suggestion that $\mathbf{TS_{1a\text{-}1a}}$ is a hydride silane complex. The activation barrier of 25.1 (25.4) [25.6, 27.8, 27.4] kcal/mol is considerably large; see also Appendix A.5.8. This large activation barrier is not consistent with the experimental result that the H1-H2 position change rapidly occurs at room temperature.

$\quad$ **Route-II**. Considering the large activation barrier of Route-I, we need to look for another reaction course for the H1-H2 position exchange. Because H1 and H2 exchange their positions simultaneously in Route-I, we then investigated stepwise position exchange of H1 and H2. In the first step, the [SiH(OMe){C(SiH$_3$)$_3$}] group moves toward the left-hand side and the H1 concomitantly moves toward the right-hand side, to afford $\mathbf{1c}$ through a transition state $\mathbf{TS_{1a\text{-}1c}}$ with a small activation barrier of 3.5 (3.7) kcal/mol, as shown in Figure 5.9. In the $\mathbf{TS_{1a\text{-}1c}}$, the W-Si distance is becoming shorter and the Si-H1 and Si-H2 distances are becoming longer; in other words, the Si-H1 and Si-H2 bonding interactions are going to be broken. In $\mathbf{1c}$, the W-Si distance is moderately shorter and the Si-H1 and Si-H2 distances are considerably longer than in $\mathbf{1a}$. The Wiberg bond indices are consistent with these geometry changes; the W-Si bond index (0.540) of $\mathbf{1c}$ is somewhat larger than that (0.393) of $\mathbf{1a}$ and the Si-H1 and Si-H2 bond indices (0.102 and 0.097, respectively) of

(A) Front view

(B) Side view

1a	**TS$_{1a-1c}$ (102.2i)**[a)]	**1c**	**TS$_{1c-1d}$ (164.8i)**	**1d**	**TS$_{1d-1a}$ (102.2i)**	**1a**
{0}[b)]	{3.5}	{3.0}	{7.6}	{3.0}	{3.5}	{0}
[0][c)]	[3.7]	[3.2]	[7.2]	[3.2]	[3.7]	[0]
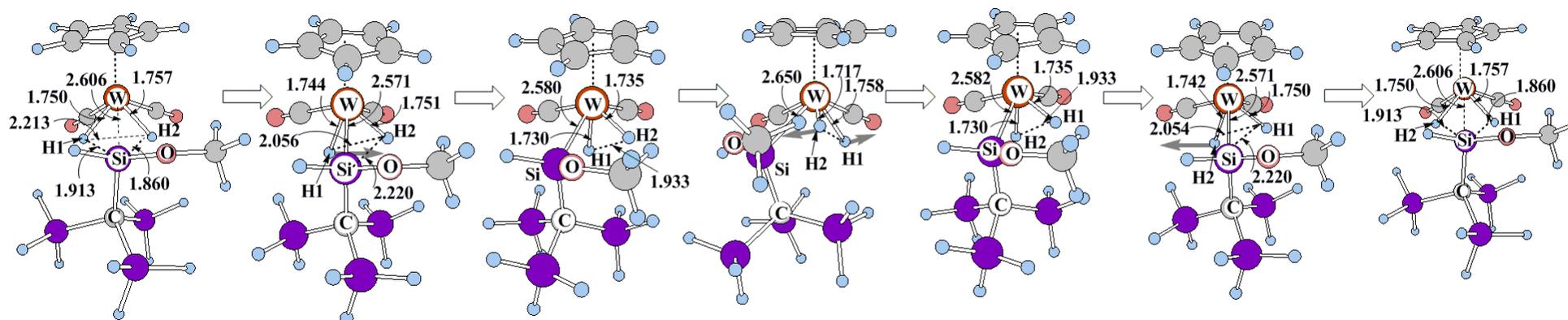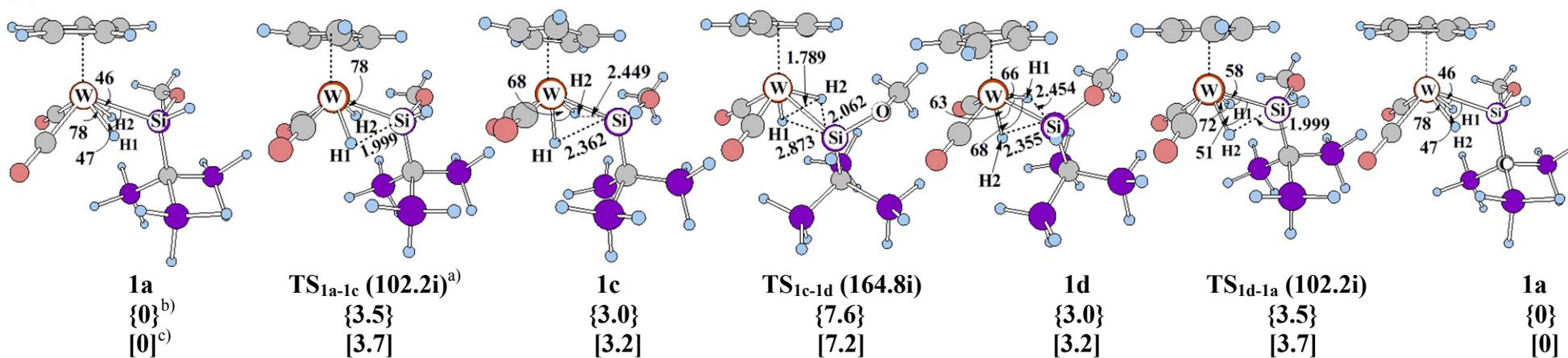
Figure 5.9. Geometry changes in H1-H2 exchange (Route-II) of Cp(CO)$_2$W(H)$_2$[SiH(OMe){C(SiH$_3$)$_3$}] **1**. Bond lengths are in angstroms and bond angles are in degree. Relative energies (in kcal/mol unit) in gas and solution phases are presented in braces.
[a)] Imaginary frequencies (in cm^{-1} unit) in transition state are presented in parenthesis. Arrows in **TS$_{1a-1c}$**, **TS$_{1c-1d}$**, and **TS$_{1d-1a}$** represent important movements of atoms in imaginary frequency.   [b)] DFT/BS-III-calculated energy change.   [c)] Solvent effect (toluene) was evaluated with the PCM method.

1c are considerably smaller than those of **1a** (0.241 and 0.281, respectively); see Appendix A.5.9. It is also noted that the H1-H2 distance (1.933 Å) is very long and the H1-H2 bond index is very small (0.044). These geometrical features and the bond indices suggest that **1c** is a dihydride silyl complex in which the W center takes a +IV oxidation state (d^2 system) in a formal sense. MOs in **1c** indicate that the W center possesses one d orbital in the occupied level, which is the HOMO; see Figure 5.8(B) for the MOs of **1c**. The HOMO-1 and HOMO-3 involve a W-Si and two W-H(hydride) bonding interactions, respectively. The electron population (1.946e) of the $\varphi_{HOMO-1}(W)$ is close to 2.0e, as shown in Table 5.5 and that (1.285e) of the $\varphi_{HOMO}(W)$ is considerably smaller than in **1a**, which is similar to that of the d^2 complex **1C**. Hence, **1c** is a dihydride silyl complex, in which the W center takes a +IV oxidation state (d^2 system). This understanding is consistent with the geometrical features of **1c** discussed above. Then, **1c** converts to **1d** through a transition state **TS$_{1c-1d}$** with a small activation barrier of 4.6 (4.0) kcal/mol. In **TS$_{1c-1d}$**, the H1-H2 axis rotates with respect to the W-H1 and W-H2 bonds. Complex **1d** is the same as **1c**, in which the positions of H1 and H2 are exchanged with each other. Hence, the **TS$_{1c-1d}$** is the transition state leading to the H1-H2 exchange. The W-Si distance becomes somewhat longer and the W-H1 distance becomes moderately longer but the W-H2 distance becomes moderately shorter in **TS$_{1c-1d}$** than those of **1c**. Also, the W-Si and W-H1 bond indices (0.432 and 0.470, respectively) of **TS$_{1c-1d}$** are moderately smaller than those of **1c** (0.540 and 0.587, respectively) and the W-H2 bond index (0.571) of **TS$_{1c-1d}$** is slightly larger than that of **1c** (0.553); see Appendix A.5.9. Though the H1-H2 distance becomes considerably shorter in **TS$_{1c-1d}$** than in **1c**, the H1-H2 distance (1.789 Å) in **TS$_{1c-1d}$** is still much longer than that (0.75 Å) of a dihydrogen molecule [62]. A very small bond index of 0.072 between the H1 and H2

also rejects the possibility of the presence of a H1---H2 interaction in **TS$_{1c\text{-}1d}$**. The very long Si-H1 distance (2.873 Å) and the very small bond index (0.013) between the Si and H1 in **TS$_{1c\text{-}1d}$** indicate the absence of the Si---H1 non-classical interaction. On the other hand, the Si-H2 distance (2.062 Å) is considerably shorter in **TS$_{1c\text{-}1d}$** than in **1c** (2.449 Å) and the Si-H2 bond index is much larger (0.205) in **TS$_{1c\text{-}1d}$** than in **1c** (0.097). These results suggest that the Si-H2 non-classical interaction certainly exists in **TS$_{1c\text{-}1d}$**, though it is not formed in **1c**. In other words, the (H)$_2$[SiH(OMe){C(SiH$_3$)$_3$}] moiety is not a silicate. Also, the much longer Si-H2 distance and the much smaller Si-H2 bond index than those of a normal silane [56] rule out the understanding that the (H)$_2$[SiH(OMe){C(SiH$_3$)$_3$}] moiety of **TS$_{1c\text{-}1d}$** is a hydride silane. These features are consistent with the electron distribution in **TS$_{1c\text{-}1d}$**, which will be described below. Finally, **1d** converts to **1a** through a transition state **TS$_{1d\text{-}1a}$** with a very small activation barrier of 0.5 (0.5) kcal/mol. This transition state **TS$_{1d\text{-}1a}$** is the same as **TS$_{1a\text{-}1c}$**. The activation barrier to complete the H1-H2 exchange is the energy difference between **TS$_{1c\text{-}1d}$** and **1a** because **1c** is less stable than **1a** and **TS$_{1c\text{-}1d}$** is at the highest energy in this H1-H2 exchange. This barrier is moderate, 7.6 (7.2) [7.2, 6.0, 8.4] kcal/mol, indicating that the H1-H2 exchange easily occurs at room temperature; see Appendix A.5.8. The moderate activation barrier arises from the presence of a non-classical Si---H2 bonding interaction in **TS$_{1c\text{-}1d}$**.

As shown in Figure 5.8(C), MOs in **TS$_{1c\text{-}1d}$** indicate that the W center possesses one d orbital in the occupied level, which is the HOMO. The HOMO-1 and HOMO-3 involve the W-Si and two W-H(hydride) bonding interactions, respectively. The electron population (1.803e) of the $\varphi_{\text{HOMO-1}}(W)$ is close to 2.0e (see Table 5.5), while that (1.546e) of the $\varphi_{\text{HOMO}}(W)$ is considerably smaller than those of **1a** and **1SiH** but considerably larger than those of **1c** and **1C**. These results suggest that the

(A) Front view
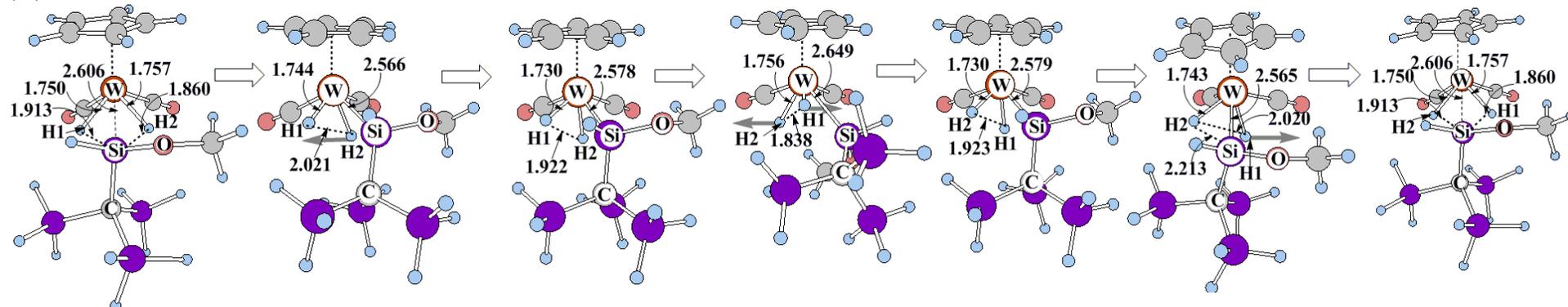
(B) Side view
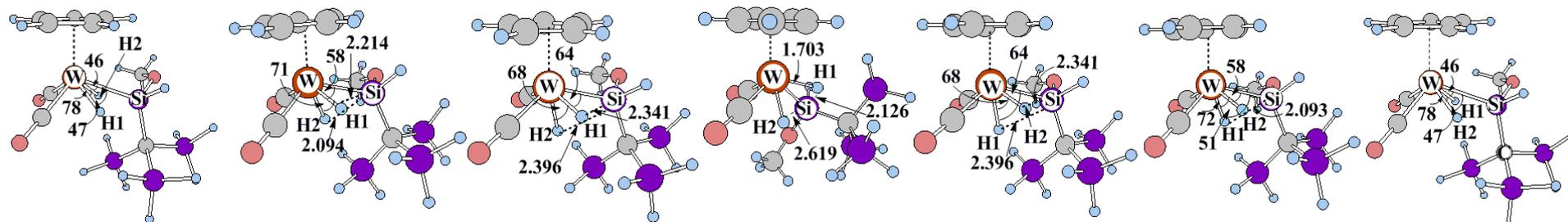
1a	TS$_{1a-1e}$ (130i)[a]	1e	TS$_{1e-1f}$ (200.6i)	1f	TS$_{1f-1a}$ (128.6i)	1a
{0}[b]	{2.7}	{2.6}	{9.1}	{2.6}	{2.7}	{0}
[0][c]	[2.8]	[2.7]	[8.8]	[2.7]	[2.8]	[0]

Figure 5.10. Geometry changes in H1-H2 exchange (Route-III) of Cp(CO)$_2$W(H)$_2$[SiH(OMe){C(SiH$_3$)$_3$}] **1a**. Bond lengths are in angstroms and bond angles are in degree. Relative energies (in kcal/mol unit) in gas[b] and solution[c] phases are presented in braces.

[a] Imaginary frequencies (in cm^{-1} unit) in transition state are presented in parenthesis. Arrows in **TS$_{1a-1e}$**, **TS$_{1e-1f}$**, and **TS$_{1f-1a}$** represent important movements of atoms in imaginary frequency. [b] DFT/BS-III calculated energy change. [c] Solvent (toluene) effect was evaluated with PCM method.

d^4 character of the W center in **TS$_{1c-1d}$** becomes considerably weaker than in **1a** and **1SiH** but considerably stronger than in **1c** and **1C**. This is because of the presence of the Si---H2 non-classical interaction. It is not easy to define which of the d^4 and d^2 electron configurations the W center takes in **TS$_{1c-1d}$**.

Route-III. Because the [SiH(OMe){C(SiH$_3$)$_3$}] group moves toward the left-hand side in Route-II (Figure 5.9), we investigated another reaction route in which the [SiH(OMe){C(SiH$_3$)$_3$}] group moves toward the right-hand side, as shown in Figure 5.10. This movement occurs concomitantly with the movement of H2 toward the left-hand side, to afford **1e** through a transition state **TS$_{1a-1e}$** with a small activation barrier of 2.7 (2.8) kcal/mol. These **TS$_{1a-1e}$** and **1e** are similar to **TS$_{1a-1c}$** and **1c**, respectively. Complex **1e** converts to **1f** through a transition state **TS$_{1e-1f}$** with moderately large activation barrier of 6.5 (6.1). In **TS$_{1e-1f}$**, the positions of the H1 and H2 are exchanged with each other. This **TS$_{1e-1f}$** is similar to **TS$_{1c-1d}$**. Finally, **1f** converts to **1a** through a transition state **TS$_{1f-1a}$** with a very small activation barrier of 0.1 (0.1) kcal/mol. This **TS$_{1f-1a}$** is essentially the same as **TS$_{1a-1e}$**. The activation barrier to complete the H1-H2 exchange is the energy difference between **TS$_{1e-1f}$** and **1a**, which is 9.1 (8.8) [8.6, 7.6, 9.7] kcal/mol; see Appendix A.5.8. These values are almost the same as those of the Route-II.

At the end of this section, we wish to mention that another transition state (**TS$_{1e-1f}$'**) is found; see Appendix A.5.11 for its geometry. In **TS$_{1e-1f}$'**, the H1-H2 distance is 0.930 Å, indicating that a dihydrogen moiety is involved in the transition state. However, **TS$_{1e-1f}$'** is more unstable than **TS$_{1e-1f}$** by 3.2 (3.2) [3.6, 1.7, 2.0] kcal/mol. Thus, it is concluded that the reaction via **TS$_{1e-1f}$'** including a dihydrogen moiety is not the easiest route.

5.4 Conclusions

The geometry, bonding nature, electronic structure, and fluxional behavior of $Cp(CO)_2(H)_2W[SiH(OMe)\{C(SiH_3)_3\}]$ **1** were theoretically investigated with the DFT, MP4(SDTQ), and CCSD(T) methods, where **1** is a model of recently synthesized tungsten dihydride silyl complex $Cp^*(CO)_2(H)_2W[SiH(OMe)\{C(SiMe_3)_3\}]$ **R1**.

The DFT-optimized geometry of **1** indicates the presence of a W-silyl and two W-hydride bonds with two weak Si---H interactions. Though the geometrical features indicate that the W center takes a d^2 electron configuration (+IV oxidation state) in a formal sense, the MO features and population analyses clearly indicate that the W center takes a d^4 electron configuration (+II oxidation state) in **1**. This means that the $(H)_2[SiH(OMe)\{C(SiH_3)_3\}]$ moiety of **1** has a silicate-like electronic structure. Though the Si-H1 and Si-H2 distances are much longer than that of the usual silicate anion, the Wiberg bond index clearly indicates the presence of the Si---H1 and Si---H2 non-classical bonding interactions in **1**. The reasonable interpretation is that the H1 and H2 form the non-classical Si-H1 and Si-H2 bonding interactions as well as the W-H1 and W-H2 non-classical bonding interactions. In addition to the presence of the Si-H1 and Si-H2 bonding interactions, the Si atom also forms a bonding interaction with the W center. The W center also forms the W-H1, W-H2, and W-Si bonding interactions in addition to the W-Cp and W-CO bonding interactions. This implies that the W center resides in an eight-coordinate environment in spite of its d^4 electron configuration, suggesting a non-classical feature of the W center.

The present theoretical study shows an interesting new type of fluxional behavior of **1**, as follows: (1) Position change of $[SiH(OMe)\{C(SiH_3)_3\}]$ around the W center easily occurs with a very small activation barrier of 2.8 (3.5) kcal/mol via a new transition state, where the DFT- and CCSD(T)-calculated values are presented without

and in parenthesis, respectively, in this section. The transition state has more silicate-like character than **1**, which leads to the small activation barrier. (2) Two hydrides easily exchange their positions with a moderate activation barrier of 7.2 (8.4) kcal/mol through a new transition state, in which neither a silane nor a dihydrogen is involved. Because of this fluxional behavior, two hydride ligands become equivalent in the NMR time scale.

In this work, we clearly elucidated the interesting non-classical electronic structure and bonding nature of **1** and a new type of fluxional behavior. It is noted that though the usual fluxional behavior was explained in terms of the transient formation of either a Si-H or a H-H bond, neither a Si-H nor a H-H bonding interaction is formed in the transition state of the H1-H2 exchange.

Bibliography

[1]   (a) Schubert, Ulrich; Ackermann, Klaus; Woerle, Barbara. *J. Am. Chem. Soc.* **1982**, *104*, 7378. (b) Rabaâ, H.; Saillard, J.Y.; Schubert, U. *J. Organomet. Chem.* **1987**, *330*, 397. (c) Schubert, U. *Adv. Organomet. Chem.* **1990**, *30*, 151. (d) Schubert, U. *Transition Met. Chem.* **1991**, *16*, 136. (e) Schubert, U.; Schwarz, M.; Moller, F. *Organometallics* **1994**, *13*, 1554. (f) Schubert, U.; Gilges, H. *Organometallics* **1996**, *15*, 2373.

[2]   Braunstein, P.; Knorr, M. *J. Organomet. Chem*. **1995**, *500,* 21.

[3]   Schneider, J. J. *Angew. Chem., Int. Ed. Engl.* **1996**, *35*, 1068.

[4]   Corey, J. Y.; Braddock-Wilking, J. *Chem. Rev*. **1999**, *99*, 175 and references therein.

[5]   Graham, W. A. G. *J. Organomet. Chem.* **1986**, *300*, 81.

[6]   (a) Fernandez, M. J.; Esteruelas, M. A.; Oro, L. A.; Apreda, M. C.; Foces-Foces, C.; Cano, F. H. *Organometallics* **1987**, *6*, 1751. (b) Esteruelas, M. A.; Oro, L. A.; Valero, C. *Organometallics* **1991**, *10*, 462. (c) Esteruelas, M. A.; Nuernberg, O.; Olivan, M.; Oro, L. A.; Werner, H. *Organometallics* **1993**, *12*, 3264. (d) Chen, W.; Edwards, A. J.; Esteruelas, M. A.; Lahoz, F. J.; Olivan, M.; Oro, L. A. *Organometallics* **1996**, *15*, 2185.

[7]   Rappoli, B. J.; Janik, T. S.; Churchill, M. R.; Thompson, J. S.; Atwood, J. D. *Organometallics* **1988**, *7*, 1939.

[8]   Duckett, S. B.; Perutz, R. N. *Chem. Commun*. **1991**, *1*, 28.

[9]   (a) Zhang, C.; Grumbine, S. D.; Tilley, T. D. *Polyhedron* **1991**, *10*, 1173. (b) Campion, B. K.; Heyn, R. H.; Tilley, T. D. *Chem. Commun*. **1992**, 1201. (c) Casty, G. L.; Lugmair, C. G.; Radu, N. S.; Tilley, T. D.; Walzer, J. F.;

Zargarian, D. *Organometallics* **1997**, *16*, 8. (d) Feldman, J. D.; Mitchell, G. P.; Nolte, J.-O.; Tilley, T. D. *J. Am. Chem. Soc*. **1998**, *120*, 11184. (e) Glaser, P. B.; Tilley, T. D. *Organometallics* **2004**, *23*, 5799. (f) Turculet, L.; Feldman, J. D.; Tilley, T. D. *Organometallics* **2004**, *23*, 2488.

[10]   (a) Jiang, Q.; Carroll, P. J.; Berry, D. H. *Organometallics* **1991**, *10*, 3648. (b) Jiang, Q.; Pestana, D. C.; Carroll, P. J.; Berry, D. H. *Organometallics* **1994**, *13*, 3679.

[11]   (a) Kreutzer, K. A.; Fisher, R. A.; Davis, W. M.; Spaltenstein, E.; Buchwald, S. L. *Organometallics* **1991**, *10*, 4031. (b) Spaltenstein, E.; Palma, P.; Kreutzer, K. A.; Willoughby, C. A.; Davis, W. M.; Buchwald, S. L. *J. Am. Chem. Soc.* **1994**, *116*, 10308.

[12]   (a) Hays, M. K.; Eisenberg, R. *Inorg. Chem*. **1991**, *30*, 2623. (b) Cleary, B. P.; Mehta, R.; Eisenberg, R. *Organometallics* **1995**, *14*, 2297.

[13]   Boardman, L. D. *Organometallics* **1992**, *11*, 4194.

[14]   Johnson, T. J.; Coan, P. S.; Caulton, K. G. *Inorg. Chem*. **1993**, *32*, 4594.

[15]   (a) Crabtree, R. H. *Stud. Surface Sci. Catal*. **1994**, *81*, 85. (b) Crabtree, R. H. *Chem. Rev. (Washington, D.C.)* **1995**, *95*, 987. (c) Crabtree, R. H. *Angew. Chem., Int. Ed. Engl*. **1993**, *32*, 789.

[16]   (a) Luo, X.-L.; Kubas, G. J.; Bryan, J. C.; Burns, C. J.; Unkefer, C. J. *J. Am. Chem. Soc*. **1994**, *116*, 10312. (b) Luo, X.-L.; Kubas, G. J.; Burns, C. J.; Bryan, J. C.; Unkefer, C. J. *J. Am. Chem. Soc*. **1995**, *117*, 1159.

[17]   Sun, J.; Lu, R. S.; Bau, R.; Yang, G. K. *Organometallics* **1994**, *13*, 1317.

[18]   (a) Nikonov, G. I.; Kuzmina, L. G.; Lemenovskii, D. A.; Kotov, V. V. *J. Am. Chem. Soc*. **1995**, *117*, 10133.   (b) Nikonov, G. I.; Kuzmina, L. G.; Lemenovskii, D. A.; Kotov, V. V. *J. Am. Chem. Soc*. **1996**, *118*, 6333. (c)

Nikonov, G. I.; Kuzmina, L. G.; Vyboishchikov, S. F.; Lemenovskii D. A.; Howard, J. A. *Chem. Eur. J.* **1999**, *5*, 2947. (d) Duckett, S. B.; Kuzmina, L. G.; Nikonov, G. I. *Inorg. Chem. Commun.* **2000**, *3*, 126. (e) G. I. Nikonov, *Angew. Chem., Int. Ed.*, **2001**, *40*, 3353. (f) Nikonov, G. I. *J. Organomet. Chem.*, **2001**, *635*, 24. (g) Nikonov, G. I.; Mountford, P.; Ignatov, S. K.; Green, J. C.; Leech, M. A.; Kuzmina, L. G.; Razuvaev, A. G.; Rees, N. H.; Blake, A. J.; Howard, JA. K.; Lemenovskii, D. A. *Dalton Trans.*, **2001**, 2903. (h) Dubberley, S. R.; Ignatov, S. K.; Rees, N. H.; Razuvaev, A. G.; Mountford, P.; Nikonov, G. I. *J. Am. Chem. Soc.* **2003**, *125,* 642. (i) Nikonov, G. I.; Mountford, P.; Dubberley, S. R. *Inorg. Chem.* **2003**, *42*, 258. (j) Osipov, A. L.; Gerdov. S. M.; Kuzmina, L. G.; Howard, J. A. K.; Nikonov, G. I. *Organometallics* **2005**, *24*, 587. (k) Dorogov, K. Y.; Yousufuddin, M.; Ho, N-N.; Churakov, A. V.; Kuzmina, L. G.; Schultz, A. J.; Mason, S. A.; Howard, JA. K.; Lemenovskii, D. A.; Bau, R.; Nikonov, G. I. *Inorg. Chem.* **2007**, *46*, 147. (l) Vyboishchikov, S. F.; Nikonov, G. I. *Organometallics* **2007**, *26,* 4160. (m) Gutsilyak, D. V.; Kuzmina, L. G.; Howard, JA. K.; Vyboishchikov, S. F.; Nikonov, G. I. *J. Am. Chem. Soc.* **2008**, *130,* 3732.

[19]   Ohff, A.; Kosse, P.; Baumann, W.; Tillack, A.; Kempe, R.; Görls, H.; Burlakov, V. V.; Rosenthal, U. *J. Am. Chem. Soc.* **1995**, *117*, 10399.

[20]   (a) Zarate, E. A.; Kennedy, V. O.; McCune, J. A.; Simons, R. S.; Tessier, C. A. *Organometallics* **1995**, *14*, 1802. (b) Simons, R. S.; Gallucci, J. C.; Tessier, C. A.; Youngs, W. J. *J. Organomet. Chem.* **2002**, *654*, 224. (c) Simons, R. S.; Panzner, M. J.; Tessier, C. A.; Youngs, W. J. *J. Organomet. Chem.* **2003**, *681*, 1.

[21]   Maseras, F.; Lledos, A. *Organometallics* **1996**, *154*, 1218.

[22] Hübler, K.; Hübler, U.; Roper, W. R.; Schwerdtfeger, P.; Wright L. J. *Chem. Eur. J.* **1997**, *3*, 1608.

[23] (a) Osakada, K.; Sarai, S.; Koizumi, T.; Yamamoto, T. *Organometallics* **1997**, *16*, 3973.   (b) Osakada, K.; Koizumi, T.; Sarai, S.; Yamamoto, T. *Organometallics* **1998**, *17*, 1868.

[24] (a) Rodriguez, V.; Donnadieu, B.; Sabo-Etienne, S.; Chaudret, B. *Organometallics* **1998**, *17*, 3809.   (b) Lachaize, S.; Sabo-Etienne, S.; Donnadieu, B.; Chaudret, B. *Chem.Commun*. **2003**, 214.

[25] Gutierrez-Puebla, E.; Monge, A.; Paneque, M.; Poveda, M. L.; Taboada, S.; Trujillo, M.; Carmona, E. *J. Am. Chem. Soc.* **1999**, *121*, 346.

[26] (a) Petri, S. H. A.; Eikenberg, D.; Neumann, B.; Stammler, H.-G.; Jutzi, P. *Organometallics* **1999**, *18*, 2615.   (b) Noveski, D.; Braun, T.; Schulte, M.; Neumann, B.; Stammler, H.-G. *Dalton Trans*. **2003**, 4075.

[27] (a) Sakaba, H.; Tsukamoto, M.; Hirata, T.; Kabuto, C.; Horino, H. *J. Am. Chem*. **2000**, *122*, 11511. (b) Sakaba, H.; Hirata, T.; Kabuto, C.; Horino, H. *Chem. Lett*. **2001**, 1078.   (c) Sakaba, H.; Hirata, T.; Kabuto, C.; Kabuto, K. *Organometallics* **2006**, *25*, 5145.   (d) Sakaba, H.; Hirata, T.; Kabuto, C.; Kabuto, K. *J. Organomet. Chem*. **2007**, *692*, 402.

[28] Baya, M.; Crochet, P.; Esteruelas, M. A.; Onate, E. *Organometallics* **2001**, *20*, 240.

[29] Yardy, N. M.; Lemke, F. R. Brammer, L. *Organometallics* **2001**, *20*, 5670.

[30] Taw, F. L.; Bergman, R. G.; Brookhart, M. *Organometallics* **2004**, *23*, 886.

[31] (a) Sakaki, S.; Ieki, M.; *J. Am. Chem. Soc*. **1991**, *113*, 5063. (b) Sakaki, S.; Ieki, M.; *J. Am. Chem. Soc*. **1993**, *115*, 2373. (c) Sakaki, S.; Ogawa, M.; Musashi, Y.; Arai, T. *Inorg. Chem*. **1994**, *33*, 1660. (d) Sakaki, S.; Ogawa, M.; Musashi,

Y.; Arai, T. *J. Am. Chem. Soc*. **1994**, *116*, 7258. (e) Sakaki, S.; Ujino, Y.; Sugimoto, M. *Bull. Chem. Soc. Jpn.* **1996**, *69*, 3047. (f) Sakaki, S.; Mizoe, N.; Sugimoto, M. *Organometallics* **1998**, *17*, 2510. (g) Sakaki, S.; Mizoe, N.; Musashi, Y.; Biswas, B.; Sugimoto, M. *J. Phys. Chem. A* **1998**, *102*, 8027.

[32]   Koga, N.; Morokuma, K. *J. Am. Chem. Soc.* **1993**, *115*, 6883.

[33]   (a) Lin, Z.; Hall, M. B. *Inorg. Chem*. **1991**, *1*, 28. (b) Cook, K. S.; Incarvito, C. D.; Webster, C. E.; Fan, Y.; Hall, M. B.; Hartwig, J. F. *Angew. Chem., Int. Ed*. **2004**, *43*, 5474.

[34]   (a) Fan, M.-F.; Jia, G.; Lin, Z. *J. Am. Chem. Soc.* **1996**, *118*, 9915. (b) Fan, M.-F.; Lin, Z. *Organometallics* **1997**, *16*, 494.   (c) Fan, M.-F.; Lin, Z. *Organometallics* **1998**, *17*, 1092. (d) Fan, M.-F.; Lin, Z. *Organometallics* **1999**, *18*, 286. (d) Ng, S. M.; Lau, C. P.; Fan, M.-F.; Lin, Z. *Organometallics* **1999**, *18*, 2484. (e) Lin, Z. *Chem. Soc. Rev.,* **2002**, *31*, 239. (f) Zhang, X. H.; Chung, L. W.; Lin, Z.; Wu, Y. D. *J. Org. Chem*.; **2008**, *73*, 820.

[35]   Jacobsen, H; Fink, M. J. *Organometallics* **2006**, *25*, 1945.

[36]   Ray, M.; Nakao, Y.; Sato, H.; Sakaki, S.; Watanabe, T.; Hashimoto, H.; Tobita, H. Submitted.

[37]   (a) Malisch, W. *J. Organomet. Chem*. **1974**, *82*, 185. (b) Malisch, W.; Hirth, U.-A.; Grun, K.; Schmeusser, M.; Fey, O.; Weis, U. *Angew. Chem. Int. Ed.* **1995,** *34,* 2500.

[38]   (a) Becke, A. D. *Phys Rev. A*. **1988**, *38*, 3098. (b) Becke, A. D. *J. Chem. Phys*. **1993**, *98*, 5648.

[39]   (a) Perdew, J. P. *In Electronic Structure of Solids*`91, Ziesche, P.; Eschrig, H., Ed.; Akademic Verlag, Berlin, **1991**; p 11. (b) Perdew, J. P.; Chevary, J. A.; Vosko, S. H.; Jackson, K. A.; Pederson, M. R.; Singh, D. J.; Fiolhais, C. *Phys.*

Rev. B. **1992**, *46*, 6671. (c) Perdew, J. P.; Chevary, J. A.; Vosko, S. H.; Jackson, K. A.; Pederson, M. R.; Singh, D. J.; Fiolhais, C. *Phys. Rev. B*. **1993**, *48*, 4978. (d) Perdew, J. P.; Burke, K.; Wang, Y. *Phys Rev. B*. **1996**, *54*, 16533.

[40]   Hay, P. J.; Wadt, W. R. *J. Chem. Phys*. **1985**, *82*, 299.

[41]   (a) Hehre, W. J.; Ditchfield, R.; Pople, J. A. *J. Chem. Phys*. **1972**, *56*, 2257. (b) Hariharan, P. C.; Pople, J. A. *Theor. Chim. Acta*. **1973**, *28*, 213. (c) Francl, M. M.; Petro, W. J.; Hehre, W. J.; Binkley, J. S.; Gordon, M. S.; DeFrees D. J.; Pople, J. A. *J. Chem. Phys*. **1982**, *77*, 3654.

[42]   Couty, M.; Hall, M. B. *J. Comput. Chem*. **1996**, *17*, 1359.

[43]   Ehlers, A. W.; Böhme, D. S.; Gobbi, A.; Höllwarth, A.; Jonas, V.; Köhler, K. F.; Stegmann, R.; Veldkamp, A.; Frenking, G. *Chem. Phys. Lett.* **1993**, *208*, 111.

[44]   Andrae, D.; Haeussermann, U.; Dolg, M.; Stoll, H.; Preuss, H. *Theor. Chim. Acta*. **1990**, *77*, 123.

[45]   Martin, J. M. L.; Sundermann, A. *J. Chem. Phys*. **2001**, *114*, 3408.

[46]   Krishnan, R.; Binkley, J. S.; Seeger, R.; Pople, J. A. *J. Chem. Phys*. **1980**, *72*, 650.

[47]   McLean, A. D.; Chandler, G. S. *J. Chem. Phys*. **1980**, *72*, 5639.

[48]   Dunning Jr, T. H. *In Modern Theoretical Chemistry, Vol. 3*, Schaefer III, H. F., Ed.; Plenum: New York, **1976**: p 1-28. The d polarization function (ζ=0.75, 0.85, 0.3247) implemented in Gaussian 03 program package (Revision C.02) was used for C, O, and Si, respectively.

[49]   (a) Dunning Jr, T. H. *J. Chem. Phys*. **1989**, *90*, 1007. (b) Woon, D. E.; Dunning Jr, T. H. *J. Chem. Phys*. **1993**, *98*, 1358.

[50]   (a) Miertuš, S.; Scrocco, E.; Tomasi, J. *Chem. Phys*. **1981**, *55*, 117. (b)

Miertuš, S.; Tomasi, J. *Chem. Phys*. **1982**, *65*, 239. (c) Cossi, M.; Barone, V.; Cammi, R.; Tomasi, J. *Chem. Phys. Lett*. **1996**, *255*, 327.

[51] Pople, J. A.; et al. *Gaussian 03,* Revision C.02, Gaussian Inc.: Wallingford, CT, **2004**.

[52] Glendening, E. D.; Reed, A. E.; Carpenter, J. E.; Weinhold, F. NBO Version, 3.1.

[53] (a) Flükiger, P.; Lüthi, H. P.; Portmann, S.; Weber, J. *MOLEKEL 4.3*, Swiss Center for Scientific Computing, Manno (Switzerland), **2000-2002**. (b) Portmann, S.; Lüthi, H. P. *MOLEKEL*, An Interactive Molecular Graphics Tool, *CHIMIA*, **2000**, *54*, 766-770.

[54] Based on a search of the Cambridge Structural Database, CSD version 5.26 (November 2004).

[55] Baker, R. T.; Calabrese, J. C.; Harlow, R. L.; Williams, I. D.; *Organometallics* **1993**, *12*, 830.

[56] Si-H bond indices are 0.753 in SiH_4, 0.754 and 0.759 in $[SiH_2(OMe)\{C(SiH_3)_3\}]$, and 0.909 and 0.915 in $[SiH_3(OMe)\{C(SiH_3)_3\}]^{-}$.

[57] We optimized a typical W(IV) complex $Cp(CO)_2W(F)_3$ by DFT/BS-I method.

[58] Kato, S.; Yamabe, S.; Fukui, K. *J. Chem. Phys*. **1974**, *60*, 572.

[59] Dapprich, S.; Frenking, G. *J. Phys. Chem*. **1995**, *99*, 9352.

[60] Burdett, J. K. *Struct. Bonding (Berlin)* **1976**, *31*, 67.

[61] Gordon, M. S.; Windus, T. L.; Burggraf, L. W.; Davis, L. P. *J. Am. Chem. Soc*. **1990**, *112*, 7167.

[62] Hay, P. J. *J. Am. Chem. Soc*. **1987**, *109*, 705.

Appendix

A.5.1 Important optimized parameters of Cp(CO)$_2$W(H)$_2$[SiH(OMe){C(SiH$_3$)$_3$}] **1**.

Table A.5.1. Basis set effects on the optimized parameters[a] of Cp(CO)$_2$W(H)$_2$[SiH(OMe){C(SiH$_3$)$_3$}] **1**.

	BS-I	BS-IV	BS-V	BS-VI	Expt
W-Si	2.606 (2.611)[a]	2.606	2.586	2.592	2.620
W-CO	1.973 (1.969)	1.964	1.969	1.967	1.962
W-CO	1.975 (1.974)	1.967	1.970	1.969	2.043
W-H1	1.750 (1.755)	1.750	1.735	1.744	-
W-H2	1.757 (1.766)	1.756	1.739	1.751	-
Si-O	1.681 (1.686)	1.689	1.711	1.679	1.660
Si-C	1.891 (1.897)	1.898	1.904	1.893	1.830
Si-H1	1.913 (1.894)	1.931	1.913	1.912	-
Si-H2	1.860 (1.814)	1.891	1.891	1.878	-
Si-H3	1.492 (1.494)	1.496	1.503	1.492	-

Bond lengths are in angstrom.
[a] In parenthesis is the optimized parameters of Cp*(CO)$_2$W(H)$_2$(SiH(OMe)(C(SiH$_3$)$_3$) **1-Cp***.

A.5.2 Wiberg bond indices of important bonds**.**

Table A.5.2 Wiberg bond indices in $Cp(CO)_2W(H)_2[SiH(OMe)(C(SiH_3)_3)]$ **1**, $Cp(CO)_2W(H)_2(CH(OMe)(C(CH_3)_3))$ **1C**, $Cp(CO)_2W(H)[SiH_2(OMe)(C(SiH_3)_3)]$ **1SiH**, and $Cp(CO)_3W[SiH(OMe)(C(SiH_3)_3)]$ **2.**

Bonds	1	1C	1SiH	2
W-Si/W-C	0.393	0.602	0.159	0.482
W-H1	0.501	0.629	0.671	-
W-H2	0.474	0.557	0.262	-
Si-H1/C-H1	0.241	0.048	0.021	-
Si-H2/C-H2	0.281	0.056	0.595	-
Si-H3/C-H3	0.889	0.915	0.898	0.876
H1-H2	0.002	0.067	0.016	-

DFT(B3PW91)/BS-III NBO calculation.

A.5.3 Conversion of Cp(CO)$_2$W(H)[SiH$_2$(OMe){C(SiH$_3$)$_3$}] **1SiH** to Cp(CO)$_2$W(H)$_2$[SiH(OMe){C(SiH$_3$)$_3$}] **1**.
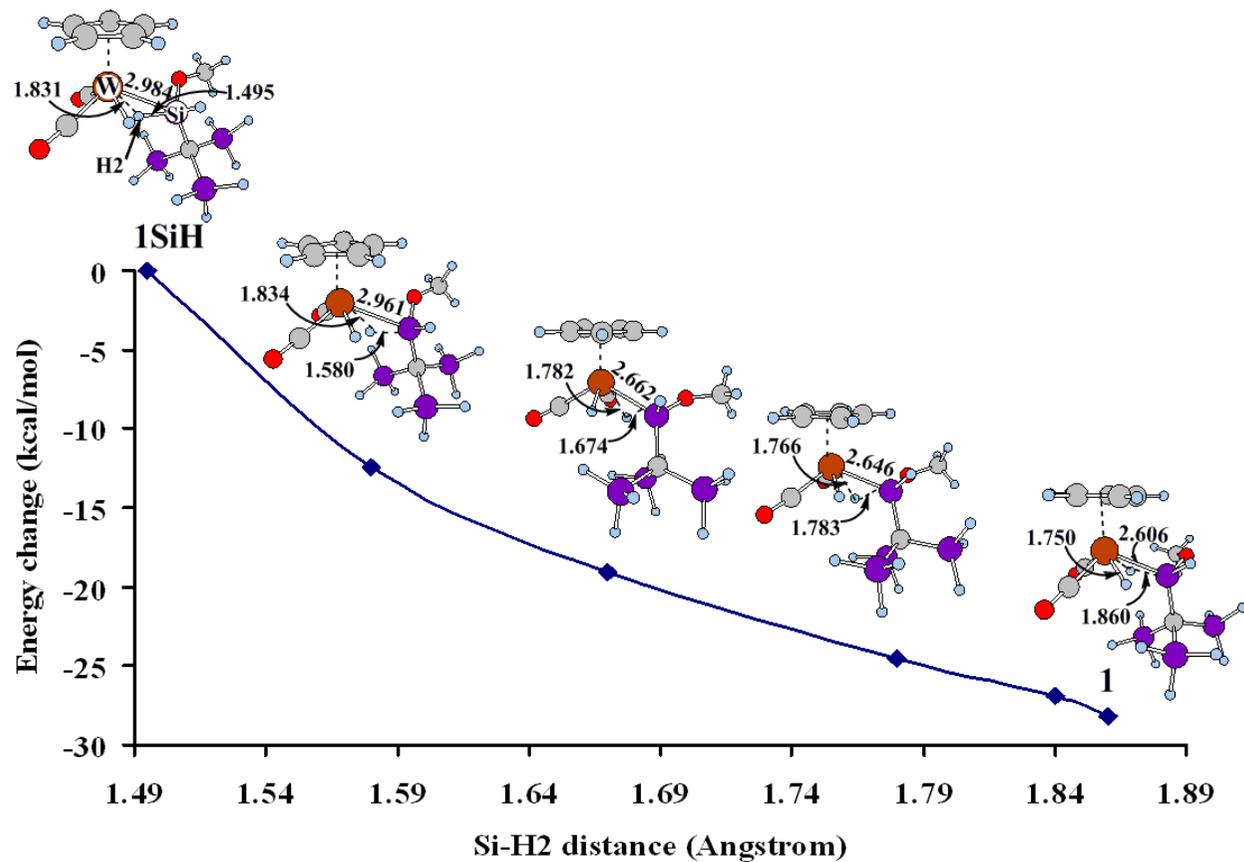
Figure A.5.1 Geometry and energy change upon going from Cp(CO)$_2$W(H)[SiH$_2$(OMe){C(SiH$_3$)$_3$}] **1SiH** to Cp(CO)$_2$W(H)$_2$[SiH(OMe){C(SiH$_3$)$_3$}] **1**.

A.5.4   Mulliken population in Cp(CO)$_2$W(H)$_2$[SiH(OMe){C(SiH$_3$)$_3$}] **1**,

Table A.5.3   Mulliken population[a)] in Cp(CO)$_2$W(H)$_2$[SiH(OMe){C(SiH$_3$)$_3$}] **1**, Cp(CO)$_2$W(H)$_2$[CH(OMe){C(CH$_3$)$_3$}]   **1C**,   Cp(CO)$_2$W(H)[SiH$_2$(OMe)(C(SiH$_3$)$_3$)] **1SiH**, Cp(CO)$_3$W[HSi(OMe)(C(SiH$_3$)$_3$)] **2**, and Cp(CO)$_2$W(F)$_3$ **3**.

Atom/Group	1	1C	1SiH	2	3
W	74.493	74.671	74.449	74.304	73.159
d	5.267	5.129	5.224	5.183	3.647
Cp(CO)$_2$W	137.408	137.391	137.487	-	135.698
H1	0.898	0.804	0.858	-	-
H2	0.954	0.776	-	-	-
Si/C	13.078	6.115	13.024	12.951	-
SiHR^{1}R^2/CHR^{1}R$^{2\ b)}$	88.740	57.028	-	88.729	-

[a)] DFT(B3PW91)/BS-III calculation.

[b)] R^1=OMe and R^2=C(SiH$_3$)$_3$ in **1** and **2**; R^1=OMe and R^2=C(CH$_3$)$_3$ in **1C**.

A.5.5 Kohn-Sham MOs in Cp(CO)$_3$W[SiH(OMe){C(SiH$_3$)$_3$}] **2** and Cp(CO)$_2$(F)$_3$ **3**.

HOMO　　　**HOMO-1**　　　**HOMO-2**

(A) Cp(CO)$_3$W[SiH(OMe){C(SiH$_3$)$_3$}] 2

HOMO　　　**HOMO-1**　　　**HOMO-2**
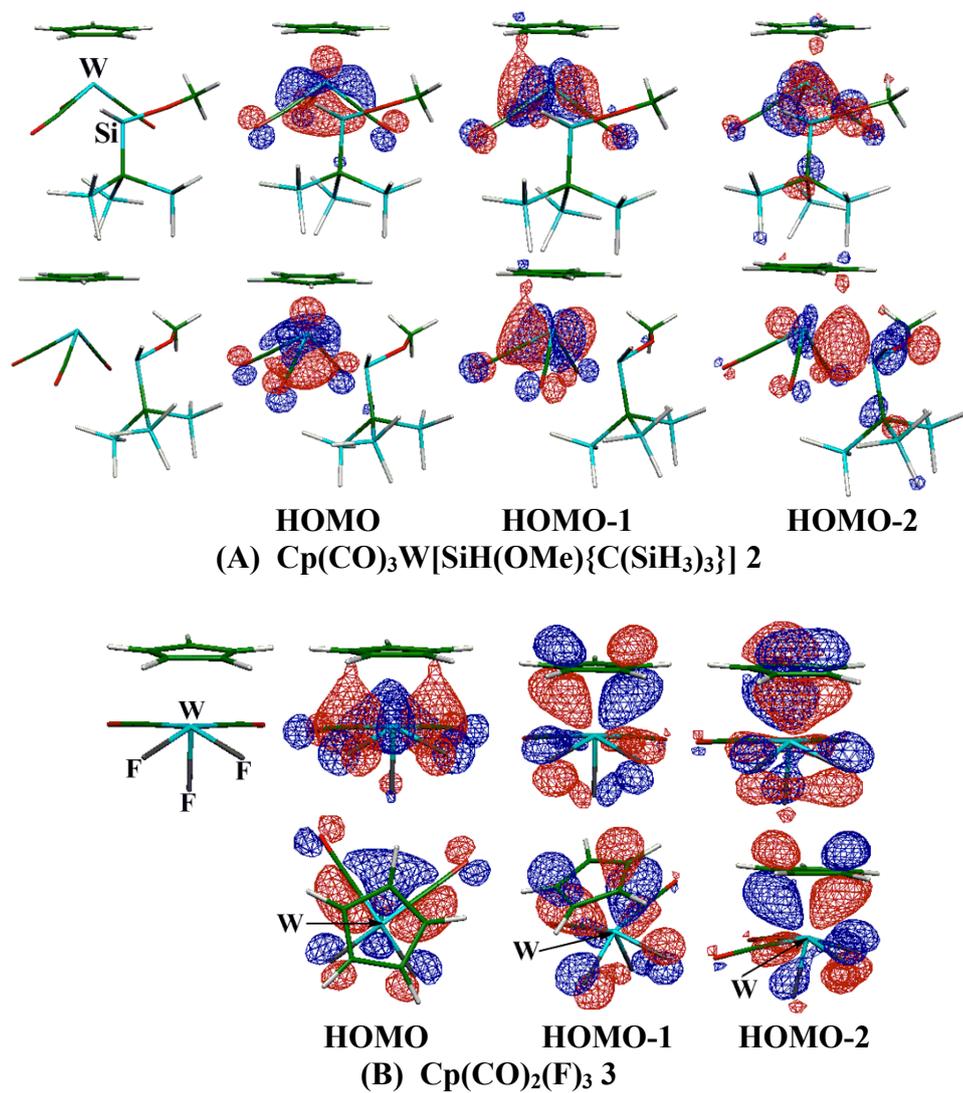
(B) Cp(CO)$_2$(F)$_3$ 3

Figure A.5.2 Several important Kohn-Sham MOs observed in Cp(CO)$_3$W[SiH(OMe){C(SiH$_3$)$_3$}] **2** and Cp(CO)$_2$(F)$_3$ **3**.

A.5.6 Destabilization energy of silicate $[SiH_3(OMe)(C(SiH_3)_3)]^-$ **4**.

Table A.5.4 Destabilization energy $(DE)^{a)}$ of silicate $[SiH_3(OMe)(C(SiH_3)_3)]^-$ **4-tbp**, **4-1**, **4-TS$_{1a-1b}$**, and **4-1b**.

Method	4-tbp	4-1	4-1b	4-TS$_{1a-1b}$
DFT	0.7 (0.3)$^{b)}$	37.6 (35.9)	44.4 (42.5)	29.1 (27.3)
MP2	1.7 (0.5)	42.5 (38.3)	50.0 (46.0)	32.5 (28.7)
MP3	1.1 (0.1)	40.7 (36.4)	47.8 (43.6)	30.9 (26.9)
MP4(DQ)	1.1 (0.1)	40.5 (36.1)	47.5 (43.2)	30.8 (26.8)
MP4(SDQ)	1.1 (0.1)	40.3 (35.9)	47.3 (43.0)	30.8 (26.7)
MP4(SDTQ)	1.3 (0.3)	40.6 (36.1)	47.6 (43.2)	31.2 (27.1)
CCSD(T)	1.2 (0.2)	39.7 (35.3)	46.4 (42.2)	30.5 (26.5)

$^{a)}$ DE = Energy difference from **4-eq**. BS-II basis set system was employed.

$^{b)}$ BS-III-calculated values are presented in parenthesis.

A.5.7 Wiberg bond index in silicate $[SiH_3(OMe)\{C(SiH_3)_3\}]^-$ **4**.

Table A.5.5 Wiberg bond index$^{a)}$ in silicate $[SiH_3(OMe)\{C(SiH_3)_3\}]^-$ **4**.

Atoms/Groups	4-eq	4-tbp	4-1
Si-H1	0.909	0.861	0.687
Si-H2	0.915	0.861	0.716
Si-H3	0.826	0.792	0.854

$^{a)}$ DFT(B3PW91)/BS-III calculation.

A.5.8 Relative energies in position change of [SiH(OMe){C(SiH$_3$)$_3$}] and H1-H2 exchange process of Cp(CO)$_2$W(H)$_2$[SiH(OMe){C(SiH$_3$)$_3$}] **1**.

Table A.5.6 Relative energies[a] in position change of [SiH(OMe){C(SiH$_3$)$_3$}] and H1-H2 exchange process of Cp(CO)$_2$W(H)$_2$[SiH(OMe){C(SiH$_3$)$_3$}] **1** calculated with various computational methods.

| | Position change of [SiH(OMe){C(SiH$_3$)$_3$}] | | H1H2 exchange process | | |
| | | | Route-I | Route-II | Route-III |
Method	TS$_{1a-1b}$	1b	TS$_{1a-1a}$	TS$_{1c-1d}$	TS$_{1e-1f}$
DFT	2.8 (2.9)[b]	0.1 (1.5)[b]	25.6 (25.1)[b]	7.2 (7.6)[b]	8.6 (9.1)[b]
MP2	4.5	1.1	28.4	6.2	8.0
MP3	3.0	-0.5	27.2	9.3	10.4
MP4(DQ)	3.6	0.1	27.3	8.4	9.7
MP4(SDQ)	3.5	0.2	27.3	8.0	9.4
MP4(SDTQ)	3.9	0.1	27.8	6.0	7.6
CCSD(T)	3.5	0.2	27.4	8.4	9.7

[a] Energy difference from **1a**. BS-II basis set system was employed.
[b] In parenthesis is the BS-III-calculated values.

A.5.9 Wiberg bond indices[a] in position change of [SiH(OMe){C(SiH$_3$)$_3$}] and H1-H2 exchange**.**

Table A.5.7 Wiberg bond indices[a] in **1b** and **TS$_{1a-1b}$** of position change of [SiH(OMe){C(SiH$_3$)$_3$}] and **TS$_{1a-1a}$**, **1c**, **TS$_{1c-1d}$**, and **TS$_{1e-1f}$** of H1-H2 exchange**.**

| | Position Change of [SiH(OMe){C(SiH$_3$)$_3$}] | | | H1-H2 Exchange Process | | |
| | | | | Route-I | Route-II | |
Bonds	1a	1b	TS$_{1a-1b}$	TS$_{1a-1a}$	1c	TS$_{1c-1d}$
W-Si	0.393	0.370	0.294	0.226	0.540	0.432
W-H1	0.501	0.541	0.497	0.555	0.587	0.470
W-H2	0.474	0.535	0.460	0.297	0.553	0.571
Si-H1	0.241	0.239	0.351	0.002	0.102	0.013
Si-H2	0.281	0.256	0.288	0.539	0.097	0.205
H1-H2	0.002	0.002	0.015	0.036	0.044	0.072

[a] DFT(B3PW91)/BS-III NBO calculation.

A.5.10 Changes in potential energy in position change of [SiH(OMe){C(SiH₃)₃}]
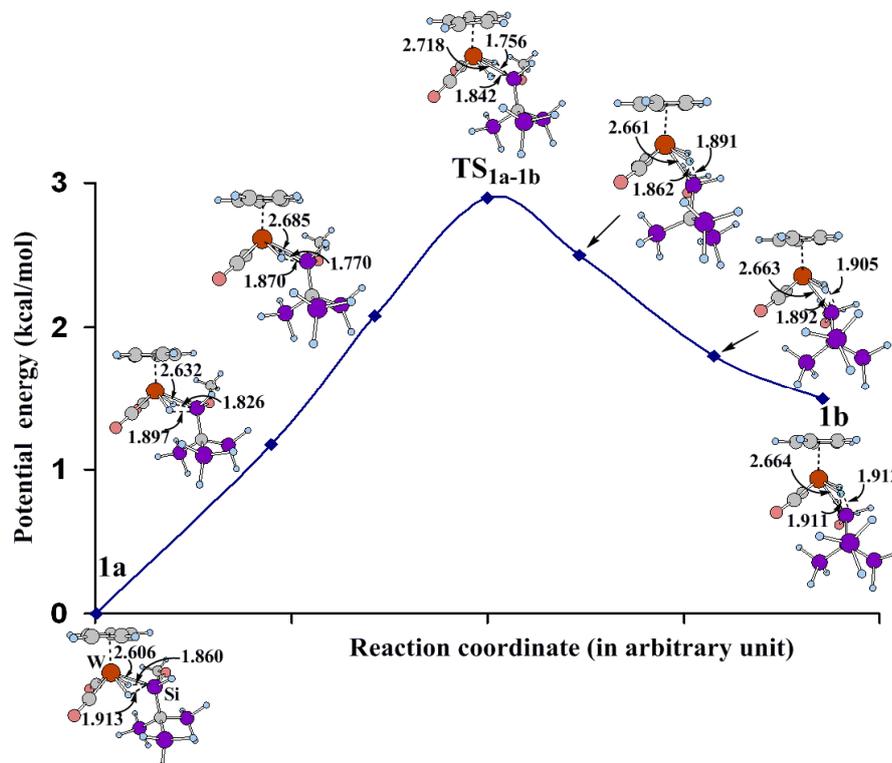
(A) Potential energy change
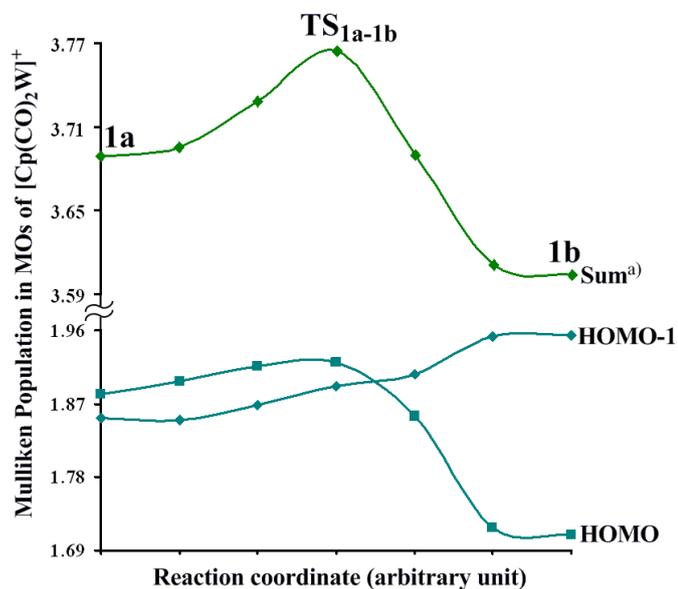
(B) Population change

in Cp(CO)₂W(H)₂[SiH(OMe){C(SiH₃)₃}] **1**.

Figure A.5.3 Changes in potential energy and d orbital population of W with reaction coordinate upon going from Cp(CO)₂W(H)₂[SiH(OMe){C(SiH₃)₃}] **1a** to Cp(CO)₂W(H)₂[SiH(OMe){C(SiH₃)₃}] **1b**.
DFT(B3PW91)/BS-III calculation.
[a] HOMO + HOMO-1.

A.5.11   Geometry of **TS₁ₑ₋₁f′** in H1-H2 exchange process of Cp(CO)₂W(H)₂[SiH(OMe){C(SiH₃)₃}] **1a**.

(A) **Front view**   (B) **Side view**

TS₁ₑ₋₁f′ (301.7i)
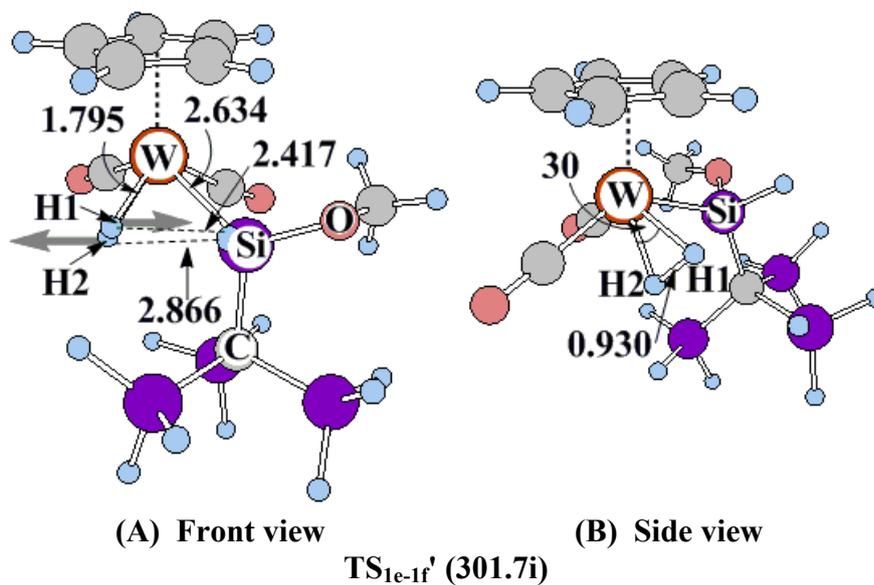
Figure A.5.4. Geometry of **TS₁ₑ₋₁f′** of Route-III in H1-H2 exchange process of Cp(CO)₂W(H)₂[SiH(OMe){C(SiH₃)₃}] **1a**.
Bond lengths are in angstroms and bond angles are in degree.
[a] The imaginary frequency is given in parenthesis. Arrows in **TS₁ₑ₋₁f′** represent important movements of atoms in imaginary frequency.

General Conclusion

Theoretical studies of new transition metal complexes containing silicon species are presented here. Their characteristic features of geometry, electronic structure, and bonding nature are discussed in detail. The density functional theory (DFT) with hybrid functional B3PW91 was mainly used for these theoretical studies. Møller-Plesset (MP) perturbation (MP2, MP3, and MP4) theory and coupled-cluster method with single and double substitutions and perturbation correction of triple excitations (CCSD(T)) were also employed to check the reliability of the DFT-calculated energies. To inspect the bonding interactions of these complexes, the LCMO (Linear Combination of Molecular Orbital) analysis was carried out, in which molecular orbital ψ_i of the total system is represented by a linear combination of molecular orbitals of fragments. The results and observations are summarized, as follows:

In chapter 1, geometry and bonding nature of $Cp(CO)_2W(CCH)(SiH_2)$ **1** and $Cp(CO)_2W(\eta^3\text{-}H_2SiCCH)$ **2** and formation reaction of **1** from **2** were theoretically investigated with the DFT, MP2 to MP4(SDTQ), and CCSD(T) methods, where **1** and **2** were adopted as models of interesting new complexes reported recently, $Cp^*(CO)_2W(CC^tBu)(SiPh_2)$ and $Cp^*(CO)_2W(\eta^3\text{-}Ph_2SiCC^tBu)$, respectively. Computational results clearly indicate that **1** involves neither a pure silacyclopropenyl group nor a pure silylene and acetylide groups and that the silylene group strongly interacts with both the W center and the acetylide group. Frontier orbitals of **1** resemble those observed in the formation reaction of silacyclopropene from silylene and acetylene. The frontier orbitals, as well as the geometry, indicate that the $(CCH)(SiH_2)$ moiety of **1** is understood in terms of an interesting intermediate species trapped by the W center in that

formation reaction. Complex **1** is easily formed from **2** through the Si-C σ-bond activation with a moderate activation barrier of 15.3, 18.8, and 15.8 kcal/mol, which are the DFT-, MP4(SDTQ)- and CCSD(T)-calculated values, respectively. This reaction takes place without change of the oxidation state of the W center. Intermediate **2** is easily formed from $Cp(CO)_2W(Me)(H_3SiC≡CH)$ via a Si-H oxidative addition followed by a C-H reductive elimination. The bonding nature of **2** is also very interesting; the non-bonding π orbital of the H_2SiCCH moiety is essentially the same as that of the propargyl group but the π conjugation between the Si and C atoms is very weak in the π orbital unlike that of the propargyl group. Thus, the electronic structure and bonding nature of **2** can be understood to be intermediate between those of tungsten $η^3$-alkynylsilyl and tungsten $η^3$-silapropargyl complexes.

In chapter 2, geometry and bonding nature of interesting new tungsten $η^3$-silaallyl/$η^3$-vinylsilyl complex $Cp(CO)_2W(η^3-H_2SiCHCH_2)$ **3** and tungsten vinyl silylene complex $Cp(CO)_2W(CHCH_2)(SiH_2)$ **4** and the conversion reaction of **3** to **4** were theoretically investigated with the DFT and CCSD(T) methods, where **3** was adopted as a model of $Cp^*(CO)_2W(η^3-Me_2SiCHCMe_2)$. Non-bonding π orbital ($φ_{nπ}$) of the $η^3-H_2SiCHCH_2$ group is similar to that of the $η^3$-allyl group except that the Si p orbital more contributes to the $φ_{nπ}$ than the C p orbital. On the other hand, the π orbital ($φ_π$) of the $η^3-H_2SiCHCH_2$ group is considerably different from that of the $η^3$-allyl group; the π-conjugation between the Si and C atoms is very weak unlike that of the $η^3$-allyl group in which the π-conjugation is considerably strong. Thus, **3** can be understood to be a species between tungsten $η^3$-vinylsilyl and tungsten $η^3$-silaallyl complexes. From geometry and frontier orbitals, **4** can be understood to be a tungsten vinyl silylene complex in which charge transfer interaction between the silylene and vinyl groups is very weak. Complex **3** is much more stable than **4** by 21.0 (20.9) kcal/mol but $Cp(CO)_2W(η^3-H_2SiCCH)$ **2** is less

stable than $Cp(CO)_2W(CCH)(SiH_2)$ **1** by 0.7 (4.9) kcal/mol, where the CCSD(T)- and DFT-calculated values are given without and in parenthesis, respectively. This means that the tungsten η^3-silaallyl/η^3-vinylsilyl complex can be isolated but the tungsten vinyl silylene complex cannot unlike the tungsten acetylide silylene complex $Cp^*(CO)_2W(CC^tBu)(SiPh_2)$ which was isolated recently. Complex **3** converts to **4** with a large activation barrier of 34.2 (33.2) kcal/mol, while **2** easily converts to **1** with a moderate activation barrier of 15.8 (15.3) kcal/mol. These differences between **2** and **3** can be interpreted as follows: Though the Si-C bond is weak in **3**, the W-(η^3-$H_2SiCHCH_2$) interaction is considerably strong. Moreover, the W-vinyl and the silylene-vinyl interactions are very weak in **4**. On the other hand, the Si-C bond is strong but the W-(η^3-H_2SiCCH) interaction is weak in **2**. Moreover, the W-acetylide and the silylene-acetylide interactions are very strong in **1**. The reasons are discussed in detail.

In chapter 3, we theoretically investigated how to stabilize a new transition metal η^3-silapropargyl/alkynylsilyl complex $CpL_2M(\eta^3$-$R^2_2SiCCR^1)$ (M = W or Mo; L = CO, PMe_3, or PF_3; Cp = C_5H_5; R^1 = H, Me, ^tBu, or CF_3; R^2 = H, Me, or F) which is an interesting silicon analogue of a transition metal η^3-propargyl complex. Though this complex was experimentally proposed as an intermediate in the synthesis of tungsten acetylide silylene complex $Cp(CO)_2W(CC^tBu)(SiPh_2)$, it has not been synthesized yet. From theoretical computations with the DFT method, we wish to propose that the combination of electron-withdrawing CF_3 on C, σ-electron-withdrawing/π-electron-donating F on Si, Mo center, and CO is the best to stabilize the η^3-silapropargyl/alkynylsilyl form. On the other hand, the combination of bulky ^tBu on C, either H or Me on Si, W center, and PMe_3 is the best to stabilize the acetylide-silylene form, which is also interesting species. The reasons are discussed.

In chapter 4, bonding nature and electronic structure of $Cp(CO)_2(SiH_2)W\text{-}CC\text{-}W(SiH_2)(CO)_2Cp$ **5** were theoretically investigated with the DFT method, where **5** was employed as a model of recently synthesized dinuclear tungsten complex $Cp^*(CO)_2(SiPh_2)W\text{-}CC\text{-}W(SiPh_2)(CO)_2Cp^*$. Computational results clearly indicate that **5** is understood not to be a disilabutadiene-bridged dinuclear complex and a cumulenic (W=C=C=W) complex but to be an ethynediyl-bridged bis(silylene) dinuclear tungsten complex which contains various charge transfer (CT) interactions between the tungsten, silylene, and ethynediyl, as follows: The CTs occur from the lone pairs (φ^{CC}_{lp}) of the ethynediyl to the unoccupied d orbital (d^W_{unoc}) of the W and from the occupied d orbital (d^W_{occ}) of the W to the π^* orbital ($\varphi^{CC}_{\pi^*}$) of the ethynediyl. Other CTs occur from the lone pair orbital (φ^{Si}_{lp}) of the silylene to the d^W_{unoc} and from the d^W_{occ} to the empty p orbital (φ^{Si}_{p}) of the silylene. Also, the CT occurs from the φ^{CC}_{π} to the φ^{Si}_{p}. These CT interactions lead to the considerably strong Si-C bonding interactions and the considerably large elongation of the C-C distance. The C-C distance is much longer than the typical C≡C triple bond distance and similar to the typical C=C double bond distance. The Si-C bond is much weaker than that of a disilabutadiene but moderately weaker than the Si-C single bond. The mixing of the φ^{CC}_{π} into the $\varphi^{CC}_{\pi^*}$ induces the π orbital polarization of the CC moiety in one plane and the reverse π orbital polarization in the perpendicular plane. These polarizations also participate in the C-C bond weakening of the ethynediyl.

In Chapter 5, geometry, bonding nature, electronic structure, and fluxional behavior of $Cp(CO)_2W(H)_2[SiH(OMe)\{C(SiH_3)_3\}]$ **6** were theoretically investigated with the DFT, MP2 to MP4(SDTQ), and CCSD(T) methods, where **6** was employed as a model of recently synthesized tungsten dihydride silyl complex $Cp^*(CO)_2W(H)_2[SiH(OMe)\{C(SiMe_3)_3\}]$ **R1**. The DFT-optimized geometry of **6** indicates the presence of a W-silyl and two W-hydride bonds with two weak Si---H

interactions, suggesting that the W center takes a d^2 electron configuration (+IV oxidation state) in a formal sense. However, analyses of molecular orbitals and electron population analysis indicate that the W center takes a d^4 electron configuration (+II oxidation state) in **6**. Theoretical interpretation is reasonably presented, as follows: The W center takes a +II oxidation state and **6** has interesting electronic structure which consists of a silicate-like $(H)_2[SiH(OMe)\{C(SiH_3)_3\}]$ moiety including two non-classical Si---H bonding interactions and a non-classical eight-coordinated W center bearing a W-Si and two W-H bonds. Interestingly NMR chemical shifts of two hydride ligands of **R1** are equivalent at room temperature despite of the presence of chiral $[SiH(OMe)\{C(SiMe_3)_3\}]$ group, indicating that **R1** exhibits a fluxional behavior which makes two hydrides equivalent. Our theoretical study reveals new type of fluxional behavior of **6**, as follows: (1) Position of $[SiH(OMe)\{C(SiH_3)_3\}]$ easily changes around the W center with a very small activation barrier of 2.8 (3.5) kcal/mol through a new transition state, where the DFT- and CCSD(T)-calculated values are presented without and in parenthesis, respectively, hereafter. In the transition state, the silicate-like electronic structure becomes stronger than in **6**. (2) Two hydrides easily exchange their positions with a moderate activation barrier of 7.2 (8.4) kcal/mol through a new transition state, in which neither a silane nor a dihydrogen is involved. Because of this fluxional behavior, two hydride ligands become equivalent, as observed by the NMR spectroscopy. The reasons of the moderate activation barrier are discussed in terms of the bonding interaction.

As discussed above, many valuable and important results are presented on the geometrical characteristics, bonding interactions, and electronic structures of new transition metal complexes containing silicon species. Their interesting geometries and bonding natures, as well as their fluxional behaviors are clearly discussed based on the fundamental understanding of electronic structure. Clear idea is proposed on how to

synthesize new transition metal complexes of silicon species. Also, correct understanding is provided on the reasons why the transition metal complexes of silicon species are similar to and/or different from their carbon analogues. The author believes that these theoretical studies provide great impact on the further development of transition metal silicon chemistry. Hopefully, this work boosts up future study on the transition metal complexes including other heavy non-transition elements.